



UNIVERSITAT
POLITÈCNICA
DE VALÈNCIA



DESIGN AND DEVELOPMENT OF A MULTI-FREQUENCY SYSTEM FOR MICROWAVE HEATING

Pablo Santón Pons

Director: Juan Vicente Balbastre Tejedor

Codirector: Ruth De los Reyes Cánovas

PhD thesis presented at Polytechnic University of Valencia for the
obtention of the PhD Eng. in Telecommunications.

Valencia, September 2022

Financial Support

The research developed in this PhD thesis has been supported by a FDGENT grant (FDGENT/2018/008) from the Valencian Regional Government (GVA).

To Lucrecia.

To my father.

To my mother.

Abstract

Microwave systems are widely used for heating applications, mainly domestic food heating. The microwave oven sales figures place it as the first domestic appliance, giving its core element, the magnetron, an unbeatable production cost margin. However, recent improvements in RF high-power generator manufacturing have pointed out not only the limitations of these systems based on the magnetron but also the main benefits of the transistors technology.

Nowadays, solid-state power amplifiers are mature enough to compete in efficiency, cost and quality with the magnetron. Transistors' main benefits are their reduced size, low operation voltages, pure frequency spectrum, lifetime, and straightforward digital control. Microwave systems based on solid-state power amplifiers have been recently introduced, although the real applications making use of them are rare. The main issue is the lack of applicator designs for specific solid-state sources that fully exploit the mentioned advantages; therefore, this is the main objective of the present PhD thesis.

Solid-State Microwave Heating (S2MH) systems are presented in this PhD dissertation as an alternative that offers enhanced heating. Fine frequency selection, adjustable output power and coherent phase sweep in multiple outputs provide the system with accurate control over the heating process. The direct outcome of this control is the production of homogeneous heating and the application of microwave technology into high-added-value temperature-sensitive processes.

The complete design and manufacture of two S2MH systems have been carried out and presented in this PhD thesis. The two designed systems are a multi-process chemical lab batch oven and an almond drying conveyORIZED oven. These two systems are composed of the Solid-State Microwave Generator System (SSMGS), consisting of four Solid-State Power Amplifiers (SSPA) with coherent wave generation, and the applicator.

The design of the SSMGS has been carried out according to the power and frequency requirements of the application. A 4 x 250 W SSPA at 2,450 MHz SSMGS has been used for the chemical processes oven, while the almond drying application needs 4 x 500 W SSPA at 915 MHz. Both SSMGS allow the individual or combined digital control of the parameters of the four amplifying modules, i.e., power, frequency and phase.

Multiphysics modelling has been thoroughly studied with special attention to the temperature-dependent thermophysical and dielectric properties of food and liquid solutions. The overall applicators' behaviour has been analysed with this tool. After completing the two PoC (Proof of Concept), the results show good agreement with the models. Both PoCs have shown promising improvements to the current state-of-the-art systems. The chemical applications PoC shows

electromagnetic field distribution improvements, independent of the application or load. On the other hand, the almonds drying system provides increased control over the process avoiding material losses through overheating.

Resumen

La utilización de sistemas de microondas para aplicaciones de calentamiento está muy extendida, principalmente por su uso en el calentamiento doméstico. El volumen de ventas del horno de microondas doméstico refleja un dato curioso: es el electrodoméstico más vendido en el mundo cada año. Por ello, el coste de producción del elemento principal, el magnetrón, presenta unos márgenes de beneficio imbatibles. Sin embargo, los avances en la fabricación de generadores de RF de alta potencia de estado sólido han puesto de manifiesto no solo las limitaciones de los sistemas basados en magnetrón sino también las grandes ventajas de la tecnología de transistores.

Actualmente, los amplificadores de potencia de estado sólido han alcanzado una madurez suficiente como para competir en eficiencia, coste y calidad de la onda generada con el magnetrón. Las principales ventajas de los transistores son un reducido tamaño, tensiones de alimentación bajas, un espectro puro en frecuencia, un mayor tiempo de vida y el control digital directo. Los sistemas de microondas con esta tecnología están siendo introducidos en el mercado desde hace diez años, aunque las aplicaciones reales que los utilizan son escasas. La principal razón es la falta de diseños de aplicadores específicos para sacar el máximo provecho a las fuentes de estado sólido. , por tanto, es éste el objetivo de la tesis doctoral.

Los sistemas S2MH (Solid-State Microwave Heating) se presentan en esta disertación doctoral como una alternativa que ofrece un calentamiento mejorado. La posibilidad de seleccionar la frecuencia exacta, ajustar la potencia de salida y realizar barridos de fase de forma coherente con múltiples iluminadores proporcionan al sistema un control preciso del proceso de calentamiento. El resultado directo de éste es un calentamiento homogéneo y el uso de la tecnología de microondas en procesos de alto valor añadido y fuerte dependencia con la temperatura.

Esta tesis doctoral presenta el trabajo realizado en el diseño y fabricación de dos sistemas S2MH: el primero es un horno estático versátil para diferentes procesos químicos, y el segundo un horno de transporte para el secado de almendras. Estos dos sistemas están formados por el SSMGS (Solid-State Microwave Generator System), que incluye cuatro amplificadores de estado sólido (SSPA) con una generación de la onda coherente, y el aplicador.

Para el diseño del SSMGS se han tenido en cuenta los requisitos de potencia y frecuencia de cada aplicación. Se ha utilizado un SSMGS con cuatro PA de 250 W a 2,450 MHz para el horno de aplicaciones químicas, mientras que el secado de almendras necesita cuatro PA de 500 W a 915 MHz. Los dos sistemas de generación de microondas permiten un control individual o combinado de los parámetros de los cuatro módulos amplificadores, i.e., potencia, frecuencia y fase.

Todo el proceso de diseño ha sido llevado a cabo mediante modelado multi-físico, poniendo un especial cuidado en las propiedades termofísicas y dieléctricas de los alimentos y soluciones acuosas que tienen una importante dependencia con la temperatura. El comportamiento completo del sistema aplicador se ha estudiado con estas herramientas. Tras la fabricación de los dos prototipos o pruebas de concepto (PoC), los resultados obtenidos presentan un comportamiento similar al modelo y muestran, además, prometedoras mejoras frente a los sistemas actuales. El sistema de aplicaciones químicas presenta mejoras en la distribución de campo, independientemente de la aplicación y la carga. Y el sistema de secado de almendras proporciona un mayor control sobre el proceso evitando la pérdida de material por sobrecalentamiento.

Resum

La utilització de sistemes de microones en aplicacions d'escalfament està molt estesa, principalment pel seu us en escalfament domèstic. El volum de ventes del forn de microones domèstic reflexa una informació curiosa: es l'electrodomèstic més venut anualment al món. Per això, el cost de producció del seu element principal, el magnetró, presenta uns marges de benefici imbatibles. No obstant això, els avanços en la fabricació de generadors de RF d'alta potència d'estat sòlid han posat de manifest tant les limitacions dels sistemes basats en magnetró, com els grans avantatges de la tecnologia de transistors.

Actualment, els amplificadors de potència d'estat sòlid són el suficientment madurs com per competir en eficiència, cost i qualitat de l'ona generada amb el magnetró. Els principals avantatges dels transistors són les dimensions reduïdes, tensions d'alimentació baixes, un espectre pur en freqüència, major temps de vida i el control digital directe. Els sistemes de microones amb aquesta tecnologia estan sent introduïts al mercat des de fa deu anys, malgrat les aplicacions reals són escasses. El principal motiu és la falta de dissenys de aplicadors específics per obtenir el màxim profit de les fonts d'estat sòlid. , por tanto, es éste el objetivo de la tesis doctoral.

Els sistemes S2MH es presenten en esta dissertació doctoral com una alternativa que ofereix un escalfament millorat. La possibilitat de seleccionar la freqüència exacta, ajustar la potència d'eixida i realitzar un rastreig de fase de forma coherent amb molts il·luminadors proporcionen al sistema un control precís del procés d'escalfament. El resultat directe d'aquest és un escalfament homogeni i el us de la tecnologia de microones en processos d'alt valor afegit i alta sensibilitat a la temperatura.

Aquesta dissertació doctoral presenta el treball realitzat en el disseny i fabricació de dos sistemes S2MH: el primer és un forn estàtic i versàtil per a diferents processos químics, i el segon es tracta d'un forn de transport per l'assecatge d'ametles. Tots dos sistemes estan formats pel SSMGS, que inclou quatre amplificadors d'estat sòlid (SSPA) amb generació coherent de l'ona, i l'aplicador.

Per al disseny del SSMGS s'han tingut en compte els requisits de potència i freqüència de cada aplicació. S'ha utilitzat un SSMGS amb quatre PA de 250 W a 2,450 MHz per al forn d'aplicacions químiques, mentre que per al d'assecatge d'ametla es necessita quatre PA de 500 W a 915 MHz. Ambdós sistemes de generació de microones permeten un control individual o combinat dels paràmetres dels quatre mòduls amplificadors, i.e., potència, freqüència i fase.

Tot el procés de disseny ha sigut realitzat amb l'ajuda del modelat multi-físic, prestant una especial atenció a les propietats termofísiques i dielèctriques dels aliments i solucions aquoses, que tenen una important dependència de la temperatura. El comportament complet del sistema

aplicador ha sigut estudiat amb estes ferramentes digitals. Després de la fabricació dels dos prototips o proves de concepte (PoC), els resultats obtinguts presenten un comportament similar al model i, a més a més, mostren millores prometedores front als sistemes actuals. El sistema d'aplicacions químiques presenta millores en la distribució de camp, independentment de l'aplicació i la càrrega. I el sistema d'assecatge d'ametlles proporciona un major control sobre el procés, evitant la pèrdua de material per sobreescalfament.

Acknowledgements

It has been four years since I was proposed to ask for a PhD grant. I can't believe I am writing these words to conclude this passionate period of my life, where we have also come through unpredictable things, such as a worldwide pandemic and a new war in Europe. I cannot finish these studies without naming everyone who participated and helped me through this effort. I just hope I don't let anyone out of these words.

First, I would like to thank Prof. Elías De los Reyes. It has been a pleasure to learn from him since he took me into his company back in 2016. I can't describe how grateful I am for these years of working, travelling and having “asmorçarets” with one of our university's most renowned researchers and academics.

While Prof. Elías appeared each morning at my office's door with a new idea, I couldn't have finished this PhD thesis without my director, Prof. Juan Vicente Balbastre. He provided me with the needed order, structure and mind clarity. He has also been thoroughly diligent with every required paperwork and with the supervision of the redaction of this PhD dissertation.

I need to thank Ruth De los Reyes, CEO of Microbiotech S.L. It has been a pleasure to work side by side on every project and learn everything related to the food industry. Her humanity and daily hard work made me grow both professionally and personally. I want to extend these words to the students that worked with us (Álvaro, Miguel, Nelson, Nora, Pepe, Samuel and Steffano) and to José.

My period in Gothenburg, Sweden, has been a before and an after in my life. I want to thank my supervisor at RISE, Birgitta Raaholt, for her support. It has been a pleasure to work with her, learning multiphysics modelling and giving me a very industrialised point of view of microwaves. Even though the limitations of the pandemic situation, it was a wonderful time. From that period, I also came back with very good friends: Leo, Kike, Javier, Luis Fernando, Michele, Mayeul, Eric and Joar.

I happened to be a corridor colleague of two of the brightest minds of our school. I must thank Prof. Mariano Baquero and Prof. Miguel Ferrando for their support, comments, and time devoted to me whenever I came up with doubts about microwave devices and antennas.

Continuing with the communications department members, I want to thank the teachers I shared lab classes with: Eva Antonino, Marta Cabedo, and, especially, Vicent Miquel Rodrigo. They have been inspiring and helpful in my discovery of university teaching.

Acknowledgements

These years have also been of significant personal growth, and I want to thank everyone who has helped and accompanied me. My friends from Mirambel, Hakuna and Machus always showing great interest in my thesis developments; my friends back in Alzira, especially Tente, Hermi, Oscar and Alberto; and my flatmates D. Ramón, Quique, Juan and Tofe.

I want to thank my family, every one of them, and especially my father, for his example as the first PhD in the family. Last but not least, I need to thank my girlfriend, Lucrecia, for her unconditional love, support and patience. I dedicate the results of this PhD thesis to them all.

I thank God for making all this possible.

Valencia, July 2022

Pablo Santón Pons

Contents

<i>Abstract</i>	<i>vii</i>
<i>Resumen</i>	<i>ix</i>
<i>Resum</i>	<i>xi</i>
<i>Acknowledgements</i>	<i>xiii</i>
<i>Contents</i>	<i>xvi</i>
<i>List of Figures</i>	<i>xx</i>
<i>List of Tables</i>	<i>xxxii</i>
<i>Abbreviations and Acronyms</i>	<i>xxxvi</i>
Chapter 1. General Information of the Thesis.	3
1.1. Context	3
1.2. Framework	5
1.3. Objectives	6
1.4. Organisation of the Thesis	7
Chapter 2. Microwave-based heating processes.	9
2.1. Background information. Theoretical basis	10
2.1.1. Complex dielectric permittivity.....	11
2.1.2. Materials classification.....	15
2.1.3. Microwaves and power.....	17
2.2. Heating and power applications using vacuum tubes.	19
2.2.1. The microwave oven.	21
2.2.2. Industrial applications.	25
2.3. Technology review. Solid-state outbreak.	27
2.3.1. Transistor technology	29
2.3.2. Solid-state power amplifiers market.....	32
2.3.3. Commercial solid-state driven microwave applicators	37
Chapter 3. Design methodology and equipment	45
3.1. Microwave system's design methodology	45
3.2. Software and equipment.	47

3.2.1.	Modelling and calculation tools	47
3.2.1.1	Electromagnetic modelling: HFSS from Ansys.	47
3.2.1.2	Multiphysics modelling: Comsol.	47
3.2.1.3	Calculation software: Matlab.	48
3.2.2.	Lab measuring devices.	48
3.2.2.1	Microwave leakage detector.	48
3.2.2.2	Vector network analyser (VNA).....	49
3.2.2.3	Infrared (IR) thermal cameras.	50
Chapter 4.	Computer-aid modelling.....	53
4.1.	Considerations to the modelling of microwave heating processes.	53
4.1.1.	Dielectric properties measurement systems.	54
4.1.1.1	Parallel plates.....	54
4.1.1.2	Coaxial probe.....	54
4.1.1.3	Transmission lines.	56
4.1.1.4	Resonant cavities.	57
4.1.1.5	Free space techniques.	57
4.1.2.	The effect of shapes and sizes.	58
4.2.	Multiphysics modelling of foodstuff.....	59
4.2.1.	Thermophysical properties.	59
4.2.1.1	Water change of state.	62
4.2.2.	Dielectric properties.	62
4.3.	Beef sample modelling example.	63
4.3.1.	Meat election: data research.	63
4.3.1.1	Data summary.....	69
4.3.2.	Beef meat defrosting and tempering.....	75
4.3.2.1	Thermophysical equations refinement.....	77
4.3.2.2	Microwave heating studies in Comsol.	78
4.3.2.3	Commercial Whirlpool oven comparison.....	79
Chapter 5.	Complementary devices design	87
5.1.	Impedance matching device.....	87
5.1.1.	Theoretical study and equations	89
5.1.2.	Coplanar waveguide structure	91
5.1.3.	Implementation.....	93
5.2.	Fast heating microwave plate.	95
5.2.1.	Asymmetric stripline structure	96
5.2.2.	Highly susceptor ceramic	97
5.2.3.	Design and manufacture	98
5.3.	EMC protection elements for in-line industrial ovens.	100
5.3.1.	Microwave exposure regulation.	101
5.3.2.	Waveguide accesses with microwave filters.	103
5.3.2.1	Study of the higher order modes.	105

5.3.2.2	Absorbent materials in the lateral walls	113
5.3.3.	Study results discussion.....	120
Chapter 6.	<i>Solid-state based system's description</i>	125
6.1.	Microwave generation: VCO and Driver	126
6.2.	Power dividers and phase shifters	126
6.3.	Solid-state power amplifiers	129
6.4.	Antennas	130
6.4.1.	Monopole antennas.....	131
6.4.1.1	Tunable monopole antennas.....	132
6.4.2.	Slotted stripline antennas.....	135
6.4.2.1	New stripline antenna design.....	135
6.4.3.	Patch antennas	144
6.4.3.1	Circular antennas.....	144
6.4.3.2	Square antennas	145
6.4.3.3	Antenna miniaturisation. New substrates.....	145
6.4.3.4	Two-frequency antennas.....	148
6.4.4.	PIFA antennas	154
6.5.	Resonant cavities.	157
Chapter 7.	<i>Microwave assisted chemical processes – 2,450 MHz ISM band.</i>	161
7.1.	Patch and wire antenna design	162
7.1.1.	Teflon-based patch antennas.....	162
7.1.2.	Monopole antennas.....	165
7.2.	Application example: chemical synthesis.	166
7.2.1.	Applicator design and implementation.....	166
7.2.1.1	Multi-source microwave generator.....	166
7.2.1.2	Antennas and cavity.....	167
7.2.1.3	Validation and start-up procedure.....	169
7.2.2.	Modelling of chemical processes.....	174
7.2.2.1	Synthesis.....	174
7.2.2.2	Calcination.....	175
7.2.2.3	Functionalisation.....	178
7.2.3.	Processes validation.....	179
7.3.	Conclusions.	179
Chapter 8.	<i>Microwave assisted almond drying – 915 MHz ISM band</i>	181
8.1.	Patch antennas studies	182
8.1.1.	With Teflon substrate	182
8.1.2.	With PEEK substrate	185
8.2.	Application example: dried fruits drying process	190
8.2.1.	Almond thermophysical and electromagnetic characterisation.....	191

8.2.1.1	Humidity characterisation	191
8.2.1.2	Dielectric properties measurements.....	192
8.2.2.	Power requirements and first tests.....	194
8.2.3.	Multi-sources electromagnetic modelling	196
8.2.4.	Development of a modular oven as a PoC (proof of concept)	201
8.2.4.1	Solid-state microwave generator	201
8.2.4.2	Static or batch oven design.....	203
8.2.4.3	Continuous or transport oven design.....	208
8.2.5.	Results	210
8.2.5.1	Load location and test preparation.....	210
8.2.5.2	Microwave generation system adjustments.....	212
8.2.5.3	Almond heating results with the static oven.....	213
8.2.5.4	Drying tests.....	216
8.2.5.5	Results of the continuous oven.....	217
8.3.	Conclusions.	219
Chapter 9.	<i>Results discussions and future work</i>.....	223
9.1.	Summary and comments	223
9.2.	Multi-frequency and AI.	225
9.2.1.	Mechanical implications.....	226
9.2.2.	Modelling implications.....	227
9.2.3.	Managing implications	228
9.2.3.1	Artificial Intelligence (AI) techniques.....	229
9.3.	Future work	230
Chapter 10.	<i>Final conclusions</i>	233
	<i>Bibliography</i>.....	237
	<i>Annex A</i>.....	249

List of Figures

Fig 1.1. Schematic of the active electronically scanned array (AESA) [2, Fig. 2.25]	4
Fig 1.2. Antenna double function for transmission and reception [2, Fig. 1.4].....	5
Fig 1.3. SSMGS block-diagram.	5
Fig 2.1. Radioelectric spectrum classification depending on the frequency - wavelength.	9
Fig 2.2. Mechanisms producing electric polarisation in dielectrics [5, Fig. 2.4].	12
Fig 2.3. Interfacial (space charge) (a), and reorientation (b) polarizations [8, Fig. 2.1].	13
Fig 2.4. Build-up (a) and decay (b) of the polarization [8, Fig. 2.5].	14
Fig 2.5. Silver (Ag): example of conductor [12]	15
Fig 2.6. Aluminium (Al): example of superconductor [13]	15
Fig 2.7. Teflon [®] (PTFE): example of a dielectric [14]	16
Fig 2.8. RT/Duroid 6202: example of a dielectric used for electronic and microwave circuitry [15]	16
Fig 2.9. Silicon: example of semiconductor [16]	16
Fig 2.10. Gallium: example of semiconductor [17].....	16
Fig 2.11. The electromagnetic spectrum [20, Fig. 1.1].	18
Fig 2.12. Randall and Boot with the first magnetron.	19
Fig 2.13. Magnetron drawing presented by Spencer for the patent request [19]	20
Fig 2.14. Comparison between the current commercial microwave ovens (left) and the first microwave oven developed by Raytheon (right) [24].	21
Fig 2.15. Components of a typical microwave oven [23, Fig. 4.2].	22
Fig 2.16. Microwave cavity with a schematic portrayal of E-field variation for the TE ₂₃₂ mode [26, Fig. 2].	23
Fig 2.17. Schematic diagram of a magnetron [28, Fig. 2].	24
Fig 2.18. Various designs of mode stirrers [23, Fig. 4.5].	25
Fig 2.19. Exploded view of a typical conveyORIZED industrial microwave oven [31, Fig. 5].....	27
Fig 2.20. RF power device family tree [38, Fig. 1.26].	29
Fig 2.21. Schematic structure of a BJT (a) and its top view (b) [38, Fig. 1.28].	30

Fig 2.22. STARTER Evaluation Kit with a 2450 MHz 250 W solid-state microwave amplifier [40].	34
Fig 2.23. PHASESHIFTER Evaluation Kit with two 2450 MHz 250 W solid-state microwave amplifiers [40].	34
Fig 2.24. Front (a) and back (b) views of LEANFA's Generator Lab Kit at 2.45 GHz and 250 W.	34
Fig 2.25. RF Energy Toolkit from pinkRF with 250 W at 2.45 GHz [43].	35
Fig 2.26. Solid-state microwave generator at 2.45 GHz and 1 kW from Muegge [44].	35
Fig 2.27. SAIREM's GMS 1000 solid-state generator with 1kW at 2.45 GHz [47].	36
Fig 2.28. SAIREM's GMS 450 solid-state generator with 450 W at 2.45 GHz [48].	36
Fig 2.29. Wattsine's 915MHz-25kW-CEWA Solid-state microwave generator [49].	37
Fig 2.30. Wattsine's 433MHz-200W-CCFA Solid State Microwave Power Generator (lab-ready) [50].	37
Fig 2.31. Wattsine's 433MHz-200W-CMFA Solid State Microwave Power Generator (integrable) [51].	37
Fig 2.32. Midea 200 W solid-state microwave oven.	38
Fig 2.33. NXP's Sage concept RF cooker.	38
Fig 2.34. Front view of the Miele's Dialog smart oven.	39
Fig 2.35. IBEX oven [58].	39
Fig 2.36. Aura-Wave ECR microwave plasma source [59, Fig. 1 (a)].	40
Fig 3.1. Velleman microwave leakage detector.	49
Fig 3.2. FieldFox Microwave Analyzer [63].	49
Fig 3.3. Optris PI 160 thermographic camera.	50
Fig 3.4. Testo 890 Thermal imager [64].	50
Fig 4.1. Parallel plates method [68].	54
Fig 4.2. Coaxial probe measurement method (left) and example of the Agilent Technologies coaxial probe (right) [68].	55
Fig 4.3. Concentrated elements schematic with a sample between the probes [70, Fig. 3].	55
Fig 4.4. Transmission/reflection measurement coaxial probes [70, Fig. 6].	55
Fig 4.5. Transmission lines method [68].	56
Fig 4.6. Complete measurement system based on CPW probe.	57
Fig 4.7. Novel CPW-based multi-frequency dielectric properties measurement device.	57
Fig 4.8. Resonant cavities method [68].	57
Fig 4.9. Free space techniques method [68].	58

Fig 4.10. Power density of radiation from S direction. TM mode (left) and TE mode (right) [95, Fig. 3.39]	58
Fig 4.11. Center overheating in a cylindrically shaped meat loaf, of radius 25 mm and $f=2,450$ MHz [96, Fig. 2.6]	59
Fig 4.12. Models for thermal conductivity of a two-component mixture: (a) perpendicular, (b) parallel and (c) dispersed. The arrow represents the heat flow direction [99, Fig. 7.1]	61
Fig 4.13. The effect of ash concentration and moisture on dielectric constant of meat samples at 2,450 MHz [104, Fig. 2]	64
Fig 4.14. The effect of the moisture and ash concentration on dielectric loss factor of meat samples at 2,450 MHz [104, Fig. 4]	64
Fig 4.15. Illustration of apparatus used to hold and measure the dielectric properties [116, Fig. 1(b)]	65
Fig 4.16. Dielectric properties, real (a) and imaginary (b) parts, of white pudding and pork luncheon roll at different temperatures and frequencies [116]	66
Fig 4.17. Equations used for the derived dielectric parameters [116]	66
Fig 4.18. Effect of added salt on the dielectric properties of meat blends at 27.12, 915 and 2450 MHz and also their temperature rises (ΔT) following a standardised heating (450 W for 1 min 30 s) at 27.12 or 2450 MHz [117, Fig. 3]	67
Fig 4.19. Effect of added fat on the dielectric properties of meat blends at 27.12, 915 and 2450 MHz and also their temperature rises (ΔT) following a standardised heating (450 W for 1 min 30 s) at 27.12 or 2450 MHz [117, Fig. 5]	67
Fig 4.20. Meat properties for the measurements [118]	68
Fig 4.21. Dielectric properties measurements by Farag et al. [118, Fig. 2]	68
Fig 4.22. Temperature dependence of the dielectric constant (left) and the dielectric loss factor (right) of chicken breast meat [119, Fig. 6]	69
Fig 4.23. Dielectric constant comparison @ 2,450 MHz.	73
Fig 4.24. Dielectric loss factor comparison @ 2,450 MHz.	74
Fig 4.25. Dielectric constant comparison @ 915 MHz.	74
Fig 4.26. Dielectric loss factor comparison @ 915 MHz.	75
Fig 4.27. Interpolation functions for the dielectric properties' definition in the model.	76
Fig 4.28. Water variables in Comsol Multiphysics.	77
Fig 4.29. Density variables in Comsol Multiphysics.	78
Fig 4.30. Thermal conductivity variables in Comsol Multiphysics.	78
Fig 4.31. Specific heat capacity variables in Comsol Multiphysics.	78
Fig 4.32. Whirlpool MD 121 geometries in Comsol.	80

Fig 4.33. Multiphysics modelling of lean beef tempering after 40 seconds of heating.....	80
Fig 4.34. Commercial microwave oven (left) and frozen meat sample inside (right).....	81
Fig 4.35. Temperature measurement setup at RISE’s labs.....	81
Fig 4.36. Sample 1 - small radius.....	82
Fig 4.37. Sample 2 - small radius.....	83
Fig 4.38. Sample 3 – big radius.....	83
Fig 4.39. Sample 4 - big radius.....	84
Fig 5.1. Double stub tuning. (a) Original circuit with the load an arbitrary distance from the first stub. (b) Equivalent circuit with the load displaced to the first stub [20, Fig. 5.7]	88
Fig 5.2. Schematic of the double slug impedance matching network.....	89
Fig 5.3. Schematic of a conventional CPW structure.....	91
Fig 5.4. Electromagnetic field distribution for even (a) and odd (b) modes.....	92
Fig 5.5. Coplanar waveguide schematic with lateral and bottom plates.....	93
Fig 5.6. Front view of the CPW. Design parameters.....	93
Fig 5.7. S11 parameter for a complete obstacle’s position sweep combination.....	94
Fig 5.8. Exploded view of the assembly in CAD.....	95
Fig 5.9. Manufactured impedance matching system prototype.....	95
Fig 5.10. Zero-thickness Centered Stripline.....	96
Fig 5.11. Centered Stripline.....	96
Fig 5.12. Off-centered stripline.....	96
Fig 5.13. Shielded stripline.....	96
Fig 5.14. New stripline structure proposed (front view)	97
<i>Fig 5.15. Thermal profile of material MBT01 when heated using 3.6kW microwave oven.....</i>	<i>97</i>
Fig 5.16. 2D Asymmetric stripline structure.....	98
Fig 5.17. Characteristic impedance of the design.....	98
Fig 5.18. The final aspect of the spiral strip (top view).....	99
Fig 5.19. Each one of the components is manufactured and prepared to be assembled.....	99
Fig 5.20. The final aspect of the device after the assembly. It has been connectorized with an N connector and painted with a non-reflective material.....	100
Fig 5.21. ERL for whole-body exposure in unrestricted environments [134].....	101
Fig 5.22. ERL for whole-body exposure in restricted environments [134].....	102
Fig 5.23. ERL for local exposure in unrestricted environments [134].....	102
Fig 5.24. ERL for local exposure in restricted environments [134].....	103

Fig 5.25. Lateral view of the access with 8 rows of metallic posts.....	104
Fig 5.26. Power outflow with 500 W as input power in two antennas.....	104
Fig 5.27. Power outflow with 1000 W as input power in two antennas.....	105
Fig 5.28. Frontal view of the access in the modelling software.....	106
Fig 5.29. Electric field for the TE ₁₀ mode with metallic posts only.....	107
Fig 5.30. Electric field for the TE ₀₁ mode with metallic posts only.....	108
Fig 5.31. Electric field for the TE ₂₀ mode with metallic posts only.....	109
Fig 5.32. Electric field for the TE ₁₁ mode with metallic posts only.....	110
Fig 5.33. Electric field for the TM ₁₁ mode with metallic posts only.....	110
Fig 5.34. Electric field for the TE ₂₁ mode with metallic posts only.....	111
Fig 5.35. Electric field for the TM ₂₁ mode with metallic posts only.....	112
Fig 5.36. Electric field for the TE ₃₀ mode with metallic posts only.....	113
Fig 5.37. Front view of the access modelled with MBT01 as an absorbent material attached to the lateral walls.....	113
Fig 5.38. Electric field for the TE ₁₀ mode with metallic posts and MBT01 slabs.....	114
Fig 5.39. Electric field for the TE ₀₁ mode with metallic posts and MBT01 slabs.....	115
Fig 5.40. Electric field for the TE ₂₀ mode with metallic posts and MBT01 slabs.....	116
Fig 5.41. Electric field for the TE ₁₁ mode with metallic posts and MBT01 slabs.....	117
Fig 5.42. Electric field for the TM ₁₁ mode with metallic posts and MBT01 slabs.....	118
Fig 5.43. Electric field for the TE ₂₁ mode with metallic posts and MBT01 slabs.....	118
Fig 5.44. Electric field for the TM ₂₁ mode with metallic posts and MBT01 slabs.....	119
Fig 5.45. Electric field for the TE ₃₀ mode with metallic posts and MBT01 slabs.....	120
Fig 5.46. Electric field for the version v0 (a) compared to the version v2 (b). TE ₀₁ mode (XZ view).....	120
Fig 5.47. Electric field for the version v0 (a) compared to the version v2 (b). TE ₁₁ mode (Isometric view).....	121
Fig 5.48. Electric field for the version v0 (a) compared to the version v2 (b). TM ₁₁ mode (XY view).....	121
Fig 5.49. Electric field for the version v0 (a) compared to the version v2 (b). TE ₂₁ mode (XY view).....	121
Fig 5.50. Electric field for the version v0 (a) compared to the version v2 (b). TM ₂₁ mode (Isometric view).....	121
Fig 6.1. Solid-state microwave system architecture.....	126
Fig 6.2. Example of a 6-bit digital phase-shifter [138].	127

Fig 6.3. “Simple” two-way power splitter from Raditek Inc. [139].....	128
Fig 6.4. “Complex” 2-way waveguide power divider example [140].....	128
Fig 6.5. Microbiotech’s stripline 1:8 (left) and 1:16 (right) power dividers.	128
Fig 6.6. Example of a microstrip microwave power divider [141].	128
Fig 6.7. Example of the block diagram of a solid-state power amplifier at 2.45 GHz and 250 W of output power [137, Fig. 5].....	129
Fig 6.8. Basic dipole antenna schematic [145, Fig. 4.1].....	131
Fig 6.9. Monopole antenna and its equivalent dipole [145, Fig. 4.16].....	131
Fig 6.10. Moving cylinder example.	132
Fig 6.11. Antenna measurement. Interior view (left) and exterior view, with the VNA (right).	133
Fig 6.12. Six manufactured antennas.	134
Fig 6.13. Manufactured antennas with the 7/16" connector separately.....	134
Fig 6.14. The slot antenna and its typical feeding structure [144, Fig. 4.67].....	135
Fig 6.15. HFSS model of the slot antenna fed by the stripline.....	136
Fig 6.16. Effect on the return losses for different slot lengths (L)	137
Fig 6.17. Effect on the return losses for different slot widths (W).....	137
Fig 6.18. Modelling of the slot antenna fed by the stripline.....	137
Fig 6.19. S11 parameter effect for different distances to upper and lower walls.....	138
Fig 6.20. S11 parameter effect for different distances to the right wall.....	138
Fig 6.21. Top cut view of the antenna assembly with the widths and lengths of each component.	139
Fig 6.22. Lateral cut view of the antenna assembly with the heights and diameters of the components.....	139
Fig 6.23. Antenna modelled feeding a box with commercial microwave oven dimensions and loaded with 2 litres of fresh water.	140
Fig 6.24. Lower part of the antenna assembly.....	141
Fig 6.25. Top and bottom view of the manufactured antenna.....	141
Fig 6.26. SIW antenna measured in an anechoic chamber.....	142
Fig 6.27. Antenna measured total electric field.....	142
Fig 6.28. 2-litre recipients and the antenna placed in the cavity.	142
Fig 6.29. Comparison of the return losses (S11(dB)) between the model and the manufactured antenna, measured in an anechoic chamber.....	143

Fig 6.30. Comparison between the S11 parameters of the measurement with the antenna feeding a commercial microwave oven and the model.	143
Fig 6.31. Patch antenna lateral cut [153, Fig. 14.3 (b)].....	144
Fig 6.32. Circular patch antenna schematic [153, Fig. 1.5 (b)].....	144
Fig 6.33. Rectangular patch antenna schematic [153, Fig. 1.5 (a)].....	145
Fig 6.34. Design variables in CST for the patch antennas [160, Fig. 7]	146
Fig 6.35. Example of a three-band U-shot microstrip/patch antenna [153, Fig. 14.55].....	148
Fig 6.36. Side view of a patch array backed by circular cavities [153, Fig. 14.41 (b)].....	149
Fig 6.37. Starting point of the 2-frequencies patch antenna modelled in HFSS.	149
Fig 6.38. Two-frequencies antenna top view with its design parameters.....	150
Fig 6.39. Final model of the 2-frequencies patch antenna.....	151
Fig 6.40. Effect of the B parameter (affecting the patch size) over the return losses at (a) 915 MHz and (b) 2,450 MHz.	151
Fig 6.41. Effect of the slot length, L, over the return losses at 2.45 GHz.	152
Fig 6.42. Effect of the vertical part of the slot, L2, over the return losses at 2.45 GHz.....	152
Fig 6.43. Effect of the slot length, L, over the return losses at 915 MHz.	152
Fig 6.44. Effect of the vertical part of the slot, L2, over the return losses at 915 MHz.	152
Fig 6.45. Effect of the Sx parameter over the S11 return losses, with Sy = 20 mm, at 2.45 GHz.	152
Fig 6.46. Effect of the Sy parameter over the return losses, with Sx = 2 mm, at 2.45 GHz.	152
Fig 6.47. Top (a) and bottom (b) views of the multi-frequency manufactured antenna.	154
Fig 6.48. Measurement results of the multi-frequency antenna in free-space.....	154
Fig 6.49. Dimetric view of the HFSS design of the PIFA antenna at 433 MHz.	155
Fig 6.50. Front a) and lateral b) views of the PIFA antenna modelled in HFSS with its design parameters.....	155
Fig 6.51. Example of the (a) L1 and (b) D parameters effect.....	156
Fig 6.52. Pictures of the PIFA antenna installed in a modified commercial microwave oven.	157
Fig 6.53. Results of the PIFA antenna at 433 MHz.....	157
Fig 6.54. Comparison between the number of possible modes and the dimension factor [165, Fig. 5.2].....	158
Fig 6.55. Power density distribution of the TE324 mode in a rectangular cavity at 2452.12 MHz [165, Fig. 5.1]	158
Fig 6.56. Lossy load effect over the resonant modes in a cavity [165, Fig. 5.6].....	158
Fig 7.1. Developed SSMGS for microwave-assisted chemical processes at 2,450 MHz.	161

Fig 7.2. Coaxial probe feed schematic [153, Fig. 14.4 (b)].....	162
Fig 7.3. Return losses of the antenna depending on the feeding point in the axes (best option).	163
Fig 7.4. Inverted dimetric view of the antenna modelled with a loaded cavity.....	163
Fig 7.5. Antenna installed in a modified microwave oven (right) and measured its RL (left)..	164
Fig 7.6. Return Losses measurement (S11) of the patch antenna. Marker M2 define the best matching frequency.	164
Fig 7.7. Complete system at 2,450 MHz and 250W solid-state microwave source controlled by a PC.	164
Fig 7.8. Monopole antenna with an N-connector designed at 2,450 MHz.....	165
Fig 7.9. Block diagram for the 2.45GHz multi-source solid-state driven system with 1kW of total output power.	167
Fig 7.10. PHASESHIFTER Evaluation Kit @ 2.45 GHz.	167
Fig 7.11. Manufactured monopole antenna and its size.	168
Fig 7.12. Antenna different location configuration.	168
Fig 7.13. Antenna array installed in metallic sheet.	169
Fig 7.14. Shielding gaskets on top of the cavity.....	169
Fig 7.15. Complete system during the set-up process.	170
Fig 7.16. Coaxial 90° transitions and cable connections to the generator.	170
Fig 7.17. Antenna nomenclature and its position in the panel.	170
Fig 7.18. Control software screenshot at maximum power where can be seen the Antenna 3 malfunctioning.....	173
Fig 7.19. Modelling of a recipient with 40 mm (left) and 100 mm (right) diameters.	174
Fig 7.20. Top and front view of the modelling at 50 mm (a,b) and 110 mm (c,d) position.....	175
Fig 7.21. Three-layer recipient for microwave-assisted calcination.	177
Fig 7.22. Multiphysics modelling in Comsol of the calcination structure in a multi-source solid- state driven microwave oven.	177
Fig 7.23. Detail of the heat pattern in the porcelain recipient after 55 seconds.	178
Fig 7.24. Radiation pattern captured with an infrared camera after 55 seconds.	178
Fig 7.25. 40 mm (left) and 100 mm (right) diameters for the functionalisation.	178
Fig 8.1. Developed conveyor oven for almond drying with the SSMGS at 915 MHz.....	181
Fig 8.2. (a) A_p and (b) A_d parameters effect.	183
Fig 8.3. Effect of Pos_x (left) and Pos_y (right) once the patch dimensions are defined.	183
Fig 8.4. Parametric study of the feeding point: diagonal movement.....	183

Fig 8.5. Matching adjustment with the corner's radio curvature.	184
Fig 8.6. Return losses of the modelled antenna.	185
Fig 8.7. Teflon squared patch antenna at 915 MHz, measured in free space (left) and inside a cavity (right).	185
Fig 8.8. Return losses for the mathematical approximation and the later improvements.	186
Fig 8.9. Comparison of the RL between the antenna modelled for a loaded cavity and free-space	187
Fig 8.10. Manufactured patch antenna at 915 MHz and PEEK substrate.	187
Fig 8.11. Example of the actions performed to verify the proper adhesive distribution.	188
Fig 8.12. Five out of six manufactured antennas and the solid-state microwave module at 915 MHz.	188
Fig 8.13. Free space measurement with VNA (left) and power tests (right).	189
Fig 8.14. Block diagram for the 915 MHz multi-source solid-state driven system with 2kW of total output power.	190
Fig 8.15. Example of an almond sample reception register file.	191
Fig 8.16. Dielectric properties measurement of an almond sample.	192
Fig 8.17. Real (left) and imaginary (right) parts of the dielectric permittivity for different humidity percentages and temperatures.	193
Fig 8.18. Microwave heating system at 915 MHz.	194
Fig 8.19. Microwave heating system at 2,450 MHz.	194
Fig 8.20. Almond sample configurations with diameters of 40 mm (left) and 80 mm (right) placed inside the multi-mode metallic cavity.	195
Fig 8.21. Hotspot effect on the almond sample at 2,450 MHz.	195
Fig 8.22. Electric field pattern modelled for the test's cavity.	196
Fig 8.23. New configuration to avoid hotspots (left) and drying results at 915 MHz (right). ..	196
Fig 8.24. The effect over the almond surface of the phase-shifting in one of the antennas from 0 to 360 grades at 915 MHz.	197
Fig 8.25. The effect over the almond surface of the phase-shifting in the right antenna from 0 to 360 grades.	198
Fig 8.26. The effect over the almond surface of the phase-shifting in the bottom antenna from 0 to 360 grades.	199
Fig 8.27. The effect over the almond surface of the phase-shifting (0-180°) in the first and third columns of antennas.	199
Fig 8.28. The effect over the almond surface of the phase-shifting (0-180°) in the second column of antennas.	200

Fig 8.29. The effect over the almond surface of the phase-shifting (0-180°) in the second row of antennas.	200
Fig 8.30. Frontal isometric view of Leanfa's PhaseShifter Kit.....	201
Fig 8.31. Rear panel view of the PhaseShifter Kit with the connections labelled.....	201
Fig 8.32. Modbus ethernet converter external installation.	202
Fig 8.33. General screenshot of LeanOn control software with the different control buttons labelled.	202
Fig 8.34. Drawings of the metallic enclosure ordered to DelValle. Luxor model.	204
Fig 8.35. Frequency-dependent shielding behaviour of the selected honeycomb [173].	205
Fig 8.36. Drawing of the metallic sheet, compatible with the top oven aperture, with the four antennas configuration.....	205
Fig 8.37. EMC viewing window and gasket dimensions drawing (left) and the 3D model (right).	206
Fig 8.38. Drawing of the window location in the oven door.....	206
Fig 8.39. Front view of the static oven with the fan on the right and the fan controller at the bottom.....	207
Fig 8.40. Isometric view of the static oven in the testbench with the computer for the control.	207
Fig 8.41. Schematic of the rolling bar with electromagnetic shielding elements.....	208
Fig 8.42. Shielding periodic structure installed in the transport oven.....	208
Fig 8.43. Internal view of the transport oven with the almond load and the patch Peek antennas installed on top.	209
Fig 8.44. Rectangular grid structure that will work as a feed hopper and a shielding element.	209
Fig 8.45. External view of the transport oven with the accesses.....	210
Fig 8.46. Initial load distribution (left) and detail of the elements used to adjust the height of the belt (right).	211
Fig 8.47. Almond distribution with regular compartments for 40 mm (left) and 80 mm (right) thickness.	211
Fig 8.48. Sample weight measurement.....	211
Fig 8.49. Meshed baskets distribution of the load.....	212
Fig 8.50. Single antenna configuration. Top view (left) and inside view (right).	213
Fig 8.51. Two antennas configuration: vertical alignment (left) and diagonal alignment (right)	213
Fig 8.52. Two antennas configuration: horizontal alignment.....	214

Fig 8.53. Example of the maximum and minimum temperature spots after the phase-shifting (φ) with two antennas separated horizontally.....	214
Fig 8.54. Four antennas configuration.....	215
Fig 8.55. Thermal images of different parts of the load show homogeneity with four sources and 80 mm of thickness.....	216
Fig 8.56. Frontal view of the definitive continuous oven with the four sources SSMGS.....	217
Fig 8.57. Detail of the extensor for the conveyor belt (left) and of the reduced free aperture (right).	217
Fig 8.58. Conveyor belt with modular lateral supports to confine the load.....	218
Fig 8.59. Top view of the definitive transport oven.....	218
Fig 9.1. High-quality EMC shielding door from MVG.....	227
Fig 9.2. Input and outputs of the control system.....	230
Fig 9.3. Diagram block of the improved SSMGS.....	231

List of Tables

Table 2.1. Maxwell's equations and the continuity equation in differential and integral forms for time-varying fields.....	10
Table 2.2. Electromagnetic classification of nonmagnetic materials in function of their dielectric properties.	17
Table 2.3. Vacuum tubes Microwave Power Sources [21].	20
Table 2.4. Early Industrial Microwave Food Applications [31].....	26
Table 2.5. A partial list of patents on solid-state microwave heating since 1971 [35].....	27
Table 4.1. Thermal property models for food components ($-40 \leq T \leq 150^{\circ}\text{C}$)	59
Table 4.2. Beef dielectric properties summary of the studied papers.....	70
Table 4.3. Chicken dielectric properties summary of the studied papers.....	71
Table 4.4. Lamb dielectric properties summary of the studied papers.....	71
Table 4.5. Pork dielectric properties summary of the studied papers.....	72
Table 4.6. Turkey dielectric properties summary of the studied papers.....	72
Table 5.1. Spiral strip dimensions.	99
Table 5.2. Mode appearance in the designed waveguide and their cut-off frequencies.....	106
Table 5.3. Study results for the first mode (TE_{10}) with metallic posts only.....	107
Table 5.4. Study results for the second mode (TE_{01}) with metallic posts only	107
Table 5.5. Study results for the third mode (TE_{20}) with metallic posts only.....	108
Table 5.6. Study results for the fourth mode (TE_{11}) with metallic posts only.....	109
Table 5.7. Study results for the fifth mode (TM_{11}) with metallic posts only.	110
Table 5.8. Study results for the sixth mode (TE_{21}) with metallic posts only.....	111
Table 5.9. Study results for the seventh mode (TM_{21}) with metallic posts only.	111
Table 5.10. Study results for the eighth mode (TE_{30}) with metallic posts only.	112
Table 5.11. Study results for the first mode (TE_{10}) with metallic posts and MBT01 slabs attached to the lateral walls.....	114
Table 5.12. Study results for the second mode (TE_{01}) with metallic posts and MBT01 slabs attached to the lateral walls.	115

Table 5.13. Study results for the third mode (TE_{20}) with metallic posts and MBT01 slabs attached to the lateral walls.....	115
Table 5.14. Study results for the fourth mode (TE_{11}) with metallic posts and MBT01 slabs attached to the lateral walls.....	116
Table 5.15. Study results for the fifth mode (TM_{11}) with metallic posts and MBT01 slabs attached to the lateral walls.....	117
Table 5.16. Study results for the sixth mode (TE_{21}) with metallic posts and MBT01 slabs attached to the lateral walls.....	118
Table 5.17. Study results for the seventh mode (TM_{21}) with metallic posts and MBT01 slabs attached to the lateral walls.	119
Table 5.18. Study results for the eighth mode (TE_{30}) with metallic posts and MBT01 slabs attached to the lateral walls.	119
Table 6.1. Tunable antennas dimensions.....	133
Table 6.2. Final antenna design parameters.	140
Table 6.3. Power and temperature measurements of the 2-litre test.....	143
Table 6.4. Final results of the PEEK patch antennas [160].....	146
Table 6.5. First design parametric studies summary.	150
Table 6.6. Final multi-frequency antenna design parameters.....	153
Table 6.7. Marker's values from Fig 6.48 in order of appearance. Squared markers point to the objective frequencies.	153
Table 6.8. PIFA final dimensions.....	156
Table 7.1. Antenna array S-parameters.	169
Table 7.2. Antenna 1 calibration measurements.....	171
Table 7.3. Antenna 2 calibration measurements.....	171
Table 7.4. Antenna 3 calibration measurements.....	171
Table 7.5. Antenna 4 calibration measurements.....	171
Table 7.6. Antenna 1 + Antenna 2 power tests.....	172
Table 7.7. Antenna 1 + Antenna 4 power tests.....	172
Table 7.8. Antenna 2 + Antenna 4 power tests.....	172
Table 7.9. Power test with the four modules activated.....	173
Table 7.10. Multi-layer calcination recipients' dimensions.	176
Table 7.11. Time improvement results on chemical processes.	179
Table 8.1. Free-space PEEK antenna measurements.	189
Table 8.2. Power tests for the antenna 1.....	189

Table 8.3. Dielectric properties of chopped almonds depending on humidity and temperature.	192
Table 9.1. Designed antennas summary.	224
Table 9.2. Example of the possible input combinations of a 2-frequencies microwave system.	228

Abbreviations and Acronyms

AESA	Active Electronically Scanned Array
AM	Amplitude Modulation
ANOVA	Analysis of Variance
DIN	Deutsches Institut für Normung
ESA	Electronically Scanned Array
FWD	Forward
d.c.	Direct Current (Zero frequency)
IMPI	International Microwave Power Institute
IoT	Internet of Things
IP	Internet Protocol
ISM	Industrial, Scientific and Medical
JPEG	Joint Photographic Experts Group
LNA	Low-Noise Amplifier
Mc	Moisture content
MMIC	Monolithic Microwave Integrated Circuits
MW	Microwaves
OS	Operative System
PCB	Printed Circuit Board
PESA	Passive Electronically Scanned Array
PLL	Phase-Locked Loop
Prof.	Professor

PTFE	Polytetrafluoroethylene
PWM	Pulse-Width Modulation
PWR	Power
RADAR	Radio Detection and Ranging
RAM	Random Access Memory
RF	Radiofrequency
RFL	Reflected
RGSEAA	Registro Sanitario de Empresas Alimentarias y Alimentos
RL	Return Losses
Rx	Reception
S2MH	Solid-State Microwave Heating
SME	Small and Medium Enterprises
SSMGS	Solid-State Microwave Generation System
Sync	Synchronised
TE	Transversal Electric
TM	Transversal Magnetic
T/R	Transmitter / Receiver
TRL	Technology Readiness Level
Tx	Transmission
USB	Universal Serial Bus
VCO	Voltage-Controlled Oscillator
Wc	Water Content

Part I

Introduction

Chapter 1. General Information of the Thesis.

1.1. Context

Microwave energy has been proved useful, efficient and effective in heating applications, both industrial and domestic [1]. Historically, microwave heating systems have been magnetron-based, providing high amount of electromagnetic power with continuous electric efficiency improvement. Although transistors technology has been widely used in electronic industry since the decade of 1970, it has currently reached enough maturity to accomplish heating jobs with prices still higher but reasonable, and efficiency similar to the magnetron technology.

This PhD dissertation relates the work on the design and development of microwave heating systems based on the so-called “Solid-State Microwave Heating”, S2MH. These systems offer generous improvements over the magnetron-based ones. The “Solid-State Microwave Generation System”, SSMGS, is the core of this system. SSMGSs provide coherent microwave generation distributed among different outputs. Frequency, phase, and power can be configured, in real-time, at each output. Moreover, the lifespan is longer, the feeding voltages are notably lower, rigidity and compactness have no competitor, and, finally, they can be easily integrated with other electronic circuitry, broadly used by the Internet of Things (IoT).

Dielectric heating, communications and radio detection are the most important applications using frequencies in the radiofrequency (RF) and microwave (MW) bands. The S2MH system proposed in this document integrates one of the key features used in the Radio Detection and Ranging (RADAR).

Since their invention, RADAR systems have steadily improved, and new MMIC (Monolithic Microwave Integrated Circuits) have introduced features and mechanisms that allow multiple operation modes. A very interesting component of new-generation radars, called electronically scanned antennas, is described in the following paragraphs extracted from [2].

“Electronically scanned antennas have been a major development of radar systems in the last 15 or more years. The simplest and most common, the passive electronically scanned array (PESA), is a planar array antenna in which a computer-controlled phase shifter is inserted in the feed system immediately behind each element. By individually controlling the phase shifters, the beam formed

by the array can be steered anywhere within a fairly wide field of regard. These antennas are often known as phased arrays.

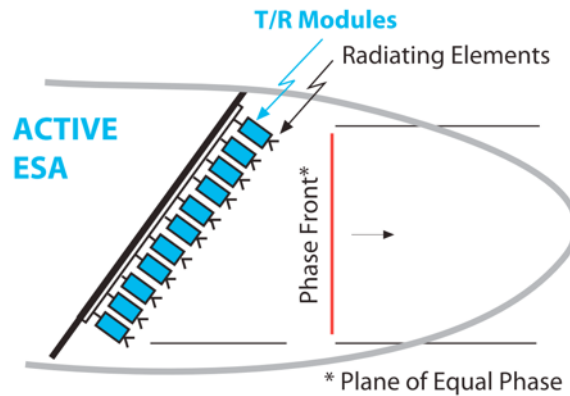


Fig 1.1. Schematic of the active electronically scanned array (AESA) [2, Fig. 2.25]

A more versatile, but considerably more expensive, implementation is the active electronically scanned array (AESA). It differs from the passive ESA in that it has a tiny solid-state transmitter/receiver (T/R) module inserted behind each radiating element (Fig 1.1). To steer the beam, provisions are included in each module for controlling both the phase and the amplitude of the signals the module transmits and receives. The transmitter and receiver components are assembled in one single T/R module. This module integrates the electronic phase shifter, the solid-state power amplifier, the LNA, circulators, and a duplexer.”

The philosophy of the AESA system can be extrapolated and used in the development of new microwave heating systems, though some precautions need to be taken.

The electric-field intensity, $E(\phi)$, produced by the radiation emitted from an antenna is a function of the amplitude and the phase of the current distribution across the antenna body. $E(\phi)$ is the aggregate of the different current contributions in the antenna area, which has been divided into three regions for mathematical approximation purposes.

The region in the immediate neighbourhood of the antenna is the near-field. It extends several antenna diameters from it and, for this reason, is usually of little importance in radar technology. Following the near-field is the Fresnel region. In this region, rays from the radiating antenna to the target are not parallel, and the antenna radiation pattern is not constant with distance. For RADAR engineers, these two regions have no application, and sometimes they call them the *reactive near-field region* and the *radiating near-field region*, respectively [3].

The farthest region from the antenna is called the far-field region. The radiating source and the target are at a sufficiently large distance from each other so that the rays originating from the antenna may be considered parallel to one another at the target. Radar antennas, and the system mentioned above, operate in the far-field region (also called Fraunhofer).

The operation region is the principal difference between the RADAR application and the solid-state-based microwave heating system. Resonant cavities like microwave ovens block the far-field wave generation.

RADAR systems base their functioning on the information provided by the transmission and reception of electromagnetic pulses. The same antenna is responsible for the wave emission and reception (see Fig 1.2).

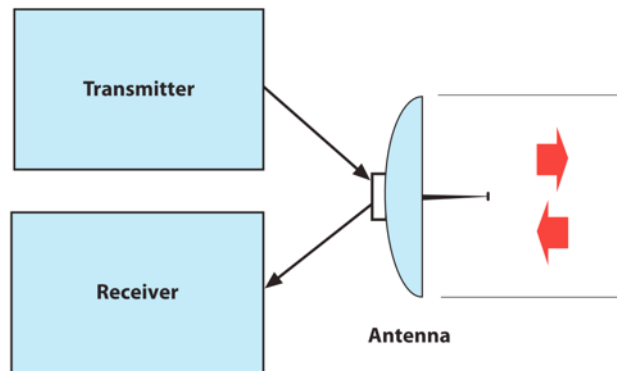


Fig 1.2. Antenna double function for transmission and reception [2, Fig. 1.4]

The proposed system consists of multiple independent, though synchronised, solid-state microwave power generators feeding a resonant cavity through high-power antennas. The information provided by the transmitted and reflected power figures and thermal imaging help decide the phase and amplitude change needed in each source or module. Like a radar system, whose purpose is to find targets, this microwave heating system optimises the power delivery to the load in real-time. Fig 1.3 shows the S2MH system complete diagram with the mentioned RADAR elements. The SSMGS corresponds to the blue blocks in Fig 1.3.

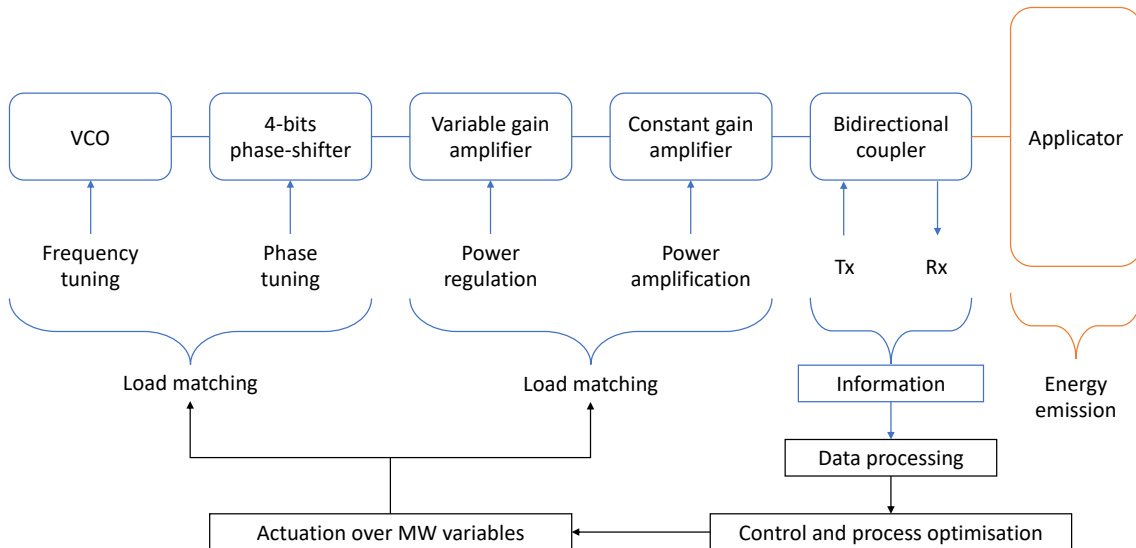


Fig 1.3. SSMGS block-diagram.

1.2. Framework

The first decade of the century’s research has been devoted to find high-performance processes with lower energetic consumption in order to reduce costs, whereas quality aspects were put in a

second place. However, nowadays research have emphasized the need of guaranteeing the quality of the commercialised food products. From a purely technological point of view, the different irreversible damages that an aliment experiences during its transformation can be reduced by choosing the adequate technique and process conditions. For instance, to achieve the maximum quality out of a dehydrated product, it is necessary optimise the drying operations. If we can also reduce the process timings, the energy cost and, furthermore, minimise the waste and disposals, a relevant processing line can be set into the market. A market that is working hard on being sustainable.

The work of this PhD dissertation has been developed in the context of a technological transfer project between Microbiotech S.L., an SME from Vilamarxant (Valencia, Spain) and the Polytechnic University of Valencia (UPV). The thesis project has been funded by the Generalitat Valenciana, through the “Subvencion para la formación de doctores en empresas valencianas (FDEGENT)”, providing the doctoral candidate with the Industrial PhD mention.

The Valencia region has characterised because of an important development in the agricultural economical sector. The vast number of important companies, as well as small ones, have made this region one of the most important Spanish regions in the food sector. It is the case of Jose Borrell S.A., a manufacturer of almond production machinery. This company has collaborated in the manufacture of one of the solutions developed in this PhD thesis: a solid-state based microwave drying system that improves the final quality of the provided by the state-of-the-art systems.

Food industry seems the perfect area to use these types of microwaves systems. However, microwave-assisted processes have also been used in other fields. Applications with high-end added value are very eligible to introduce the S2MH systems due to the advantages it delivers. Chemical processes fit this condition because they need a highly accurate control over the heating process. The design and validation of new chemical processes, or the improvement of currently ones, is the main work of the Redolí Group at the University of Valencia (UV). The other designed and manufactured solid-state based system of this thesis has been devoted to this aim.

The PhD work has also been developed at an international centre, the Research Institutes of Sweden (RISE). The research stay in Gothenburg, Sweden, for four months during the third year of the thesis, also enables the candidate to apply for the International PhD mention.

1.3. Objectives

The primary purpose of this PhD thesis is to design, manufacture and validate the performance of the S2MH systems. These aim to apply RADAR technology advances and specific antenna design to foster the fully exploitation of the solid-state technology advantages against the magnetron. The most important one is the capacity to change digitally and in real time the electromagnetic field distribution, which can be done through multi-illumination and power, frequency and phase control. This thesis aims to demonstrate that the S2MH systems allow the design of enhanced microwave heating processes, i.e., higher efficiency, temperature homogeneity and improved control.

The specific objectives to reach the defined goal are:

- Identify the technology/components needed to benefit from using S2MH over magnetron (e.g., phase shifters, optimum antenna designs, power amplifiers, etc.)
- Identify two applications that can demonstrate these benefits.
- Design the identified required components.
- Develop adequate simulation models for the design of these components.
- Determine, and if needed, design and manufacture the complimentary devices necessary for the best performance of the technology (e.g., dielectric properties measurement systems, microwave filters, etc.)
- Design and manufacture a microwave oven per application using the designed technologies/devices.
- Validate the performance and its potential over the EM field distribution.
- Verify the improvements against the magnetron-based systems.

1.4. Organisation of the Thesis

This thesis has been organized in four parts, ten chapters and one annex.

The first part, *Introduction*, is composed of two chapters, 1 and 2, that set the basis for the entire thesis. **Chapter 1** describes the general information of the thesis, whereas **Chapter 2** provides a complete review of the microwave heating systems and those based on solid-state technology. In this chapter the theoretical basis are also presented.

The second part, *Materials and Methods*, is composed of three chapters: 3, 4 and 5. **Chapter 3** defines the design methodology of the SSMGS, which is similar to the one used to design other microwave heating systems. This chapter also describes all the equipment and software tools used in the design process. **Chapter 4** comprises a foodstuff dielectric properties' review and their use in a multiphysics modelling, the main design tool for the thesis results. Finally, in **Chapter 5** auxiliar equipment developed within the PhD work is presented.

The third part of the document, *Results*, is divided in three more chapters: 6, 7 and 8. **Chapter 6** contains the general description of the proposed SSMGS and the different components' design is explained in detail. **Chapter 7** comprises the design and manufacture of a microwave oven with the SSMGS for microwave-assisted chemical processes. This work has been developed in the 2,450 MHz frequency band. **Chapter 8**, analogously to the chapter seven, is devoted to the conveyORIZED oven with the SSMGS for the almond drying industry. It includes all the components' design, development and validation.

The fourth part, *Conclusions*, collects all the work carried out. It is divided in two chapters and the annexes. **Chapter 9** summarizes the different achievements and novelties of the thesis and presents the faced challenges. It also includes the description of the future work. Finally, **Chapter 10** provides the final conclusions. In Chapter 4, an exhaustive foodstuff dielectric properties search is conducted. The data retrieved is arranged in a comprehensive format in **Annex A**.

Chapter 2. Microwave-based heating processes.

Microwaves are electromagnetic waves operating in the spectrum frequency band between 300 MHz and 300 GHz (Fig 2.1). James Clerk Maxwell foretold its existence and the rest of the electromagnetic waves in 1864 [4]. He proved that electricity, magnetism, and even light resulted from the same electromagnetic field. In 1888, Heinrich Rudolf Hertz was able to generate and detect for the first time radiofrequency electromagnetic waves, confirming Maxwell's theory.

This second chapter aims to give a complete and thorough view of the most important aspects of the electromagnetic field theory and its relation to microwave heating technology. First, some theoretical information on the mathematical aspects of this theory is exposed. This introduction shows the reader how these physical concepts are related to materials, mainly foodstuff.

The second section of the chapter reviews microwave technology and the main heating applications. Finally, the upcoming technological revolution with the emergence of the solid state is presented. The advantages of this technology are shown, thus justifying why it was chosen for this PhD dissertation.

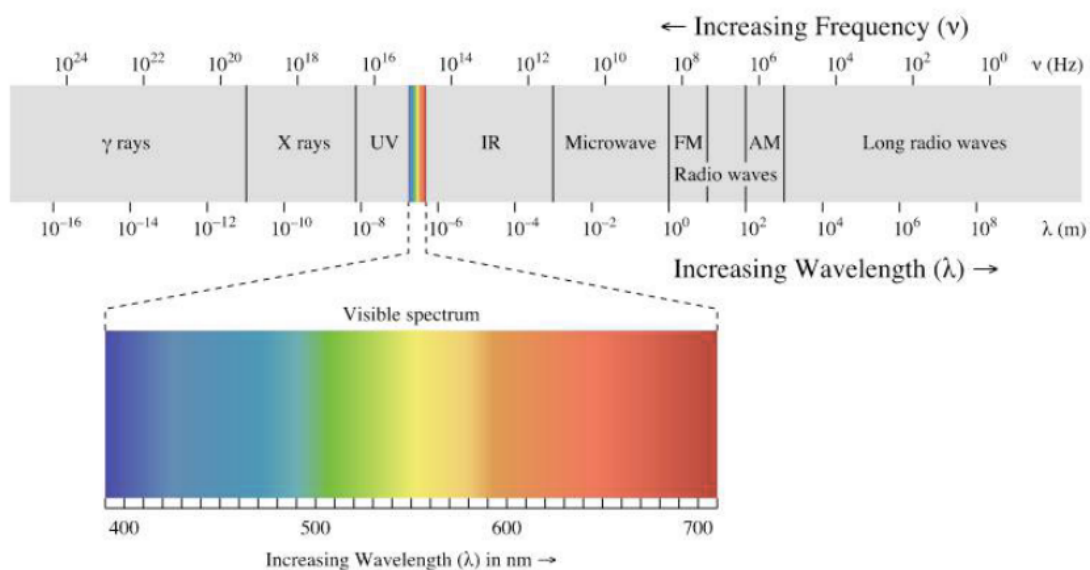


Fig 2.1. Radioelectric spectrum classification depending on the frequency - wavelength.

2.1. Background information. Theoretical basis.

Electromagnetic field theory is a discipline dealing with the study of charges, either at rest or in motion, that produce currents and electric-magnetic fields [5]. These electric and magnetic fields are defined by the well-known Maxwell's equations, which are laws of the physics. They can be written either in differential or integral form, as shown in Table 2.1.

Table 2.1. Maxwell's equations and the continuity equation in differential and integral forms for time-varying fields.

Differential form	Integral form
$\nabla \times \boldsymbol{\mathcal{E}} = -\boldsymbol{\mathcal{M}}_i - \frac{\partial \boldsymbol{\mathcal{B}}}{\partial t}$	$\oint_C \boldsymbol{\mathcal{E}} \cdot d\boldsymbol{l} = - \iint_S \boldsymbol{\mathcal{M}}_i \cdot d\boldsymbol{s} - \frac{\partial}{\partial t} \iint_S \boldsymbol{\mathcal{B}} \cdot d\boldsymbol{s}$
$\nabla \times \boldsymbol{\mathcal{H}} = \boldsymbol{\mathcal{J}}_i + \boldsymbol{\mathcal{G}}_c + \frac{\partial \boldsymbol{\mathcal{D}}}{\partial t}$	$\oint_C \boldsymbol{\mathcal{H}} \cdot d\boldsymbol{l} = \iint_S \boldsymbol{\mathcal{J}}_i \cdot d\boldsymbol{s} + \iint_S \boldsymbol{\mathcal{J}}_c \cdot d\boldsymbol{s} + \frac{\partial}{\partial t} \iint_S \boldsymbol{\mathcal{D}} \cdot d\boldsymbol{s}$
$\nabla \cdot \boldsymbol{\mathcal{D}} = q_{ev}$	$\oiint_S \boldsymbol{\mathcal{D}} \cdot d\boldsymbol{s} = Q_e$
$\nabla \cdot \boldsymbol{\mathcal{B}} = q_{mv}$	$\oiint_S \boldsymbol{\mathcal{B}} \cdot d\boldsymbol{s} = Q_m$
$\nabla \cdot \boldsymbol{\mathcal{J}}_{ic} = -\frac{\partial q_{ev}}{\partial t}$	$\oiint_S \boldsymbol{\mathcal{J}}_{ic} \cdot d\boldsymbol{s} = -\frac{\partial}{\partial t} \iiint_V q_{ev} dv = -\frac{\partial Q_e}{\partial t}$

The so-called constitutive parameters are used to characterise the macroscopic electrical and magnetic properties of linear media. In isotropic media, these parameters are represented by time varying functions, namely permittivity (ε), permeability (μ) and conductivity (σ). The physical magnitudes in the equations above are related among them by means of the constitutive parameters, which are, in general, functions of the position within the medium, and the frequency of operation. These parameters are obtained through the following relations in the *time domain*, where $*$ stands for the convolution operator.

- The electric flux density, $\boldsymbol{\mathcal{D}}$, and the electric field intensity, $\boldsymbol{\mathcal{E}}$, are related by the time-varying permittivity of the medium (Farads/meter), ε .

$$\boldsymbol{\mathcal{D}} = \varepsilon * \boldsymbol{\mathcal{E}} \quad (2.1)$$

- The magnetic flux density, $\boldsymbol{\mathcal{B}}$, and the magnetic field intensity, $\boldsymbol{\mathcal{H}}$, are related by the time-varying permeability of the medium (Henries/meter), μ .

$$\boldsymbol{\mathcal{B}} = \mu * \boldsymbol{\mathcal{H}} \quad (2.2)$$

- The conduction current density, $\boldsymbol{\mathcal{J}}_c$, and the electric field intensity, $\boldsymbol{\mathcal{E}}$, are related by the time-varying conductivity of the medium (Siemens/meter), σ .

$$\mathbf{J}_c = \sigma * \mathbf{E} \quad (2.3)$$

Assuming an $e^{j\omega t}$ time dependence, it is possible to replace the time derivatives in Table 2.1 with $j\omega$. Maxwell's equations in phasor form then become

$$\nabla \times \mathbf{E} = -j\omega \mathbf{B} - \mathbf{M} \quad (2.4)$$

$$\nabla \times \mathbf{H} = j\omega \mathbf{D} + \mathbf{J} \quad (2.5)$$

$$\nabla \cdot \mathbf{D} = \rho \quad (2.6)$$

$$\nabla \cdot \mathbf{B} = 0 \quad (2.7)$$

Equations (2.1)-(2.3) can also be related in phasor form

$$\mathbf{D} = \varepsilon_0 \mathbf{E} + \mathbf{P}_e = \boldsymbol{\varepsilon} \mathbf{E} \quad (2.8)$$

$$\mathbf{B} = \mu_0 (\mathbf{H} + \mathbf{P}_m) = \boldsymbol{\mu} \mathbf{H} \quad (2.9)$$

$$\mathbf{J} = \sigma \mathbf{E} \quad (2.10)$$

Applying (2.8) and (2.9) to the Maxwell's equations these can be rewritten as

$$\nabla \times \mathbf{E} = -j\omega \boldsymbol{\mu} \mathbf{H} - \mathbf{M} \quad (2.11)$$

$$\nabla \times \mathbf{H} = j\omega \boldsymbol{\varepsilon} \mathbf{E} + \mathbf{J} \quad (2.12)$$

$$\nabla \cdot \mathbf{D} = \rho \quad (2.13)$$

$$\nabla \cdot \mathbf{B} = 0 \quad (2.14)$$

2.1.1. Complex dielectric permittivity.

The most used dielectric property is the material permittivity, which describes how the electromagnetic waves propagated across it, how much are the waves reflected on the surface, and how much energy absorption occurs when the wave passes through it [6]. From a macroscopic point of view, the dielectric properties (permittivity) determine the electromagnetic energy interaction with the materials.

The dielectric materials have the ability to store electric charge like a capacitor. This ability is called polarisation. This phenomenon happens due to the positive and negative charge displacements from their balance points, caused by the applied electric field and constrained by the atomic and molecular forces [7] (see Fig 2.2).

The origin of heating with high-frequency electromagnetic waves lies in the ability of the electric field to polarise the charges in the material and the inability of this polarisation to follow extremely rapid reversals of the electric field [8].

There are four polarisation mechanisms: ionic, orientation, atomic and electronic. Their main characteristics are explained by C. A. Balanis in [5, pp. 42–43] as follows:

1. *Dipole or Orientation Polarisation:* This polarisation is evident in materials that, in the absence of an applied field and due to their structure, possess permanent dipole moments that are randomly oriented. The dipoles tend to align with the fields. Such materials are known as polar materials, and water is an excellent example of them.
2. *Ionic or Molecular Polarisation:* This polarisation is evident in materials, such as sodium chloride (NaCl), that possess positive and negative ions and tend to displace themselves when an electric field is applied.
3. *Electronic Polarisation:* This polarisation occurs in atoms, where electrons can be displaced with respect to the nucleus. This polarisation occurs in all substances.
4. *Atomic Polarisation:* The atoms can be moved in crystals or molecules in this last polarisation. Together with atomic polarisation, electronic polarisation gives most dry solids a permittivity of the order of $\epsilon' < 10$. When only these two mechanisms are present, the material is almost lossless at microwave frequencies. Atomic, or vibration, polarization is closely related to electronic polarisation but, because of the much greater mass to be moved, the resonant frequencies of atomic polarisation are lower [9].



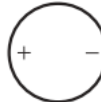

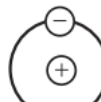

Mechanism	No applied field	Applied field
Dipole or orientational polarization		
Ionic or molecular polarization		
Electronic polarization		

Fig 2.2. Mechanisms producing electric polarisation in dielectrics [5, Fig. 2.4].

In Fig 2.3, a more detailed schematic representation of the Maxwell – Wagner and orientation polarisation due to an alternating electric field is provided. These two mechanisms, along with d.c. conductivity, are the basis of high-frequency heating [8].

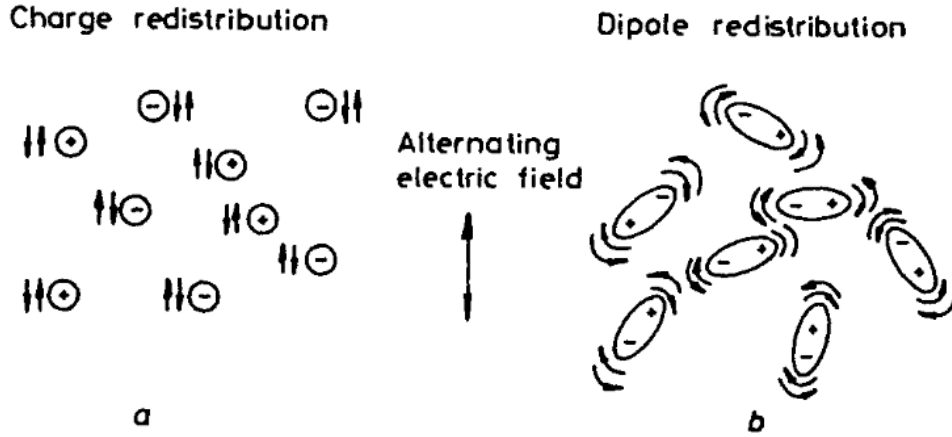


Fig 2.3. Interfacial (space charge) (a), and reorientation (b) polarizations [8, Fig. 2.1].

In real dielectrics, to account for the losses, the permittivity attains a complex form given by

$$\varepsilon = \varepsilon' - j\varepsilon'' = \varepsilon'(1 - \tan\delta) = \varepsilon_0(1 + \chi_e) \quad (2.15)$$

where the real part, ε' , is the material permittivity, or dielectric constant, and the imaginary part, ε'' , is the loss factor, and χ_e is the electric susceptibility. A thorough demonstration of the complex nature of the permittivity can be found, for instance, in [8, pp. 8–9].

When retrieving dielectric properties information from bibliography and databases, sometimes it is given in complex form (real and imaginary parts), and others as relative permittivity and loss tangent.

The real part of the dielectric permittivity (ε') measures the capacity of the material to store electrical energy, whereas the imaginary part (ε'') measures the electrical energy dissipation in the material that is turned into thermal energy (this is the reason why it is also called dielectric loss factor).

It is essential to underline that these two parameters are mainly dependent on frequency and temperature. This behaviour is due to the fact that, for many materials, the time constants for the establishment and decay of the polarisation occur at times comparable to the periods of oscillation of the high-frequency signal [8]. Appreciating this fact through experiments with electrolytes (dipolar polarisation), the Dutch engineer and physicist Peter Debye came up with the well-known equation that defines the dielectric constant as a function of the frequency:

$$\varepsilon = \varepsilon' - j\varepsilon'' = \varepsilon_\infty + \frac{\varepsilon_s - \varepsilon_\infty}{1 + j\omega\tau} \quad (2.16)$$

In (2.16), ε_s and ε_∞ stand for the dielectric constants at d.c. and very high frequencies, respectively; whereas τ is the relaxation time of the system, which controls the build-up and decay of the polarisation shown in Fig 2.4 as the external field is applied or removed respectively. \mathbf{P}_2 and \mathbf{P}_1 are the dipolar and distortion polarization vectors, being \mathbf{P}_2 when the polarisation is out of phase with the applied electric field \mathbf{E} .

By separating the real and imaginary parts of the complex dielectric constant given by (2.16), the specific equations for each parameter can be obtained:

$$\varepsilon' = \varepsilon_{\infty} + \frac{\varepsilon_s - \varepsilon_{\infty}}{1 + \omega^2\tau^2} \quad (2.17)$$

$$\varepsilon'' = \frac{(\varepsilon_s - \varepsilon_{\infty})\omega\tau}{1 + \omega^2\tau^2} \quad (2.18)$$

Debye's interpretation of this relaxation time is given in terms of dipolar rotation against frictional forces in the medium. Using Stoke's theorem, Debye derived the following expression for the relaxation time of the spherical dipole:

$$\tau = \frac{4\pi r_q^3 n_v}{k_b T} \quad (2.19)$$

where n_v is the viscosity of the medium, r_q is the radius of the rotating dipole, and k_b is Boltzmann's constant. However, this approximation is not accurate enough for solid dielectrics, where viscosity is the dominant mechanism. Later studies, such as the one performed by Cole and Cole in 1941 [10], obtained more approximative equations for this relaxation time.

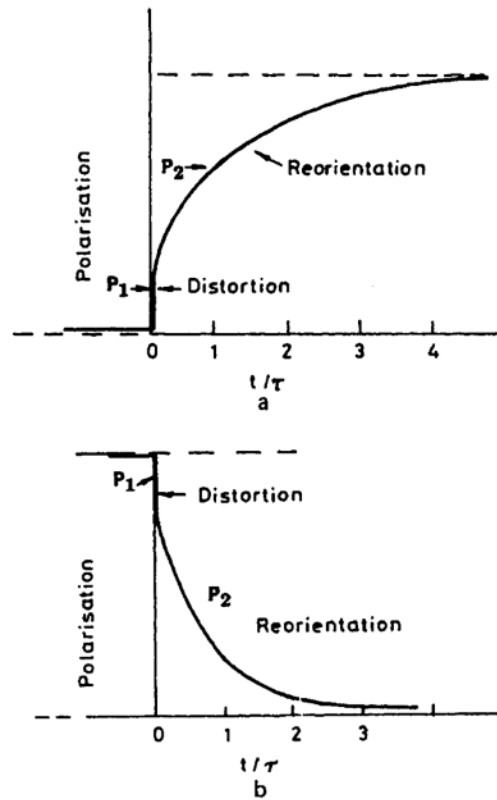


Fig 2.4. Build-up (a) and decay (b) of the polarization [8, Fig. 2.5].

2.1.2. Materials classification.

In general, materials are classified as dielectric, magnetic, or conductor, depending on whether polarisation (electric displacement current density), magnetisation (magnetic displacement current density), or conduction (conduction current density) is the prevailing phenomenon.

Another class of material comprises semiconductors, which bridge the gap between dielectrics and conductors where neither displacement nor conduction currents, in general, prevail.

When classifying materials according to their macroscopic parameters, it should be noted that the terms insulator, semiconductor, conductor, and magnetic material are used to indicate the dominant responses of different materials. All materials have some response to magnetic fields, but their response is usually minimal, except for ferromagnetic and ferrimagnetic types, and their permeability values do not significantly differ from μ_0 . Most ferromagnetic materials are highly conductive, but we call them magnetic materials, as their magnetic properties are the most significant in their applications. For superconductors, the Meissner effect shows that they are excellent magnetic materials, but in microwave electronics, people are more interested in their surface impedance [11, p. 11].

Materials of these kinds of characterisation appear in this thesis dissertation. For instance:

- The metallic compounds are defined as conductors. They have very high conductivity, usually in the range of 10^4 to 10^8 (Ωm)⁻¹. There are two types of notable conductors: perfect conductors and superconductors. A perfect conductor is a theoretical model with infinite conductivity at any frequency, e.g., silver (Fig 2.5). Superconductors have exceptional electromagnetic properties when they are under the threshold temperature, known as the critical temperature, e.g., aluminium (Fig 2.6). For d.c. electric fields, their conductivity is virtually infinite; but for high-frequency electromagnetic fields, they have complex conductivities.



Fig 2.5. Silver (Ag): example of conductor [12]



Fig 2.6. Aluminium (Al): example of superconductor [13]

- The different substrates used in electronic PCBs, as well as the air, are defined as dielectric components. Also named insulators, they have very low conductivity, usually in the range of 10^{-12} to $10^{-20} (\Omega\text{m})^{-1}$. Often, we assume insulators are nonmagnetic, so that is why they are actually dielectrics. In theoretical analysis of dielectric materials, an ideal model, perfect dielectric, is often used, representing a material whose permittivity's imaginary part is assumed to be zero: $\epsilon'' = 0$. For microwave components, two commonly used dielectrics are Teflon[®] (see Fig 2.7) and Duroid[®] (see Fig 2.8)



Fig 2.7. Teflon[®] (PTFE): example of a dielectric [14]



Fig 2.8. RT/Duroid 6202: example of a dielectric used for electronic and microwave circuitry [15]

- The semiconductor materials appear within the solid-state technology explanation. Their conductivity is higher than that of a dielectric but lower than that of a conductor. Usually, the conductivities of semiconductors at room temperature are in the range of 10^{-7} to $10^4 (\Omega\text{m})^{-1}$. The most common solid-state transistors are made of silicon, Si (Fig 2.9) and gallium, Ga (Fig 2.10).



Fig 2.9. Silicon: example of semiconductor [16]

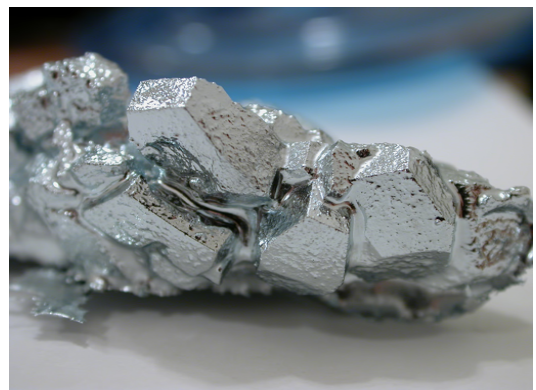


Fig 2.10. Gallium: example of semiconductor [17]

From the electromagnetic point of view, another parameter can be used to make this classification. Instead of using the electric conductivity, the real and imaginary part of the complex dielectric constant can be used. In

Table 2.2 can be seen a comprehensive summary of this classification.

Table 2.2. Electromagnetic classification of nonmagnetic materials in function of their dielectric properties.

Classification		ϵ'	$\tan\delta$	Behaviour
Conductors		∞	-	Reflects or conducts microwaves through its surface. (Example: metallic materials)
Dielectrics	Transparent	1 – 3	< 0.001	Microwaves have no noticeable effect on the material and the same thing other way around. (Example: air or Teflon)
	Absorbent	-	> 0.1	The microwave energy transmitted into the material is absorbed and transformed into heat (thermal energy). Depending on the ϵ' the transmission is different. (Example: water, foodstuff...)
	Isolators	> 20	< 0.001	It is not a conductor, but the high permittivity value makes it behave as a mirror. (Example: resins)

2.1.3. Microwaves and power.

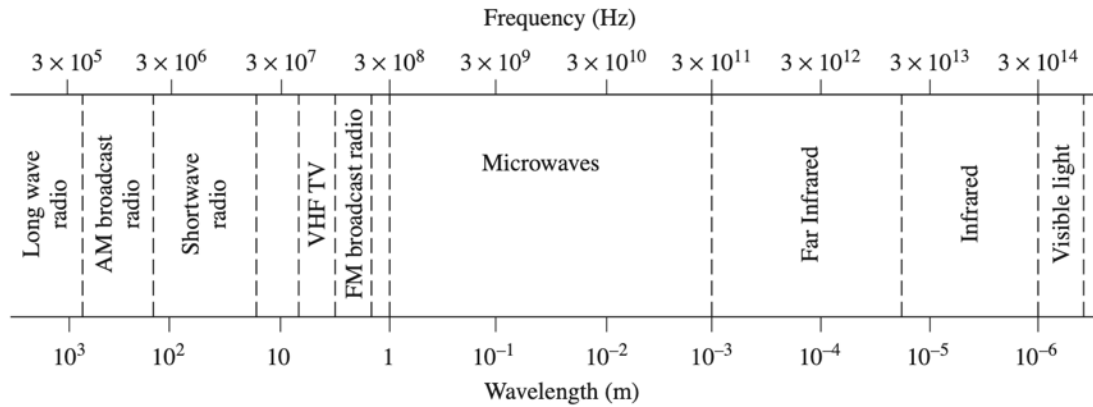
In wireless communication systems, electromagnetic fields are used to transport information over long distances. To accomplish this, information must be associated with electromagnetic fields. This transport of energy is accomplished, as stated by Maxwell, even in the absence of any intervening medium.

The power supplied to the system will follow the *conservation of power law* (2.20). This law states that within a volume V , bounded by a closed surface S , the supplied power \mathcal{P}_s [W] equals to the power \mathcal{P}_e [W] exiting S plus the power \mathcal{P}_d [W] dissipated within that volume plus the rate of change (increase if positive) of the electric (\mathcal{W}_e [J]) and magnetic (\mathcal{W}_m [J]) energies stored within that volume.

$$\mathcal{P}_s = \mathcal{P}_e + \mathcal{P}_d + \frac{\partial}{\partial t}(\mathcal{W}_e + \mathcal{W}_m) \quad (2.20)$$

In 1895, seven decades after the invention of the telephone, the first radio transmission was demonstrated by Marconi [18]. From that moment on, the electromagnetic fields were used to transmit information through different technologies, mainly communication antennas. The evolution of these communication techniques has been inserted in the history books, from the first phone call to the R.A.D.A.R (radio detection and ranging), a crucial technology for the result of

World War II. During the study of the R.A.D.A.R. application, the heat transfer from electromagnetic waves and foodstuff was discovered. The microwave heating applications were patented by Percy Spencer in 1950 [19].



Typical Frequencies		Approximate Band Designations	
AM broadcast band	535–1605 kHz	Medium frequency	300 kHz–3 MHz
Short wave radio band	3–30 MHz	High frequency (HF)	3 MHz–30 MHz
FM broadcast band	88–108 MHz	Very high frequency (VHF)	30 MHz–300 MHz
VHF TV (2–4)	54–72 MHz	Ultra high frequency (UHF)	300 MHz–3 GHz
VHF TV (5–6)	76–88 MHz	L band	1–2 GHz
UHF TV (7–13)	174–216 MHz	S band	2–4 GHz
UHF TV (14–83)	470–890 MHz	C band	4–8 GHz
US cellular telephone	824–849 MHz	X band	8–12 GHz
	869–894 MHz	Ku band	12–18 GHz
European GSM cellular	880–915 MHz	K band	18–26 GHz
	925–960 MHz	Ka band	26–40 GHz
GPS	1575.42 MHz	U band	40–60 GHz
	1227.60 MHz	V band	50–75 GHz
Microwave ovens	2.45 GHz	E band	60–90 GHz
US DBS	11.7–12.5 GHz	W band	75–110 GHz
US ISM bands	902–928 MHz	F band	90–140 GHz
	2.400–2.484 GHz		
	5.725–5.850 GHz		
US UWB radio	3.1–10.6 GHz		

Fig 2.11. The electromagnetic spectrum [20, Fig. 1.1].

When dielectric materials with relatively high dielectric loss factors are subjected to radiofrequency (RF) electric fields (both high-frequency and microwave frequencies, as shown in Fig 2.11) of sufficient intensity, they absorb energy by conversion of the electric field energy into heat energy within the materials. The phenomenon is known as RF dielectric heating, high-frequency dielectric heating, or microwave heating, depending on the frequencies employed. The degree of heating depends on the amount of absorbed power and on the characteristics of the material.

Two parameters that can be obtained from dielectric properties to understand how and how much heat will be generated on a material: the heat generation density and the penetration depth.

The amount of heat in watts per cubic meter (W/m^3) depends on the frequency, the loss factor (ϵ'') and the electric field strength, as given by (2.21):

$$Q_{gen} = 2\pi f \epsilon_0 \epsilon'' |\vec{E}_{rms}|^2 (W/m^3) \quad (2.21)$$

The penetration depth, d_p , indicates the distance, measured from the object surface inwards, with a 66% wave attenuation and, therefore, represents the effective heating area. This parameter depends on both the real and imaginary parts of the dielectric constant (ϵ' and ϵ''), the light speed (in m/s) and the frequency (in Hz):

$$d_p = \frac{c}{2\pi f \sqrt{2\epsilon' \left(\sqrt{1 + \left(\frac{\epsilon''}{\epsilon'}\right)^2} - 1 \right)}} \quad (m) \quad (2.22)$$

2.2. Heating and power applications using vacuum tubes.

For nearly 70 years, every microwave application was for communication or R.A.D.A.R. purposes. With the appearance of heating applications using electromagnetic waves, some frequency bands were reserved internationally for industrial, scientific, and medical (ISM) purposes. Among these frequency bands, three of them get special attention in heating applications because of their wavelength compared to the size of the objects to be heated. From larger wavelengths to shorter ones: 433 MHz, 915 MHz and 2.45 GHz. The domestic microwave oven is one of the most popular applications, although it is not the only one: industrial heating, sterilization, disinfection, drying, boiling, synthesis of materials, plasma generation, etc.

Research and development evolution in microwave energy applications had one of its most important milestones in 1940 when John Randall and Harry Boot (Fig 2.12) invented the high-frequency magnetron at Birmingham University, United Kingdom. This tube, which can generate high microwave powers while keeping its size small compared to similar devices, had a crucial contribution to the development of World War II.



Fig 2.12. Randall and Boot with the first magnetron.

Being the core of the R.A.D.A.R system, the magnetron provided the British army with a very important strategic advantage against the German invasion. It allowed them to detect smaller targets, and it was possible to board them in anti-submarine aircraft and small boats. That is how the magnetron was named “the valve that won the war”.

In 1945, Percy Spencer, an engineer from Raytheon Corporation, was conducting research on the efficient production of magnetrons and achieved a daily production increase from seventeen to two thousand nine hundred units per day. The widespread knowledge marks that moment as the first experience of microwave heating, when Spencer noticed how a candy bar had melted in his shirt pocket after having been one of his magnetrons operating. This resulted in the first patented foodstuff microwave heating device (Fig 2.13).

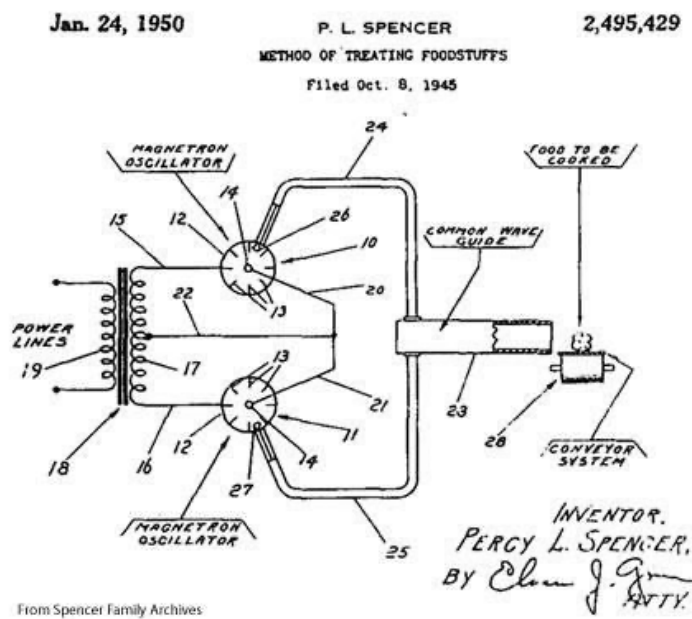


Fig 2.13. Magnetron drawing presented by Spencer for the patent request [19]

After the magnetron, other microwave power sources were developed to achieve even higher output powers. A comparison of the main features between the magnetron, klystron and gyrotron is provided in Table 2.3.

Table 2.3. Vacuum tubes Microwave Power Sources [21].

Attribute	Magnetron	Klystron	Gyrotron
Acquisition cost	\$0.01-\$0.1/W	Higher	Much higher
Efficiency	70-85%	30-60%	40%
Operating voltage	4-20 kV	20-50 kV	
Cooling	Air/water	Water	Cryogenic

<i>X-rays</i>		No	Maybe	Maybe
	2.45 GHz	1-30 kW	30-100 kW	
<i>CW power</i>	915 MHz	30-100 kW		
	10-30 GHz	Not practical		100 kW and up

2.2.1. The microwave oven.

Raytheon Corporation was a pioneer in developing and marketing early microwave ovens. The first Raytheon microwave oven was introduced to a select audience of food editors, home economists, restaurateurs, and airline operators in October 1946 in New York City [22]. This oven was huge, standing over 1.7 m tall, weighing around 340 kg, and costing about \$5000 (around \$61000 in 2019). While this oven was physically large, it just was able to heat sandwiches due to its small cavity dimensions. A production oven with a larger, more useful cavity, was introduced in early 1947, called the *RadarRange* (Fig 2.14). But it was still very large, measuring over 1.5 m tall, 0.6 m wide, and 0.6 m deep. The weight had been trimmed down to a mere 300 kg, and the cost pared down to the \$2000 range [23].



Fig 2.14. Comparison between the current commercial microwave ovens (left) and the first microwave oven developed by Raytheon (right) [24].

Later, in 1952, oven technology was licensed to Tappan, who introduced the first home microwave oven three years later. In those twenty years, the fierce competition between the electronic manufacturers pushed engineers to design smaller ovens with more power and features. Those manufacturers were General Electric (Boston, United States), Bruder Corporation (acquired by Litton Industries), Philips Company (Eindhoven, The Netherlands), Sharp Corporation (Osaka, Japan) and Panasonic Corporation (Osaka, Japan).

Even though GE (General Electric) produced a model operated at 915 MHz to address the problem of limited microwave penetration, the 2.45 GHz frequency band was predominant. These companies tried to improve these ovens throughout the years by combining them with different technologies. The turntable, for instance, was introduced by Sharp Corporation in its model R-600 in 1966. The first humidity sensor was invented in Sweden by P.O. Risman [25] and was initially used in Husqvarna (Stockholm, Sweden) ovens.

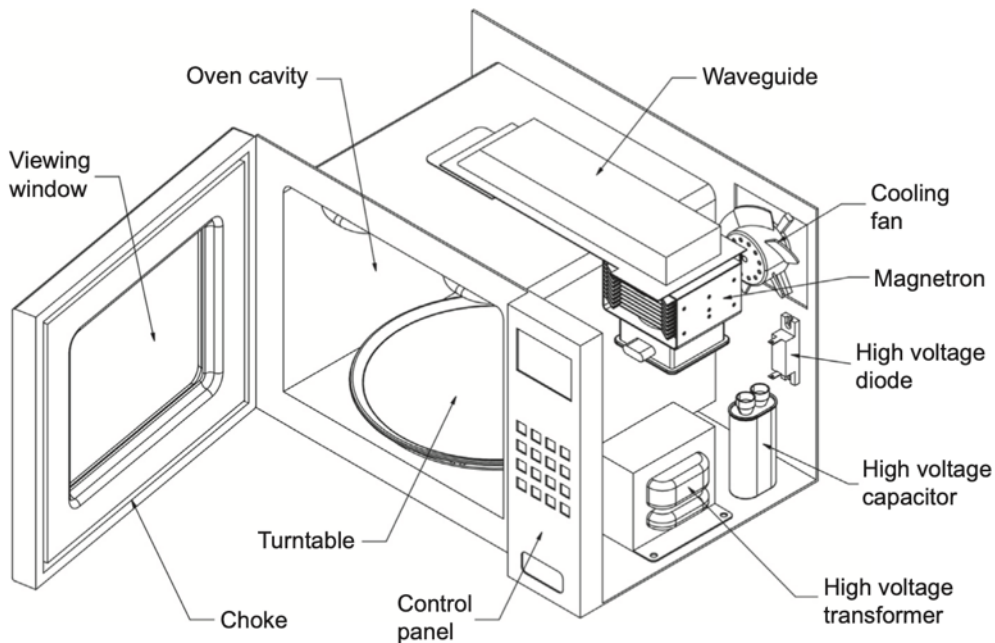


Fig 2.15. Components of a typical microwave oven [23, Fig. 4.2].

Microwave ovens became the killer application we know today by mid-1970s when they became to be a standard appliance in American kitchens, with sales of microwave ovens exceeding sales of gas ranges for the first time.

Fig 2.15 shows a good schematic of the actual microwave oven, with its main parts:

- **Viewing window.** A metallic microperforated sheet is used to prevent microwave leakage while allowing to have a partial view of the inside of the oven. To protect this metallic sheet a plastic cover is used. It keeps also the humidity level within the oven and helps have a clean device.
- **Oven cavity.** Microwaves are applied to the material to be heated in a multimode cavity whose dimensions have been thoroughly designed in order to have proper matching at the working frequency band, normally 2.45 GHz. In 1970, Harold S. Hauck wrote a paper

about the design considerations for microwave oven cavities, giving an approximate equation (2.23) for the resonant frequency wavelength and the different modes present [26].

$$\lambda = \frac{2}{\sqrt{\left(\frac{M}{W}\right)^2 + \left(\frac{N}{D}\right)^2 + \left(\frac{P}{H}\right)^2}} \quad (2.23)$$

Where λ is the wavelength of the resonant frequency; M , N , and P are the wavenumbers or half-waves of variation of E field in the W , D , and H directions, respectively; and W , D , and H are the width, depth and height of the cavity. Fig 2.16, shows an example of the TE_{232} mode in a cavity with the mentioned parameters.

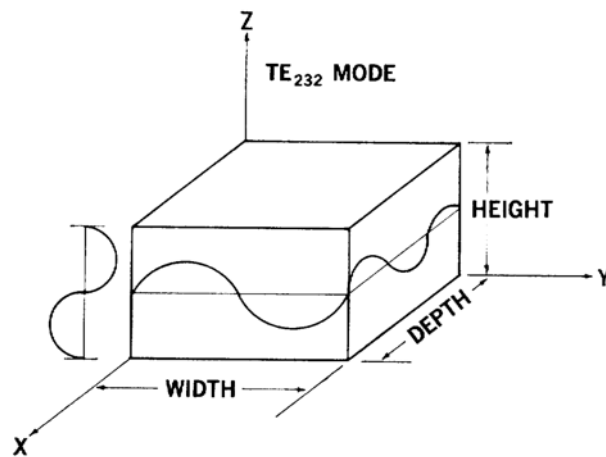


Fig 2.16. Microwave cavity with a schematic portrayal of E -field variation for the TE_{232} mode [26, Fig. 2].

- **Waveguide.** A non-standard waveguide, also called a launcher, is used to guide the microwaves from the magnetron to the oven. This device is designed to have return losses as low as possible. One of the oven design parameters is the location of the launcher on the cavity walls [27]. A power divider can be used to feed several launchers in order to achieve more homogenous field patterns within the cavity.
- **Magnetron.** It is the core of the microwave oven. A cylindrical cathode is at the axis, several millimeters from a hollow circular anode (see Fig 2.17). Inside the anode, there are a number of cavities designed to resonate at the desired frequency; in commercial ovens, this frequency is 2.45 GHz. A voltage of several kilovolts is applied between the electrodes and a magnetic field is applied parallel to the axis [28].

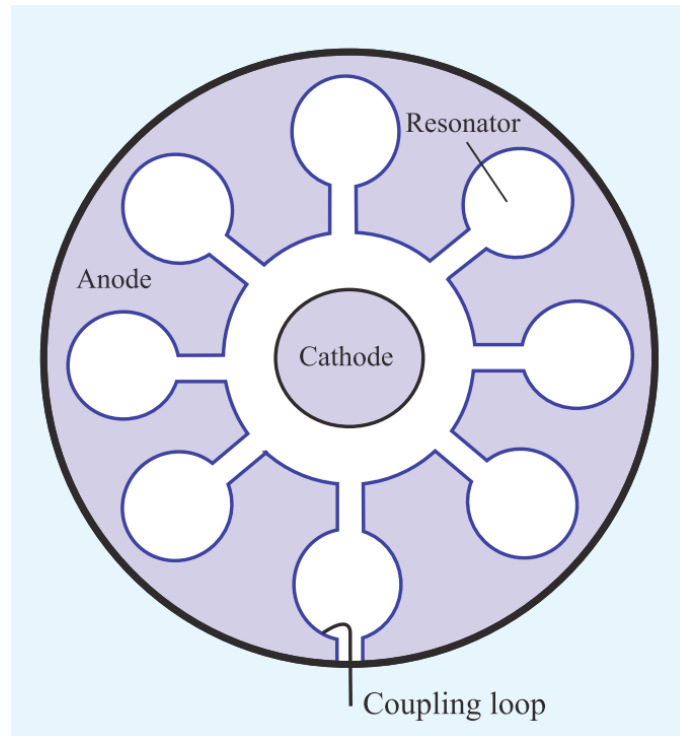


Fig 2.17. Schematic diagram of a magnetron [28, Fig. 2].

- **Cooling fan.** One critical aspect of magnetron-based heating systems is the considerable heating rate of this kind of vacuum tubes. Frequency instability caused by high-temperature values in the magnetron provokes it to malfunction, showing issues to perform in an efficient way. Cooling fans are extremely necessary to prevent overheating the magnetron. A good cooling rate will also improve the user comfort by noise reduction and energy consumption.
- **High voltage transformer.** It is necessary to produce the high voltage (about 2200 V) needed to operate. A transformer provides a low voltage (3.3 V) with high current potential to the filament inside the magnetron. This hot filament is also the cathode of the magnetron.
- **High voltage diode.** It converts alternating current (AC) to direct current (DC), which doubles the voltage and powers the magnetron. Without this diode, the magnetron would not receive enough voltage to operate [29].
- **High voltage capacitor.** It holds onto dangerous amounts of electricity even after the microwave has been unplugged [30]. This device, in conjunction with the diode, boost the voltage at the magnetron to almost 4000 V DC.
- **Control panel.** The user interface to manage the operative of the oven.
- **Turntable.** To obtain acceptable heating homogeneity, commercial and industrial ovens rely on relative motion between the food and the electromagnetic fields inside the oven.

The more economic ovens use the turntable, while more advanced appliances (typical in professional kitchens) use mode stirrers, some of which have very complex designs (see Fig 2.18).

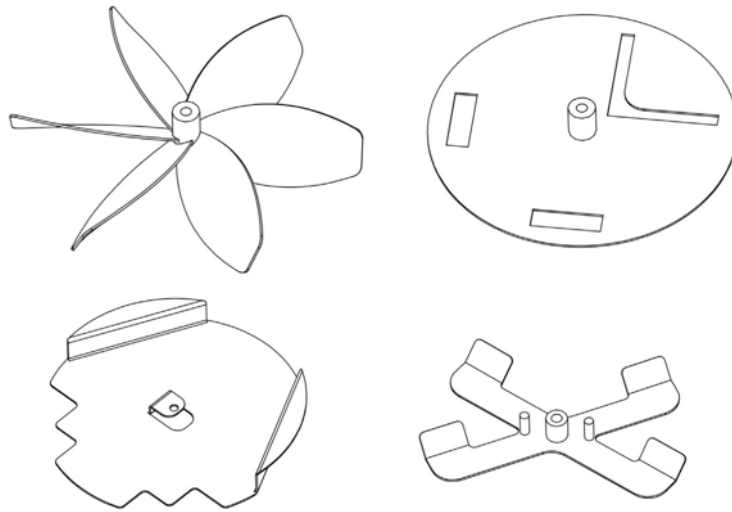


Fig 2.18. Various designs of mode stirrers [23, Fig. 4.5].

- **Choke.** There are two ways to seal in microwave energy with the door: contact and choke seal. Choke seals are widely used in domestic microwave ovens. They are designed as a quarter wave stub around the door perimeter.

2.2.2. Industrial applications.

Although GE had marketed a microwave oven operating at 915 MHz, a combination range model, in the late 60s and early 70s, its manufacture was halted in the mid-70s. Since then, the frequency of 2,450 MHz has become the worldwide frequency for all consumer and commercial microwave ovens. In the industrial area, however, the use of the 915 MHz frequency has become dominant, although some equipment operates at 2,450 MHz [21]. Some of the first industrial microwave food applications are listed in Table 2.4.

Raytheon acquired Amana Refrigeration, Inc. in the mid-1960s and built industrial microwave ovens not only for the food industry but also for the rubber and foundry. Others, like Microdry Corporation or Astex were centred on the food industry and microwave plasma technology, respectively.

Dielectric heating of agricultural materials through the application of high-frequency electric fields and electric fields associated with microwave energy has been also considered for other applications. These include drying products such as grain and seed, controlling stored-product insects, seed treatment to improve germination, improving the nutritional value of products, controlling product-borne plant and animal pathogens, and inactivating weed seed and plant-infecting organisms in soils [6].

Table 2.4. Early Industrial Microwave Food Applications [31].

<i>Application</i>	<i>Frequency (MHz)</i>	<i>RF Power</i>	<i>Manufacturer</i>
<i>Potato chips</i>	915	50 kW	Raytheon/Litton
<i>Pasta drying</i>	915	50 kW	Microdry
<i>Bacon cooking</i>	915	50 kW	Microdry/Raytheon
<i>Chicken cooking</i>	2,450	2.5 kW per module	Litton Industries
<i>Tempering</i>	915	25 kW	Raytheon
<i>Doughnut proofing</i>	2,450	30 kW	DCA Industries

The American microwave guru Bob Schiffmann wrote a book chapter in 2001 [1] that contributed to increasing the general knowledge of industrial microwave systems for food processing. In this chapter an exhaustive study and description of the different applications, including:

- Meat and poultry cooking.
- Bacon precooking.
- Tempering meat, poultry, fish, butter and fruit.
- Baking and proofing dough.
- Drying snacks and vegetables.
- Pasteurizing ready meals and pasta.

Other industrial applications are rubber vulcanisation [32] or soil disinfection [33].

Fig 2.19 shows the exploded view of an example of a conveyORIZED industrial microwave oven for food processing. These systems have several design requirements that differentiate them from the domestic ovens:

- The accesses for loading and unloading the oven (openings) are much larger than a wavelength, thus posing a design challenge to reduce the microwave leakage.
- The operating power is on the order of 10 to several hundred kW.
- They may be under severe ambient conditions such as extreme temperature, high humidity and water spray, among others.
- Modular construction often involves that the power generators, the cavity applicator, and the control system are separated.
- They require to ensure high reliability to work 24/7.

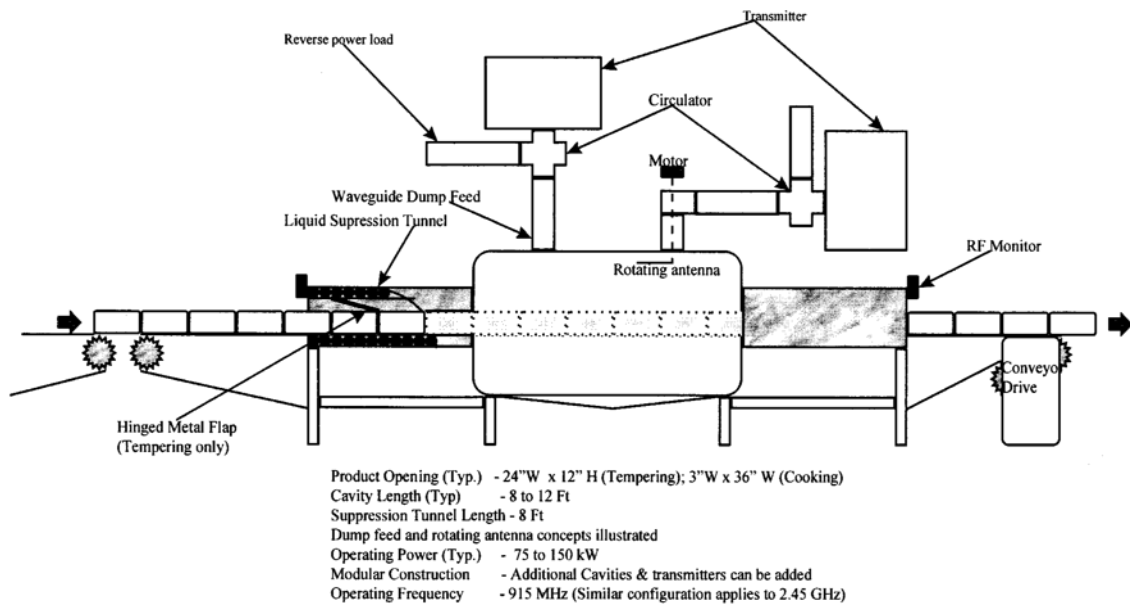


Fig 2.19. Exploded view of a typical conveyorized industrial microwave oven [31, Fig. 5].

2.3. Technology review. Solid-state outbreak.

The idea of using solid-state technology in microwave systems for cooking dates back to the 1970s', when several patents were presented. However, the innovation of the scientists and engineers was by far more advanced than the technology maturity. Radiofrequency (RF) power amplifiers are not the subject to Moore's famous extrapolation, which predicted the exponential growth in processing power of the last fifty years. Smaller transistors with lower operating voltage are particularly well suited for digital circuitry, but with high power amplifiers, high voltages are needed. A single high-power RF transistor can handle peak currents large enough to start a small car [34].

Communications and radar applications have driven transistor development. These two are high-value applications with high peak-to-average power ratios (pulses). In contrast, solid-state cooking is mainly based on continuous wave (CW), with a peak to average power ratio of 1. Moreover, it must be economically accessible with a similar price to the consumer ovens.

Table 2.5 lists some of the main inventions around solid-state microwave heating from 1971 to 2016. Inventors have been adding features to their patents such as heatsinks, dipole antennas, technology combinations, multiple sources, frequency change, etc.

Table 2.5. A partial list of patents on solid-state microwave heating since 1971 [35]

Year	Title	Inventor	Patent No
1971	Solid-state microwave oven	Bruce R. McAvoy	US 3557333

1972	Solid-state microwave heating apparatus	Kern K. Cheng	US 3691338
1975	Hybrid microwave heating apparatus	Tetsuro Ohtani	US 3867607
1977	Microwave heating apparatus with improved multiple couplers and solid-state power source	Rudolph A. Dehn	US 4006338
1978	Solid-state microwave oven power source	Samuel H. Bickel	US 4097708
1980	Controlled heating microwave ovens	Alejandro MacKay	US 4196332
1980	Controlled heating microwave ovens using different operating frequencies	Alejandro MacKay	CA 1081796
1983	Microwave oven having controllable frequency microwave power source	Tomotaka Nobue	US 4415789
1985	Microwave heating apparatus with solid-state microwave oscillating device	Hisashi Okatsuka	US 4504718
1995	Microwave oven, in particular for rapid heating to high temperature	Patrick Jackuault	US 5420401
1995	Solid-state microwave generating array material, each element of which is phase controllable, and plasma processing systems	Jerome J. Cuomo	EP 0459177
1996	Active RF cavity including a plurality of solid-state transistors	Bernard R. Cheo	US 5497050
1996	Microwave power radiator for heating applications	Derrick J. Page	US 5558800
2004	Microwave heating using distributed semiconductor sources	Peter Handinger	US 20040206755
2010	Microwave oven switching between predefined modes	Ulf E. Nordh	US 20100155392
2011	Microwave heating apparatus	Tomotaka Nobue	US 20110108548
2013	Microwave oven with antenna array	Ranjit Gharpurey	US 20130175262
2015	Microwave oven using solid-state amplifiers and antenna array	Jose A. Lima	US 20150136760
2016	Versatile microwave heating apparatus	Olle Niklasson	US 9332597

2.3.1. Transistor technology

Many active devices are currently available for use in RF power amplifiers (PA), and RF power transistors are available in packaged, die, and grown-to-order forms. Continuous research activities result in the development of a variety of RF solid-state devices, which can be roughly grouped into two main classes, i.e. the Bipolar-Junction Transistors (BJTs) or the Field Effect Transistors (FETs) [36], [37]. Among them, different and improved structures have been proposed, including Heterojunction Bipolar Transistors (HBTs) Metal Oxide Semiconductor Field Effect Transistors (MOSFETs), Laterally Diffused Metal Oxide Semiconductor FETs (LDMOSFET), Metal Semiconductor FETs (MESFETs) and High Electron Mobility Transistors (HEMTs), as schematically depicted in Fig 2.20 [38].

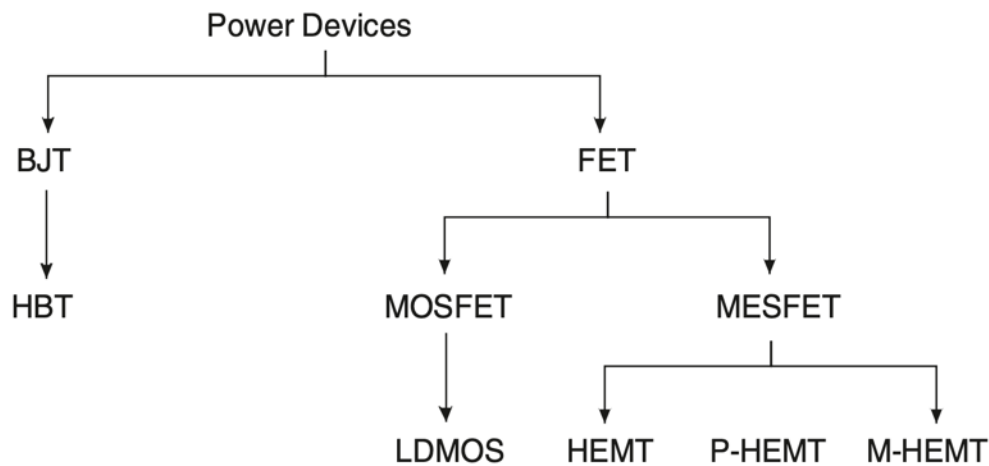


Fig 2.20. RF power device family tree [38, Fig. 1.26].

According to Raab et al., who conducted a study of the different types of technologies used for manufacturing transistors [39], their more interesting features are:

a. Bipolar Junction Transistor (BJT)

The Si BJT is the original solid-state RF power device dating back to the 1960s. Since the BJT is a vertical device, obtaining a high collector-breakdown voltage is relatively simple, and the power density is very high. Si BJTs typically operate from 28 V supplies and are still in use at frequencies up to 5 GHz, especially in high-power (1 kW) pulsed applications such as radar.

b. Metal-Oxide-Silicon Field-Effect Transistor (MOSFET)

MOSFETs are constructed with insulated gates. Topologies with either vertical or lateral current flows are used in RF applications, and most of them are produced by a double-diffusion process. Vertical RF power MOSFETs (VMOS) are useable through very high frequency (VHF) and ultra-high frequency (UHF). Gemini-packaged devices can deliver up to 1 kW at high frequency (HF) and 100s of watts at VHF. VMOS devices typically operate from 12, 28, or 50 V supplies, although some devices can operate from 100 V or more.

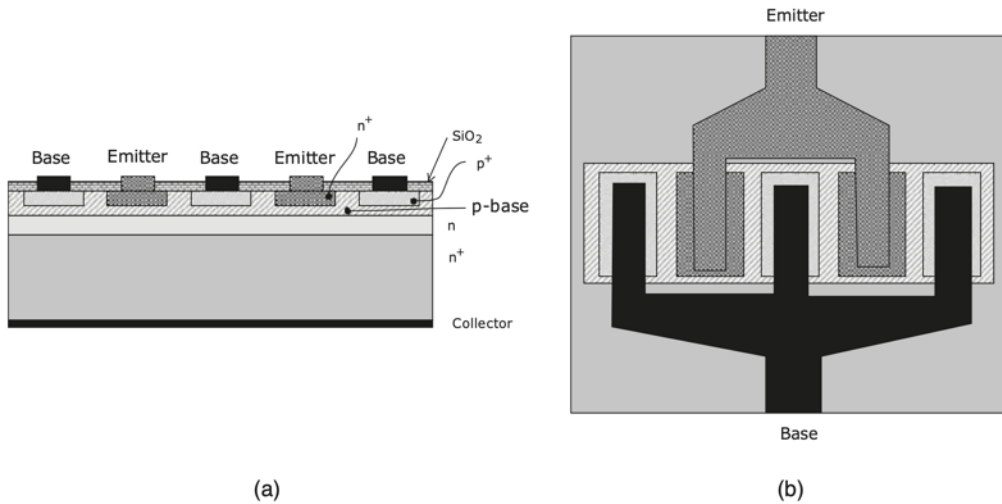


Fig 2.21. Schematic structure of a BJT (a) and its top view (b) [38, Fig. 1.28].

c. Laterally Diffused MOS (LDMOS)

LDMOS (Laterally Diffused Metal-Oxide-Silicon) transistors are especially useful at UHF and lower microwave frequencies. The direct grounding of its source eliminates bond-wire inductance that produces negative feedback and reduces gain at high frequencies. This also eliminates the need for the BeO insulating layer commonly used in other RF-power MOSFETs [39]. They are relatively low-cost compared to other devices for this frequency range and are currently the device of choice for use in high-power transmitters at 900 MHz and 2 GHz.

After some generations, LDMOS transistor technology has been optimised for current markets, leading to an LDMOS-law of around 3% efficiency improvement every 2-3 years. Like Moore's law, this will slow as physical limitations become apparent, but it has been broadly valid for a decade. This increase in efficiency and power delivery capability has made this technology a reality for microwave cooking systems.

Schwartz et al. presented in 2006 at the IMPI-40 a solid-state microwave heater. This laboratory heater stands as the first use of an LDMOS amplifier for microwave heating purposes known to this author.

d. GaAs Metal Semiconductor FET (GaAs MESFET)

GaAs MESFETs are JFETs based upon GaAs and a Schottky gate junction. They have higher mobility than Si devices do and are therefore capable of efficiently operating at higher frequencies. GaAs MESFETs are widely used to produce microwave power, with capabilities of up 200 W at 2 GHz and 40 W at 20 GHz in packaged devices.

e. Heterojunction FET (HFET) / High- Electron-Mobility Transistor (HEMT)

HFETs and HEMTs improve the MESFET geometry by separating the Schottky and channel functions. Added to the basic MESFET structure is a heterojunction consisting

of an n-doped AlGaAs Schottky layer, an undoped AlGaAs spacer, and an undoped GaAs channel.

This transistor is known in the literature by a wide variety of different names, including MODFET (Modulation-Doped FET), TEGFET (Two-dimensional Electron-Gas FET), and SDFET (Selectively Doped FET). It is also commonly called an HFET (Heterostructure FET).

GaAs HEMTs/HFETs with working frequency (f_T) as high as 158 GHz are reported. PAs based upon these HEMTs exhibit 15 W outputs at 12 GHz with a power-added efficiency (PAE) of 50 per cent. Outputs of 100 W are available at S-band from packaged devices.

f. Pseudomorphic HEMT

The pseudomorphic HEMT (pHEMT) further improves upon the basic HEMT by employing an InGaAs channel. The efficiency of PAs using pHEMTs does not begin to drop until about 45 GHz, and they can be used up to frequencies as high as 80 GHz. Power outputs vary from 40 W at the L band to 100 mW at the V band. While pHEMTs are generally grown to order, a packaged device, pHEMT, has recently become available.

g. InP HEMT

The InP HEMT has a higher gain and efficiency than the GaAs pHEMT, with the PA efficiency dropping at 60 GHz. However, it has a lower breakdown voltage (typically 7 V) and must therefore be operated from a relatively low drain-voltage supply (e.g., 2 V). This results in lower output per device and possible loss in the combiners required to achieve a specified output power.

InP HEMTs have been manufactured with maximum frequency (f_{max}) as high as 600 GHz, and amplification has been demonstrated at frequencies as high as 190 GHz. The efficiency does not begin to drop until about 60 GHz. Power levels range from 100 to 500 mW per chip.

h. Metamorphic HEMT (mHEMT)

The mHEMT allows channels with high-In content to be built on GaAs substrates. The higher electron mobility and higher peak saturation velocity result in higher gain than a pHEMT.

i. Heterojunction Bipolar Transistor (HBT)

HBTs are typically based on the compound-semiconductor material AlGaAs/GaAs. Currently, available AlGaAs/GaAs HBTs can produce several watts and are widely used in wireless handsets; GaAs HBTs are also widely used in MMIC circuits at frequencies up to X band and can operate in PAs at frequencies as high as 20 GHz.

j. SiC MESFET

The high thermal conductivity of the SiC substrate is beneficial in high-power applications. The higher operating voltage and associated higher load impedance considerably simplify output networks and power combining. SiC MESFETs typically operate from a 48 V supply. Devices with outputs of 10 W are currently available, and 60 W or more output powers have been demonstrated experimentally. The cost of SiC devices is about ten times that of Si LDMOS.

k. GaN HEMT

GaN offers the same high break-down voltage of SiC but even higher mobility. However, they have a lower thermal conductivity; hence, GaN devices must be built with substrates such as SiC or diamond.

Although LDMOS technology is the most commonly used for high power solid-state devices, the noticeable performance advantages of the steadily improving and growing GaN technology are the trigger to pursue low-cost, high-volume manufacturing. Companies like MACOM, AMPLEON, QORVO, INFINEON, NXP, and RFHIC presented in 2016 GaN transistors capable of handling 300 W at 2.45 GHz.

l. Monolithic Microwave Integrated Circuit (MMIC)

MMICs integrate RF power devices and matching/decoupling elements such as on-chip inductors, capacitors, resistors, and transmission lines. The proximity of these elements to the RF-power devices is essential for input, output, and inter-stage matching at microwave and millimetre-wave frequencies.

Building a solid-state microwave power amplifier consists of designing the best combination for the different types of transistors depending on the application, i.e., working frequency, continuous or pulsed wave, maximum power, etc.

Solid-state transistor manufacturers, such as Ampleon, arQana, NXP, Macom, Richardson Electronics, etc., can provide transistors mounted with the other components or sell an amplifier block called a pallet. This pallet comprises all the essential elements for a solid-state power source: oscillator, transistor, and gain amplifiers. A complete description of every part is provided in 6.3 section.

2.3.2. Solid-state power amplifiers market

The emergence of this new technology has shaken the microwave sector. Transistor companies have started to build solid-state microwave power modules in order to sell their products; new companies have entered the market offering modules and kits with lower prices than the traditional microwave device manufacturers, who have been seen themselves forced to adapt their

portfolios and include the solid-state power amplifiers along with their perfectly mastered magnetron generators and waveguide devices.

The possibility of buying a solid-state module or kit has helped small companies with low manufacturing and electronic assembly capacity develop their own microwave devices by combining the different functional blocks of a typical microwave system: source, antenna/applicator, and cavity. Microbiotech S.L. is one of these companies that have developed several systems for a wide variety of applications and sectors (RTC-2015-3421-5, RTC-2016-4946-3, IMINOE/2020/90).

Among the market, several companies offer more mature microwave solid-state modules. Most of the devices these manufacturers have extensively tested and are readily reliable are centred in 2.45 GHz and with output powers around 250 W. Devices operating at other frequencies such as 433 MHz, 915 MHz or 5.8 GHz are also available, and some of them offer up to 700 W for a single power amplifier and a single output. The majority of these devices, due to the lack of massive and redundant use in applications, are served under demand, which allows the customer to choose between several configurations. The options can be separated in:

- Maximum output power: 50, 100, 200, 250, 500, 700 W...
- Working frequency band: 433 MHz, 868 MHz, 915 MHz, 2.45 GHz, 5.8 GHz...
- Cooling system: liquid cooling or air cooling. For output powers over 500 W, it is strongly recommended to use liquid cooling, for it offers better performance.
- Control system: some devices can have a touchscreen to manage the configuration, others come with a proprietary computer software interface, or they can be sold without any user-friendly interface, and the customer can design and develop its control.
- Power source: in 2022, it is rare to find a solid-state microwave module without its power source, but in 2018, for instance, it was very common to have to buy the power source separately, mostly when purchasing in the Asiatic market.

The Italian manufacturer **Leanfa Srl**, based in Ruvo di Puglia (Bari, Italy), is one of those companies focused on solid-state technology. They have a complete range of microwave modules for industrial, scientific, and medical applications, from 10 W to 2,500 W at most ISM frequency bands.

It is interesting to point out what they call “Evaluation Kits” from all their products. These modules are “ready for a true plug-and-play experience” [40]. They support two configurations: 1) the Starter Evaluation Kit (Fig 2.22) is built around one generator, while the 2) Phaseshifter Evaluation Kit (Fig 2.23) is built around two or four generators, which are synchronised with an advanced synthesiser. This second one is a very interesting product that allows multiple heating combinations. They offer these kits in different powers and frequencies and are controlled by their *LeanOn* Control and Monitoring application for Windows OS.

Another interesting product of this company is the GENERATOR LAB KIT (Fig 2.24), specifically designed for experimental laboratory use. This hybrid device combines 200 W at 450 kHz and 200 W at 2.45 GHz and is equipped with a touch-screen user interface [41].

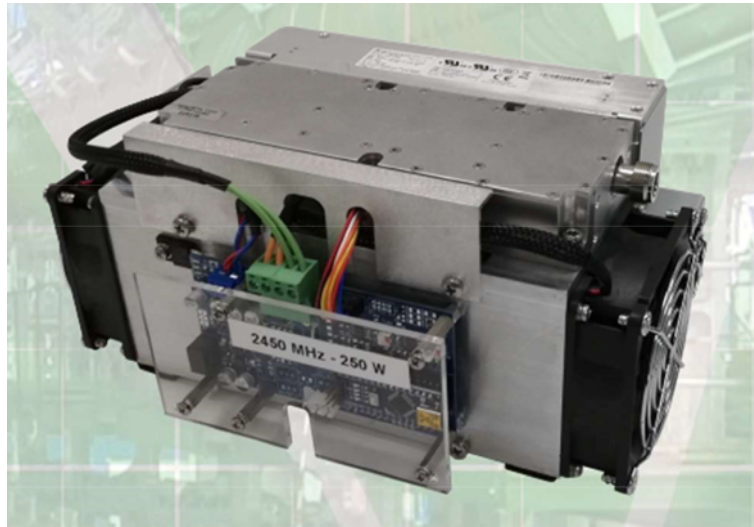


Fig 2.22. STARTER Evaluation Kit with a 2450 MHz 250 W solid-state microwave amplifier [40].



Fig 2.23. PHASESHIFTER Evaluation Kit with two 2450 MHz 250 W solid-state microwave amplifiers [40].



Fig 2.24. Front (a) and back (b) views of LEANFA's Generator Lab Kit at 2.45 GHz and 250 W.

Continuing with the solid-state centred companies, the Dutch **pinkRF** is the other big producer. It was established in 2015 with the aim to “bridge the knowledge gap between end system functionality and the solid-state RF energy generation and control” [42]. They are based in Nijmegen (The Netherlands) and recently have become partners with America’s Odyssey to work with RF repair.

They have power amplifiers available in 250, 500 and 1,000 W at 915 MHz and 2,450 MHz frequency bands. However, combining different amplifiers, they are capable of reaching 4 KW

of CW. Their market-ready *RF Energy Toolkits* are a clear competitor to LEANFA's Lab kit. They can be designed to work at 2,450 MHz up to 300 W or 915 MHz with maximum power of 1 kW. Unlike the LEANFA one, these cannot have output powers lower than 50 W. [43]



Fig 2.25. *RF Energy Toolkit* from pinkRF with 250 W at 2.45 GHz [43]

MUEGGE (Reichelsheim, Germany) is one of the most important companies of microwave components worldwide. It was founded in 1986, and it has been specialised in magnetron manufacturing, waveguide components, high-power microwave systems with power up to 50 kW and plasma systems and components. Their only solid-state microwave generator works at 2,450 MHz and reaches 1 kW of output power with a coaxial output connector (Fig 2.26).



Fig 2.26. Solid-state microwave generator at 2.45 GHz and 1 kW from Muegge [44].

SAIREM (Lyon, France) is one of the most important industrial microwave ovens manufacturers in Europe. They have a complete range of magnetron-based products, with the magnetrons manufactured by them. They have specialised in the food industry with transport ovens with magnetrons and microwave plasma generators for synthetic diamond.

SAIREM has been interested in solid-state technology since 2008 [45]. Among their products, they offer one generator at 2,450 MHz and 1 kW (Fig 2.27) and two lab-ready generators with 200 W and 450 W, respectively (Fig 2.28). One interesting feature of these two last devices is the capability to adjust the frequency automatically within the band to optimise the return losses of the system. This feature works through the SAIREM Auto-tune patented algorithm [46].



Fig 2.27. SAIREM's GMS 1000 solid-state generator with 1kW at 2.45 GHz [47].



Fig 2.28. SAIREM's GMS 450 solid-state generator with 450 W at 2.45 GHz [48].

Wattsine (Chengdu, Sichuan, China) is the explicit exponent when considerable solid-state power is needed. This company is fully solid-state centred and can reach output powers up to 25 kW and 20 kW at 915 MHz (Fig 2.29) and 2,450 MHz, respectively.

On the lower range of power, they have different solutions according to the need of the application or environment. For example, Wattsine is one of the few companies that offer solid-state power amplifiers at 433 MHz with 200 W, both as a piece of lab equipment (Fig 2.30) with its touch-

screen control interface and as an integrable device (Fig 2.31) with nothing else than the power amplifier and the air-cooling system (it also needs the power source).



Fig 2.29. Wattsine's 915MHz-25kW-CEWA Solid-state microwave generator [49]



Fig 2.30. Wattsine's 433MHz-200W-CCFA Solid State Microwave Power Generator (lab-ready) [50]



Fig 2.31. Wattsine's 433MHz-200W-CMFA Solid State Microwave Power Generator (integrable) [51]

2.3.3. Commercial solid-state driven microwave applicators

Integrating these solid-state microwave sources into microwave oven applicators has been one of the challenges in the foodstuff microwave heating sector. As previously stated, magnetrons became economic due to the domestic microwave oven killer application. The advantages of the solid-state technology for microwave heating have been clearly stated; however, there are just a few commercial ovens using this technology in the market.

One of the first solid-state driven microwave ovens was developed by the transistors maker Ampleon along with the Chinese consumer appliances manufacturer Midea [52] (see Fig 2.32). They claim that their work “has resulted in Midea launching what is believed to be the world’s first commercially available solid-state RF energy oven”. This oven consists of a small cavity feed with 200 W and a single antenna working at 2,450 MHz. They designed an oven capable of working connected to the electrical network or with a 24 Vdc battery.



Fig 2.32. Midea 200 W solid-state microwave oven.

The transistor manufacturer NXP also developed their concept oven for smart microwave cooking based on solid-state technology. They called it *Sage concept RF cooker* [53], although this seems more a tool to sell transistors than a microwave cooking solution (Fig 2.33).



Fig 2.33. NXP's Sage concept RF cooker.

The German appliance manufacturer Miele also got interested in solid-state technology. This well-established company developed a professional-oriented oven called Dialog [54] (see Fig 2.34). It uses a combination of solid-state, hot-air and conventional convection heating systems. There is little information available online on technical features, but it is definitely professional-

oriented or only for very wealthy families due to its high cost: 7,990€ [55]. This oven has been developed using the technology patented by the Israeli company Goji Food Solutions, whose work has been focused on developing solid-state-based hardware, algorithms and software to control their systems relying on vast food databases. They have registered more than two hundred patents worldwide in this technology [56].



Fig 2.34. Front view of the Miele's Dialog smart oven.

Another example of a cooking microwave oven with solid-state technology is the IBEX Oven (see Fig 2.35). This oven was developed by a company named IBEX, based in Illinois, United States. Their only product is a hybrid microwave and convection oven with smart heating for different preselected processes. It is clearly oriented to professional kitchens such as restaurants and hotels. It has a retail price of \$18,000 and uses a real-time, adaptive, heat-sensing system that uses heating algorithms designed for custom menus and common kitchen operations. Programming and uploading recipes and unique cooking functions is available via a USB port to expand menu offerings [57].



Fig 2.35. IBEX oven [58]

Plasma generation is an application where solid-state sources have acted as a trigger. Microwaves have been used to produce high-density plasmas for industrial and laboratory applications such as low-temperature diamond deposition, exhaust gas abatement, thin-film deposition, etc. [59]. To meet industrial requirements on plasma generation, i.e., larger-scale processing with high density and uniformity, companies like Sairem have developed new equipment. In this case, the

AuraWave system (see Fig 2.36) with multiple 200 W solid-state microwave generators with fine control over the frequency range from 2.4 to 2.5 GHz. These generators represent an important step forward due to the spectral quality, much better than that of a magnetron generator. This spectral quality is directly related to an excellent spectrum from the first watts.



Fig 2.36. *Aura-Wave* ECR microwave plasma source [59, Fig. 1 (a)]

Part II

Materials and Methods

Chapter 3. Design methodology and equipment

The third chapter of this PhD dissertation contains the methodology's description and an explanation of every tool, both software and hardware, used in the development of the thesis.

It is presented here the methodology followed for the design of new microwave systems. The second section of this chapter is devoted to describing the computer programs and lab equipment used to conduct each one of the steps presented in the methodology.

3.1. Microwave system's design methodology.

The designing process of a microwave heating system comprises different aspects: applicator dimensions, load location and energetic requirements. The method used consists of seven steps:

a) Microwave heating feasibility.

The first step is to verify the interaction between microwaves and the desired load. A simple method is heating a small, though representative, sample of the material and checking the temperature increase. Using solid-state microwave generators, it is possible to adjust the power delivery, verify the return losses and precisely control the amount of power that theoretically is being given to the sample.

The first study is usually made in a modified commercial oven at 2,450 MHz. If the sample does not respond to the microwaves or the product requirements need higher wavelengths, a bigger oven is used with a 915 MHz solid-state microwave generator.

The objective of this first step is to check, through measurements, the energy requirements, i.e., the power needed to increase the desired temperature in a defined timeframe.

b) Applicator requirements.

Every application has its own requirements, functionalities, initial conditions, etc. The key to a successful design is to adapt the applicator as much as possible to the heating process. To this purpose, several questions must be addressed: should the oven be static or continuous? It is possible to use solid-state generators or high-power magnetron must be used (for cost reduction) instead? If solid-state is the choice, is better to use air or water cooling systems? Does the applicator structure, i.e., antennas, waveguides, etc., need mechanical movement? How much load needs to be introduced in the system at a time?

All these questions must be answered by the client/customer. Therefore, fluid communication between the manufacturer and the client is highly desired. Most times, the first step is to define a common vocabulary and never take anything for granted.

c) Load characterisation.

The next step is to fully characterise the load sample that needs to be heated. It is important to look up in the literature the thermophysical and dielectric properties of the product. If these properties are temperature dependent, an accurate characterisation is needed.

If possible, measurements are used to verify these properties. Being the most critical, the dielectric properties' measurements; which is extensively described later in this Chapter.

d) Electromagnetic modelling.

Once the dimensions of the applicator are approximatively defined, and the load is properly characterised, the electromagnetic modelling step takes place. This study can be performed in the time-domain, i.e., by means of finite-difference, time-domain (FDTD) methods, or in the frequency domain, i.e., using the finite elements method (FEM). The selected tool is the FEM-based HFSS from Ansys.

The goal of this step is to tune the applicator design to improve the power delivery within a specified area of interest. This area of interest is the location of the sample that sometimes needs to be optimised.

e) Multiphysics modelling.

A first verification of the electromagnetic model is carried out through multiphysics modelling tools, like Comsol Multiphysics. It is used to solve mixed (i.e., coupled) physics' problems. Electromagnetic or microwave heating involves, primarily, electromagnetism and heat transfer physics. Therefore, multiphysics tools must be used to model them.

f) Prototype manufacture and modelling refinement.

Once the proper behaviour of both computer-aid models is verified, a prototype needs to be built. This equipment should be prepared for possible changes; therefore, removable parts or pre-

defined adjustment variables must be included in the design to take full advantage of the prototype.

The multiphysics study is refined by means of the manufactured prototype and, using an iterative process, the model is adjusted to the measures. This is important for further developments of the system, the heating process or application changes.

g) Market ready device.

Finally, the market-ready, (i.e., a TRL9 system), is manufactured. However, this step is well beyond the scope of research works, like the present PhD.

3.2. Software and equipment.

3.2.1. Modelling and calculation tools

3.2.1.1 Electromagnetic modelling: HFSS from Ansys.

The high-frequency electromagnetic fields modelling tool HFSS is a 3D finite elements method (FEM) based simulation software developed by Ansys. It is used for designing and simulating high-frequency electronic products such as antennas, RF or microwave components, high-speed interconnects, filters, IC packages and printed circuit boards. Worldwide engineers use Ansys HFSS software to design high-frequency, high-speed electronics found in communications systems, advanced driver assistance systems (ADAS), satellites, and internet-of-things (IoT) products [60].

Simulations are based on finite element calculations, integral equations and advanced hybrid methods. HFSS provides a 3D complete wave precision allowing the prototype creation in reduced time-space. As explained before, this software has been used for the electromagnetic modelling steps, including the design of antenna systems, applicators and resonant cavities, as well as microwave circuitry.

3.2.1.2 Multiphysics modelling: Comsol.

COMSOL Multiphysics® is a general-purpose simulation software used in all fields of engineering, manufacturing, and scientific research. The software brings fully coupled multiphysics and single-physics modelling capabilities, simulation data management, and user-friendly tools for building simulation applications. Add-on modules provide specialized functionality for electromagnetics, structural mechanics, acoustics, fluid flow, heat transfer, and chemical engineering. Interfacing products are available for CAD and other third-party software. All add-on products from the product suite connect seamlessly with COMSOL Multiphysics® for a modelling workflow that remains the same regardless of what you are modelling [61].

Electromagnetic and heat transfer physics have been used to model the solid-state based microwave ovens and their different applications.

It is important to note that both electromagnetic and multiphysics modelling are helpful tools but do not show the reality. It is very easy to obtain “good” results, i.e., convergence in the equation solvers and visual field distribution and electromagnetic parameters. That’s why the verification has to be made by the engineer. Moreover, a profound knowledge of the physics and structures involved is mandatory to reduce the unnecessary calculations that increase the computational cost, i.e., a bigger processor and RAM are needed in the computer and operation times are incommensurate.

3.2.1.3 Calculation software: Matlab.

MATLAB[®] is a programming platform explicitly designed for engineers and scientists to analyse and design systems and products. The heart of Matlab is the Matlab language, a matrix-based language allowing the most natural expression of computational mathematics [62].

It has been used to perform every mathematical calculation, field post-processing and graphic creation for the thesis dissertation.

3.2.2. Lab measuring devices.

3.2.2.1 Microwave leakage detector.

A microwave leakage detector is a passive security device that every person working on a microwave system design and validation needs to carry. It measures the microwave power in mW/cm^2 and, once the detected signal exceeds the defined threshold, it emits visual and acoustic warnings.

The model used (see Fig 3.1) is the DVMEMF (Velleman Inc., BE). It offers a detection signal range of 0 - 9.99 mW/cm^2 , and the alarm value is set at 5 mW/cm^2 .

It has been used whenever the microwave generators are ON and has also been used to check the different signal values in the different parts of the manufactured systems.



Fig 3.1. Velleman microwave leakage detector.

3.2.2.2 Vector network analyser (VNA).

Vector Network Analysers (VNA) and Spectrum Analysers (SA) are two of the most important electromagnetism lab equipment. A VNA injects a signal into the network and then monitors its response. It can measure the amplitude and phase responses in a defined frequency bandwidth. Although SAs share many functionalities with VNAs, the main difference between them is that SAs are intended for analysing the introduced signal nature, whereas VNAs generate the signal and use it to analyse the network or device under test.



Fig 3.2. FieldFox Microwave Analyzer [63]

There are devices in the market that integrate both analysers into one single device. It is the case of the used in this thesis. The Keysight's FieldFox N9917A (see Fig 3.2) is a portable analyser with VNA, SA, built-in power meter, vector voltmeter, and more. It has two RF ports (N-connectors) and can measure all four S-parameters simultaneously. It has been used to measure

the return losses of the designed antennas, as well as the oven's characteristic impedances. The model used is capable of measuring from 30 kHz to 18 GHz with up to 1 dBm output power.

3.2.2.3 Infrared (IR) thermal cameras.

Being able to graphically measure the thermal distribution of temperature in materials is a must in the microwave heating system's design. Classical pyrometers can measure the temperature at a single point, but given the heterogeneous heating produced by microwave ovens, it is necessary to have a complete thermal picture.

Microbiotech owns an optical pyrometer, concretely, the Optris PI 160 (Optris, Berlin, GE). This camera is controlled by the software CompactConnector provided by the same company. With this software, a video of the temperature evolution is recorded. It has been used for every thermal measurement performed at Microbiotech's labs.



Fig 3.3. Optris PI 160 thermographic camera.

The thermal camera used at the RISE labs in Sweden is the testo 890 (Testo SE & Co. KGaA, Titisee-Neustadt, GE). This is a professional thermal imager with thermal sensitivity of < 40 mK. It offers sequence capturing, humidity calculation, JPEG storage function and other practical features.



Fig 3.4. Testo 890 Thermal imager [64]

Chapter 4. Computer-aid modelling

Getting the aid of electronic devices such as computers and highly specialized lab equipment is the key to better understanding problems and offering solutions. This fourth chapter of the dissertation comprises the description of the foodstuff microwave heating modelling, including the involved equations, the food thermophysical and dielectric properties.

It is important to note that software tools help understand what's happening in a very complex process, but it can never be taken as reality. Modelling is used in an iterative process that goes from a very simplified model of the problem to the most similar reflection to reality, even though it will never be the same. Given that, it is essential to define assumptions, boundary conditions, and expected results to lead the modelling to a better agreement with reality.

The first section of the chapter is devoted to explaining the limitations and aspects that need to be taken into account when performing electromagnetic and multiphysics modelling jobs. It describes the importance of dielectric properties and shape in microwave heating modelling. It also shows the main dielectric properties measurement systems.

The second part of the chapter shows the modelling example of the defrosting and tempering of beef meat. Part of this work was presented at the 18th Ampere conference [65].

4.1. Considerations to the modelling of microwave heating processes.

One of the challenging aspects of the microwave heating modelling of food is the definition of the dielectric and thermophysical properties of the food material. Bengtsson and Ohlsson [66] stated that the heat generated by a microwave source rises with the dielectric loss of the food material. It is essential to note that the dielectric properties of foods are affected by frequency, temperature and composition.

The other important aspect is the effect of the load's shape and size. Their importance is such that most of the recent improvements in the microwave-assisted cooking sector has been the research and development of new packaging solutions that provide better heating. A valuable reference in this field is "Development of Packaging and Products for Use in Microwave Ovens" [27].

4.1.1. Dielectric properties measurement systems.

Reliable dielectric properties measurement systems must be used to define the material's behaviour with microwaves. The choice of which measurement method must be used depends on the sample size and shape and the application. There are five predominant dielectric measurement methods: parallel plates, coaxial probes, transmission lines, resonant cavities, and free space.

4.1.1.1 Parallel plates.

The parallel plates method (see Fig 4.1) consists of inserting a thin material slab between two metallic plates, working as electrodes. It is, therefore, a structure similar to a capacitor and the dielectric constant, ϵ' , is calculated from the capacitance, C_p . The loss factor, ϵ'' , is obtained from the dissipation factor, D_f [67]. It presents the advantage of sample simplicity: the material has to be prepared as a thin slab (lower than 10 mm width). On the other hand, the disadvantages are the surface roughness limitations and the required constant electric field, forcing the system to work at frequencies lower than 1 GHz.

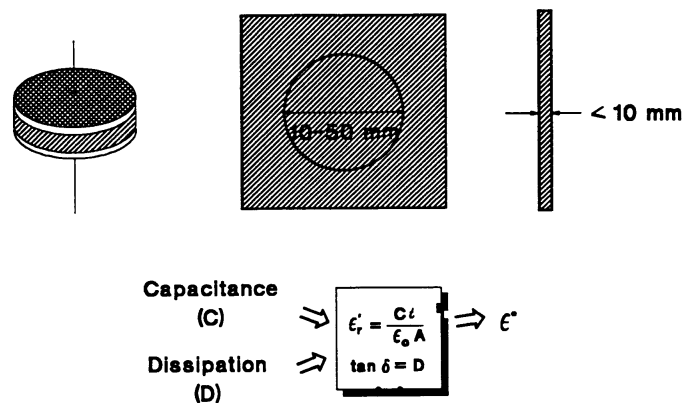


Fig 4.1. Parallel plates method [68].

4.1.1.2 Coaxial probe.

The open-ended coaxial probe is basically a sectioned transmission line. The material's dielectric properties are obtained by placing with direct planar contact the probe to the solid sample or submerged into a liquid or semi-solid sample. The electromagnetic fields at the end of the probe penetrate the material and change with its contact. The complex dielectric constant can be obtained from the reflected signal measurement, S_{11} [69]. A typical coaxial probe measurement system comprises a VNA, the coaxial probe and a computer for the measurement processing and calculations (see Fig 4.2).

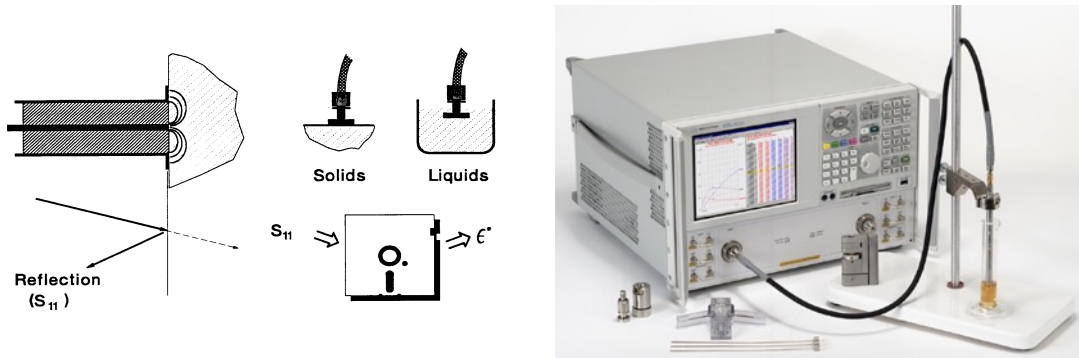


Fig 4.2. Coaxial probe measurement method (left) and example of the Agilent Technologies coaxial probe (right) [68].

The processing software usually calculates the complex permittivity assuming some conditions: the material is isotropic and non-magnetic, the interface between the material and the probe is perfect, so no air is allocated there, and the sample can be considered as infinite at the working frequency. These conditions are not always feasible; thus, some error is introduced. The interface challenge has limited the results' precision and hindered the method for liquid materials.

It is also possible to use coaxial probes with transmission measurements. A novel system based on using two coaxial probes (see Fig 4.4) has been developed by Santón et al. [70]. Considering the sample as a thin and flat slab, probes can be seen as a 2-port pi network (see Fig 4.3). Using a two-step measurement procedure (with and without sample), can be obtained the dielectric properties.

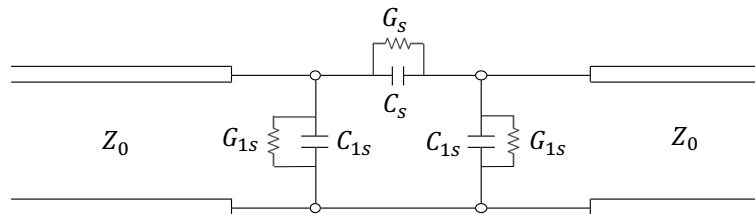


Fig 4.3. Concentrated elements schematic with a sample between the probes [70, Fig. 3]

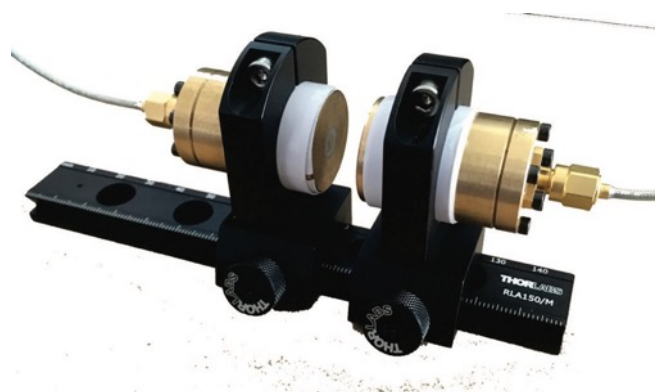


Fig 4.4. Transmission/reflection measurement coaxial probes [70, Fig. 6]

4.1.1.3 Transmission lines.

Transmission line techniques are based on placing the material under test (MUT) inside a transmission line section. It is usually a rectangular waveguide or an air-filled coaxial line (see Fig 4.5). They present the interesting characteristic of covering a wide frequency band, but the samples need to be cut to the transmission shape, which is not always easy. Coaxial lines present the wider band and the more challenging sample shape, while the waveguide's sizes make it easier to prepare a sample, although the cutoff frequency of the guide limits the bandwidth. Traditionally, it has been used in reflection configuration (a single port) [71]–[75] or combining transmission and reflection measurements (two ports) [76]–[84].

In the shorted lines (reflection method), the sample is positioned at the end of the transmission line, and the dielectric properties are obtained from the reflection coefficient S_{11} . The electromagnetic solution obtained from this technic leads to equations with a sole adequate value out of multiple solutions. Therefore, some previous knowledge of the estimated value or taking measurements at different frequencies is needed to increase accuracy. On the other hand, the two-port-based method can determine the permittivity, ϵ_r , and the permeability, μ_r , through the reflected signals (S_{11} and S_{22}) and the transmitted ones (S_{21} and S_{12}) obtained from the VNA.

Both methods present the uncertainty introduced by the air gaps between the sample and the transmission line walls. In addition, the bandwidth margin can be reduced due to superior modes appearance because of sample inhomogeneities.

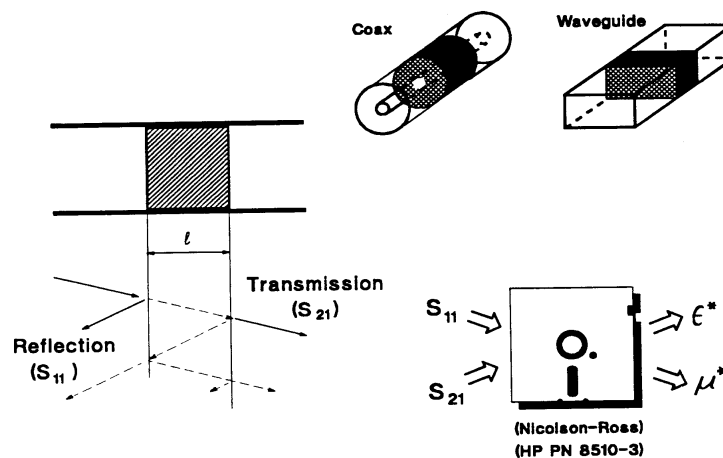


Fig 4.5. Transmission lines method [68].

Coplanar waveguide (CPW) consists of a microstrip line with two metallic plates on both sides of the strip. A CPW-based dielectric properties measurement system has been designed [85] with a slab of the material whose complex permittivity value wants to be obtained on top of it. The system's scattering matrix (S_{11} and S_{21}) with the “unknown” material is measured between two reference planes. This device can measure the dielectric constant and dielectric loss factor in the 433 – 2,450 MHz frequency range. This work has been presented in a poster at the IMPI's 56th Annual Microwave Power Symposium [86].



Fig 4.6. Complete measurement system based on CPW probe.

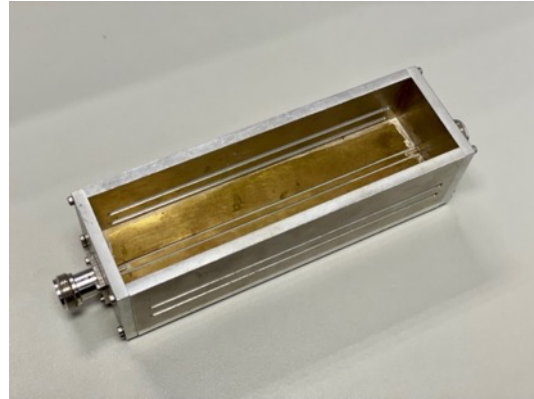


Fig 4.7. Novel CPW-based multi-frequency dielectric properties measurement device.

4.1.1.4 Resonant cavities.

A high-quality factor, Q , is the principal characteristic of resonant cavities. As the name indicates, the best behaviour occurs at a specific frequency (see Fig 4.8). When a dielectric material sample is introduced inside such a cavity, the resonant frequency is slightly reduced, as well as the Q factor. From these changes, it is possible to calculate both the permittivity and permeability of the material at the resonant frequency.

Perturbational approximations improve the measurement accuracy with resonant cavities [87]–[89]. However, these techniques are limited by sample size and permittivity. For materials with low losses, some corrections have been developed from specific cavity modes [90]–[92].

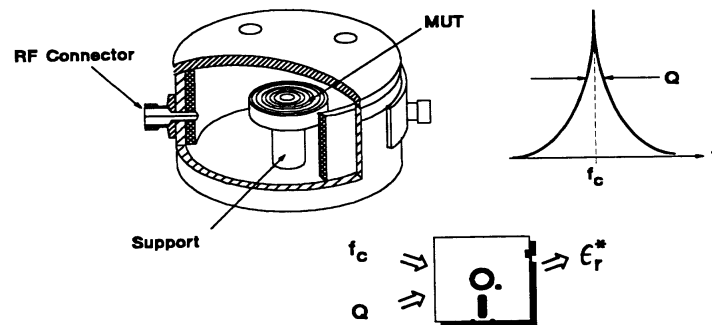


Fig 4.8. Resonant cavities method [68].

4.1.1.5 Free space techniques.

Antennas and metallic surfaces are used for the free space dielectric properties techniques (see Fig 4.9). It can be done with a single antenna (reflection) or with two or more antennas (transmission). The algorithms used are the same as in the transmission line method. Free space is the measurement option when the sample is big, flat and thin. It is also helpful for samples that need to be tested at high temperatures.

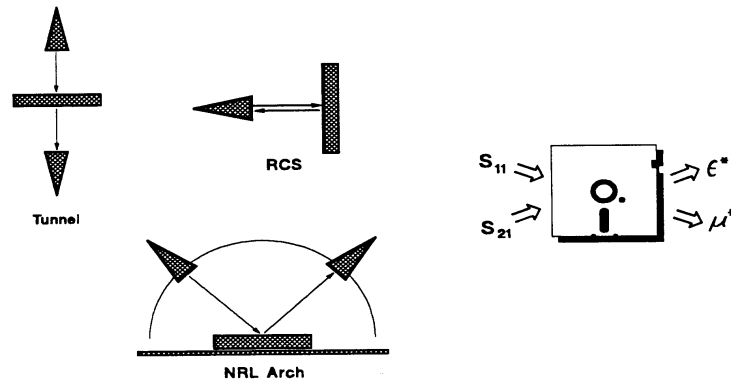


Fig 4.9. Free space techniques method [68].

This non-contact technique is non-destructive and usually works at frequencies higher than 10 GHz to avoid the effect of the border. Moreover, it can reconstruct tomographic images and is extensively used in medical applications [93], [94].

4.1.2. The effect of shapes and sizes.

The load geometry affects its microwave heating. Some shapes and sizes can create highly concentrated heating patterns, a critical situation to avoid in order to reach heating homogeneity. Hot spots (or cold) making severe temperature differences and even burnings are the outcome of this effect. It can be found in the borders, for rectangular loads, or at the centre of spherical and cylindrical loads. There are also stationary wave patterns in big and flat loads.

The border effect is perfectly seen at the sharp edges of the samples. A non-resonant diffraction phenomenon caused by the parallel to the edge electric field component is the responsible. The higher the dielectric constant, the higher the overheating. The same effect occurs for smaller edge angles. Fig 4.10 shows the role of the polarization (TM and TE) in the border effect.

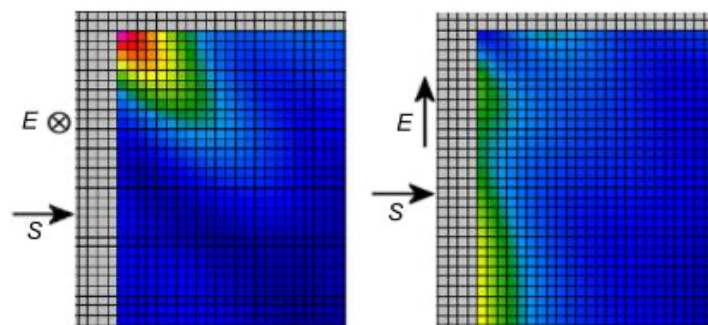


Fig 4.10. Power density of radiation from S direction. TM mode (left) and TE mode (right) [95, Fig. 3.39]

These diffraction phenomena produce a high energy concentration at the load's centre for cylindrical and spherical geometries (see Fig 4.11). This effect is conditioned to the load's diameter, the working frequency and penetration depth in the load.

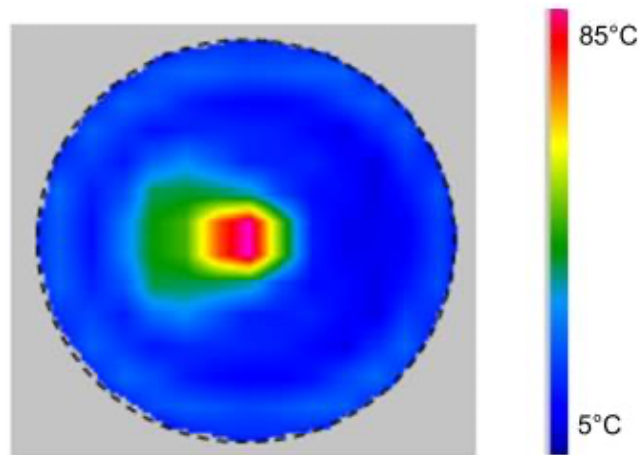


Fig 4.11. Center overheating in a cylindrically shaped meat loaf, of radius 25 mm and $f=2,450$ MHz [96, Fig. 2.6]

4.2. Multiphysics modelling of foodstuff.

4.2.1. Thermophysical properties.

The thermal properties of food and liquids must be known to perform the different heat transfer calculations, one of the two physics included in the microwave heating. The most important thermophysical properties are density, specific heat, thermal conductivity and thermal diffusivity. Several methods are available to measure these properties; however, needing to perform measurements every time a food sample is modelled is not the wisest option.

Most foodstuff contains water, protein, fat, carbohydrate, fibre, and ash. Choi and Okos [97] presented in 1986 a paper defining the approximative equations of the main food constituents' thermophysical properties. These equations can be seen written, with the temperature expressed in °C, in chapter 9 of the ASHRAE Handbook [98].

Nevertheless, when the model is prepared in Comsol for electromagnetic heating, only four thermophysical properties are strictly required: density (ρ), thermal conductivity (k), specific heat capacity (c_p) and thermal diffusivity (α). Table 4.1 contains the equations that define these properties for the main constituents.

Table 4.1. Thermal property models for food components ($-40 \leq T \leq 150^\circ\text{C}$)

Thermal property	Food component	Approximative equation
Density [kg/m ³]	Water	$\rho_w = 9.9718 \times 10^2 + 3.1439 \times 10^{-3}T - 3.7574 \times 10^{-3}T^2$
	Ice	$\rho_{ice} = 9.1689 \times 10^2 - 1.3071 \times 10^{-1}T$

	Protein	$\rho_{prot} = 1.3299 \times 10^3 - 5.1840 \times 10^{-1}T$
	Fat	$\rho_{fat} = 9.2559 \times 10^2 - 4.1757 \times 10^{-1}T$
	Ash	$\rho_{ash} = 2.4238 \times 10^3 - 2.8063 \times 10^{-1}T$
Thermal conductivity [W/(m·K)]	Water	$k_w = 5.7109 \times 10^{-1} + 1.7625 \times 10^{-3}T - 6.7036 \times 10^{-6}T^2$
	Ice	$k_{ice} = 2.2196 - 6.2489 \times 10^{-3}T + 1.0154 \times 10^{-4}T^2$
	Protein	$k_{prot} = 1.7881 \times 10^{-1} + 1.1958 \times 10^{-3}T - 2.7178 \times 10^{-6}T^2$
	Fat	$k_{fat} = 1.8071 \times 10^{-1} - 2.7604 \times 10^{-4}T - 1.7749 \times 10^{-7}T^2$
	Ash	$k_{ash} = 3.2962 \times 10^{-1} + 1.4011 \times 10^{-3}T - 2.9069 \times 10^{-6}T^2$
Specific heat [kJ/(kg·K)]	Water (- 40 – 0°C)	$c_{wu} = 4.1289 - 5.3062 \times 10^{-3}T + 9.9516 \times 10^{-4}T^2$
	Water (0 – 150°C)	$c_{wo} = 4.1289 - 9.0864 \times 10^{-5}T + 5.4731 \times 10^{-6}T^2$
	Ice	$c_{ice} = 2.0623 + 6.0769 \times 10^{-3}T$
	Protein	$c_{prot} = 2.0082 + 1.2089 \times 10^{-3}T - 1.3129 \times 10^{-6}T^2$
	Fat	$c_{fat} = 1.9842 + 1.4733 \times 10^{-3}T - 4.8008 \times 10^{-6}T^2$
	Ash	$c_{ash} = 1.0926 + 1.8896 \times 10^{-3}T - 3.6817 \times 10^{-6}T^2$

The Engineering Properties of Foods book [99] presents the thermophysical properties of a mixture. Considering that every foodstuff can be modelled as a homogenous mixture of constituents, the different properties can be united under addition laws.

The law of addition of specific volumes allows good estimation of the mixture's density (4.1), where ρ is the density of the mixture, x_i is each of the components' mass fraction and ρ_i the densities of the constituents.

$$1/\rho = \sum x_i/\rho_i \quad (4.1)$$

Two models can be used to define the thermal conductivity of multi-component foods. They represent the two limiting values. The perpendicular model assumes that the constituents are disposed in layers perpendicular to the heat flow (see Fig 4.12 (a)). The second model is the

parallel model, in which the constituents are arranged as layers parallel to the heat flow (see Fig 4.12 (b)).

The law of addition of thermal resistances in series defines the conductivity for the perpendicular model (4.2), where k_{\perp} is the thermal conductivity of the food according to the perpendicular model, $\epsilon_i = x_i/\rho_i$ is the volume fraction of each constituent and k_i are the thermal conductivities of the constituents.

$$k_{\perp} = 1 / \sum \epsilon_i / k_i \quad (4.2)$$

The conductivity for the parallel model, k_{\parallel} , is obtained now following (4.3).

$$k_{\parallel} = \sum \epsilon_i k_i \quad (4.3)$$

A mixing model combining the two limiting values (4.4) is often used as estimation, with g as a constant between 0 and 1. For $g = 0.5$, the conductivity, k_{mix} , is the arithmetic mean of k_{\perp} and k_{\parallel} .

$$k_{mix} = gk_{\perp} + (1 - g)k_{\parallel} \quad (4.4)$$

Finally, the conductivity, k , of a two-component food consisting of a continuous and a dispersed phase (see Fig 4.12 (c)), can also be modelled by a formula adopted from Maxwell's dielectric theory and adapted by Eucken (4.5). In this equation, k_c is the continuous phase thermal conductivity, k_d is the thermal conductivity of the dispersed phase, and $\epsilon_d = x_d/\rho_d$ is the volume fraction of the dispersed phase.

$$k = k_c \frac{2k_c + k_d - 2\epsilon_d(k_c - k_d)}{2k_c + k_d + \epsilon_d(k_c - k_d)} \quad (4.5)$$

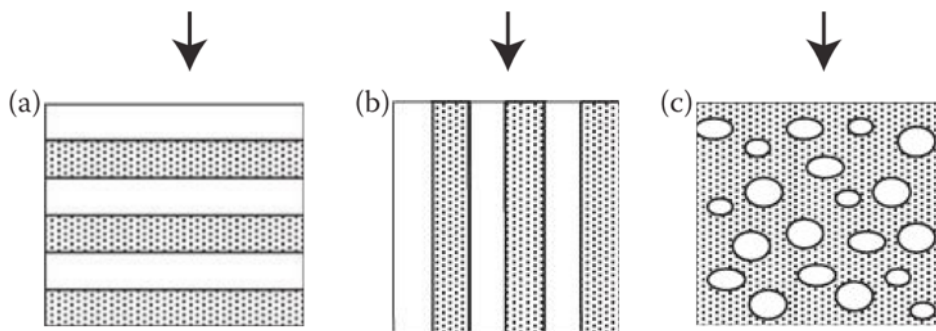


Fig 4.12. Models for thermal conductivity of a two-component mixture: (a) perpendicular, (b) parallel and (c) dispersed. The arrow represents the heat flow direction [99, Fig. 7.1].

Fibre has not been taken into account despite its effect on the thermal conductivity of nonporous materials. Frozen and unfrozen meat present different behaviours when the heat flows parallel to muscle fibres. Concretely 30% and 10% higher, respectively. However, obtaining information on

this property is not an easy procedure, given the heterogeneity and diversity of samples of the same material.

The thermal diffusivity (4.6) depends on all three parameters detailed above.

$$\alpha = \frac{k}{\rho c_p} [J/(m^3 \cdot K)] \quad (4.6)$$

4.2.1.1 Water change of state.

A critical situation is given by the change of state of the water. Knowing the actual liquid water content is essential given the differences between water and ice and microwaves. Note that the heat capacity equations described in Table 4.1 differ for the water when the temperature is under and over the fusion temperature, T_f . The ice content is obtained by (4.7),

$$x_{ice}(T) = \begin{cases} \frac{1.105 * x_w}{1 + \frac{0.7318}{\ln(T_f - T + 1)}}, & T < 272.15 K - T_f \\ 0, & T \geq 272.15 K - T_f \end{cases} \quad (4.7)$$

and the liquid water content is obtained, therefore, as in (4.8).

$$x_{wl}(T) = x_w - x_{ice}(T) \quad (4.8)$$

4.2.2. Dielectric properties.

The vast amount of data in the literature for the dielectric properties of most known food and beverages makes it possible to electromagnetically model the foodstuff with considerable accuracy. The first action is to define the operation frequency and look for dielectric properties at that frequency band. Some typical ISM frequency bands have more data available than others, e.g., 2,450 MHz (sometimes approximated at 3 GHz). The second step is to find among the available data studies that show differences in the dielectric properties with the materials' composition and temperature. This gives the researcher a more comprehensive vision of the problem.

Bengtsson and Ohlsson [66] also stated that for some of the parameters (e.g., composition in terms of certain constituents), the impact of the dielectric properties is relatively moderate. Things also depend on the type of application, e.g., if phase changes are included. Different studies have shown this effect, e.g., [100] studied the impact of the frequency in an ample range, while [101] and [102] did their studies concerning the composition. Most data of all kinds of food products are already available. In most cases, the new data agree with the study by Bengtsson and Ohlsson [103], considered and referenced in many books as accurate reference data.

The dielectric constant in a multiphysics modelling must include the temperature dependency. In some cases, authors have obtained approximative equations, like in [104] and [105]. In others,

the easiest way to define the temperature dependency is by defining paired values. The following subsection gives a thorough explanation of the permittivity definition.

4.3. Beef sample modelling example.

As a part of the PhD studies, the work related to acquiring the required knowledge on multiphysics modelling using Comsol Multiphysics® was done during a research stay in Gothenburg, Sweden. The Agrifood and Bioscience area of the Research Institutes of Sweden (RISE) was the receiving research centre. The vast experience of their leader, Birgitta Raaholt, has been an essential asset in the thesis development and the election of her centre for the research stay. Their main work has been devoted to modelling food behaviour with microwaves [106]–[114]. An excellent example of her knowledge in the field can be found in her chapter written for the *Development of Packaging and Products for Use in Microwave Ovens* book [96].

The objective of the stay was to model a meat sample in a standard microwave oven. Afterwards, several verification tests were carried out with a commercial oven. This work aims to properly define the electromagnetic and thermophysical equations used in a multiphysics modelling environment. With this, we will be able to work with any kind of food load and design microwave ovens and systems for the desired application.

The first step is to select the best meat for the modelling. It must be easy to find, as much homogeneous as possible, i.e., without skin, bones, etc. Still, the most important thing is that their dielectric and thermophysical properties (or composition) need to be available and verified by different authors.

4.3.1. Meat election: data research.

Exhaustive research work has been carried out to find the suitable meat type. The most interesting papers are described below, ordered per year, collecting dielectric properties data at 915 and 2,450 MHz, the two most used frequencies for microwave heating applications.

In April 1994, Bodakian and Hart presented a paper [115] about beef and chicken permittivity. It is explanatory and a good introduction to the dielectric properties' measurement field, including the study of conductivity. However, both meat samples were measured in the range of 1 Hz to 1 MHz.

Sipahioglu et al. [104] published in 2003 in the *JMPEE* (Journal of Microwave Power and Electromagnetic Energy) a very interesting paper with data at 2,450 MHz for chicken and beef, among other foodstuffs. The dielectric properties were measured (in triplicate) using the open-ended coaxial probe 85070B from Hewlett-Packard, Palo Alto, CA, USA. The temperature range covered was 15 to 65 °C, and the ash and moisture content (%) were also measured (see Fig 4.13 and Fig 4.14).

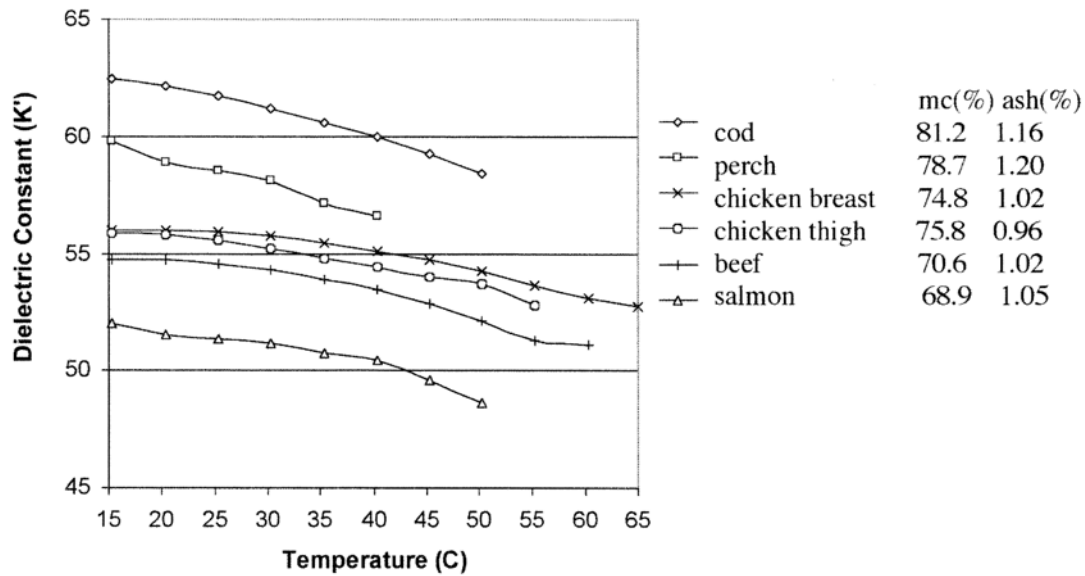


Fig 4.13. The effect of ash concentration and moisture on dielectric constant of meat samples at 2,450 MHz [104, Fig. 2].

Two approximative equations for the real (4.9) and imaginary (4.10) parts of the dielectric constant were defined from these measurements. In these equations, M is the moisture content percentage, T is the temperature in $^{\circ}\text{C}$, and A the ash content percentage. The coefficient of determination, R^2 , obtained is 0.82 and 0.89, respectively. The paper compares their results with the equations and previous studies with some equivalent data, mainly the beef sample.

$$\varepsilon' = 6.49 + 0.689 M - 0.0748 T \quad (4.9)$$

$$\varepsilon'' = -608 - 0.107 T + 0.00177 T^2 + 12.6 M - 0.0839 M^2 + 279 A - 122 A^2 \quad (4.10)$$

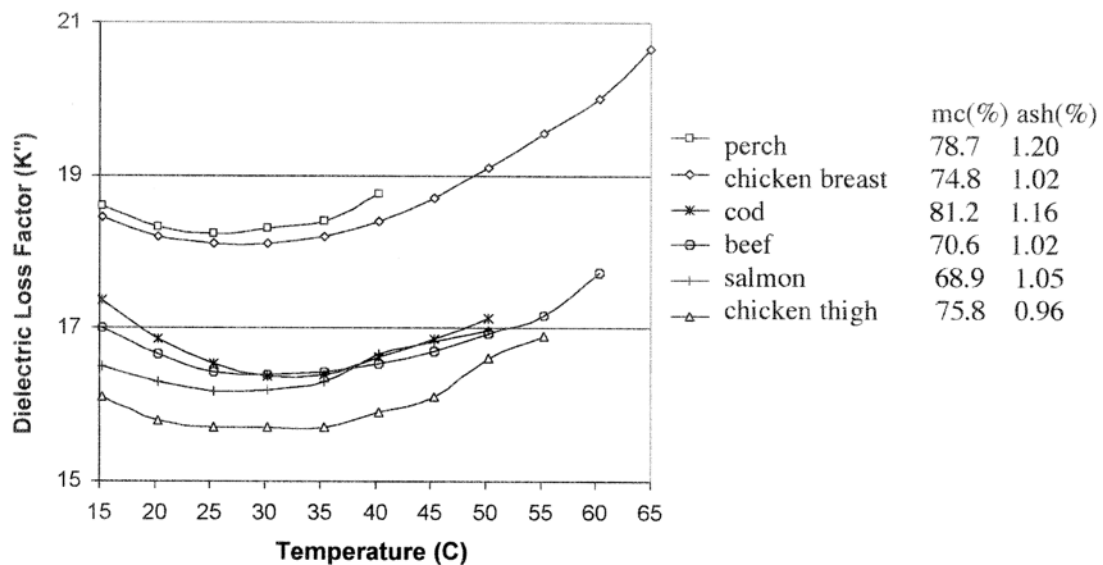


Fig 4.14. The effect of the moisture and ash concentration on dielectric loss factor of meat samples at 2,450 MHz [104, Fig. 4].

More recently, in 2004, Zhang published a paper centred on meat batters in a temperature range [116]. The measurements of different batters were carried out in the temperature range of 5 – 85 °C at 20 °C intervals. The measurement method is based on a complex and well-designed coaxial probe system, as shown in Fig 4.15. They also measured the thermal conductivity, heat capacity and, through calculations, the penetration depth.

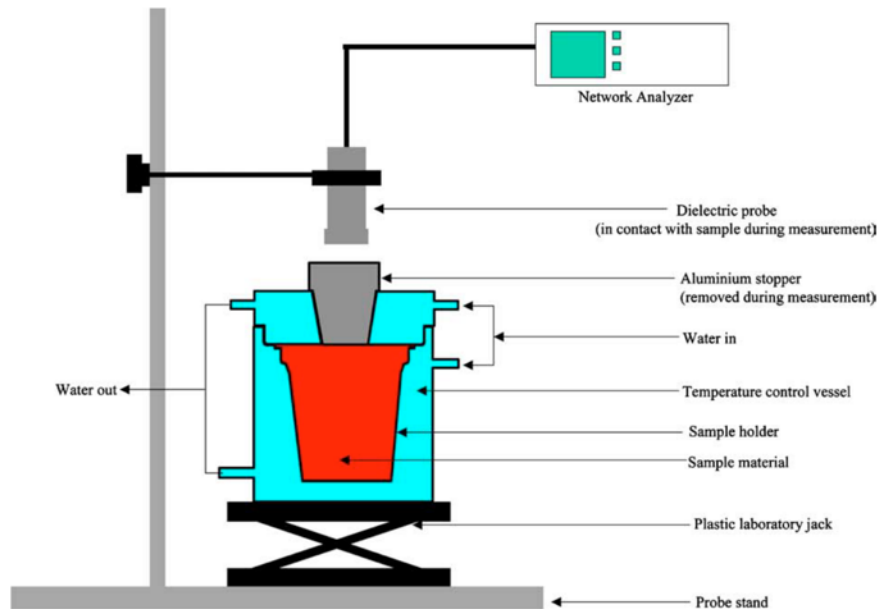


Fig 4.15. Illustration of apparatus used to hold and measure the dielectric properties [116, Fig. 1(b)].

The dielectric properties, shown in Fig 4.16, were measured at 27.12, 896, 915 and 2,450 MHz. It is enlightening to see the minimal but apparent differences between two close frequency bands like 896 and 915 MHz. Another clear conclusion is that the penetration depth decreases with the temperature at 2,450 MHz.

Table 5
The effect of temperature on ϵ' of white pudding and pork luncheon roll meat batters

Temperature (°C)	White pudding				Pork luncheon roll			
	27.12 MHz	896 MHz	915 MHz	2450 MHz	27.12 MHz	896 MHz	915 MHz	2450 MHz
5	44.24	37.48 ^{bc}	37.38 ^b	33.00 ^{ab}	46.60	40.13 ^a	40.03 ^a	36.08 ^a
25	42.63	36.72 ^{bc}	36.57 ^b	32.83 ^{ab}	46.59	39.71 ^a	39.61 ^a	35.90 ^a
45	42.03	38.83 ^c	38.72 ^b	34.64 ^b	47.24	36.49 ^a	36.39 ^a	33.01 ^a
65	41.71	35.67 ^{ab}	35.56 ^a	31.45 ^{ab}	50.22	39.60 ^a	39.49 ^a	35.63 ^a
85	47.85	33.84 ^a	33.72 ^a	29.97 ^a	50.19	34.93 ^a	34.82 ^a	31.16 ^a
P value	NS	0.001	0.001	0.023	NS	NS	NS	NS

^{a-c}Means in the same column with unlike letters are different ($P < 0.05$).

(a)

Table 6
The effect of temperature on ϵ'' of white pudding and pork luncheon roll meat batters

Temperature (°C)	White pudding				Pork luncheon roll			
	27.12 MHz	896 MHz	915 MHz	2450 MHz	27.12 MHz	896 MHz	915 MHz	2450 MHz
5	880.41 ^a	42.09 ^a	41.32 ^a	21.92 ^a	526.66 ^a	28.48 ^a	28.01 ^a	17.14 ^a
25	1118.17 ^{ab}	48.31 ^a	47.42 ^a	23.09 ^{ab}	701.76 ^b	32.86 ^a	32.27 ^a	18.03 ^{ab}
45	1457.18 ^c	59.82 ^b	58.68 ^c	26.85 ^c	855.51 ^b	34.49 ^{ab}	33.85 ^{ab}	18.32 ^{ab}
65	1631.39 ^c	58.59 ^b	57.46 ^{bc}	25.61 ^{bc}	938.11 ^c	41.22 ^b	40.43 ^b	21.03 ^b
85	1350.15 ^{bc}	50.64 ^{ab}	49.64 ^{ab}	23.34 ^{ab}	933.21 ^c	32.45 ^a	31.85 ^a	16.24 ^a
P value	0.000	0.000	0.000	0.005	0.000	0.004	0.004	0.014

^{a-c}Means in the same column with unlike letters are different ($P < 0.05$).

(b)

Fig 4.16. Dielectric properties, real (a) and imaginary (b) parts, of white pudding and pork luncheon roll at different temperatures and frequencies [116].

Also in 2004, Lyng and Zhang published their work on the effect of the ingredients used for meat manufacture on the dielectric properties [101]. The paper includes a review table with the dielectric properties of foodstuff until then published. They measured at 2,450 MHz the dielectric properties of chicken, lamb, beef, pork and turkey with different salt, fat and moisture contents, among others. Derived values like the reflected power (P_r), the transmitted power (P_t), the tan delta ($\tan\delta$), and the penetration depth (d_p) are used to compare the different behaviours (see Fig 4.17). Although it is not helpful for the lack of temperature dependency, some interesting conclusions can be derived.

Calculated parameter	Equation	Units	Source
Power reflected (Pr)	$P_r = \left(\frac{\sqrt{\epsilon'} - 1}{\sqrt{\epsilon'} + 1} \right)^2$	%	Buffler (1993)
Power transmitted (Pt)	$P_t = 1 - P_r$	%	Buffler (1993)
Tan Delta (Tan δ)	$\tan \delta = \frac{\epsilon''}{\epsilon'}$	Dimensionless	Engelder and Buffler (1991)
Penetration Depth (d_p)	$d_p = \frac{i\sqrt{2}}{2\pi} \left\{ \epsilon' \left[\sqrt{1 + \left(\frac{\epsilon''}{\epsilon'} \right)^2} - 1 \right] \right\}^{-1/2}$	cm	Buffler (1993)

Fig 4.17. Equations used for the derived dielectric parameters [116]

In general, for most of the meats and ingredients measured, ϵ' and P_r and more noticeably ϵ'' , $\tan\delta$ and d_p tend to decrease with increasing frequency while P_t tends to increase with increasing frequency. At 2,450 MHz, strong correlations are noted between ϵ' vs moisture, ϵ'' vs moisture, fat and to a lesser extent, protein, $\tan\delta$ vs protein and also d_p vs moisture, protein or fat.

Later in 2007, the work focused on three specific components: fat, water and salt [117]. In this case, the dielectric properties were measured at 23 °C at 27.12, 915 and 2,450 MHz.

At frequencies between 300 and 3,000 MHz, ϵ'' increased with increasing salt content. The addition of salts tends to elevate ϵ'' as a consequence of the addition of conductive charge carriers. At all measured frequencies, increasing salt content also had a negative effect on the d_p . It is also worth noting that at all frequencies, an inverse relationship existed between ϵ'' and d_p . As ϵ'' increased at the higher salt concentrations, d_p decreased. Therefore, at microwave frequencies for a product with a high salt content, a substantial percentage of the incident electromagnetic radiation will be absorbed near the product's surface, leading to a significant temperature differential between the outer and inner regions of the product. All these comments can be seen graphically in Fig 4.18.

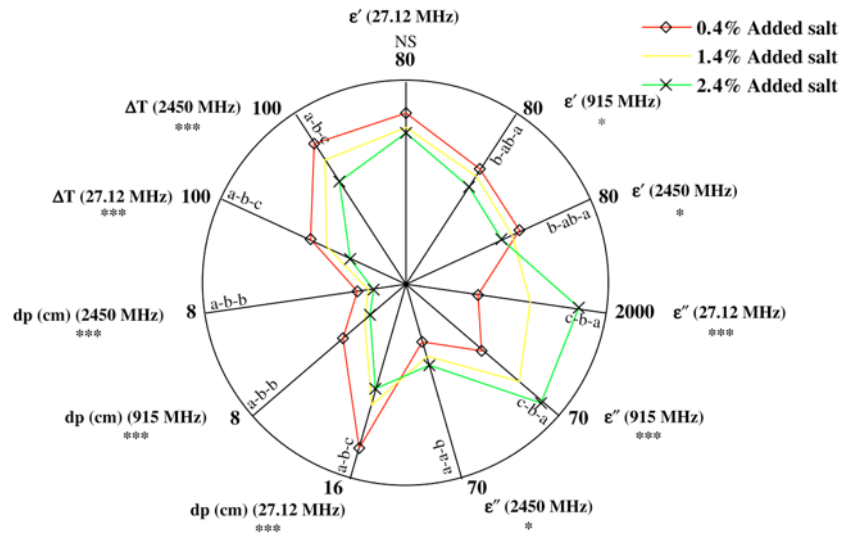


Fig 4.18. Effect of added salt on the dielectric properties of meat blends at 27.12, 915 and 2450 MHz and also their temperature rises (ΔT) following a standardised heating (450 W for 1 min 30 s) at 27.12 or 2450 MHz [117, Fig. 3].

Fig 4.19 shows the results of the measurements with added fat. From this graph can be obtained the following conclusions. The fat content increase depresses both ϵ' and ϵ'' values at all measured frequencies. It is thought that more fat content is related to a water reduction, explaining the lower microwave interaction with microwaves. Lower dielectric constant values are usually related to faster heating rates; however, it can be seen that the effect does not present significant ΔT improvements.

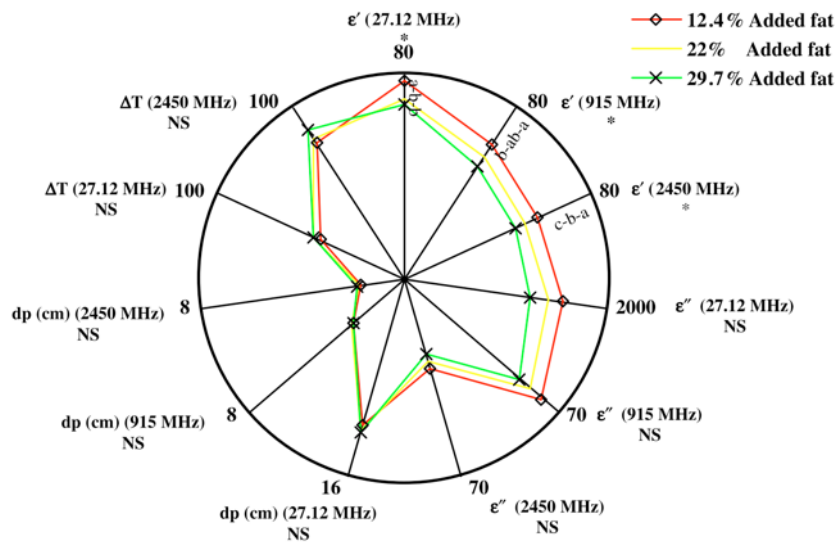


Fig 4.19. Effect of added fat on the dielectric properties of meat blends at 27.12, 915 and 2450 MHz and also their temperature rises (ΔT) following a standardised heating (450 W for 1 min 30 s) at 27.12 or 2450 MHz [117, Fig. 5].

Finally, the water content effect is analysed but with no meaningful information due to the high moisture content of the blends. However, their results agree with the current knowledge: ϵ' increases with the moisture content, and the higher the moisture content the higher the reduction in ϵ'' with the temperature increase [103].

In 2008, Farag et al. [118] presented a study of beef meat blends' dielectric and thermophysical properties over -18 to 10 °C. This study meets some of the requirements defined above: blends

are nearly homogeneous samples; their property values are consistent with other work, and the data is temperature and frequency dependent. They studied the dielectric and thermophysical properties at -18, -15, -10, -5, -3, -1, +1, +5 and +10 °C. The different blends are beef lean (with low fat content, 50:50 mixture and beef fat. The meat constituents can be seen in Fig 4.20. and the measurement results are shown in Fig 4.21.

Table 2
Proximate analysis of meat used in the study

Product	Moisture (%)	Fat (%)	Protein (%)	Ash (%)
Beef lean	67.8 ^a	11.8 ^c	17.9 ^a	0.8 ^a
50:50 mixture	48.2 ^b	36.1 ^b	13.7 ^b	0.6 ^b
Beef fat	26.3 ^c	65.7 ^a	7.8 ^c	0.3 ^c
SE	0.67	1.26	0.38	0.03

^{a,b,c} Means in the same column with unlike letters are different ($P < 0.05$).

Fig 4.20. Meat properties for the measurements [118]

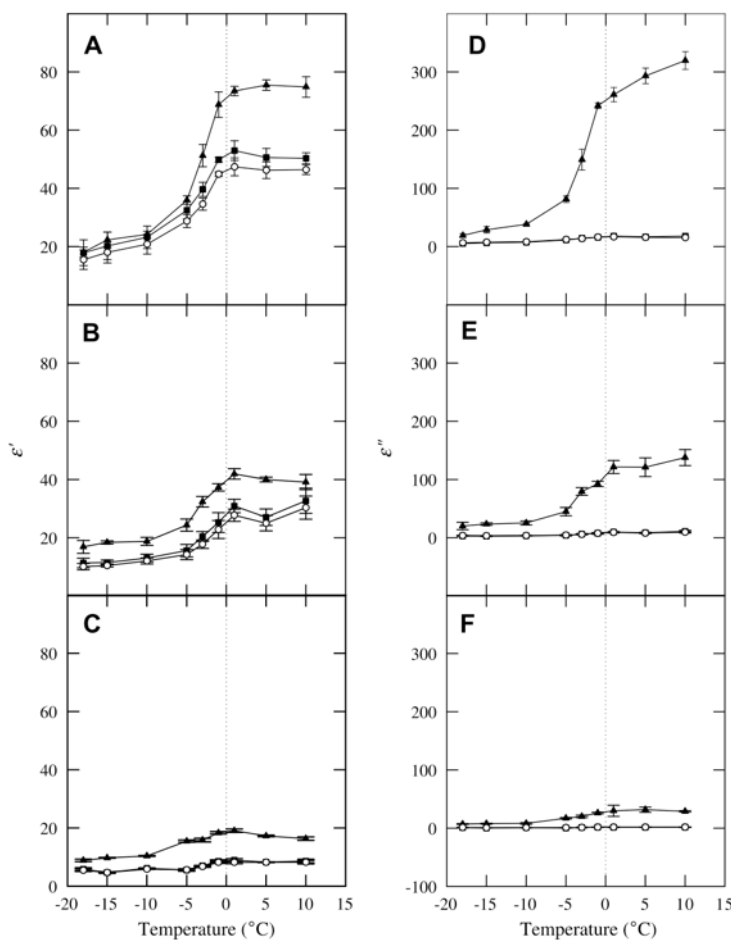


Fig. 2. Dielectric constant (ϵ') and loss factor (ϵ'') as functions of temperature and frequency (▲) 27.12 MHz; (■) 896 MHz and (○) 2450 MHz for (A/D) lean beef, (B/E) 50:50 mixture and (C/F) fat.

Fig 4.21. Dielectric properties measurements by Farag et al. [118, Fig. 2]

Another study with temperature dependency was presented by Trabelsi in 2015, in this case, with chicken meat [119]. The dielectric properties measurement equipment is an open-ended coaxial-line probe between 200 MHz and 20 GHz. The measurements were done at temperatures ranging from -20 to +25 °C and performed in a temperature-controlled chamber. The temperature

increments were 5°C for temperatures between -20 to -5 °C and +5 to +25 °C. For temperatures between -5 and +5 °C, more precision is needed, so the increment was +1 °C.

Their work pointed out, as can be seen in Fig 4.22, the following aspects of temperature-dependency of the dielectric properties:

- For temperatures below -2 °C, the dielectric properties are either frequency-independent or decrease slightly with frequency, which reflects the ice-like behaviour of the water in the chicken breast meat.
- For temperatures between 0 and 25 °C, the water molecule dipoles are freer to rotate with the electric field, and thus both ϵ' and ϵ'' are much higher than values measured below 0 °C.
- The range -2 to 0°C is affected by the phase change, where a total dipolar relaxation takes place at the T_f .

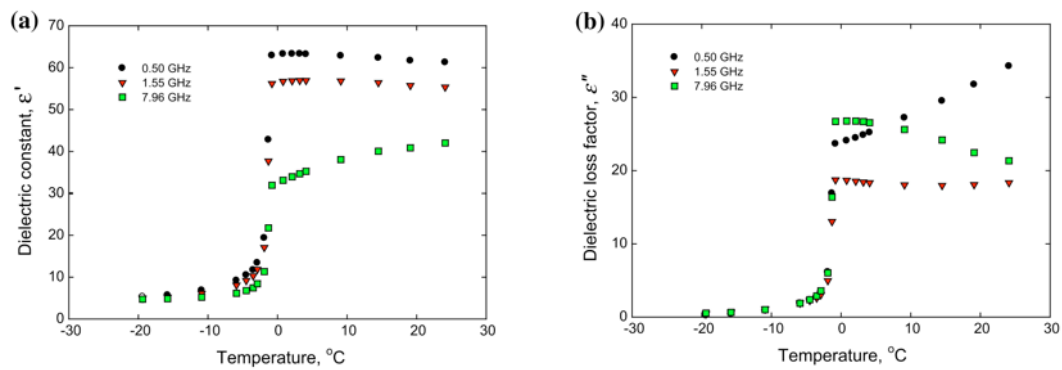


Fig 4.22. Temperature dependence of the dielectric constant (left) and the dielectric loss factor (right) of chicken breast meat [119, Fig. 6]

Gómez-Salazar presented in 2021 a paper on rabbit meat measuring [105]. They also used the open-ended coaxial measurement method. The obtained data agree with the equation proposed to define the dielectric constant (4.11), where a and b are regression constants. The R^2 is higher than 0.93 for each experiment.

$$\epsilon' = a \log_{10} f + b \quad (4.11)$$

The main conclusion is that ϵ' decreased with increasing temperature in the frequency range from 0.5 to 12 GHz. On the other hand, the loss factor generally increased with increasing temperature at low frequencies (< 2 GHz). Differences between the dielectric properties are related to changes in protein denaturation and shrinkage of the muscle fibres during the thermal process. With increasing temperature, muscles release intracellular fluids containing soluble constituents, including polar and ionic compounds.

4.3.1.1 Data summary.

The most important data retrieved in the previous papers have been arranged and compared to validate the results and make the best material choice. The data presented in each paper has been

processed with a graph scanner tool and set in tables that can be seen in Annex A. A summary of the information available for each kind of meat is shown in Table 4.2 - Table 4.6.

Table 4.2. Beef dielectric properties summary of the studied papers.

<i>Beef</i>					
Ref.	Author	Sample properties	Frequencies	Equations	Comments
[120]	Riedel 1957	Raw beef. Density 1.15 g/cm ³ . Wc 65%. No salt added	2,450 MHz	-	Enthalpy and ice content. Temperature range [-40,+80]°C
[87]	Bengtsson 1971	Raw beef	2,800 MHz	-	A validated reference in the field
		Cooked beef			
[121]	Ohlsson 1975	Raw beef. Wc 72.7%, Fat 2.7%	900 MHz	-	Temperature [40,140] °C
[104]	Sipahioglu 2003	Wc 70.6%, Ash 1.02%	2,450 MHz	(4.9) (4.10)	Compared with other authors.
[116]	Lyng 2004	Wc (%) 71.5, Protein (%) 21.3, Fat (%) 6.1, Ash (%) 0.83, Salt (%) 0.11	2,450 MHz	-	Mean value obtained from a heating process (4 to 65°C)
[122]	Brunton 2006	Raw beef	915, 2,450 and 3,000 MHz	-	Temperature [5,80] °C
[117]	Zhang 2007	Salt (%) 0.4, 1.4 and 2.4; Fat (%) 12.4, 22 and 29.7; Water (%) 21, 25 and 29	915 and 2,450 MHz	-	Results in ANOVA radial format. Measured at 23 °C
[118]	Farg 2008	Beef lean. Wc 67.8%, Fat 11.8%, Protein 17.9%, Ash 0.8%	896 and 2,450 MHz	-	Thermophysical properties measurements
		50:50. Wc (%) 67.8, Fat (%) 11.8, Protein			

		(%) 17.9, Ash (%) 0.8			
		Fat. Wc (%) 67.8, Fat (%) 11.8, Protein (%) 17.9, Ash (%) 0.8			

Table 4.3. Chicken dielectric properties summary of the studied papers.

<i>Chicken</i>					
Paper	Author	Sample properties	Frequencies	Equations	Comments
[104]	Sipahioglu 2003	Chicken breast. Mc (%) 74.8 Ash (%) 1.02	2,450 MHz	(4.9) (4.10)	Compared with other authors.
[101]	Lyng 2004	Chicken breast. Mc (%) 73.6, Protein (%) 24.3, Fat (%) 1.2, Ash (%) 0.86, Salt (%) 0.13	2,450 MHz	-	Mean value obtained from a heating process (4 to 65°C)
[123]	Trabelsi 2012	Chicken breast. Mc (%) 75. Different water holding capacity and pH	500 MHz and 8 GHz	-	
[119]	Trabelsi 2015	Chicken breast	From 200 MHz to 20 GHz	-	Temperature range [-19.4 , +25] °C

Table 4.4. Lamb dielectric properties summary of the studied papers.

<i>Lamb</i>					
Paper	Author	Sample properties	Frequencies	Equations	Comments
[101]	Lyng 2004	Lamb leg. Mc (%) 73.0, Protein (%) 21.9, Fat (%) 3.6,	2,450 MHz	-	Mean value obtained from a heating process (4 to 65°C)

		Ash (%) 1.48, Salt (%) 0.14			
--	--	-----------------------------	--	--	--

Table 4.5. Pork dielectric properties summary of the studied papers.

<i>Pork</i>					
Paper	Author	Sample properties	Frequencies	Equations	Comments
[116]	Zhang 2004	Pork luncheon roll. Mc (%) 60.4, Fat (%) 15.1, Protein (%) 11.3, Carbohydrate (%) 11.4, Ash (%) 1.8, Salt (%) 1.2	896, 915 and 2,450 MHz	-	Thermophysical properties too
		White pudding. Mc (%) 61.2, Fat (%) 15.8, Protein (%) 10.8, Carbohydrate (%) 9.1, Ash (%) 3.1, Salt (%) 2.3			
[101]	Lyng 2004	Pork shoulder. Mc (%) 73.9, Protein (%) 20.1, Fat (%) 4.4, Ash (%) 1.13, Salt (%) 0.08	2,450 MHz	-	Mean value obtained from a heating process (4 to 65°C)
		Pork back. Mc (%) 19, Protein (%) 3.9, Fat (%) 76.1, Ash (%) 0.2, Salt (%) 0.07			
[117]	Zhang 2007	Pork batter. Salt (%) 0.4, 1.4 and 2.4; Fat (%) 12.4, 22 and 29.7; Water (%) 21, 25 and 29	915 and 2,450 MHz	-	Results in ANOVA radial format. Measured at 23 °C

Table 4.6. Turkey dielectric properties summary of the studied papers.

<i>Turkey</i>					
Paper	Author	Sample properties	Frequencies	Equations	Comments
[116]	Lyng 2004	Turkey breast. Mc (%) 74.5, Protein (%) 24.1, Fat (%) 0.4, Ash (%) 0.98, Salt (%) 0.07	2,450 MHz	-	Mean value obtained from a heating process (4 to 65°C)

From the information available in these tables, it is decided to work with beef meat. There is enough dielectric and thermophysical properties data available at the two most interesting working frequencies, with temperature constituents' dependency information. In the beef summary, there are more references shown than in the previous section. Once it has been seen that is the best choice, more research has been carried out.

Fig 4.23 - Fig 4.26 compare the different dielectric property values at 915 and 2,450 MHz retrieved from the available data. In these graphs, it can be seen the high agreement between the authors at 2,450 MHz (there is more data, though) than for 915 MHz. It is interesting to see that the data provided by Bengtsson and Farag are similar. The dielectric loss factor at 915 MHz (see Fig 4.26), for instance, has a similar tendency even though the measurements are taken at different temperatures.

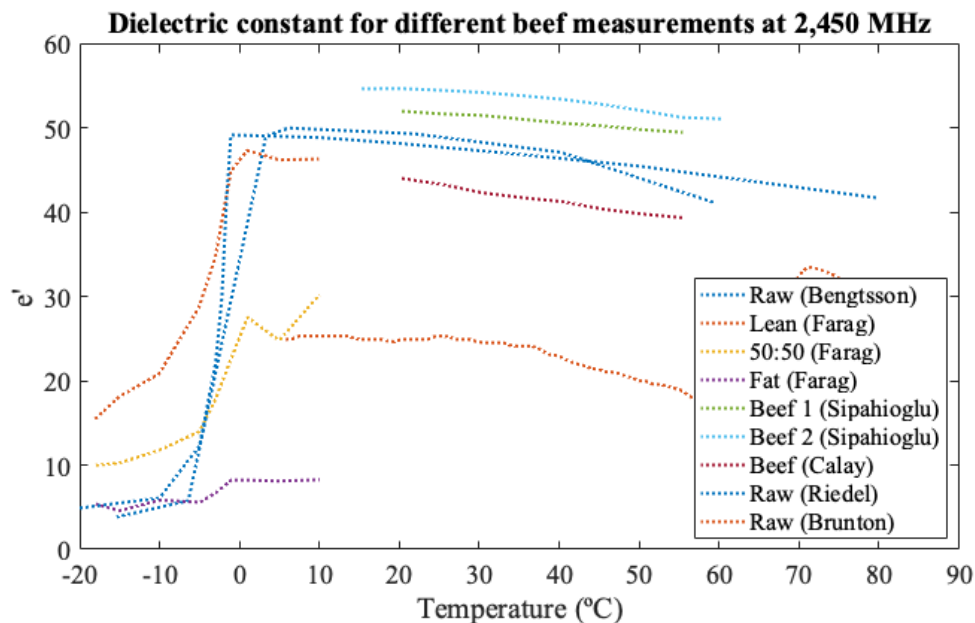


Fig 4.23. Dielectric constant comparison @ 2,450 MHz.

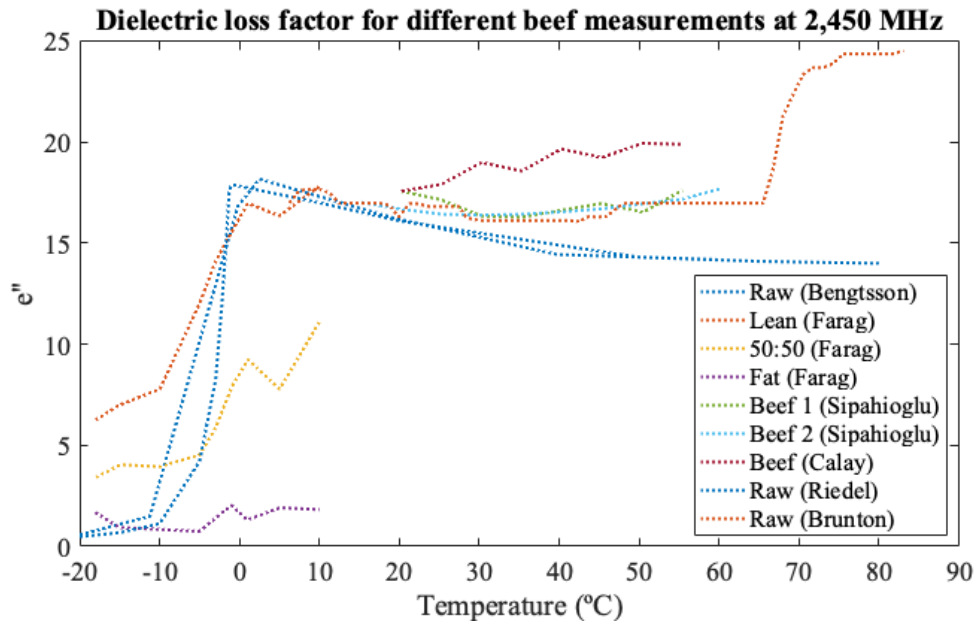


Fig 4.24. Dielectric loss factor comparison @ 2,450 MHz.

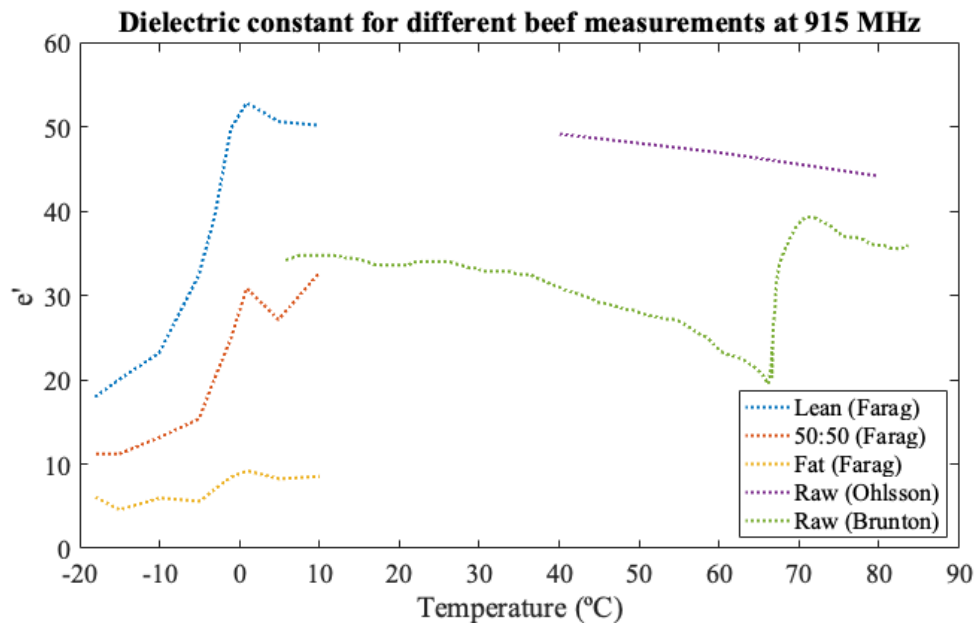


Fig 4.25. Dielectric constant comparison @ 915 MHz.

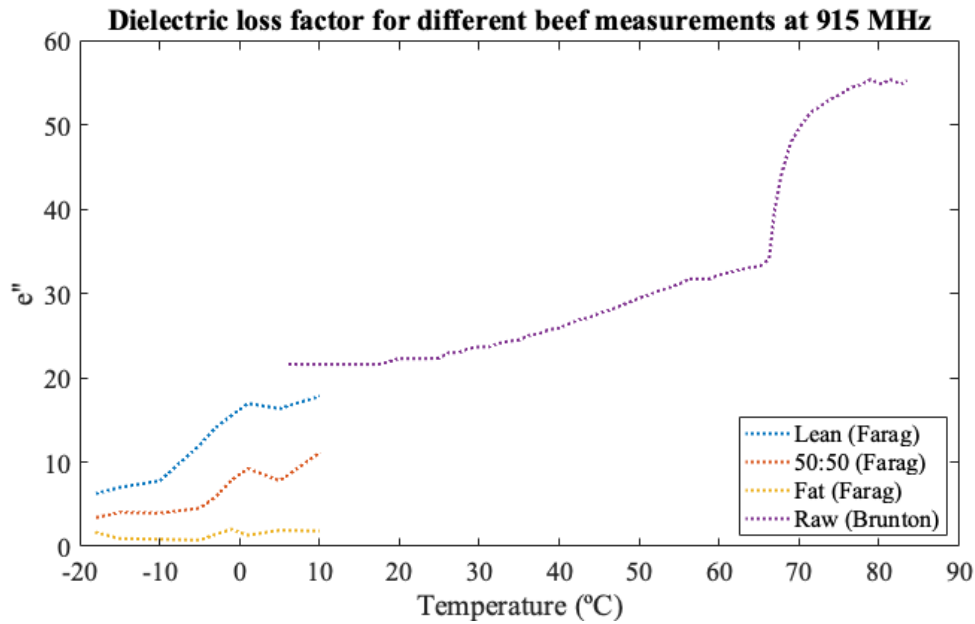


Fig 4.26. Dielectric loss factor comparison @ 915 MHz.

4.3.2. Beef meat defrosting and tempering.

Within the extensive data available in the literature, the study presented by Farag in [118] meets the temperature range of interest to the current project. The most interesting composition is lean beef, whose constituents are 67.8% moisture, 11.8% fat, 17.9% protein, and 0.8% ash. The fusion temperature for beef meat is $T_f = -1.76$ °C. This composition is also used for the mass and volume fractions needed in the thermophysical equations.

The functions or equations used to define a material's property in Comsol Multiphysics can be introduced in three possible ways [124]:

- Analytic: Specifies the properties as functions of one or more arguments or as independent variables, such as temperature or pressure. First, the mathematical expression defining the function is introduced. Later, the arguments and their value range are entered.
- Interpolation: It is used to describe properties that are defined by a table or file containing values of the function at discrete points, also named paired values. Later, the function behaviour between the data points and outside the data range is specified.
- Piecewise: This method is useful for describing properties with different definitions at different intervals. One can enter the start and end points for each interval and the function relevant to each interval, as well as choose the interpolation and extrapolation methods.

The figure displays two screenshots of a software interface for defining interpolation functions. The left pane shows a tree view of material properties, with 'Real permittivity (e1)' selected in the top screenshot and 'Imaginary permittivity (e2)' selected in the bottom screenshot. The right pane shows the 'Definition' dialog for the selected property, with 'Local table' as the data source and a table of temperature (t) vs. function value (f(t)).

Top Screenshot: Real permittivity (e1)

Definition dialog:

- Data source: Local table
- Function name: e1

t	f(t)
255	15.5
258	18.1
263	20.85
268	28.71
270	34.51
272	44.88
274	47.36
278	46.24
283	46.35

Bottom Screenshot: Imaginary permittivity (e2)

Definition dialog:

- Data source: Local table
- Function name: e2

t	f(t)
255	6.25
258	6.99
263	7.78
268	12
270	14.13
272	15.55
274	17
278	16.35
283	17.83

Fig 4.27. Interpolation functions for the dielectric properties' definition in the model.

In this case, the relative permittivity and loss factor are defined in the interpolation format. Fig 4.27 shows how the data (in the -18 to +10 °C temperature range and 2,450 MHz) has been introduced into the software.

The piecewise function has been used twice: the heat capacity, different equations for water in the frozen and unfroze regions, and the ice content, reflected in (4.7). The rest of the thermophysical properties have been introduced with analytical functions. These functions put together the equations in Table 4.1 and the law of addition equations (4.1) - (4.6). However, this procedure leads to very long equations, with a high risk of committing a writing error. The following equation for the thermal conductivity is shown as an example:

$$\begin{aligned}
TC = & (5.7109E - 1 + 1.7625E - 3 * t - 6.7036E - 6 \\
& * t^2)^{(w/(9.9718E2 + 3.1439E - 3 * t - 3.7574E \\
& - 3 * t^2)) * (1.8071E - 1 - 2.7604E - 4 * t \\
& - 1.7749E - 7 * t^2)^{(f/(9.2559E2 - 4.1757E - 1 \\
& * t)) * (2.2196 - 6.2489E - 3 * t + 1.0154E - 4 \\
& * t^2)^{(ic/(9.1689E2 - 1.3071E - 1 * t))} \\
& * (3.2962E - 1 + 1.4011E - 3 * t - 2.9069E - 6 \\
& * t^2)^{(a/(2.4238E3 - 2.8063E - 1 * t))} \\
& * (1.7881E - 1 + 1.1958E - 3 * t - 2.7178E - 6 \\
& * t^2)^{(p/(1.3299E3 - 5.1840E - 1 * t))}
\end{aligned} \tag{4.12}$$

Where t is the temperature, w is the water percentage, f is the fat content, ic is the ice content, a is the ash percentage, and p is the protein content.

4.3.2.1 Thermophysical equations refinement.

Another option for the thermophysical parameter definition provided by the software is used to cope with the equation lengths problem presented above. The definitions section inside the component permits defining variable tables. In our case, the equations have been ordered according to the thermophysical parameter.

Fig 4.28 shows the equations related to the water definitions. Comsol operates with the temperature in Kelvins and is needed a variable conversion for the equations, T_{cal} . This table integrates the equations for the water and ice percentages according to the equations presented earlier in subsection 4.2.1.1 and the Debye equations for the water dielectric properties (explained in Chapter 2). Fig 4.29 shows the density variables table, with the constituents' densities and the law of addition equation.

Fig 4.30 contains the thermal conductivity equations, including the mixing methods described previously in the text. Fig 4.31 shows the specific heat capacity equations, improving the simple equations by considering the dry solid content and the apparent specific heat.

Name	Expression	Unit	Description
Tcal	T-273.16	K	Temperature conversion to °C
Fi	$\text{if}(T < T_f, 1 - 1.105 / (1 + 0.7138 / \log(T_f - T + 1)), 1)$		Liquid water volume
dFidTA...	$\text{if}(T < T_f, 1.105 * 0.7138 / ((T_f - T + 1) * (\log(T_f - T + 1) + 0.7138)^2), 0)$		Fi derived
Xice	$(1 - Fi) * X_w$		Ice percentage
theta	$1 - 300 / T$	1/K	Temp. change of variable
e0	$77.66 - 103.3 * \text{theta}$	1/K	static dielectric constant water
einf	$0.066 * e_0$	1/K	infinity dielectric constant water
relaxf	$(20.27 + 146.5 * \text{theta} + 314 * \text{theta}^2) * 1E9$ [1/s]		Relaxation frequency
erDeb	$(e_0 - \text{einf}) / (1 - j * (f_0 / \text{relaxf})) + \text{einf}$		Debye equation

Fig 4.28. Water variables in Comsol Multiphysics.

Name	Expression	Unit	Description
Dw	$(9.9718E2 + 3.1439E-3 \cdot T_{cal} - 3.7574E-3 \cdot T_{cal}^2)$		Water density
Dfat	$(9.2559E2 - 4.1757E-1 \cdot T_{cal})$	K	Fat density
Dice	$(9.1689E2 - 1.3071E-1 \cdot T_{cal})$	K	Ice density
Dash	$(2.4238E3 - 2.8063E-1 \cdot T_{cal})$	K	Ash density
Dprot	$(1.3299E3 - 5.184E-1 \cdot T_{cal})$	K	Protein density
Dfib	$(1.3115E3 - 3.6589E-1 \cdot T_{cal})$	K	Fiber density
SumFV	$X_w \cdot Fi/D_w + X_{fat}/D_{fat} + X_{ice}/D_{ice} + X_{ash}/D_{ash} + X_{prot}/D_{prot} + X_{fib}/D_{fib}$		Partial law addition
density	$1/SumFV$		Law addition

Fig 4.29. Density variables in Comsol Multiphysics.

Name	Expression	U	Description
Tcw	$(5.7109E-1 + 1.7625E-3 \cdot T_{cal} - 6.7036E-6 \cdot T_{cal}^2)$		Water thermal conduct.
Tcfat	$(1.8071E-1 - 2.7604E-4 \cdot T_{cal} - 1.7749E-7 \cdot T_{cal}^2)$		Fat thermal conduct.
Tcice	$(2.2196 - 6.2489E-3 \cdot T_{cal} + 1.0154E-4 \cdot T_{cal}^2)$		Ice thermal conduct.
Tcash	$(3.2962E-1 + 1.4011E-3 \cdot T_{cal} - 2.9069E-6 \cdot T_{cal}^2)$		Ash thermal conduct.
Tcprot	$(1.7881E-1 + 1.1958E-3 \cdot T_{cal} - 2.7178E-6 \cdot T_{cal}^2)$		Protein thermal conduct.
Tcfib	$(1.8331E-1 + 1.2497E-3 \cdot T_{cal} - 3.1683E-6 \cdot T_{cal}^2)$		Fibers thermal conduct.
Tcpl	$(X_w \cdot Fi/D_w \cdot T_{cw} + X_{ice}/D_{ice} \cdot T_{cice} + X_{fat}/D_{fat} \cdot T_{cfat} + X_{ash}/D_{ash} + T_{cprot} \cdot X_{prot}/D_{prot} + T_{cfib} \cdot X_{fib}/D_{fib})/SumFV$		Parallel addition
Tcpp	$SumFV/(X_w \cdot Fi/D_w \cdot T_{cw} + X_{ice}/D_{ice} \cdot T_{cice} + X_{fat}/D_{fat} \cdot T_{cfat} + 1/T_{cash} \cdot X_{ash}/D_{ash} + 1/T_{cprot} \cdot X_{prot}/D_{prot} + 1/T_{cfib} \cdot X_{fib}/D_{fib})$		Perpendicular addition
Tcc	$gamma \cdot T_{cpp} + (1 - gamma) \cdot T_{cpl}$		Mixed thermal conduct.

Fig 4.30. Thermal conductivity variables in Comsol Multiphysics.

Name	Expression	Uni	Description
Cpwu	$(4.1289 - 5.3062E-3 \cdot T_{cal} + 9.9516E-4 \cdot T_{cal}^2) \cdot 1000$		Water under 0°C specific heat
Cpwo	$(4.1289 - 9.0864E-5 \cdot T_{cal} + 5.4731E-6 \cdot T_{cal}^2) \cdot 1000$		Water over 0°C specific heat
Cpfat	$if(T_{cal} < -40, (1.9842 + 1.4733E-3 \cdot (-40) - 4.8008E-6 \cdot (-40)^2), if(T_{cal} > 150, (1.9842 + 1.4733E-3 \cdot 150 - 4.8008E-6 \cdot 150^2), (1.9842 + 1.4733E-3 \cdot T_{cal} - 4.8008E-6 \cdot T_{cal}^2))) \cdot 1000$		Fat specific heat
Cpash	$if(T_{cal} < -40, (1.0926 + 1.8896E-3 \cdot (-40) - 3.6817E-6 \cdot (-40)^2), if(T_{cal} > 150, (1.0926 + 1.8896E-3 \cdot 150 - 3.6817E-6 \cdot 150^2), (1.0926 + 1.8896E-3 \cdot T_{cal} - 3.6817E-6 \cdot T_{cal}^2))) \cdot 1000$		Ash specific heat
Cpprot	$if(T_{cal} < -40, (2.0082 + 1.2089E-3 \cdot (-40) - 1.3129E-6 \cdot (-40)^2), if(T_{cal} > 150, (2.0082 + 1.2089E-3 \cdot 150 - 1.3129E-6 \cdot 150^2), (2.0082 + 1.2089E-3 \cdot T_{cal} - 1.3129E-6 \cdot T_{cal}^2))) \cdot 1000$		Protein specific heat
Cpice	$if(T_{cal} < -40, (2.0623 + 6.0769E-3 \cdot (-40), if(T_{cal} > 150, (2.0623 + 6.0769E-3 \cdot 150), (2.0623 + 6.0769E-3 \cdot T_{cal}))) \cdot 1000$	K	Ice specific heat
Cpfib	$if(T_{cal} < -40, (1.8459 + 1.8306E-3 \cdot (-40) - 4.6509E-6 \cdot (-40)^2), if(T_{cal} > 150, (1.8459 + 1.8306E-3 \cdot 150 - 4.6509E-6 \cdot 150^2), (1.8459 + 1.8306E-3 \cdot T_{cal} - 4.6509E-6 \cdot T_{cal}^2))) \cdot 1000$		Fibers specific heat
Cpw	$if(T - 273.16 <= 0, Cpwu, Cpwo)$		Water specific heat selection
Cpss	$(Cpfat \cdot X_{fat} + Cpash \cdot X_{ash} + Cpprot \cdot X_{prot} + Cpfib \cdot X_{fib}) \cdot (1 + \tau_{ao})$		Dried solid specific heat
Integral	$1000 \cdot if(T <= T_f, if(T - 273.16 < -40, (4.1289 - 2.0623) \cdot (-40) + (-5.3062E-3 - 6.0769E-3) \cdot 2 \cdot (-40)^2 + 9.9516E-4 \cdot (-40)^3), (4.1289 - 2.0623) \cdot (273.16 - T) + (-5.3062E-3 - 6.0769E-3) \cdot T + 9.9516E-4 \cdot T^2)$		Integral for the refinement
Cpa	$Cpss + \tau_{ao} \cdot Cpice + \tau_{ao} \cdot Fi \cdot (Cpw - Cpice) + \tau_{ao} \cdot d(Fi, T) \cdot (\lambda_{\text{lambda}_0} - \text{Integral})$		Aparent specific heat
Ca	$1550 + 1260 \cdot X_{ss} - (X_w - 0.4 \cdot X_{prot}) \cdot \lambda_{\text{lambda}_0} \cdot (T - 273) / T_{cal}^2$		Specific heat
Cabs	$Ca \cdot (1 + \tau_{ao})$		Absolute specific heat

Fig 4.31. Specific heat capacity variables in Comsol Multiphysics.

4.3.2.2 Microwave heating studies in Comsol.

One of the multiphysics studies consists of a two steps study. This is the study predetermined or recommended by Comsol Multiphysics for microwave heating [125]. The study consists of a first frequency-domain electromagnetic study, followed by a time-domain heat transfer study. The multiphysics electromagnetic heating node is responsible for coupling the results of the electromagnetic study, i.e., the field pattern in the cavity creating an energy source, with the heat transfer study that applies the energy to the load during a time period.

This multiphysics method is valid as long as the dielectric properties of the load do not change (or the variation is not relevant) with the temperature evolution. Given the interest in modelling a beef sample's defrosting, thawing and tempering process, another type of study is needed.

The second option is a single-step study called Frequency-Transient. This study is used to compute temperature changes over time together with the electromagnetic field distribution in the frequency domain. It is crucial, however, to acknowledge the limitations of this method. Comsol's user guide says:

“Only use this study when the power transfer from the fields to any susceptible variables occurs at twice the angular frequency set by the study. In a large number of cases, the thermal time constant of an object of interest is substantially greater than the angular frequency of the

electromagnetic radiation. In order to solve the problem in the time domain, tens or hundreds of thousands of RF cycles need to be computed by the solver before the problem evolves to the periodic steady-state solution. By solving for the fields in the frequency domain, the change in the fields over a single RF cycle does not need to be resolved and thus the periodic steady state solution is reached much more rapidly. This means that the transient, thermal response of an object is computed by this study, but any (small) fluctuations in temperature over any given RF cycle are not.” [126]

If the modelling of a microwave heating process does not include the phase change, i.e., the initial temperature is above 5 °C, and the superior limit temperature is 100 °C. Most foods’ dielectric properties have a linear behaviour with a slight change in this temperature range.

4.3.2.3 Commercial Whirlpool oven comparison.

A comparison between the commercial, domestic microwave oven model and a series of heating measurements has been made to verify the proper functioning of the equations described above.

The model used is the Whirlpool MD 121 (Whirlpool Corporation, Michigan, USA). The calibration method used to obtain the actual power of the oven is the IEC 60705 standard. The measurement is made with a water load in a glass container. The water temperature is initially below ambient temperature and is raised to approximately ambient temperature by heating in the microwave oven. This procedure ensures that the heat losses and the heat capacity of the container have a minimum effect. The specific conditions of the tests are described here.

At the start of the test, the oven and the empty container are at ambient temperature (20 ± 5 °C). Potable water having an initial temperature of 10 ± 1 °C is used for the test. The water temperature is measured immediately before it is poured into the container. A quantity of $1,000 \pm 5$ g of water is added to the container and its actual mass obtained. The container is then immediately placed in the centre of the oven shelf, which is in its lowest normal position. The oven is operated and the time for the water temperature to attain 20 ± 2 °C is measured. The oven is then switched off and the final water temperature is measured within 60 s. It is important to stir the water before the measure.

The microwave output power is calculated from (4.13), where P is the microwave output power, in watts; m_w is the mass of water, in grams; m_c is the mass of the container, in grams; T_0 is the ambient temperature in Celsius degrees; T_1 and T_2 are the initial and final temperatures of the water, in Celsius degrees; and t is the heating time, in seconds, excluding the magnetron filament heating-up time.

$$P = \frac{4.187 \cdot m_w(T_2 - T_1) + 0.55 \cdot m_c(T_2 - T_0)}{t} \quad (4.13)$$

The microwave output power is stated in watts, rounded to the nearest 50W. The results throw that the oven’s efficiency is 73.78%. Therefore, the power value used for the model is 750 W.

The oven has been created in Comsol Multiphysics, as shown in Fig 4.32. The feeding ports are two, although the generation is made by a single 1 kW magnetron. The model also includes the rotating plate and the meat sample.

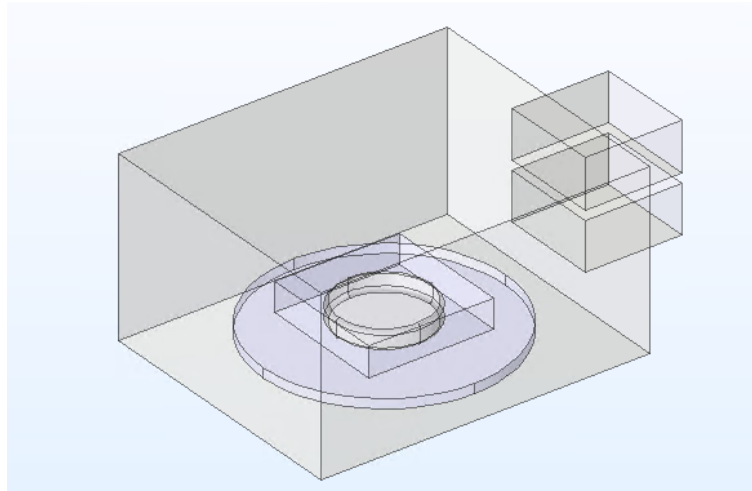


Fig 4.32. Whirlpool MD 121 geometries in Comsol.

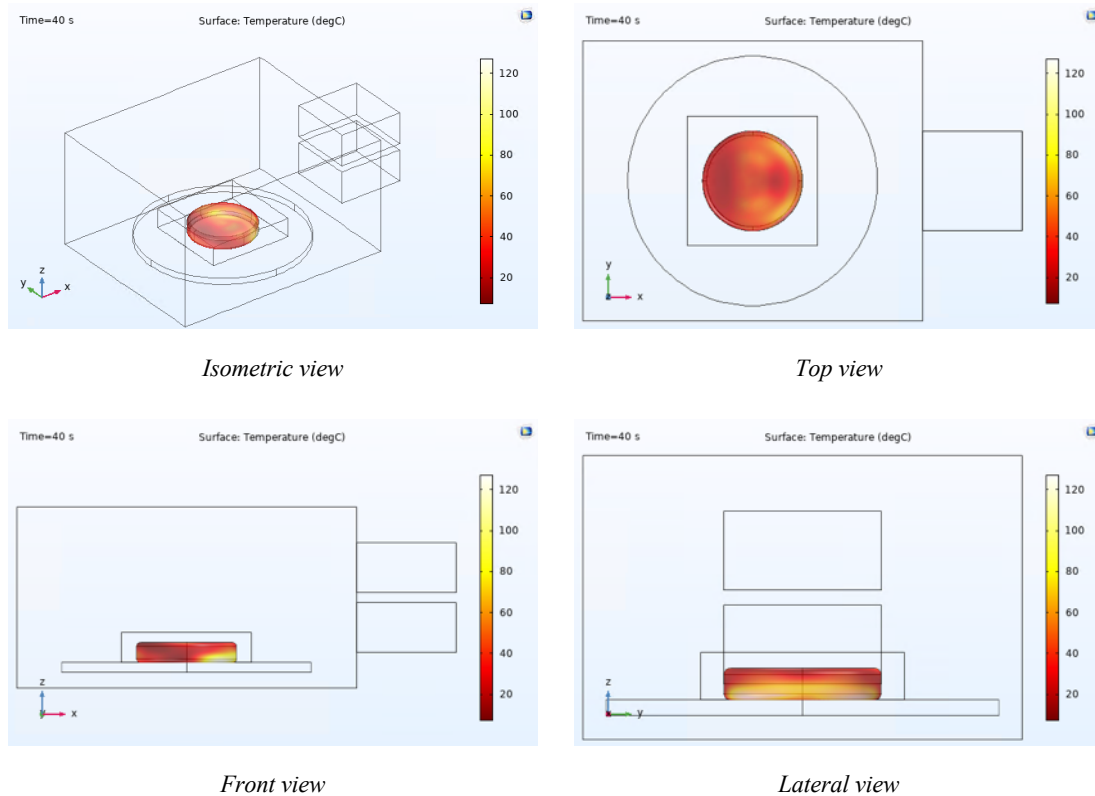


Fig 4.33. Multiphysics modelling of lean beef tempering after 40 seconds of heating.

The study consists of a one-minute single Frequency-Transient step at the 2,450 MHz working frequency. The results of the tempering study are shown in Fig 4.33.

The heating configuration is the same as the modelling. The meat batter (lean beef) has been prepared into cylindrical metallic recipients (two sizes) and frozen to $-18\text{ }^{\circ}\text{C}$. The samples are centred in the oven (see Fig 4.34), and full power is applied for 60 seconds. Every 20 seconds,

the sample is extracted, and the temperature measured with an IR camera. This is the only way to follow the process, even though it provokes discontinuity in the heating process. Fig 4.35 shows the measurement setup.

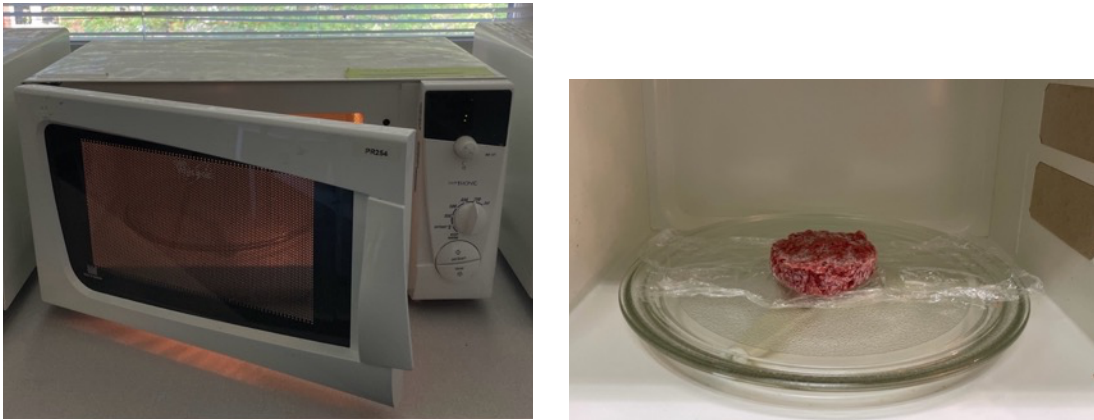
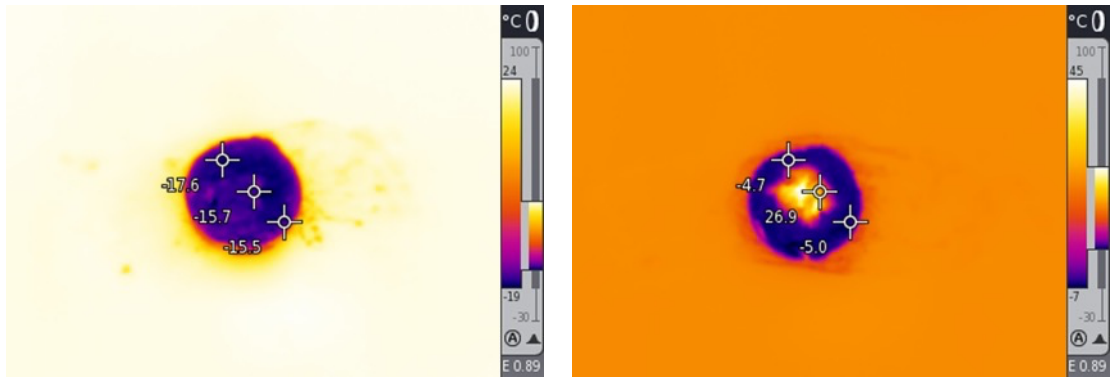


Fig 4.34. Commercial microwave oven (left) and frozen meat sample inside (right).

Fig 4.36 - Fig 4.39 show the thermal images of the four tested samples in four time steps: 0, 20, 40 and 60 seconds. Every $t_3=60\text{ s}$ from samples 2 to 4 has been taken with a dish below the beef sample to prevent the liquid spread created at higher temperatures, as shown in Fig 4.36 d).

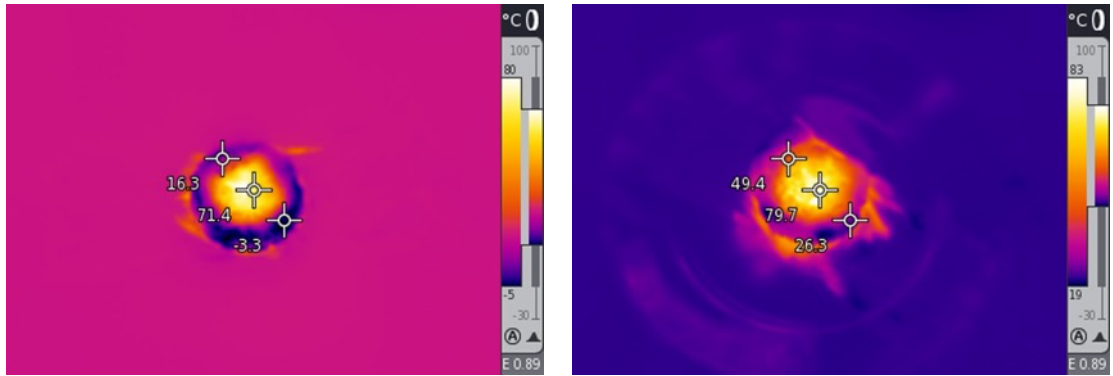


Fig 4.35. Temperature measurement setup at RISE's labs.



a) t_0

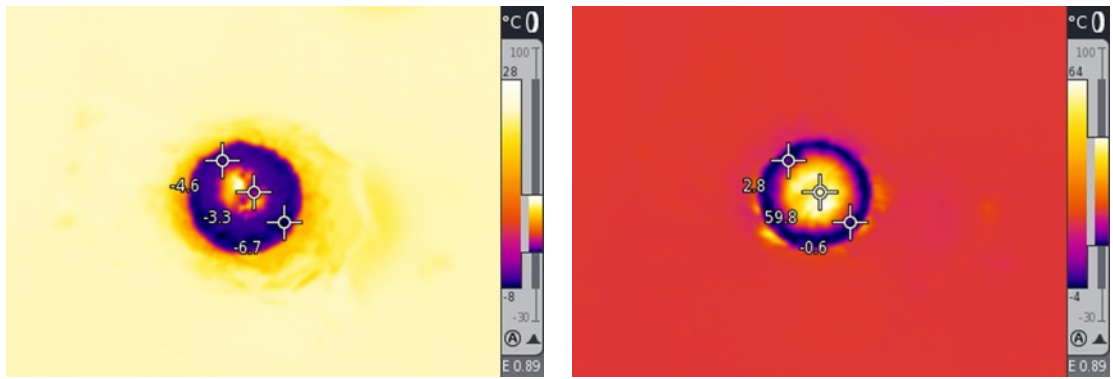
b) $t_1 = 20\text{ s}$



c) $t_2 = 40\text{ s}$

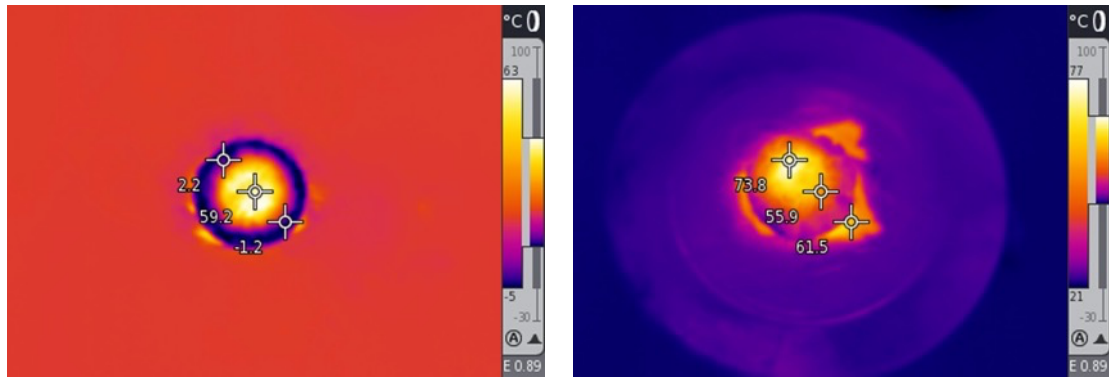
d) $t_3 = 60\text{ s}$

Fig 4.36. Sample 1 - small radius.



a) t_0

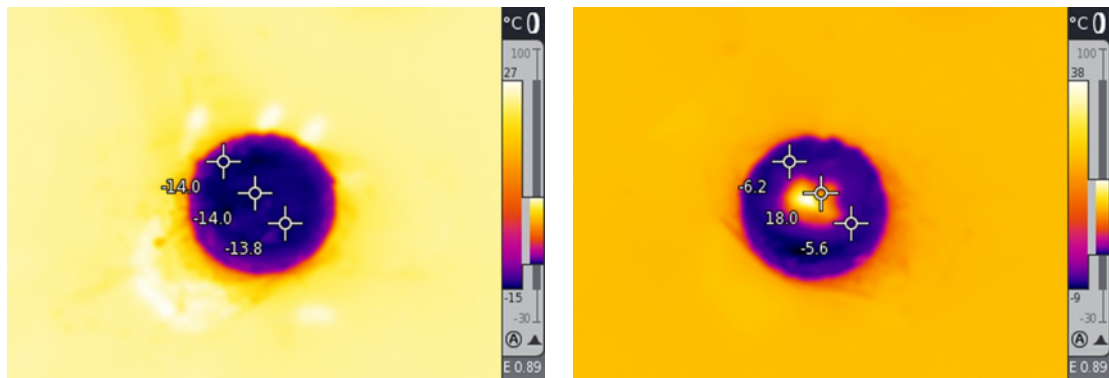
b) $t_1 = 20\text{ s}$



c) $t_2 = 40\text{ s}$

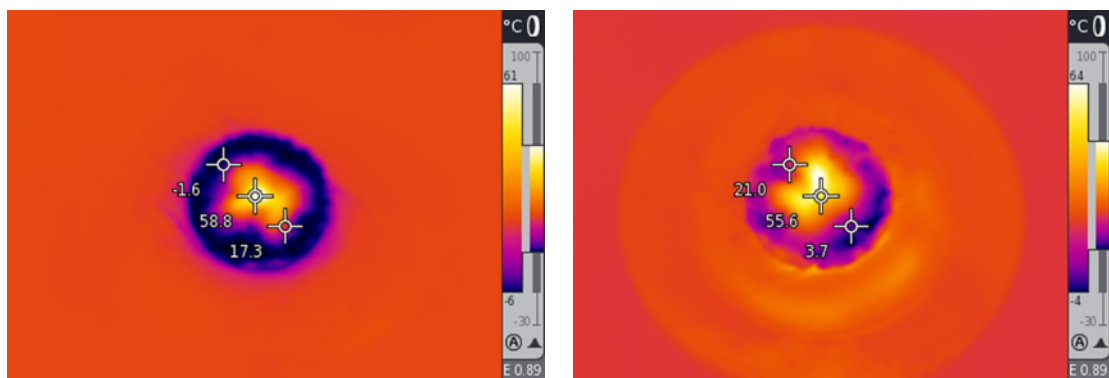
d) $t_3 = 60\text{ s}$

Fig 4.37. Sample 2 - small radius



a) t_0

b) $t_1 = 20\text{ s}$



c) $t_2 = 40\text{ s}$

d) $t_3 = 60\text{ s}$

Fig 4.38. Sample 3 – big radius.

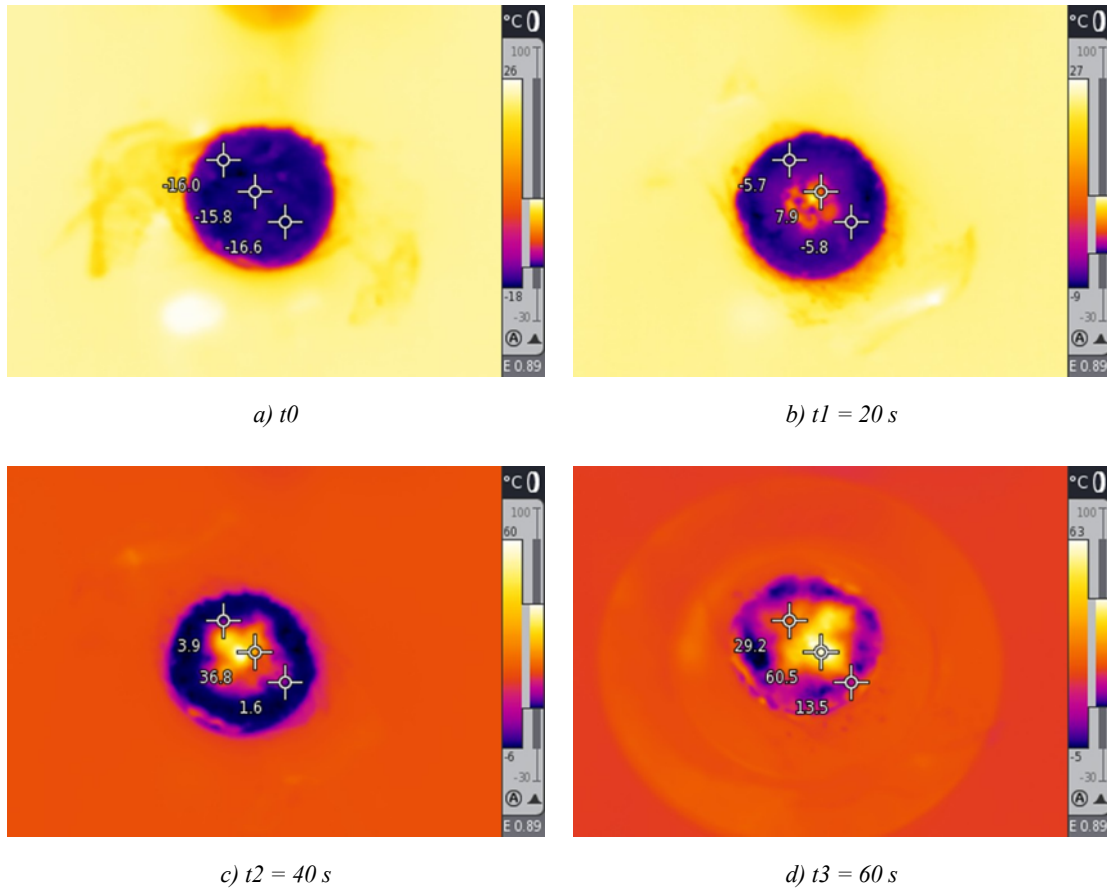


Fig 4.39. Sample 4 - big radius.

From these results can be extracted the following conclusions:

- The equations for the thermophysical properties are accurate.
- It needs refinement in the dielectric properties, mainly the melting region and for higher temperature values.
- The water created and leaked after the heating had not been modelled. It is very complex.
- An improvement in the plate's rotating effect is needed for the modelled to reflect the homogeneity of the measurements.

Despite the needed upgrades for the domestic oven modelling, the work developed is good enough to be used as "initial values" for future microwave modelling.

Chapter 5. Complementary devices design

Alongside the core research activities conducted during the thesis, several pieces of equipment came across during the work. The devices and studies explained in this chapter aim to fill a complementary-technology gap needed to achieve the thesis goals. They encompass an impedance matching device, a fast-heating microwave plate, and shielding elements for continuous ovens.

The impedance matching device was designed and discovered within the work done for the dielectric properties measurement device based on a coplanar waveguide structure explained in 4.1.1.3.

The second device is a fast-heating microwave plate. It responds to and fits into this project because of the need for hybrid microwave-convection heating systems in the food industry. It is, furthermore, a later development of the patent WO2016051003A1 [127] owned by Microbiotech S.L.

To conclude this chapter, the complete study carried out to design the protective elements that ensure the compliance with the electromagnetic compatibility (EMC) requirements of the industrial application explained in detail in Chapter 8 is described.

5.1. Impedance matching device.

A common concept intrinsically related to microwave devices and circuitry, i.e., antennas, filters, power dividers and combiners; is impedance matching. These elements must be matched to the feeding network connected. This allows to yield the best efficiency possible, i.e., obtaining antennas capable to reach longer distances (in far-field radiation cases), lowering the power consumption of the systems and reducing the working temperature range of the components used. In summary, it is a technique that ensures the maximum power transfer achieved by removing the reflected waves generated when a signal is transmitted between two devices with different characteristic impedance Z_0 .

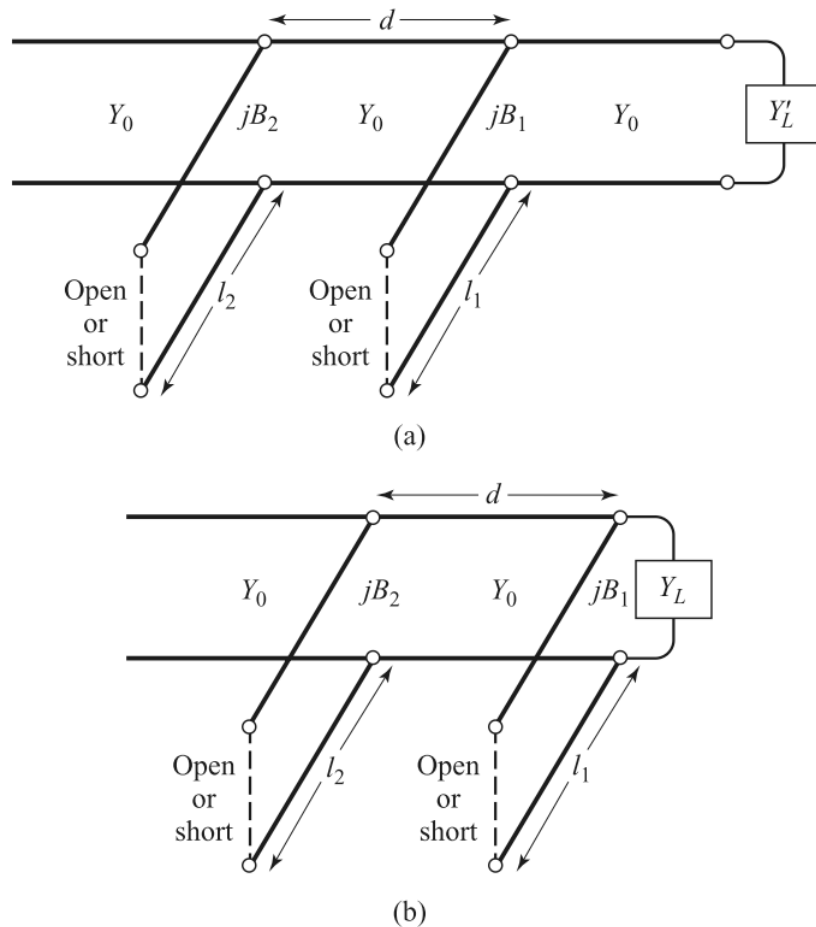


Fig 5.1. Double stub tuning. (a) Original circuit with the load an arbitrary distance from the first stub. (b) Equivalent circuit with the load displaced to the first stub [20, Fig. 5.7]

The interaction between microwaves and loads inside a cavity considerably changes throughout the heating process, which means that the matching of the antenna to the material being heated can vary from complete matching to maximum reflectivity. Hence, an adaptive impedance matching device was identified as a complementary device necessary for proper heating processes or lab works.

The most common and straightforward impedance matching network is the L-network configuration with two lumped elements (resistors, capacitors or inductors). Another way to design an impedance matching network is to use distributed elements, i.e., transmission lines. This type of impedance matching network is extensively explained by Pozar [20] (see Fig 5.1) and Ida [128] and can be used as adaptive impedance matching devices. A coaxial or stripline device (distributed elements) should be used to maintain the TEM-based device approach of the solid-state microwave generators, with the main advantage of frequency independence.

After a search for impedance matching devices in coaxial structure, the number of them available in the market capable of supporting high power inputs (i.e., N connectorized at least) is very low. Therefore, it was decided to work on a multipurpose device like the one explained in the previous chapter.

Prof. Elías De los Reyes worked on the design of a double slug matching impedance network using a TEM structure [129]. This method (see Fig 5.2) presents A and B as defined elements and

l and l_1 as the two degrees of freedom. So, the whole network presents an S_{22}^T with a variable amplitude according to l length while, length l_1 controls the phase. The network is matched when $Z = Z_0$.

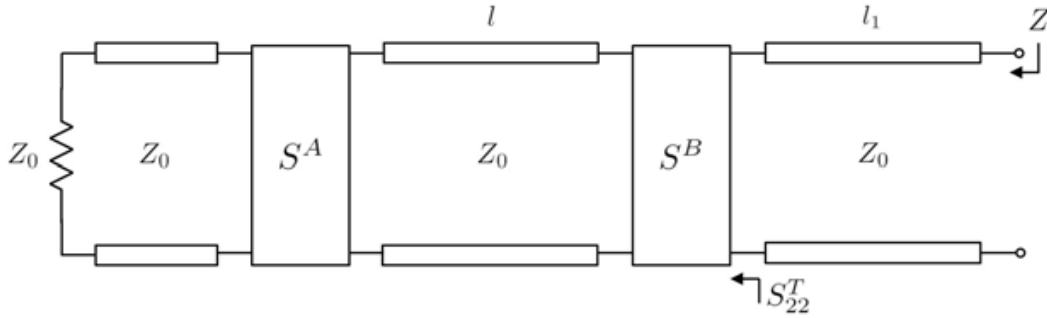


Fig 5.2. Schematic of the double slug impedance matching network.

5.1.1. Theoretical study and equations

The element A , representing a lossless reciprocal network, is characterised by the Scattering matrix (5.1)

$$[S^A] = \begin{bmatrix} S_{11}^A & S_{12}^A \\ S_{21}^A & S_{22}^A \end{bmatrix} \quad (5.1)$$

Element B can also be defined by the same Scattering matrix as in (5.2)

$$[S^B] = \begin{bmatrix} S_{11}^B & S_{12}^B \\ S_{21}^B & S_{22}^B \end{bmatrix} \quad (5.2)$$

In order to work with a simplified equation, element B and the line with length l can be described as a whole in (5.3), where β is the propagation constant $\beta = 2\pi/\lambda$.

$$[S_l^B] = \begin{bmatrix} S_{11}^B e^{-2j\beta l} & S_{12}^B e^{-2j\beta l} \\ S_{21}^B e^{-2j\beta l} & S_{22}^B e^{-2j\beta l} \end{bmatrix} \quad (5.3)$$

It is possible now to obtain the equation (5.4) of the aggregate of both elements A and B , S_{22}^T .

$$S_{22}^T = \frac{S_{22}^B - \Delta^B e^{-2j\beta l} S_{22}^A}{1 - S_{11}^B S_{22}^A e^{-2j\beta l}} \quad (5.4)$$

Where Δ^B is the determinant of $[S^B]$, assuming that it is symmetric:

$$\Delta^B = S_{11}^B S_{22}^B - S_{12}^B{}^2 \quad (5.5)$$

Considering that the reference planes are such that the matrixes S^A and S^B are (5.6) and (5.7), this determinant is $\Delta^B = 1$.

$$[S^A] = \begin{bmatrix} -\sqrt{1-a^2} & ja \\ ja & -\sqrt{1-a^2} \end{bmatrix} \quad (5.6)$$

$$[S^B] = \begin{bmatrix} -\sqrt{1-b^2} & jb \\ jb & -\sqrt{1-b^2} \end{bmatrix} \quad (5.7)$$

Then, introducing the following variable change:

$$\sqrt{1-a^2} = X \quad (5.8)$$

$$\sqrt{1-b^2} = Y \quad (5.9)$$

$$e^{-2j\beta l} = Z \quad (5.10)$$

equation (5.4) can be written as:

$$S_{22}^T = \frac{-Y + XZ}{1 - XYZ} \quad (5.11)$$

In (5.11), X and Y are complex constants.

Taking into account that $ZZ^* = 1$ is the equation of a circumference representing complex numbers with radius equal to one and $\lambda/2$ -periodic phase, (5.11) is the bilinear transformation of $ZZ^* = 1$ into another circumference in the (X,Y) plane.

The center, C, and radius, R, coordinates can be straightforwardly obtained:

$$C = \frac{-Y(1 - X^2)}{1 - X^2Y^2} \quad (5.12)$$

$$R = \frac{X(Y^2 - 1)}{1 - X^2Y^2} \quad (5.13)$$

The maximum and minimum values of the S_{22}^T module, when S_A and S_B are equal are:

$$S_{22_{MAX}}^T = \frac{X + Y}{1 + XY} = \frac{2\sqrt{1-a^2}}{2-a^2} = 1 \text{ if } a \ll 1 \quad (5.14)$$

$$S_{22_{MIN}}^T = \frac{Y - X}{1 - XY} = 0 \quad (5.15)$$

This condition implies that the Smith chart of impedance can be completely covered by adjusting the position of these two obstacles along the transmission line.

5.1.2. Coplanar waveguide structure

A microstrip is a transmission line made of a conductive strip on top of a dielectric sheet which, in general, includes a ground plane at the bottom of both elements. The constitutive elements of the conventional coplanar waveguide (CPW) structure are three conductive parts, and a dielectric one. Two of the conductive elements behave as the ground plane, and the other one is the active strip. These three metallic elements are on top of a dielectric sheet separated by two identical gaps giving the structure its characteristic aspect (see Fig 5.3).

The effective dielectric constant, the characteristic impedance of the line, and its attenuation are given by the central strip width (W), as well as the gap (g) between this strip and the lateral ground strips, their thickness (t) and the dielectric permittivity of the substrate (ϵ_r).

Due to the existence of three conducting elements, this structure supports two fundamental modes with zero cut-off frequency: 1) the known as “even mode”, with the same potential in the ground planes, and 2) the “odd mode” whose ground potentials show the same magnitude but opposite sign. Both modes are called “quasi-TEM” and present different effective dielectric constants and dispersion properties because of the resultant electric and magnetic fields (Fig 5.4).

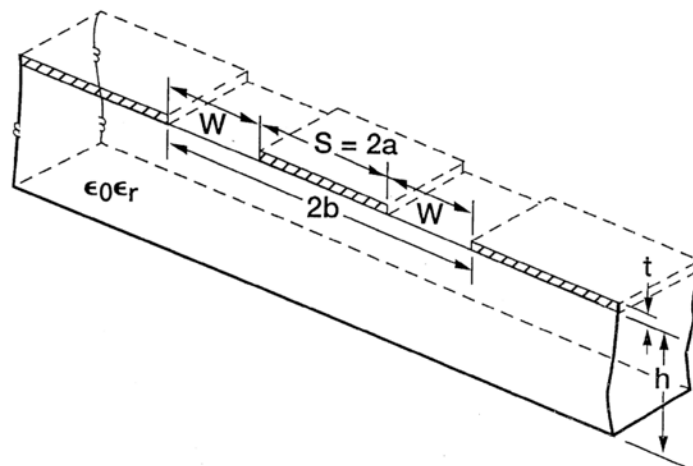


Fig 5.3. Schematic of a conventional CPW structure.

Fig 5.4 shows that the even mode presents symmetry regarding the symmetry plane, low dispersion, and generally is used for circuitry designs. Its electric field lines start (or end) at the central strip and end (or start) at the two ground planes. The magnetic field lines enclose the central conductor. If the current is conducted through the main strip, the current densities on the ground planes have opposite directions. On the other hand, electric field lines for the odd mode start at one ground plane and end in the other ground plane, meaning that the potentials of both ground planes have different signs, i.e., they present different potential.

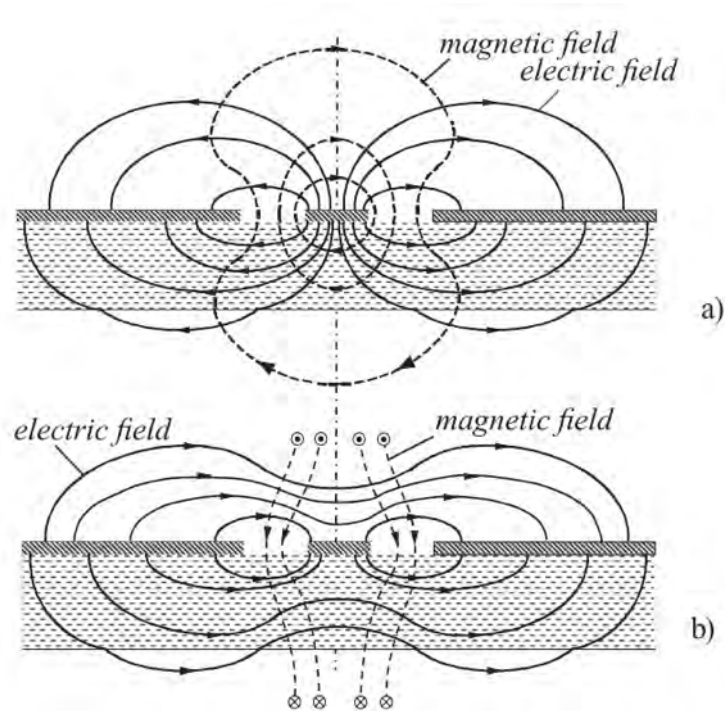


Fig 5.4. Electromagnetic field distribution for even (a) and odd (b) modes.

The characteristics of the even mode produce more significant losses than the odd mode. This can be related to the high electromagnetic field concentration within the gaps between conductors, leading to higher losses inside the main strip and the borders of the ground planes. Increasing the gap will reduce these losses and increase the dispersion, so a good agreement between losses and electromagnetic field dispersion must be chosen when designing these structures with a low-loss approach. However, this property is of great advantage for the present application because the aim is to transmit with a high and concentrated field distribution.

A metallic plane can be added at the bottom of the structure, although making the electric field of the even mode to be dispersed through the dielectric element. This dispersion is called “parallel-plate” and produces a parasite mode that affects the effective permittivity of the primary mode at very high frequencies. This effect can be suppressed, and the benefits of having an element that encloses somehow the electromagnetic radiation to the strip are really interesting.

Placing two metallic lateral plates is enough to suppress the named parasite modes. These plates connect the ground planes with the bottom one creating a short circuit and stopping the propagation of the prescribed mode.

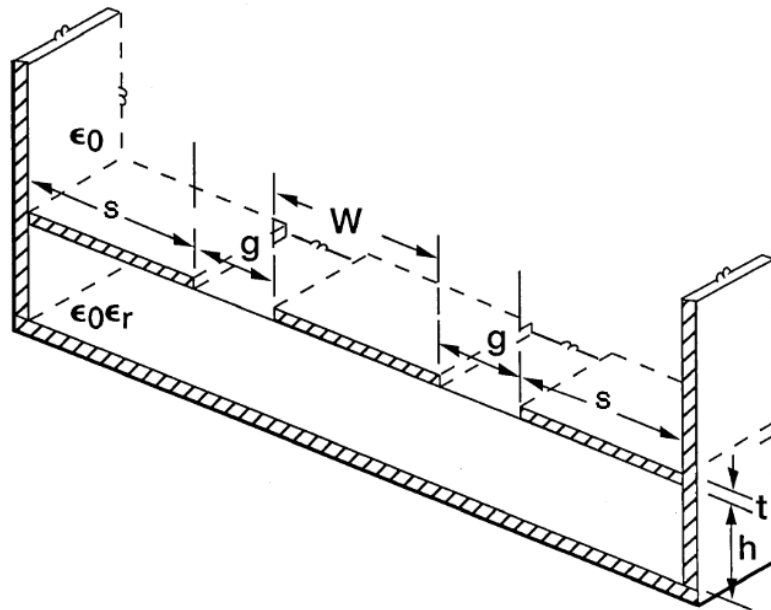


Fig 5.5. Coplanar waveguide schematic with lateral and bottom plates.

5.1.3. Implementation

The behaviour of this transmission line depends directly on the two gaps (g), the central conductor width (w), the total width (a) and the dielectric height (h), as well as the thickness of the metallic parts (t). All these design parameters can be seen in Fig 5.6.

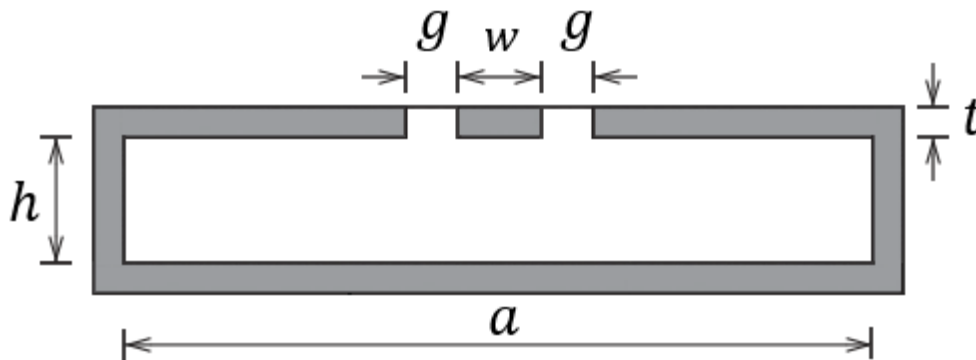


Fig 5.6. Front view of the CPW. Design parameters.

The material chosen for the dielectric part is Teflon[®] (PTFE). This material is easily machinable, relatively affordable and its dielectric properties fits the application: presents low losses and the permittivity value of 2.1 grants a good electromagnetic field distribution and propagation. The metallic parts are designed in aluminum and copper, two metals with good conductivity and mechanic rigidity.

The electromagnetic modelling tool HFSS has been used to evaluate the different dimensions and variables. It has been necessary to control the appearance of high order modes, especially when working at the frequencies 2.45 and 5.8 GHz. Once the CPW dimensions are defined (are those that shares the CPW dielectric properties measurement probe described in Chapter 3), the next step is to define the material and its thickness that is going to be used to create the obstacles

mentioned in subsection 5.1.1. of this chapter. An obstacle like the one designed, transforms the transmission line into a capacitor when placed on it. The capacitance is given by $C = \epsilon_0 \epsilon_r \frac{S}{d}$, so the most important material's property is the permittivity.

The obstacle width is set to 12 mm in order to cover completely the central strip and the gaps. A wider piece does not affect to the results. The other parameters, obstacle length, thickness and permittivity of the material are studied to find the optimum values.

The shorter the obstacle is, the closer the $|\rho|$ value is to the Smith chart's $|\rho_{MAX}|$. If a major part of the Smith chart wants to be covered, i.e., to be able to match nearly every impedance, the obstacle length should be 10 mm.

In order to cover most of the Smith chart it is necessary to evaluate what materials, i.e., permittivity values, are the best. At 2.45 GHz permittivity values above 5 offers a maximum radius of $|\rho| = 0.85$. With $\epsilon_r = 10$, this radius is extended to $|\rho| = 0.93$. Due to the effect of a lower frequency, the permittivity is set to 10 to assure the performance of the impedance matching system. The material used in this prototype (alumina), whose permittivity is around.

A parametric study including all the possible configurations of the two elements is done and the results are shown in Fig 5.7. The variety of impedances that can be covered and matched by this device shows its vast versatility for different microwave networks and devices.

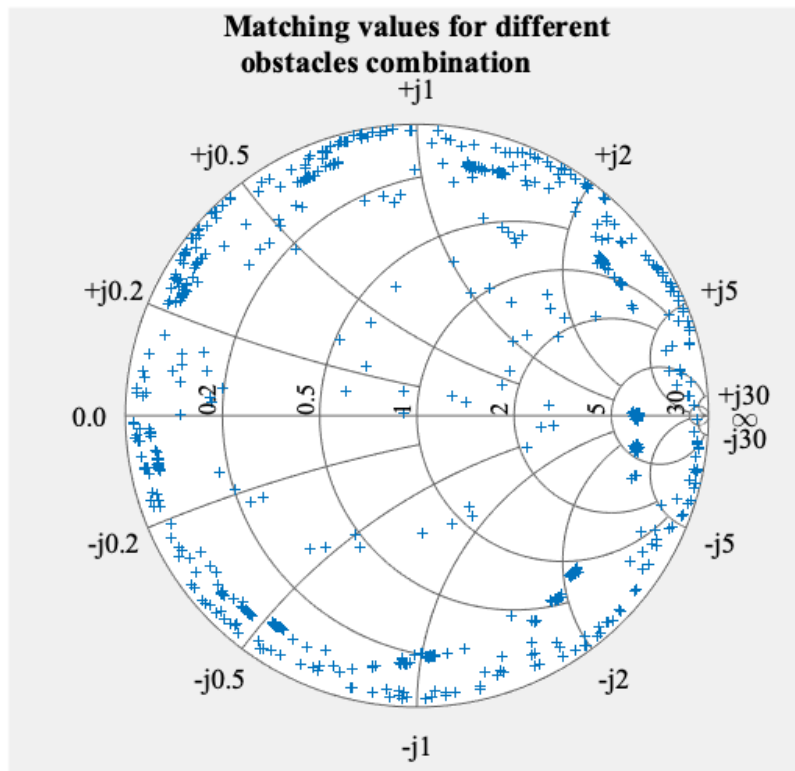


Fig 5.7. S_{11} parameter for a complete obstacle's position sweep combination.

The complete assembly of the prototype can be seen in CAD design (Fig 5.8) and manufactured (Fig 5.9). The alumina sheet is placed at the bottom of the lower metallic obstacle (the upper one is used to fix the obstacle in the transmission line).

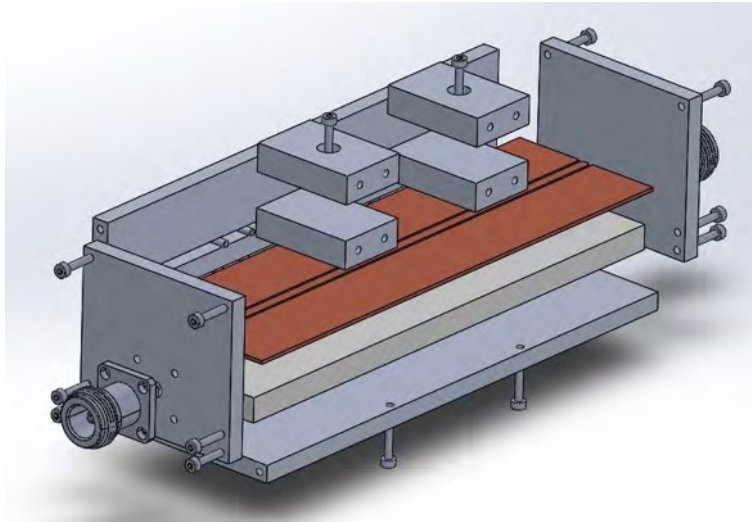


Fig 5.8. Exploded view of the assembly in CAD.



Fig 5.9. Manufactured impedance matching system prototype.

5.2. Fast heating microwave plate.

Chapter 2 describes how microwaves are related to the heat energy production. Prior to them, two different sources have been traditionally used: those based on electrical resistors and those based on the combustion of fossil fuels. The lack of control of electrical resistors and the environmental

impact of non-renewable sources lead to a problem that needs to be solved, when the interaction between the material to be heated and the microwaves is not possible.

The approach applied with this coplanar waveguide structure is to use electrical power (renewable sources can produce that) similarly to conventional systems but using dielectric electrothermal transducers instead of resistors.

Altogether with the typical microwave heating process, microwaves can transfer thermal energy by means of thermodynamic mechanisms (mainly radiation and conduction) materials that cannot be directly heated using microwave technology due to issues like their electromagnetic properties, size, etc.

A new fully lossy asymmetric stripline structure has been developed for that purpose. This kind of structure allows working with high input powers without any resonant structure or hazardous open ones. It may be used as a heater or combined within a microwave oven for hybrid heating.

5.2.1. Asymmetric stripline structure

Stripline structure refers to a strip sandwiched between ground planes [130]. It has also been classified into different types, depending on its relations: Zero-Thickness Centered Stripline (Fig 5.10), Centered Stripline (also known as Triplate® or Sandwich Line)(Fig 5.11), Off-center Stripline (Fig 5.12) or Shielded Stripline (Fig 5.13).

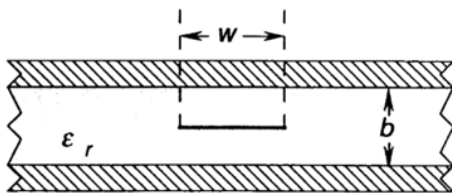


Fig 5.10. Zero-thickness Centered Stripline.

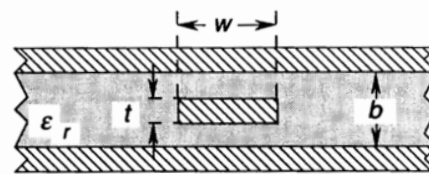


Fig 5.11. Centered Stripline.

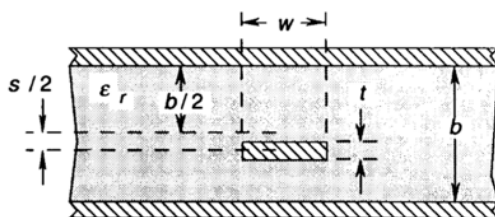


Fig 5.12. Off-centered stripline.

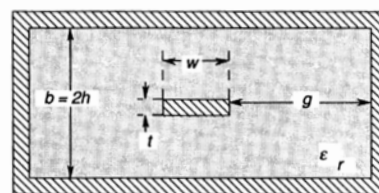


Fig 5.13. Shielded stripline.

The TEM structure used for the solution proposed is an enclosed (or shielded) asymmetric stripline. This structure allows minimising a microwave system, as far as TEM transmission lines do not need to have sizes comparable to the wavelength. The conventional asymmetric configuration consists of a strip closer to one ground plane than the other. The solution considered in this work it is even more asymmetric than the typical one because the dielectric materials are different on each side: while one of them is entirely lossless (Teflon®), the other one consists of a high susceptor ceramic [131], as it is shown in Fig 5.14. This will ensure that only one of the structure's faces is heated while the other remains cold. This structure could be named "Shielded off-centred asymmetric stripline".

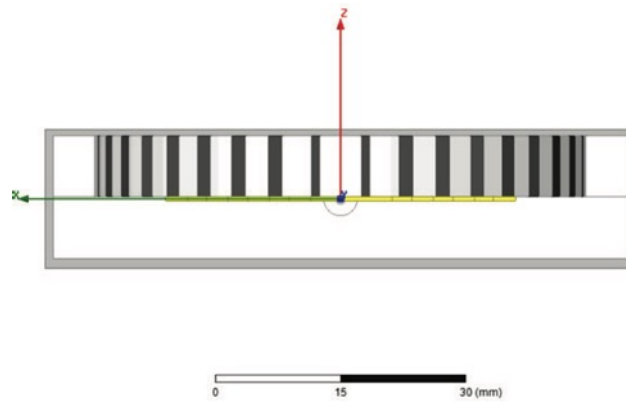


Fig 5.14. New stripline structure proposed (front view)

As it has been discussed above, all typical stripline structures have a uniform dielectric material with a fixed ϵ_r . This fact makes the equations developed in the bibliography a mere indicative guide to design the asymmetric device proposed. It must be completed, therefore, with computer-aid electromagnetic modelling tools.

5.2.2. Highly susceptor ceramic

The most crucial element of the structure presented above is the ceramic material, MBT-01, developed by Microbiotech S.L. The main benefit of working with this material is that the heating rate is non-reciprocal (see Fig 5.15): it can reach high temperatures in short periods while the cooling process is slower (similar to a normal ceramic one).

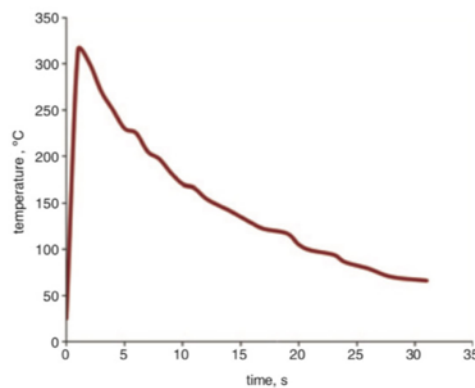


Fig 5.15. Thermal profile of material MBT01 when heated using 3.6kW microwave oven.

The named company has patented this ceramic and its integration with microwave technology, alongside the Spanish National Research Council (CSIC) and the Polytechnic University of Valencia (UPV) [127]. Following some research done by [131], a solution has been reached for the issue presented: a small device for fast heating using microwave sources.

This ceramic susceptor ensures fast heating with low power input, thus allowing a proper heat transfer to any kind of environment. The transmitted microwave energy can be controlled to obtain the required heating rate. This allows getting an appropriate process of heating that is strongly needed in most processes, which is the main difference with electrical resistors-based systems.

5.2.3. Design and manufacture

First of all, a parametric study with 2DExtractorDesign of Ansys has been done. The result obtained is that, for the given materials' dielectric properties and thicknesses, the strip width must be 2.7 mm to get a 50 Ω characteristic impedance for this asymmetric structure (Fig 5.17) [132].

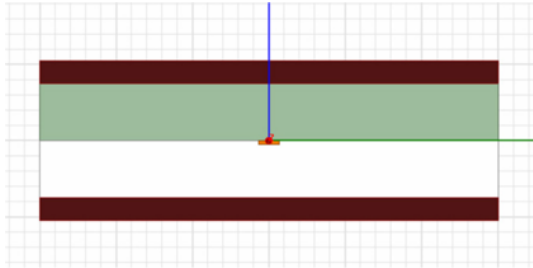


Fig 5.16. 2D Asymmetric stripline structure.

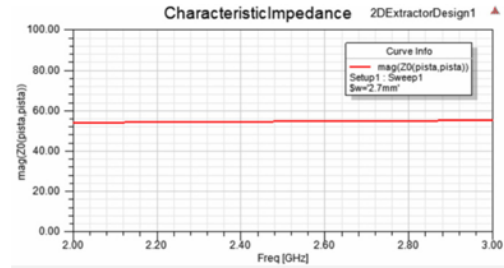


Fig 5.17. Characteristic impedance of the design.

Once the strip width is defined, a spiral strip has been designed inside the stripline structure to achieve the described performance and transmit all the consumed energy by the ceramic to the upper ground plane. The design parameters were the separation between turns and the total length to transfer, in a homogeneous way, all the conducted microwave to the susceptor. For this purpose, the HFSS software of the Ansys suite was used.

After having measured the actual parameters of the dielectric properties of the ceramic material ($\epsilon_r = 14$ and $\tan\delta = 0.2$), a 1-port device was drawn and modelled.

The predefined example in HFSS of a spiral wire was integrated as a starting point. The main objective was to have a spiral strip under the maximum of a circular ceramic disc. For this purpose, two aspects were considered: the width of the strip had to be close to the calculated in previous works (2.7 mm), and there had to be enough separation between turns of the spiral to avoid any electric arc when working with high input powers.

The aspect of the final spiral strip can be seen in Fig 5.18, and the main values of the design parameters for this spiral strip are shown in Table 5.1.

The prototype was manufactured by assembling five different elements depicted in Fig 5.19:

- One EMC shielding box without the top and bottom faces.
- Two copper sheets to enclose the top and bottom of the prototype.
- Two Teflon slabs.
- The spiral strip made of copper, which is embedded in one of the Teflon slabs.
- An MBT-01 cylinder with the same thickness of the Teflon slabs, and inserted totally in the middle of the other Teflon slab.

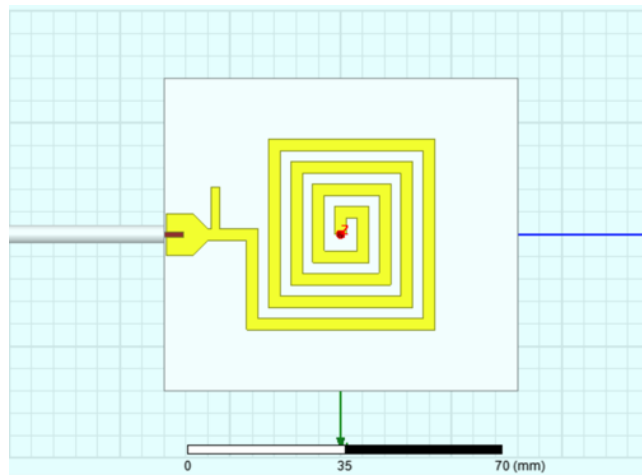


Fig 5.18. The final aspect of the spiral strip (top view)

Table 5.1. Spiral strip dimensions.

Main parameters of the spiral stripline		
Definition	Symbol	Value
Strip width	w	2.63 mm
Separation between turns	s	5 mm
Number of turns	n	4
Strip thickness	t	0.5 mm

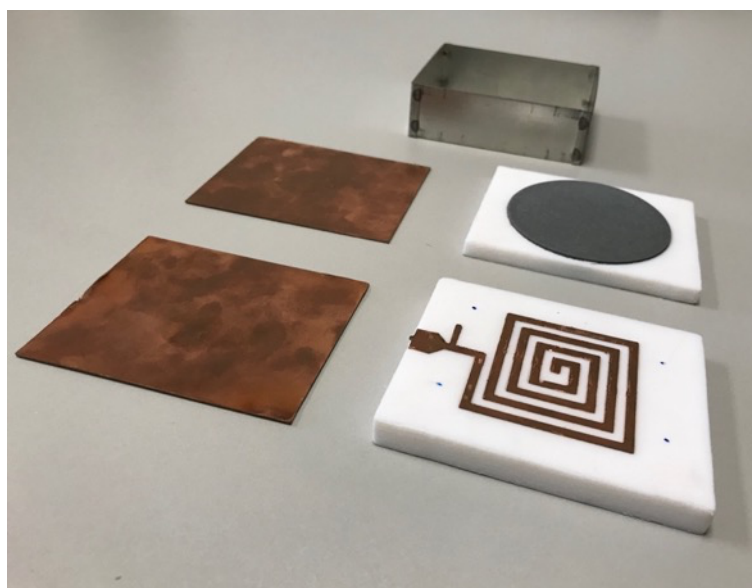


Fig 5.19. Each one of the components is manufactured and prepared to be assembled.

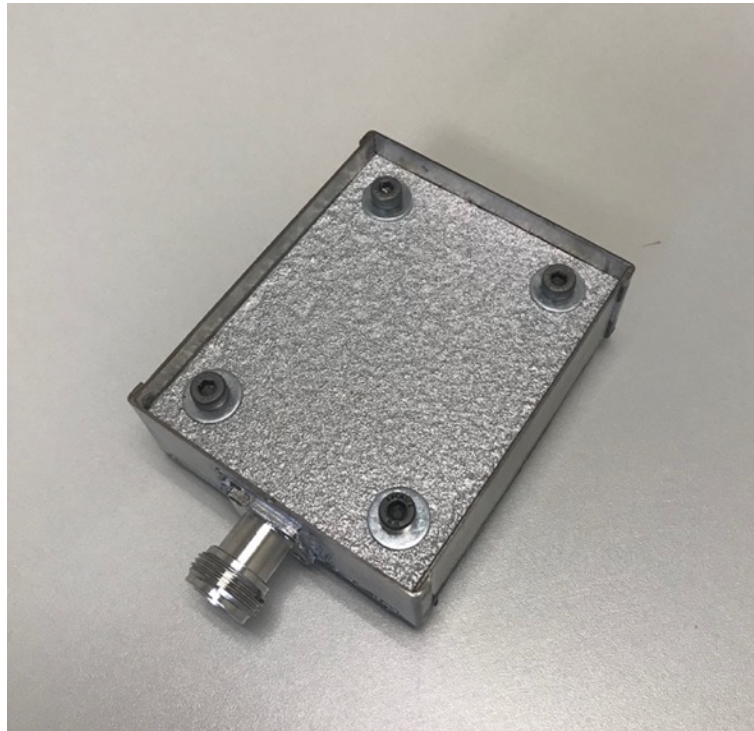


Fig 5.20. The final aspect of the device after the assembly. It has been connectorized with an N connector and painted with a non-reflective material.

The final result of the assembly is shown in Fig 5.20. Four screws were placed at the corners to adjust all the elements and a N-type coaxial connector was used to feed the device. Finally, the device was tested showing good results of heating rate and efficiency for different input powers. The results of these tests were presented in an international conference [133].

5.3. EMC protection elements for in-line industrial ovens.

Within the project “Evaluación e Integración en Línea del Proceso de Secado de Almendras mediante Microondas Generadas con Estado Sólido (Improsec)”, a non-static oven devoted to the integration of microwave technology in conjunction with other conventional technologies for fruit drying was developed and built. The non-static condition performance of this oven led to the design of microwave filters techniques.

The electromagnetic waves in the microwave frequency range are part of the so-called non-ionizing radiation, i.e., they cannot modify nor change the human cellular structure, as X-rays or Gamma rays do. However, elevated exposure to electromagnetic waves may result in health problems due to overheating of the parts of the body exposed to the radiation.

Being exposed to high energy may produce excessive heating, as it happens with any heat source. Taking into account that energy (E) is related to the power (P) and time (t) as in (5.16), when high power applications are taking place, the exposure times must be short enough so as not to produce any significant harm.

$$E(J) = P(W) \times t(s) \quad (5.16)$$

5.3.1. Microwave exposure regulation.

The ICNIRP (International Commission on Non-Ionizing Radiation Protection) is commissioned to define, alongside the WHO (World Health Organization), the protocols, figures and exposure limits for protection against non-ionizing radiation like the one the system involved in the project might create. The IEEE also offers a Standard for Safety Levels with Respect to Human Exposure to Electric, Magnetic, and Electromagnetic Fields [134], which is in line with the limits of the last ICNIRP report [135]. These limits depend on two main aspects:

1. The working frequency band.
2. Exposure type: local or whole-body. In turn, it distinguishes between two kinds of environments:
 - a. Unrestricted. Neither qualified personnel access control nor specific equipment is required.
 - b. Restricted. Qualified personnel equipped with personal protection.

The frequency range used in the microwave oven designed for the Improsec project, is 915 MHz. Taking this into account, and the last ICNIRP and IEEE reports the following Electromagnetic Radiation Limits (ERL) framed in red have to be fulfilled.

Table 7—ERLs for whole-body exposure of persons in unrestricted environments (100 kHz to 300 GHz) [see Figure 3 for graphical representation]

Frequency range (MHz)	Electric field strength (E) ^{a,b,c} (V/m)	Magnetic field strength (H) ^{a,b,c} (A/m)	Power density (S) ^{a,b,c} (W/m ²)		Averaging time (min)
			S_E	S_H	
0.1 to 1.34	614	$16.3 / f_M$	1000	$100\,000 / f_M^2$	30
1.34 to 30	$823.8 / f_M$	$16.3 / f_M$	$1800 / f_M^2$	$100\,000 / f_M^2$	30
30 to 100	27.5	$158.3 / f_M^{1.668}$	2	$9\,400\,000 / f_M^{3.336}$	30
100 to 400	27.5	0.0729	2		30
400 to 2000	—	—	$f_M / 200$		30
2000 to 300 000	—	—	10		30

NOTE— S_E and S_H are plane-wave-equivalent power density values, based on electric or magnetic field strength respectively, and are commonly used as a convenient comparison with ERLs at higher frequencies and are sometimes displayed on commonly used instruments.

^a For exposures that are uniform over the dimensions of the body, such as certain far-field plane-wave exposures, the exposure field strengths and power densities are compared with the ERLs in Table 7. For more typical nonuniform exposures, the mean values of the exposure fields, as obtained by spatially averaging the plane-wave-equivalent power densities or the squares of the field strengths, are compared with the ERLs in Table 7. (See notes to Table 7 through Table 11 in 4.3.5.)

^b f_M is the frequency in MHz.

^c The E , H , and S values are those rms values unperturbed by the presence of the body.

Fig 5.21. ERL for whole-body exposure in unrestricted environments [134]

Table 8—ERLs for whole-body exposure of persons permitted in restricted environments (100 kHz to 300 GHz) [see Figure 4 for graphical representation]

Frequency range (MHz)	Electric field strength (E) ^{a,b,c} (V/m)	Magnetic field strength (H) ^{a,b,c} (A/m)	Power density (S) ^{a,b,c} (W/m ²)		Averaging time (min)
			S_E	S_H	
0.1 to 1.0	1842	$16.3 / f_M$	9000	$100\,000 / f_M^2$	30
1.0 to 30	$1842 / f_M$	$16.3 / f_M$	$9000 / f_M^2$	$100\,000 / f_M^2$	30
30 to 100	61.4	$16.3 / f_M$	10	$100\,000 / f_M^2$	30
100 to 400	61.4	0.163	10		30
400 to 2000	—	—	$f_M / 40$		30
2000 to 300 000	—	—	50		30

NOTE— S_E and S_H are plane-wave-equivalent power density values, based on electric or magnetic field strength respectively, and are commonly used as a convenient comparison with ERLs at higher frequencies and are sometimes displayed on commonly used instruments.

^a For exposures that are uniform over the dimensions of the body, such as certain far-field plane-wave exposures, the exposure field strengths and power densities are compared with the ERLs in Table 8. For more typical nonuniform exposures, the mean values of the exposure fields, as obtained by spatially averaging the plane-wave-equivalent power densities or the squares of the field strengths, are compared with the ERLs in Table 8. (See notes to Table 7 through Table 11 in 4.3.5.)

^b f_M is the frequency in MHz.

^c The E , H , and S values are those rms values unperturbed by the presence of the body.

Fig 5.22. ERL for whole-body exposure in restricted environments [134]

These two limits, 4.5 W/m^2 and 22.5 W/m^2 , for unrestricted and restricted environments, respectively, are considered whole-body exposure. However, these figures are a bit laxer when the exposure is local. The limits for this situation are the following:

Table 9—Local exposure ERLs (100 kHz to 6 GHz)—Persons in unrestricted environments^o

Frequency range (MHz)	Electric field strength (E) ^{a,b,c,d} (V/m)	Magnetic field strength (H) ^{a,b,c,d} (A/m)	Power density (S) ^{a,b,c,d} (W/m ²)	
			S_E	S_H
0.1 to 1.34	1373	$36.4 / f_M$	5000	$500\,000 / f_M^2$
1.34 to 30	$1842 / f_M$	$36.4 / f_M$	$9000 / f_M^2$	$500\,000 / f_M^2$
30 to 100	61.4	$353 / f_M^{1.668}$	10	$47\,000\,000 / f_M^{3.336}$
100 to 400	$21.2 \times f_M^{0.232}$	$0.0562 \times f_M^{0.232}$		$1.19 \times f_M^{0.463}$
400 to 2000	—	—		$1.19 \times f_M^{0.463}$
2000 to 6000	—	—		40

NOTE 1—Below 6 GHz, portable devices are typically tested for DRL compliance (e.g., SAR), for which distinct limits for head and torso, pinnae and limbs are defined.

NOTE 2— S_E and S_H are plane-wave-equivalent power density values, based on electric or magnetic field strength respectively, and are commonly used as a convenient comparison with ERLs at higher frequencies and are sometimes displayed on commonly used instruments.

^a Determined in air at the location of the body surface.

^b Spatial and temporal peaks averaged over 6 min.

^c f_M is the frequency in MHz.

^d The E , H and S values are those rms values unperturbed by the presence of the body.

^e See notes to Table 7 through Table 11 in 4.3.5.

Fig 5.23. ERL for local exposure in unrestricted environments [134]

Table 10—Local exposure ERLs (100 kHz to 6 GHz)—Persons permitted in restricted environments^c

Frequency range (MHz)	Electric field strength (E) ^{a,b,c,d} (V/m)	Magnetic field strength (H) ^{a,b,c,d} (A/m)	Power density (S) ^{a,b,c,d} (W/m ²)	
			S_E	S_H
0.1 to 1.0	4119	$36.4/f_M$	45 000	$500\,000/f_M^2$
1.0 to 30	$4119/f_M$	$36.4/f_M$	$45\,000/f_M^2$	$500\,000/f_M^2$
30 to 100	137.3	$36.4/f_M$	50	$500\,000/f_M^2$
100 to 400	$47.3 \times f_M^{0.232}$	$0.125 \times f_M^{0.232}$	$5.93 \times f_M^{0.463}$	
400 to 2000	—	—	$5.93 \times f_M^{0.463}$	
2000 to 6000	—	—	200	

NOTE 1—Below 6 GHz, portable devices are typically tested for DRL compliance (e.g., SAR), for which distinct limits for head and torso, pinnae and limbs are defined.

NOTE 2— S_E and S_H are plane-wave-equivalent power density values, based on electric or magnetic field strength respectively, and are commonly used as a convenient comparison with ERLs at higher frequencies and are sometimes displayed on commonly used instruments.

^a Determined in air at the location of the body surface.

^b Spatial and temporal peaks averaged over 6 min.

^c f_M is the frequency in MHz.

^d The E , H , and S values are those rms values unperturbed by the presence of the body.

^e See notes to Table 7 through Table 11 in 4.3.5.

Fig 5.24. ERL for local exposure in restricted environments [134]

5.3.2. Waveguide accesses with microwave filters.

A continuous-flow industrial microwave oven, like the one designed for the project referred above, poses a technical challenge to prevent microwave leakage. The apertures (accesses) are much larger than the wavelength and no door array, like in the so-called “vestibule” ovens, is feasible. When the aperture’s height is greater than a quarter of a wavelength, reactive microwave chokes do not work [21].

To ensure the ERLs, different methods have been reported in the literature; the most relevant ones are those based on periodical metallic structures [136].

The most common approach is to place metallic posts in a rectangular waveguide with a separation between them of approximately $\lambda_g/4$. The rule of thumb says that each row of these metallic posts offers attenuation of 10 dB on the power at the beginning of the waveguide, in the exit access.

In the project referred to above, where the working frequency band used is 915 MHz, to obtain the 60 dB attenuation required to fulfil the authorities’ limits, the length needed for the access will follow the equation (5.17)

$$L_{access} = 6 * \frac{\lambda_T}{4} = 49.14cm \quad (5.17)$$

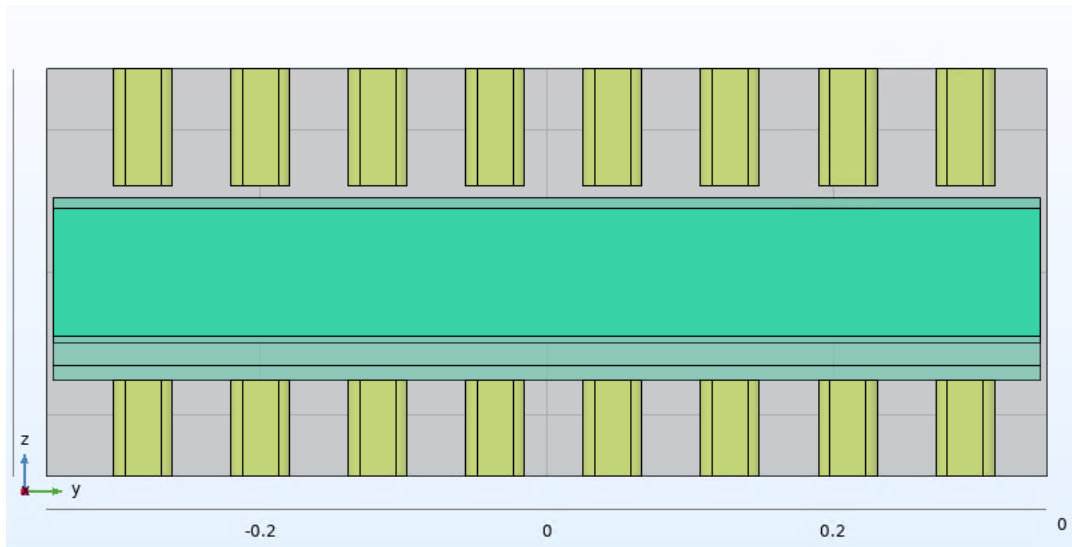


Fig 5.25. Lateral view of the access with 8 rows of metallic posts.

This first approach was studied with an electromagnetic modelling software. The results of the power outflow through the access with 500 W and 1 kW as input power in the antennas feeding the cavity are shown in Fig 5.26 and Fig 5.27, respectively. It can be seen that six rows will fulfil the restricted environment requirements. For this first prototype, height rows have been used as can be seen in Fig 5.25.

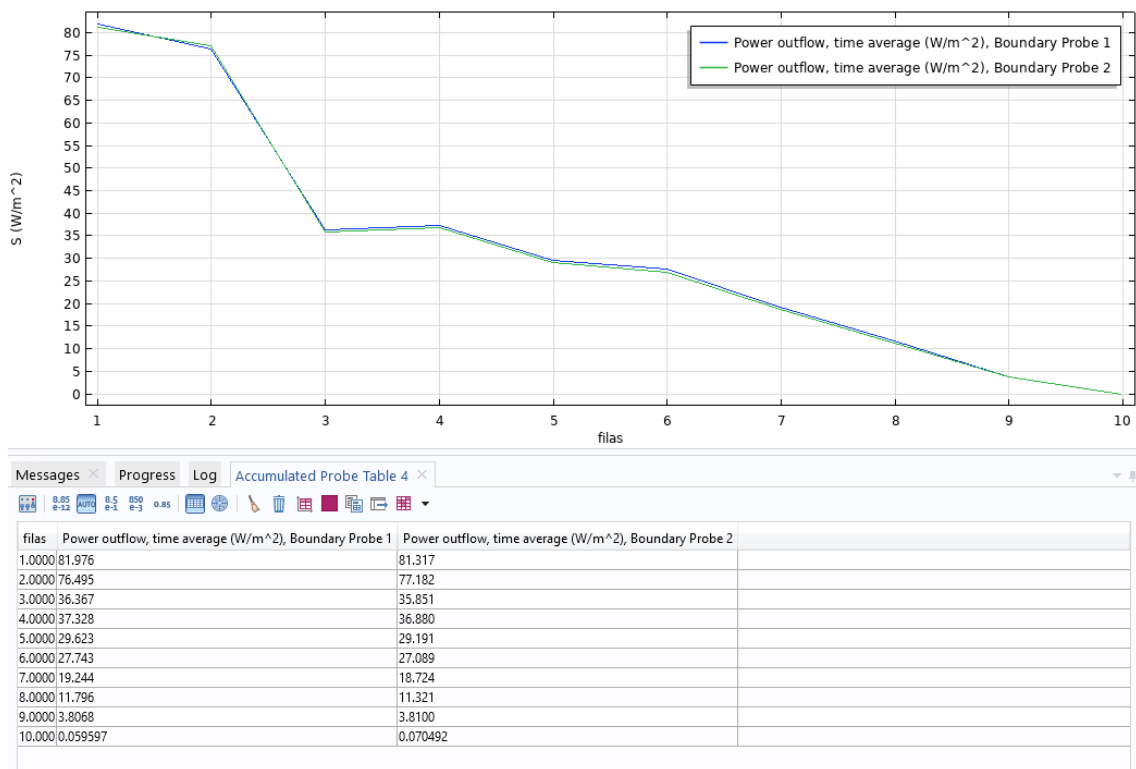


Fig 5.26. Power outflow with 500 W as input power in two antennas.

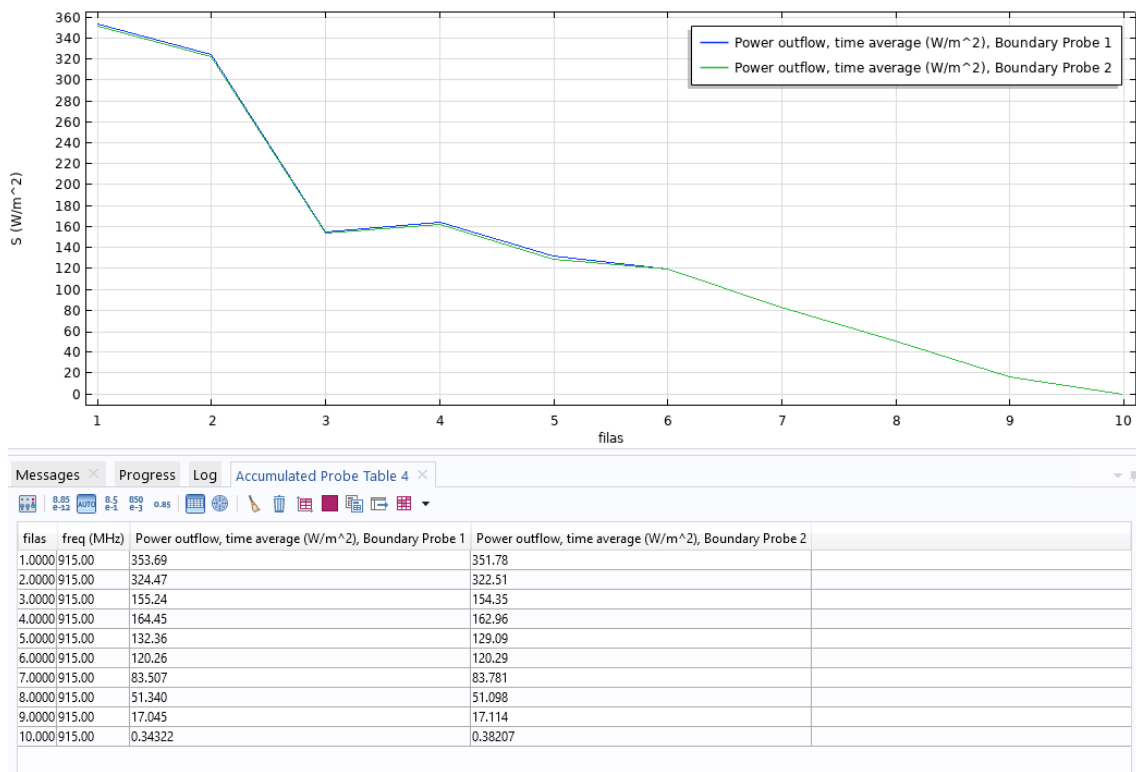


Fig 5.27. Power outflow with 1000 W as input power in two antennas.

A thorough study was performed to test what would happen with the sole waveguide. This study brought attention to the fact that more than the TE₁₀ mode was being propagated and, as a result, the resultant power outflow is greater than the permitted.

5.3.2.1 Study of the higher order modes.

The first design was developed taking into account the posts as the only protective elements. Fig 5.28 shows the components of the access. The yellow elements are the metallic posts and the blue ones represent a Teflon tray and three Teflon slabs on each lateral wall. This configuration was used for the study of the superior modes.

For a given waveguide, its dimensions define the cut-off frequency of each electromagnetic mode. In a waveguide, these can be transversal electric (TE) or transversal magnetic (TM); and their cut-off frequency is given by:

$$f_c(Hz) = \frac{c}{2\pi\sqrt{\epsilon'}} * \sqrt{\left((M) * \frac{\pi}{a}\right)^2 + \left((N) * \frac{\pi}{b}\right)^2} \tag{5.18}$$

Where *M* and *N* are the modes' indexes, epsilon the dielectric constant of the material filling the guide (in this case is air, so the value is 1); and *a* and *b* are the waveguide width and height, respectively. The waveguide designed for the access is 520 mm x 285 mm (*a* x *b*), resulting in the following cut-off frequencies for each mode that appears.

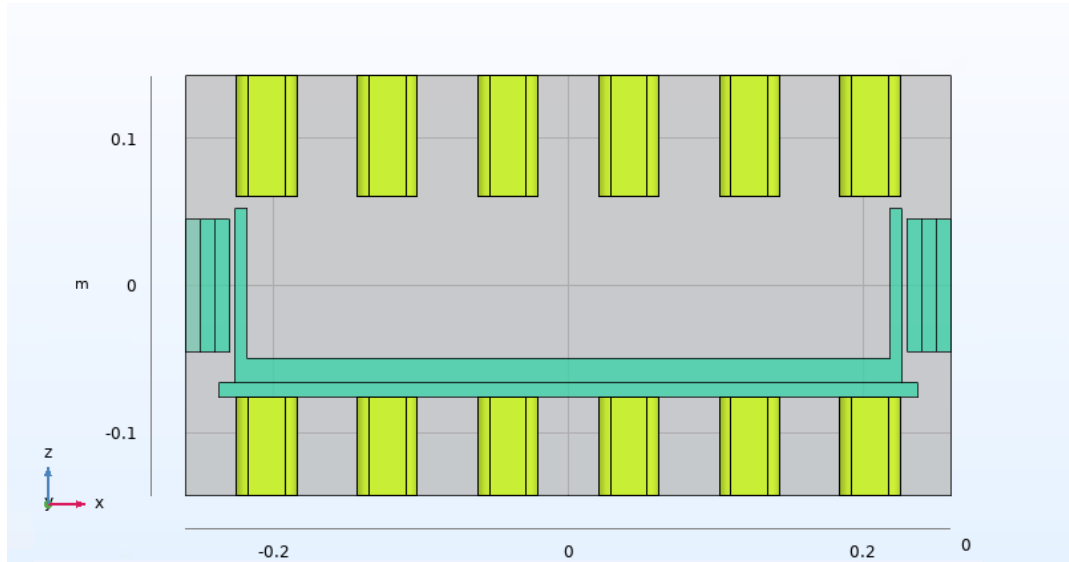


Fig 5.28. Frontal view of the access in the modelling software.

Table 5.2. Mode appearance in the designed waveguide and their cut-off frequencies.

Mode number (order of appearance)	Frequency (MHz)	TE Modes	TM Modes
1	288.461538461538	"TE1,0"	
2	526.315789473684	"TE0,1"	
3	576.923076923077	"TE2,0"	
4 – 5	600.181946930183	"TE1,1"	"TM1,1"
6 – 7	780.928003682604	"TE2,1"	"TM2,1"
8	865.384615384615	"TE3,0"	
9 – 10	1012.86664610584	"TE3,1"	"TM3,1"

Given that the working frequency is 915 MHz the last two modes, TE₃₁ and TM₃₁, will not be propagated through the access.

The study consists of measuring the scattering parameters for each mode. These values are directly related through (5.19) and (5.20) to the input (P_{In}) and output (P_{Out}) power in the access:

$$P_{In} = P_{fwd} * (1 - |S_{11}|^2) \quad (5.19)$$

$$P_{Out} = P_{In} * |S_{21}|^2 \quad (5.20)$$

where S_{11} and S_{21} are the scattering parameters, and P_{fwd} is the generated power. For this study, 100 W have been used. To understand graphically what wave distribution has each mode, the

electric field is also plotted in the three main cuts: XY, XZ and YZ. An isometric view is also plotted.

First mode: TE₁₀

Table 5.3 shows that this mode is completely negligible in the access. These kinds of modes (TE_{M0}) are affected directly by the periodic metallic structure.

Table 5.3. Study results for the first mode (TE₁₀) with metallic posts only.

f_c (MHz)	S11 (dB)	S21(dB)	S11	S21	P_{IN}	P_{OUT}
288	-2.95e-5	-55.367	1	2.906e-6	0.0013	8.445e-10

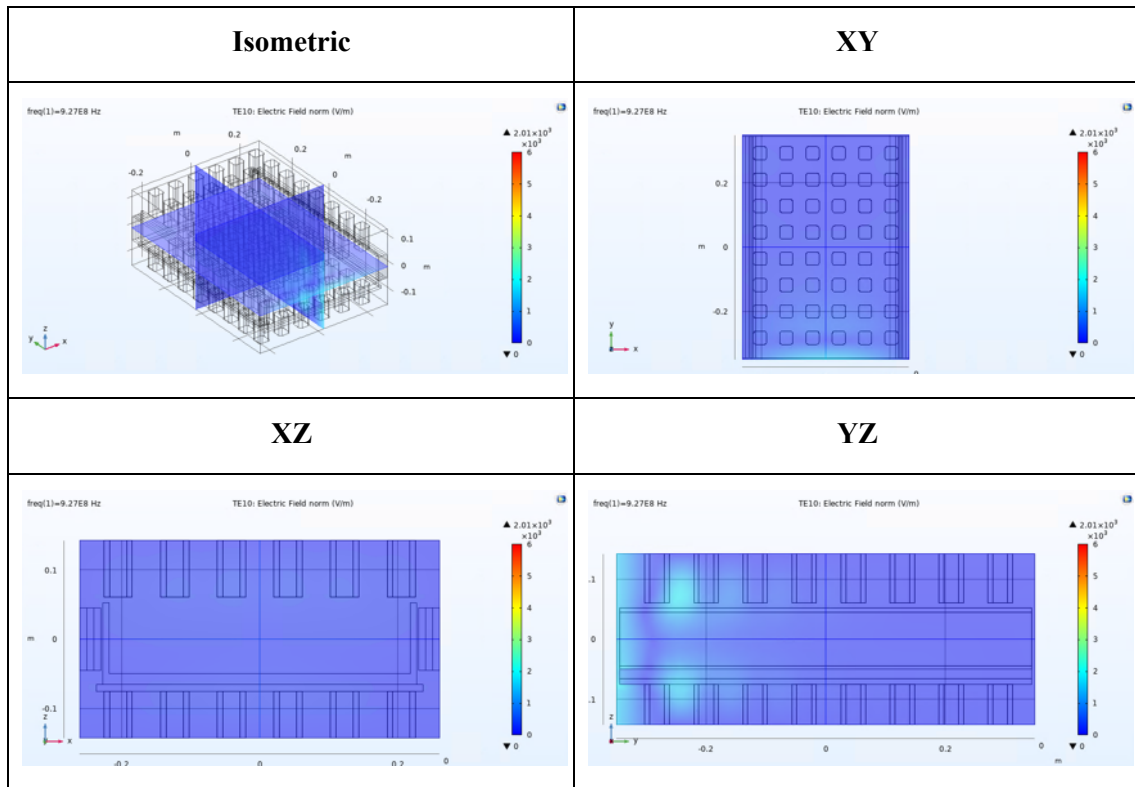


Fig 5.29. Electric field for the TE₁₀ mode with metallic posts only.

Second mode: TE₀₁

This second mode is the main cause of the microwave propagation to the exterior of the machine. A periodic electric field with higher values around the lateral walls is the reason for that, as it can be seen in Fig 5.30. The output power exceeds 90% of the input power.

Table 5.4. Study results for the second mode (TE₀₁) with metallic posts only

f_c (MHz)	S11 (dB)	S21(dB)	S11	S21	P_{IN} (W)	P_{OUT} (W)
526	-13.29	-0.209	0.0469	0.9530	99.78	90.8239

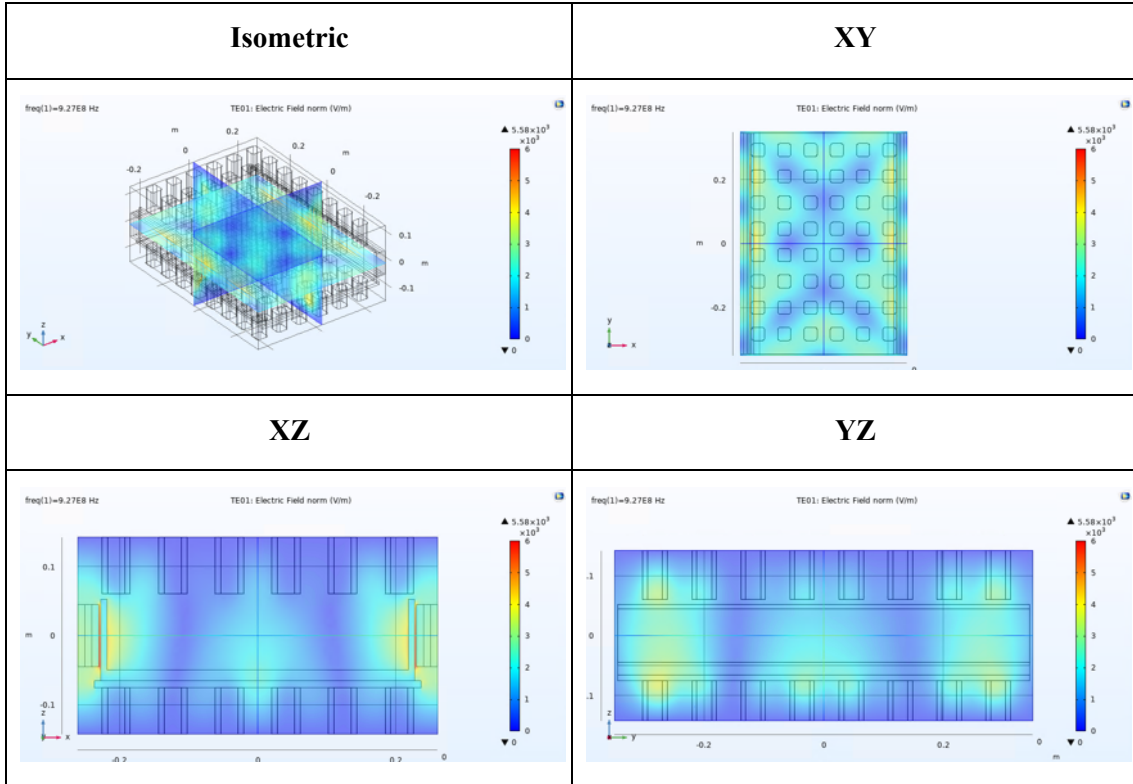


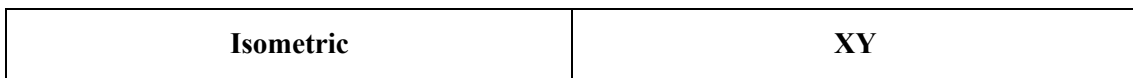
Fig 5.30. Electric field for the TE_{01} mode with metallic posts only.

Third mode: TE_{20}

As stated before, both the output power and the electric field will have low levels due to the effect of the metallic post.

Table 5.5. Study results for the third mode (TE_{20}) with metallic posts only

f_c (MHz)	S11 (dB)	S21(dB)	S11	S21	P_{IN} (W)	P_{OUT} (W)
577	-5.798e-4	-38.72	0.9999	1.3428e-4	0.0267	1.803e-6



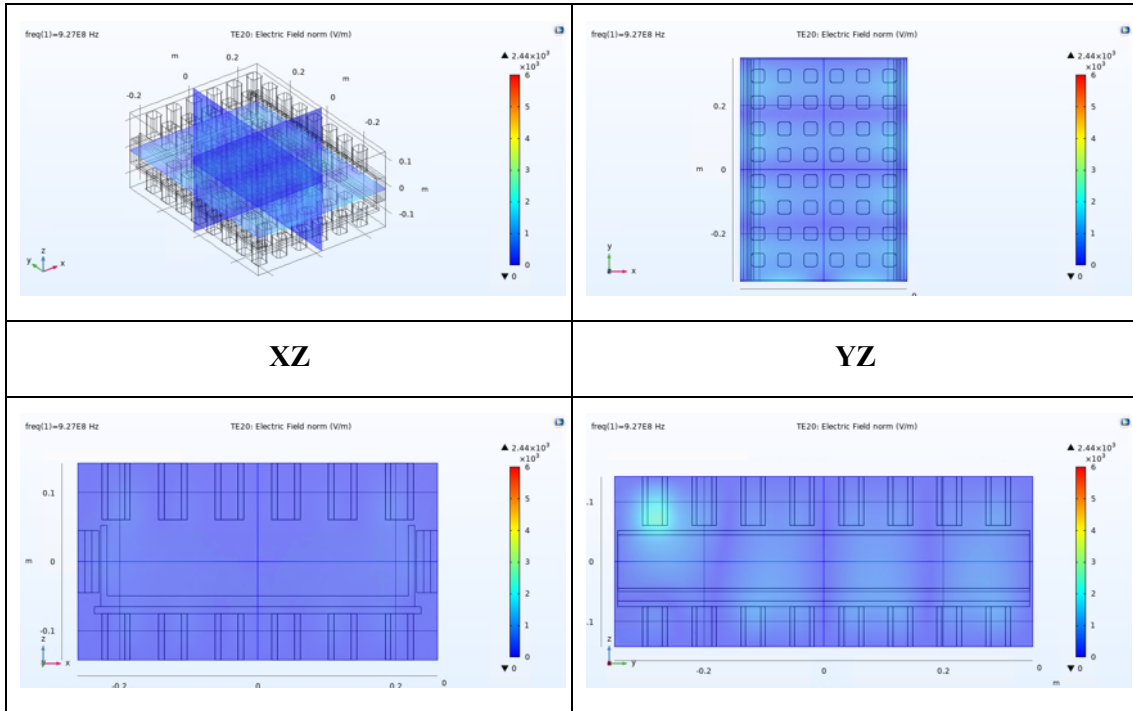


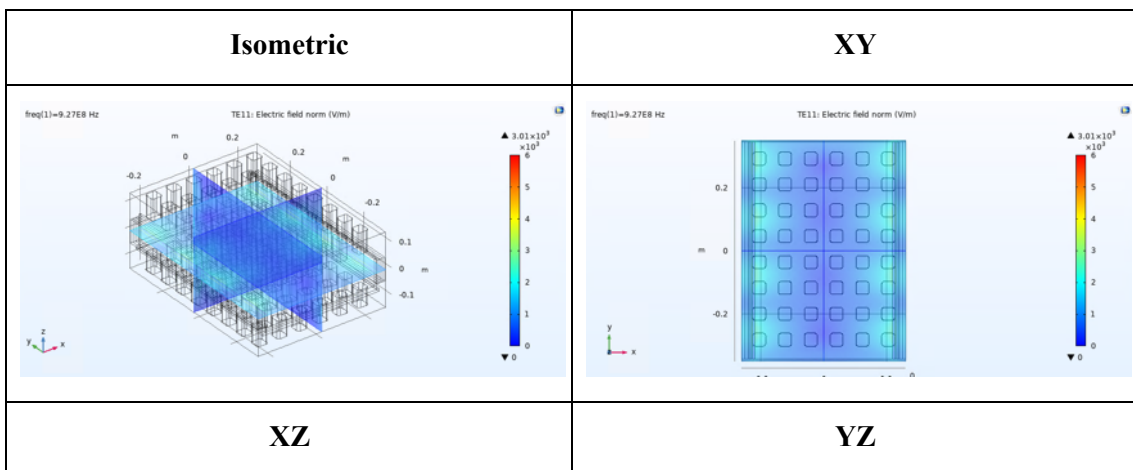
Fig 5.31. Electric field for the TE_{20} mode with metallic posts only.

Fourth mode: TE_{11}

Similarly to the second mode, this TE_{11} shares with it the strong presence of the lateral electric field. It can be seen graphically that its levels are lower than in the second mode, and that is related to the output power; which is close to 85% of the input power.

Table 5.6. Study results for the fourth mode (TE_{11}) with metallic posts only.

f_c (MHz)	S11 (dB)	S21(dB)	S11	S21	P_{IN} (W)	P_{OUT} (W)
600	-10.906	-0.3678	0.0812	0.9188	99.3411	84.419



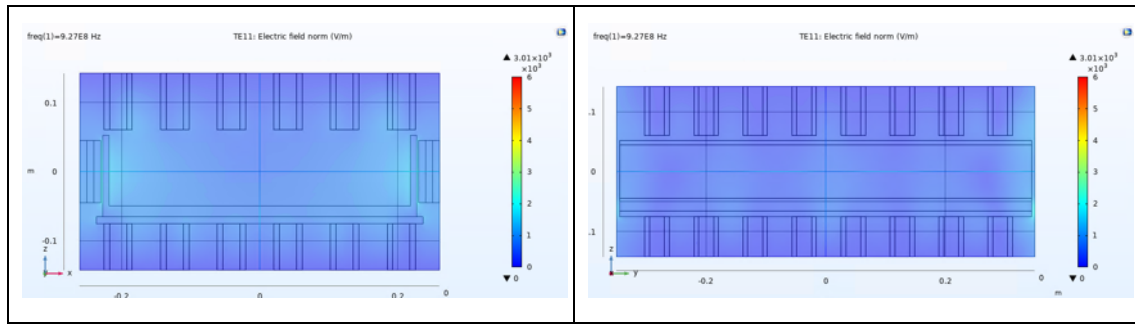


Fig 5.32. Electric field for the TE_{11} mode with metallic posts only.

Fifth mode: TM_{11}

The fifth mode, corresponding with the TM_{11} , can carry a high amount of energy periodically through the lateral walls, as can be seen in Fig 5.33, XY. The filtering effect is almost inexistent as can be seen with the resultant output power.

Table 5.7. Study results for the fifth mode (TM_{11}) with metallic posts only.

f_c (MHz)	S11 (dB)	S21(dB)	S11	S21	P_{IN} (W)	P_{OUT} (W)
600	-18.16	-0.067	0.0153	0.9847	99.9767	96.9617

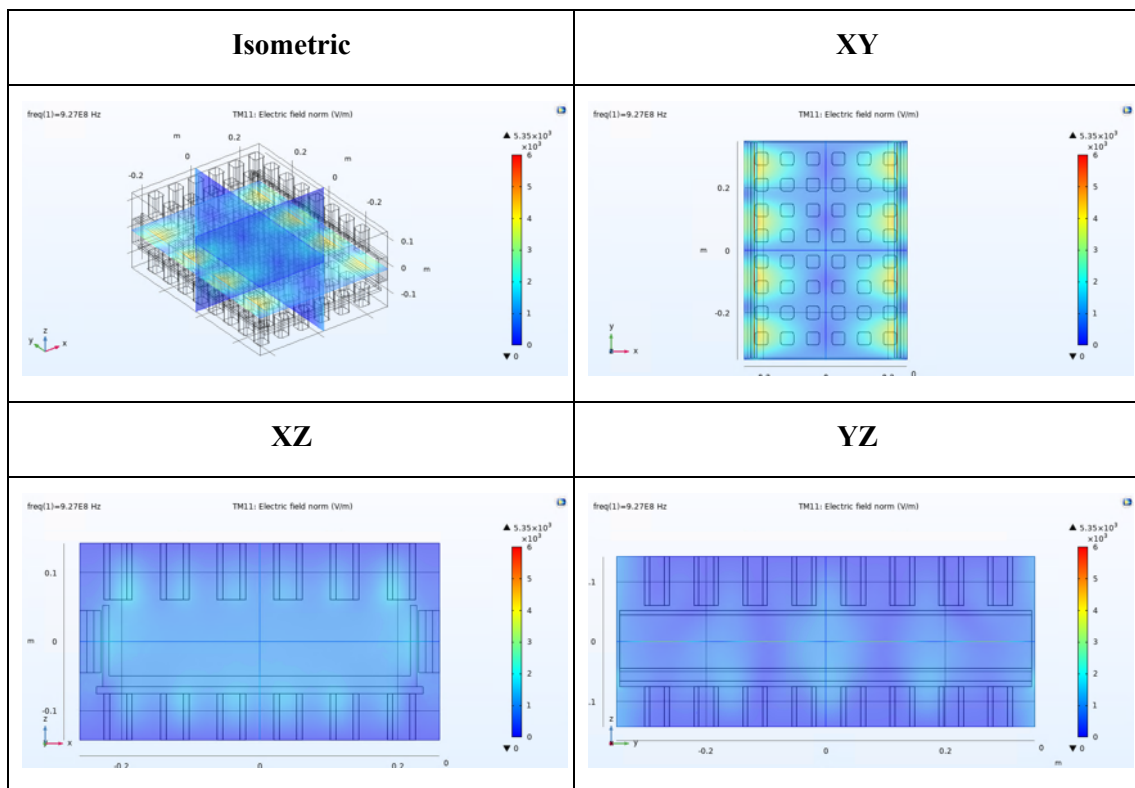


Fig 5.33. Electric field for the TM_{11} mode with metallic posts only.

Sixth mode: TE₂₁

With the TE₂₁ a curious effect happens. The output power is over the 50% (i.e., lower than in the previous mode) but the electric field has higher values in every one of the planes. The mismatching in the input port is the responsible.

Table 5.8. Study results for the sixth mode (TE₂₁) with metallic posts only.

f_c (MHz)	S11 (dB)	S21(dB)	S11	S21	P_{IN} (W)	P_{OUT} (W)
780	-6.23	-1.18	0.2382	0.7621	94.3246	58.0765

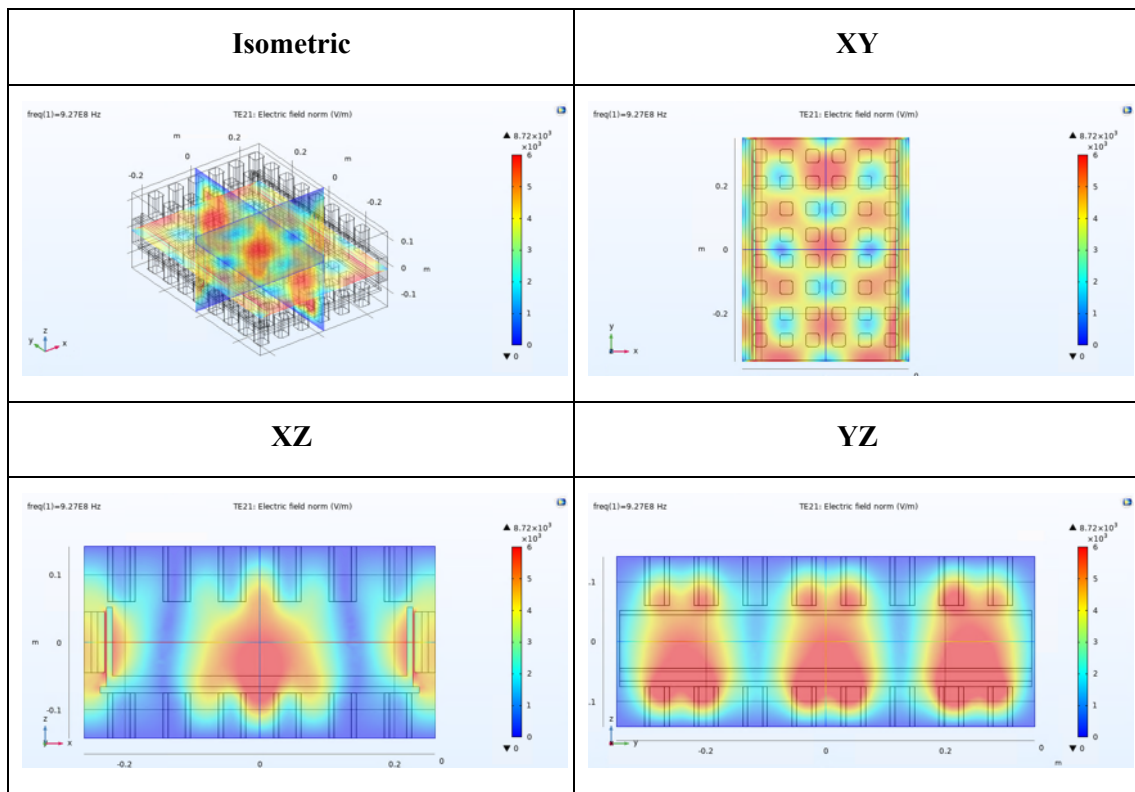


Fig 5.34. Electric field for the TE₂₁ mode with metallic posts only.

Seventh mode: TM₂₁

Table 5.9. Study results for the seventh mode (TM₂₁) with metallic posts only.

f_c (MHz)	S11 (dB)	S21(dB)	S11	S21	P_{IN} (W)	P_{OUT} (W)
780	-1.528	-5.279	0.7034	0.2966	50.5234	8.7943

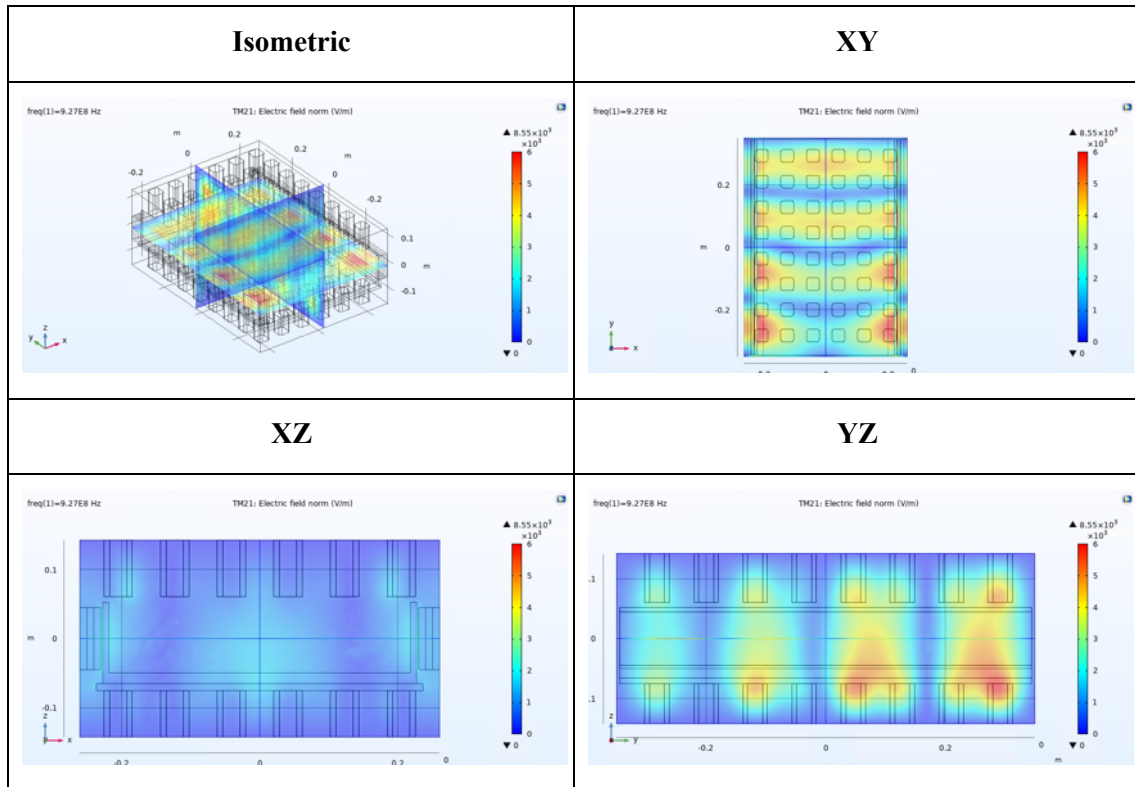


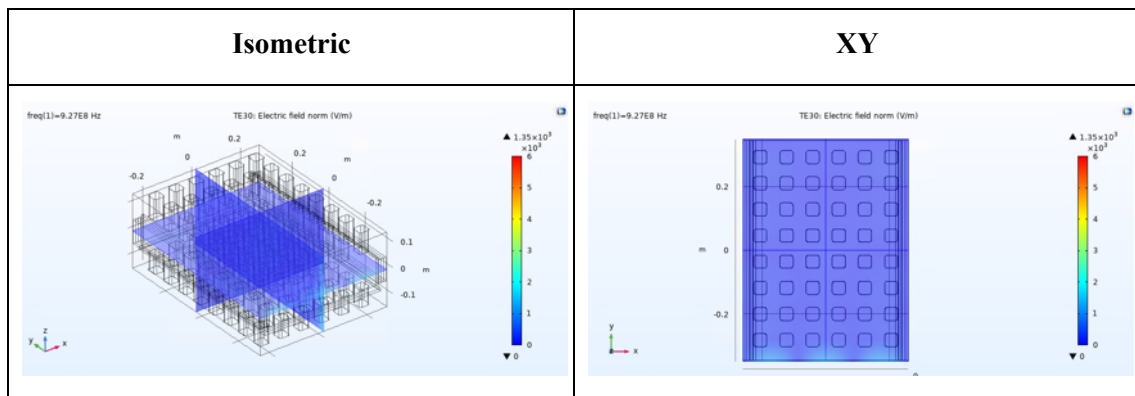
Fig 5.35. Electric field for the TM_{21} mode with metallic posts only.

Eighth mode: TE_{30}

The last mode behaves like all the previous with $N = 0$, confirming the noticeable effect of the periodic metallic structure.

Table 5.10. Study results for the eighth mode (TE_{30}) with metallic posts only.

f_c (MHz)	S11 (dB)	S21(dB)	S11	S21	P_{IN} (W)	P_{OUT} (W)
865	-1.15e-5	-57.82	1	1.652e-6	5.25e-4	2.729e-10



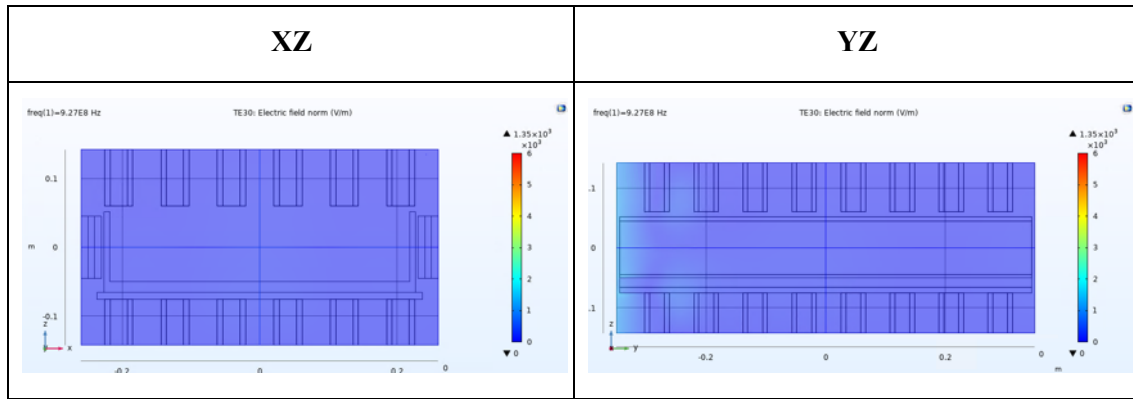


Fig 5.36. Electric field for the TE_{30} mode with metallic posts only.

The results of this first study showed that some of the modes were carrying enough power outside the access, infringing the limits defined before. To solve that, a second filtering element was placed and the same mode study was performed.

5.3.2.2 Absorbent materials in the lateral walls

Linear tunnels with absorbing walls have been historically rejected because of two reasons. First, they will tend to absorb a significant amount of energy impinging on them at the tunnel cavity interface. When the amount of energy is significant, heat transfer issues appear requiring the use of liquid absorbers and continuous heat exchanging systems. This last solution is already used by well-known companies to ensure radiation levels. Second, when tunnel openings approach a wavelength, assuming perfectly absorbing walls, the tunnels become impractical because of free space propagation [21].

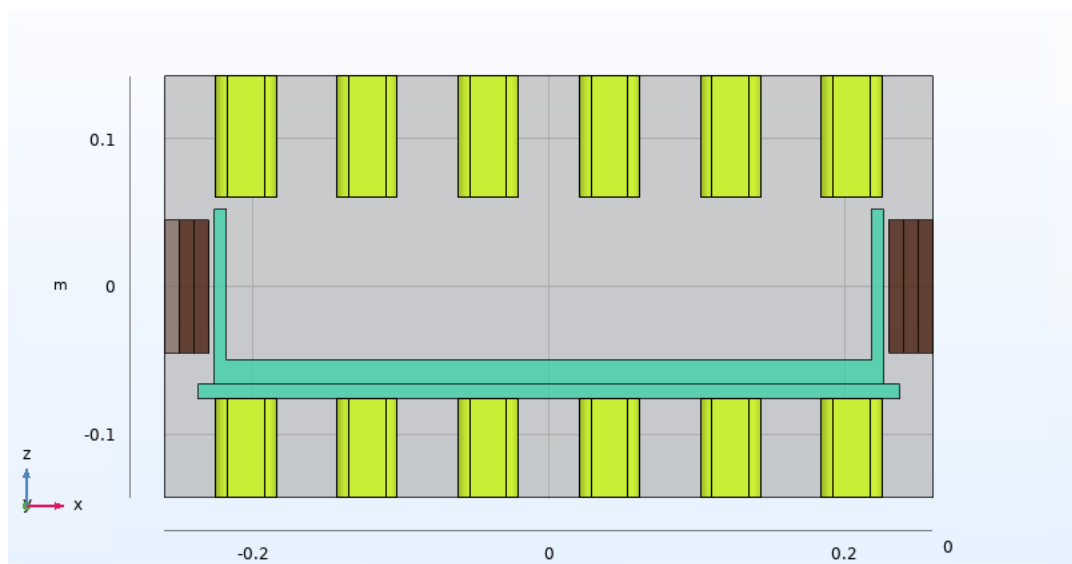


Fig 5.37. Front view of the access modelled with MBT01 as an absorbent material attached to the lateral walls.

However, due to the restrained amount of power used in this prototype, and as a combination of different filtering elements, the MBT01 technical ceramic has been thought to replace the three Teflon slabs (Fig 5.37). One important result obtained when placing this material is that the

electric field was considerably reduced, producing the constraining of microwaves inside the oven.

The results of the study are shown down below. It keeps the same structure as the last subsection, but includes in the results table both versions: v0 for the Teflon[®] slabs and v2 for the study with MBT01 absorbent slabs with 30mm of thickness.

First mode: TE_{10} ($f_c = 288$ MHz)

This first mode was already attenuated so slight differences should be seen when adding this new material. As can be seen in the table below, this material absorbs some power at the beginning of the waveguide, but the output remains beneath contempt.

Table 5.11. Study results for the first mode (TE_{10}) with metallic posts and MBT01 slabs attached to the lateral walls.

Version	S11 (dB)	S21(dB)	S11	S21	P _{IN} (W)	P _{OUT} (W)
v0	-2.95e-5	-55.367	1	2.906e-6	0.0013	8.445e-10
v2	-0.2034	-46.148	0.9542	2.4277e-5	8.9416	5.27e-9

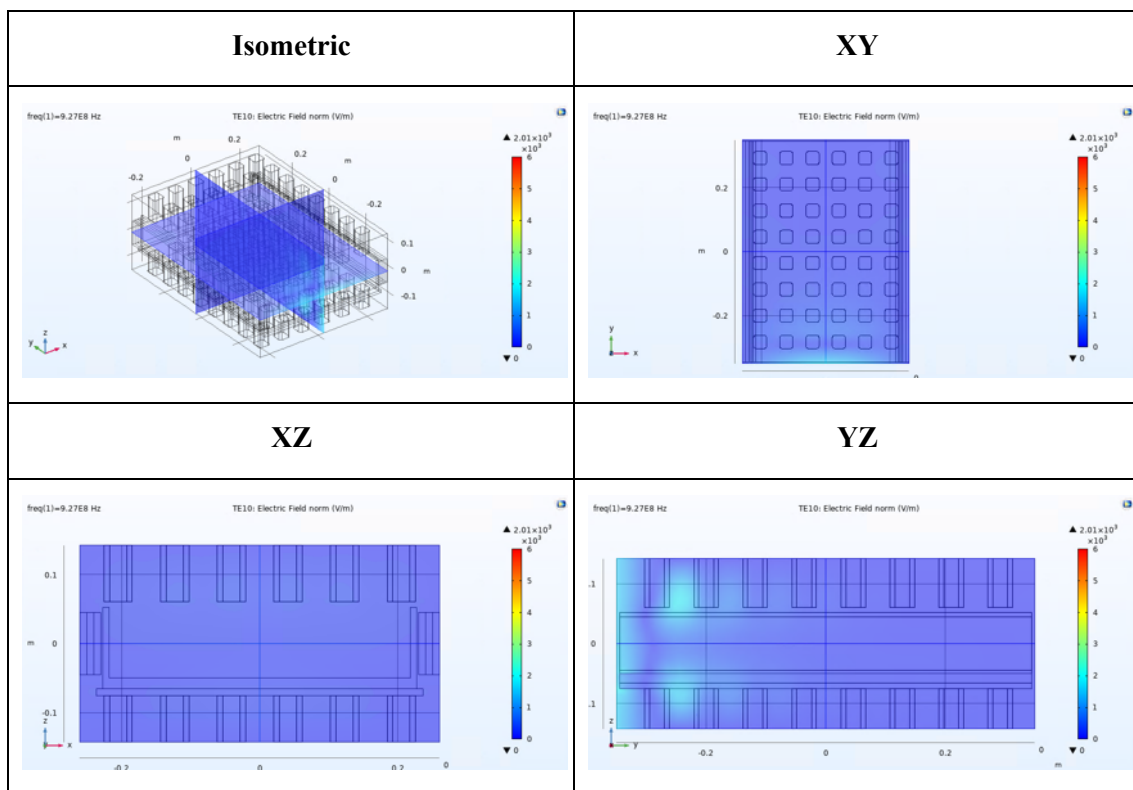


Fig 5.38. Electric field for the TE_{10} mode with metallic posts and MBT01 slabs.

Second mode: TE₀₁ ($f_c = 526$ MHz)

Here can be seen an important improvement: the output power is around 1.5% while in the first version it was 90%.

Table 5.12. Study results for the second mode (TE₀₁) with metallic posts and MBT01 slabs attached to the lateral walls.

Version	S11 (dB)	S21(dB)	S11	S21	P _{IN} (W)	P _{OUT} (W)
v0	-13.29	-0.209	0.0469	0.9530	99.78	90.8239
v2	-36.004	-9.066	2.509e-4	0.124	100	1.5374

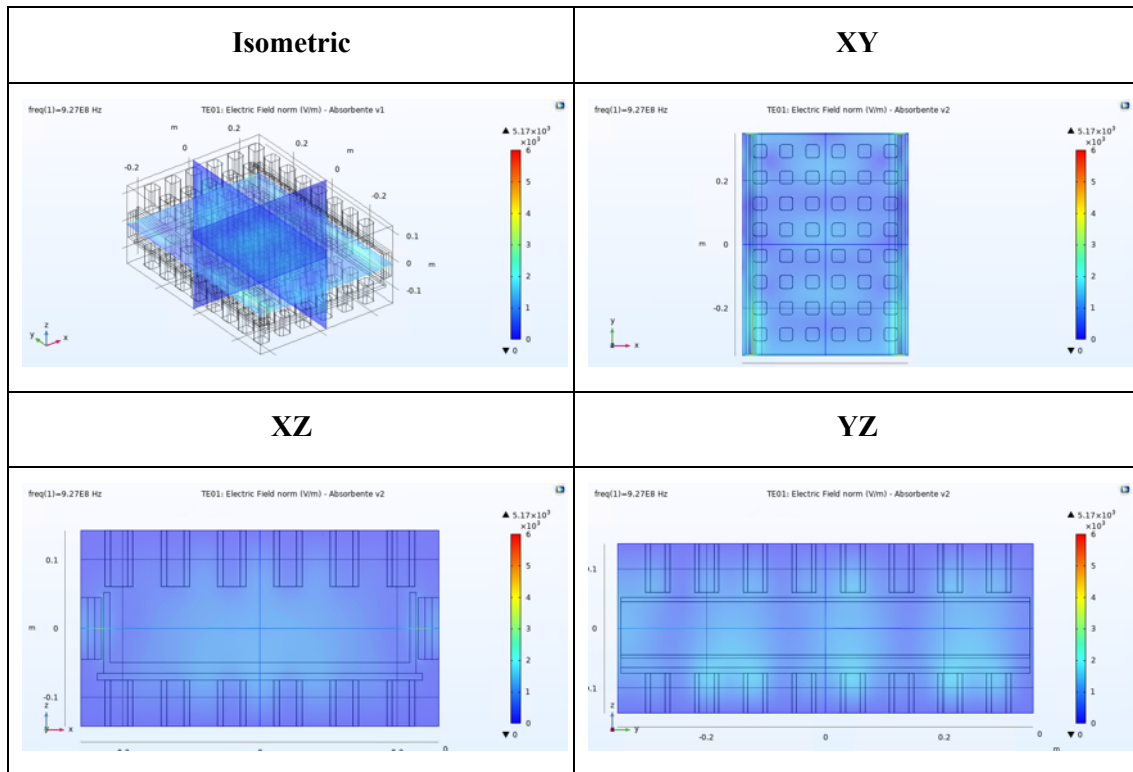


Fig 5.39. Electric field for the TE₀₁ mode with metallic posts and MBT01 slabs.

Third mode: TE₂₀ ($f_c = 577$ MHz)

Table 5.13. Study results for the third mode (TE₂₀) with metallic posts and MBT01 slabs attached to the lateral walls.

Version	S11 (dB)	S21(dB)	S11	S21	P _{IN} (W)	P _{OUT} (W)
v0	-5.798e-4	-38.72	0.9999	1.3428e-4	0.0267	1.803e-6

v2	-0.4129	-43.637	0.9093	4.3281e-5	17.3163	3.244e-8
----	---------	---------	--------	-----------	---------	----------

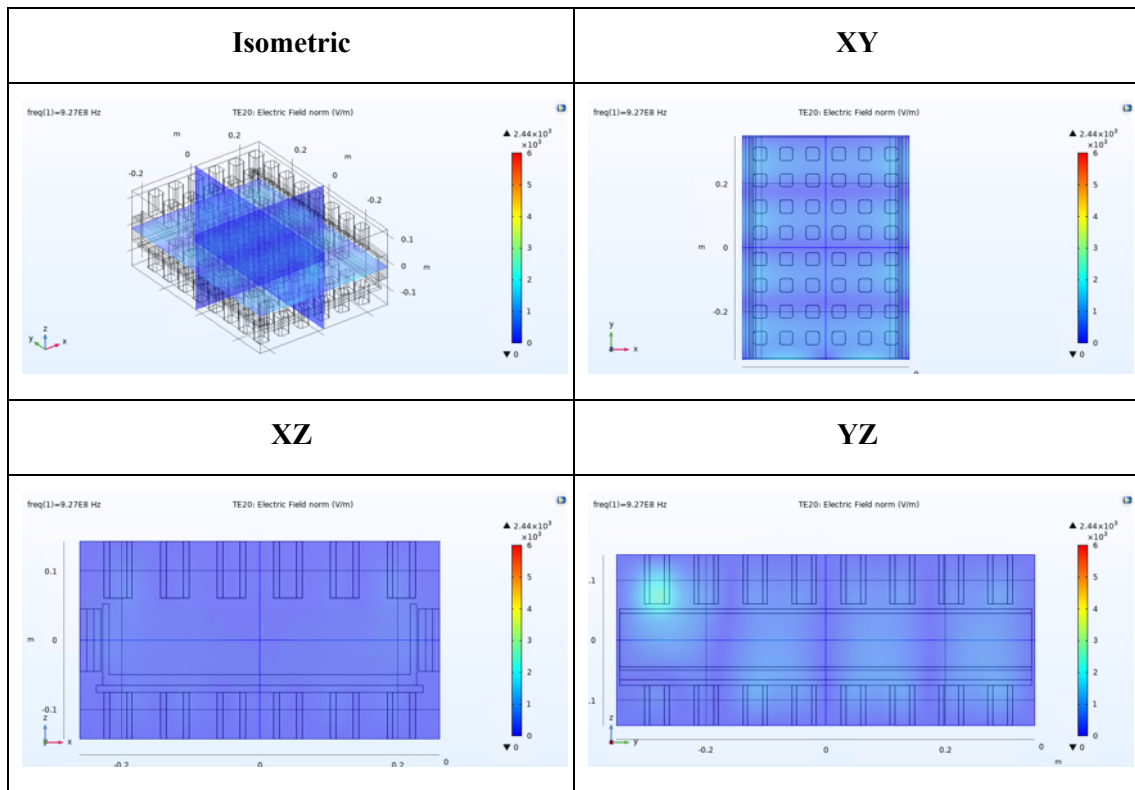


Fig 5.40. Electric field for the TE₂₀ mode with metallic posts and MBT01 slabs.

Fourth mode: TE₁₁ (f_c = 600 MHz)

The fourth mode, carrying nearly the 85% of the power out of the waveguide, is now reduced to less than 0.1% with the v2.

Table 5.14. Study results for the fourth mode (TE₁₁) with metallic posts and MBT01 slabs attached to the lateral walls.

Version	S ₁₁ (dB)	S ₂₁ (dB)	S ₁₁	S ₂₁	P _{IN} (W)	P _{OUT} (W)
v0	-10.906	-0.3678	0.0812	0.9188	99.3411	84.419
v2	-14.658	-15.959	0.0342	0.0254	99.8829	0.0642

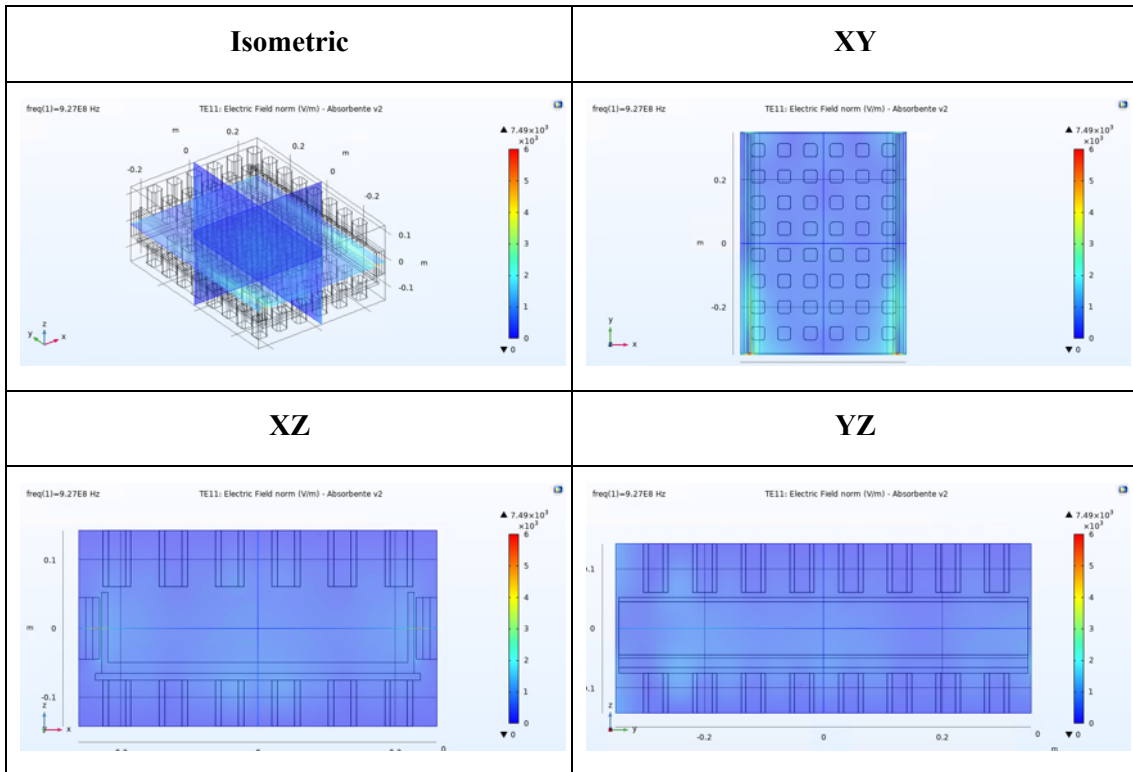


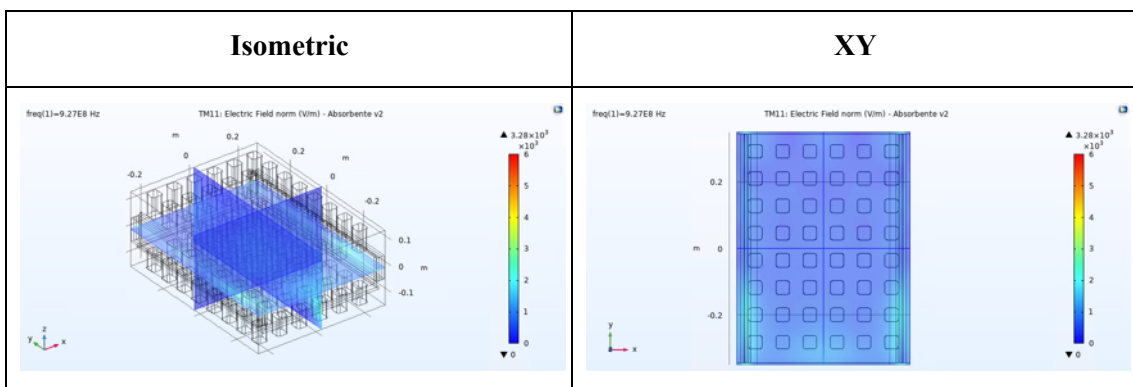
Fig 5.41. Electric field for the TE_{11} mode with metallic posts and MBT01 slabs.

Fifth mode: TM_{11} ($f_c = 600$ MHz)

With the TM_{11} , the output power reduction from v0 to v2 is even higher than with the previous mode.

Table 5.15. Study results for the fifth mode (TM_{11}) with metallic posts and MBT01 slabs attached to the lateral walls.

Version	S11 (dB)	S21(dB)	S11	S21	P_{IN} (W)	P_{OUT} (W)
v0	-18.16	-0.067	0.0153	0.9847	99.9767	96.9617
v2	-4.0045	-19.094	0.3977	0.0123	84.1839	0.0128



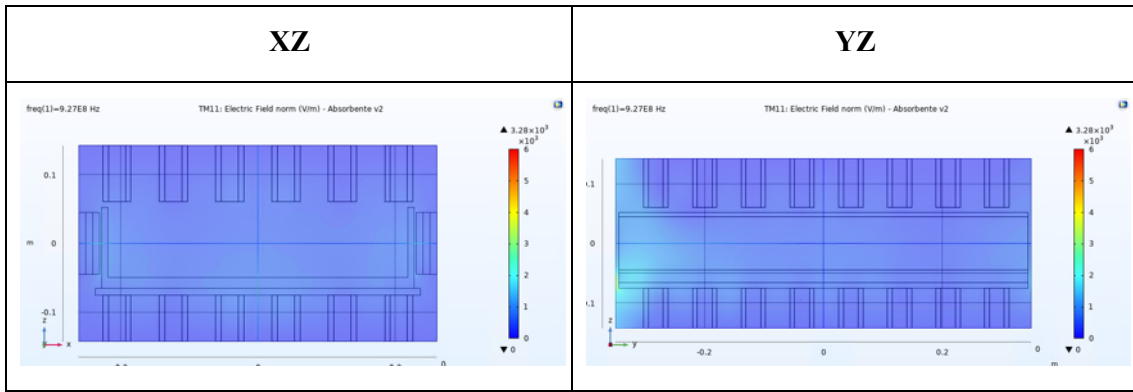


Fig 5.42. Electric field for the TM_{11} mode with metallic posts and MBT01 slabs.

Sixth mode: TE_{21} ($f_c = 780$ MHz)

When comparing these results with the ones mentioned in 0, it can be seen the suppression of this high electric field distribution.

Table 5.16. Study results for the sixth mode (TE_{21}) with metallic posts and MBT01 slabs attached to the lateral walls.

Version	S11 (dB)	S21(dB)	S11	S21	P_{IN} (W)	P_{OUT} (W)
v0	-6.23	-1.18	0.2382	0.7621	94.3246	58.0765
v2	-2.1724	-27.406	0.6064	0.0018	63.2278	2.087e-4

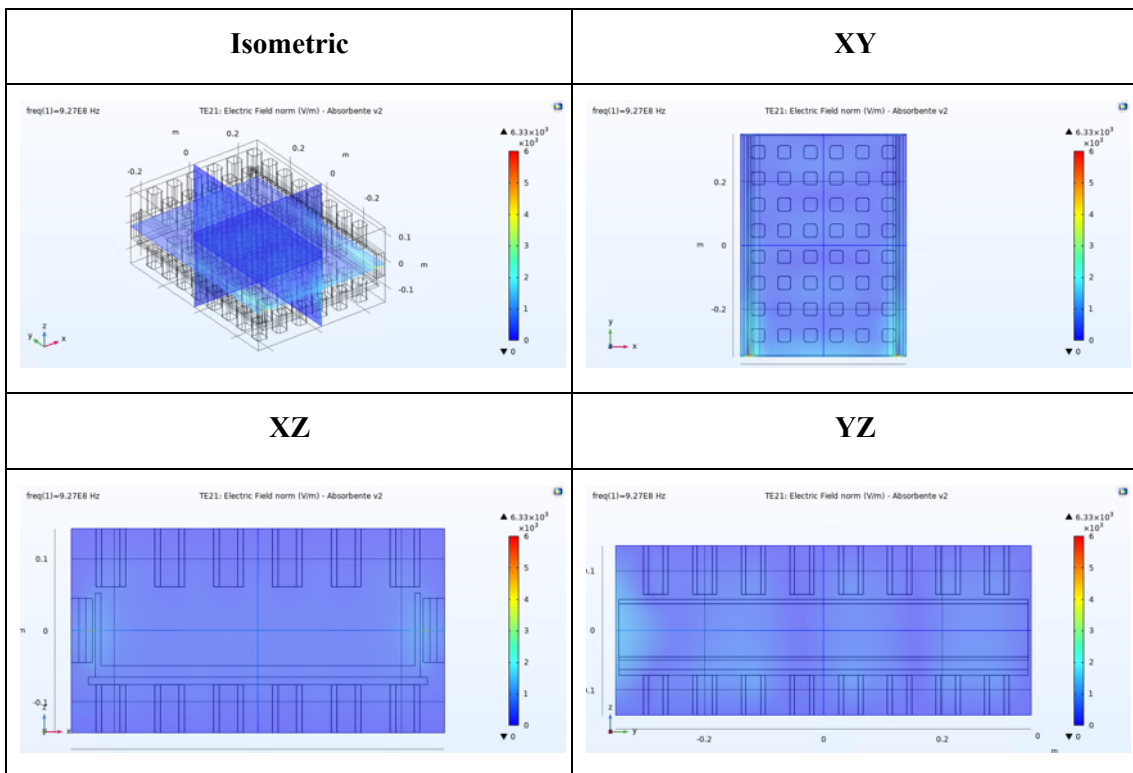


Fig 5.43. Electric field for the TE_{21} mode with metallic posts and MBT01 slabs.

Seventh mode: TM_{21} ($f_c = 780$ MHz)

Table 5.17. Study results for the seventh mode (TM_{21}) with metallic posts and MBT01 slabs attached to the lateral walls.

Version	S11 (dB)	S21(dB)	S11	S21	P _{IN} (W)	P _{OUT} (W)
v0	-1.528	-5.279	0.7034	0.2966	50.5234	8.7943
v2	-12.269	-14.323	0.0593	0.037	99.6483	0.1361

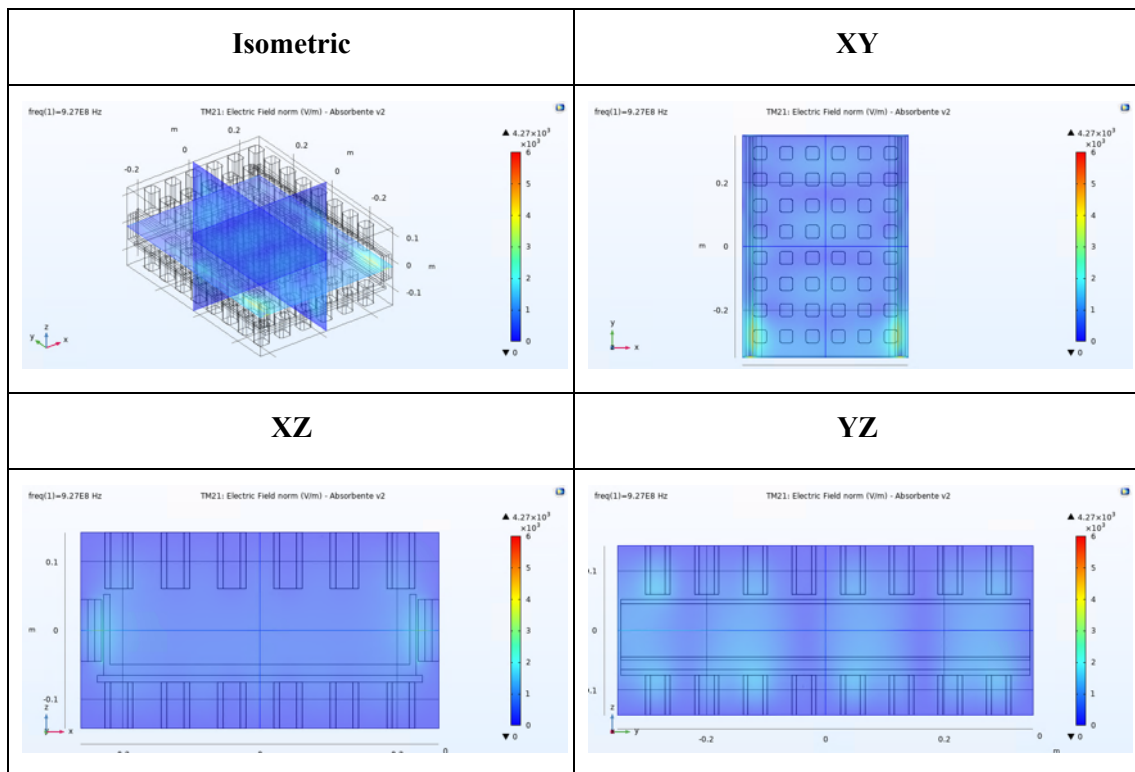


Fig 5.44. Electric field for the TM_{21} mode with metallic posts and MBT01 slabs.

Eighth mode: TE_{30} ($f_c = 865$ MHz)

Table 5.18. Study results for the eighth mode (TE_{30}) with metallic posts and MBT01 slabs attached to the lateral walls.

Version	S11 (dB)	S21(dB)	S11	S21	P _{IN} (W)	P _{OUT} (W)
v0	-1.15e-5	-57.82	1	1.652e-6	5.25e-4	2.729e-10
v2	-0.262	-49.456	0.9414	1.13e-5	11.3681	1.46e-9

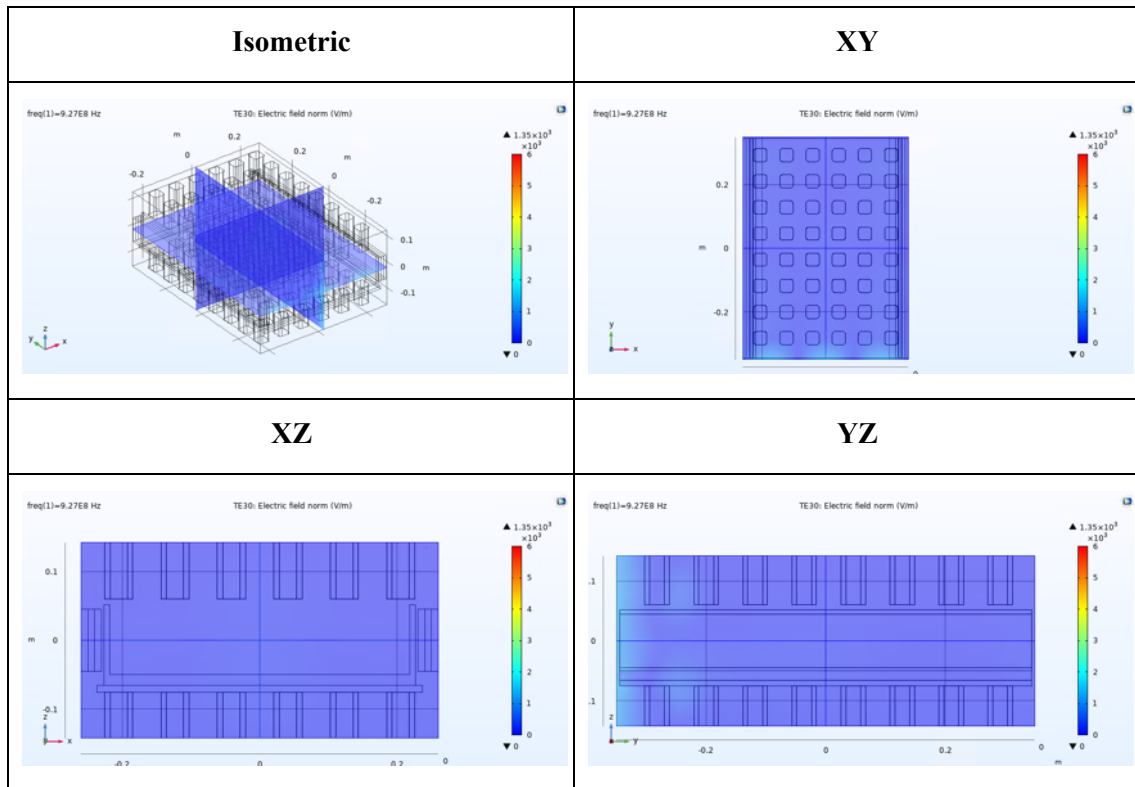


Fig 5.45. Electric field for the TE_{30} mode with metallic posts and MBT01 slabs.

5.3.3. Study results discussion

The five modes that have experienced an important change from v0 and v2 are the TE_{01} , TE_{11} , TM_{11} , TE_{21} and TM_{21} . These modes have in common that they are capable to transport energy through the electric field formed, mainly, alongside the lateral walls.

With the absorbent material these modes have suffered a severe attenuation as can be seen in Fig 5.46 – Fig 5.50.

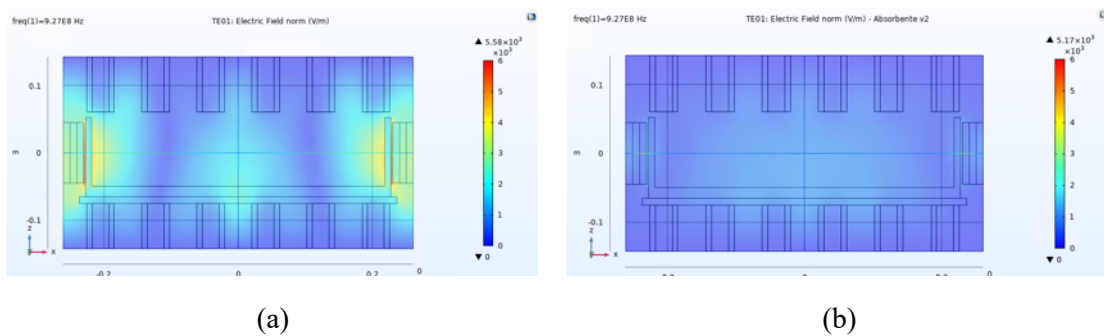


Fig 5.46. Electric field for the version v0 (a) compared to the version v2 (b). TE_{01} mode (XZ view).

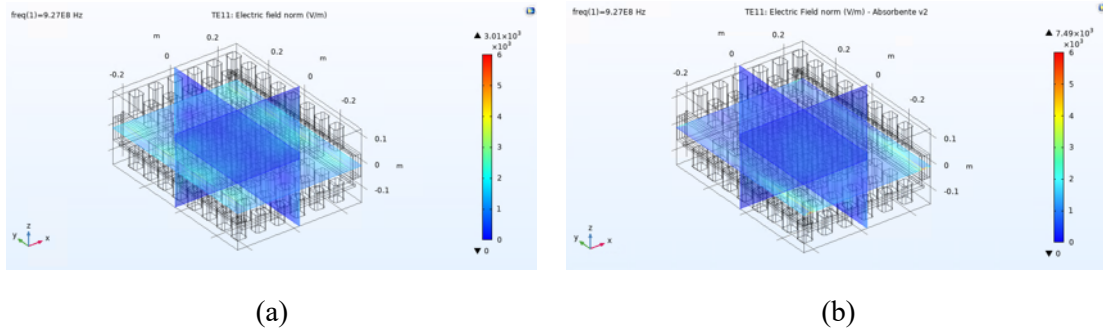


Fig 5.47. Electric field for the version v0 (a) compared to the version v2 (b). TE_{11} mode (Isometric view).

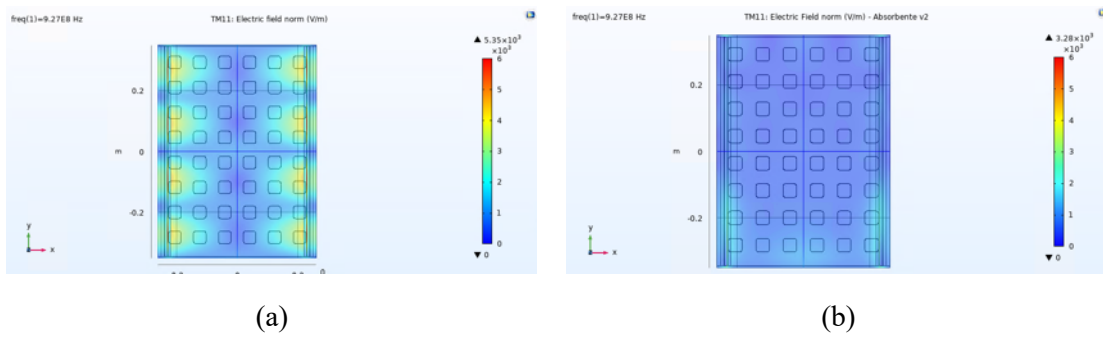


Fig 5.48. Electric field for the version v0 (a) compared to the version v2 (b). TM_{11} mode (XY view).

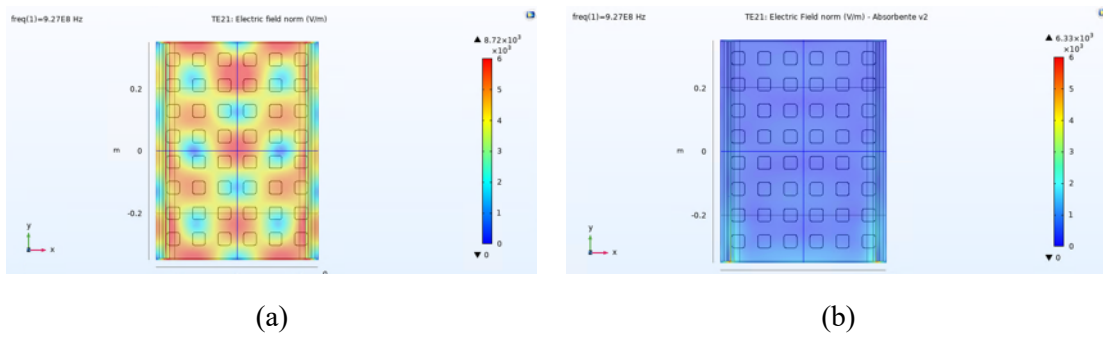


Fig 5.49. Electric field for the version v0 (a) compared to the version v2 (b). TE_{21} mode (XY view).

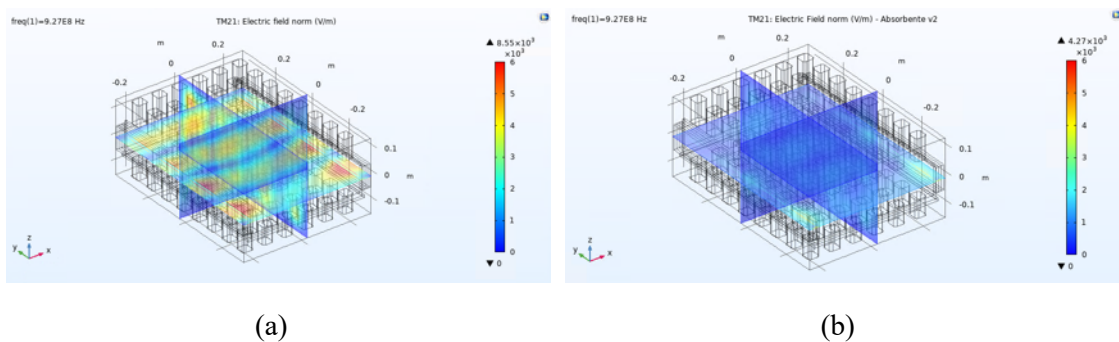


Fig 5.50. Electric field for the version v0 (a) compared to the version v2 (b). TM_{21} mode (Isometric view).

Part III

Results

Chapter 6. Solid-state based system's description

Solid-state microwave systems present clear and varied design and behaviour differences compared to vacuum tube heating applications. Precise power control, fine frequency adjustment, phase-shifting capability, fast response and low voltage requirements are some of the main advantages. This third part of the document compiles all the results directly related to designing, developing, and manufacturing the solid-state driven microwave heating system with multiple sources at different frequencies.

Chapter 6 includes the description of the system architecture, with three specific subsections: the microwave generation (solid-state power amplifier), the control and wave manipulation (phase-shifting and power lectures) and the applicators (antennas). This last subsection includes the complete theoretical description of the different designed antennas. Several of these have been implemented and integrated into the final systems, while others have been designed and manufactured but not chosen to be used in the system. This chapter also describes these last antennas' design process and measurements.

The system proposed in this doctoral thesis, the S2MH, consists of two main blocks: the Solid-State Microwave Generator System (SSMGS) and the applicator. Fig 6.1 shows a summary of all the elements comprising these two blocks.

The SSMGS is responsible for generating, distributing, and amplifying the microwave signal. The Voltage Control Oscillator (VCO) is responsible for generating the small microwave signal at the working frequency. The Driver amplifies this signal to give the required input power to the power amplifier.

The proposed system relies on multiple illuminations; hence, the microwave signal needs to be divided, in our case, by four identical paths. Each path is now managed independently. First, the phase-shifting takes place while still working with low voltages (slotted lines in Fig 6.1), and second, the main amplification process. The power amplifier allows choosing from zero to maximum power, watt per watt. In this stage, frequency tuning is also possible but restricted to some conditions explained later in the document.

High-power coaxial cables (the bold lines in Fig 6.1) conduct the output power from the SSMG to the second block: the applicator oven. The oven construction can be batch (static) or a tunnel

(continuous). Antennas are used to match the cavity and its load to the 50Ω impedance of the SSMG. These antennas have one thing in common: they have a transversal electromagnetic (TEM) structure similar to the SSMG.

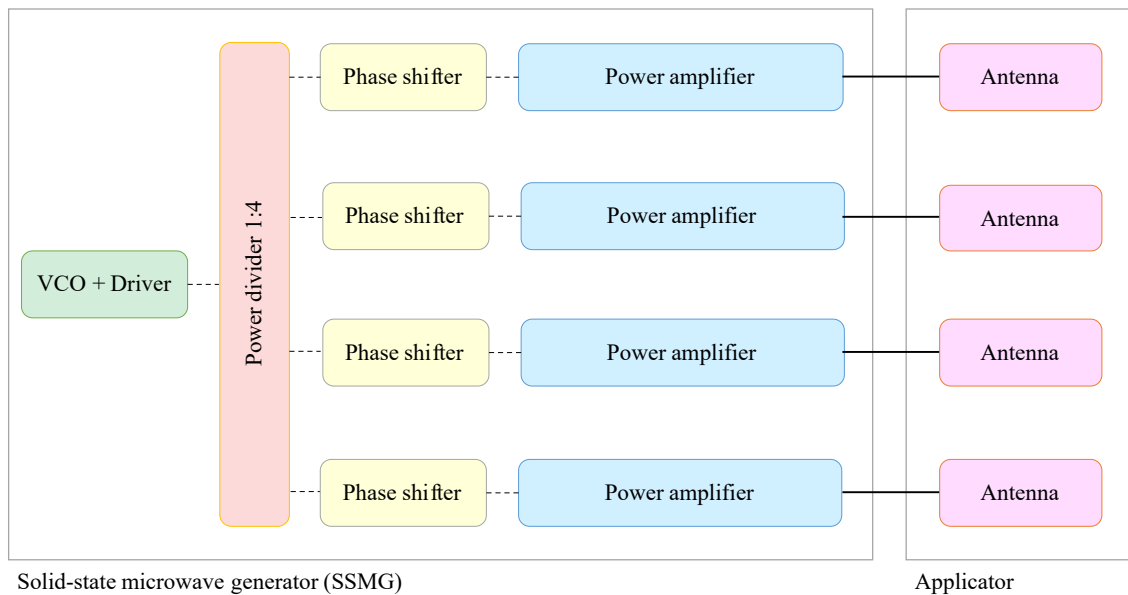


Fig 6.1. Solid-state microwave system architecture.

6.1. Microwave generation: VCO and Driver

Microwave oscillators are at the heart of all RF and microwave systems. Voltage-controlled oscillators (VCO) represent the most common form of oscillators. A VCO is a three-terminal active device that oscillates at the desired frequency band. It commonly uses a varactor diode to tune its frequency within the band [137].

A medium-power amplifier amplifies the RF output power from the VCO with a fixed gain level. This amplifier is also called Driver.

6.2. Power dividers and phase shifters

In RADAR, “the phased array is a directive antenna made up of individual radiating antennas generating a radiation pattern whose shape and direction is determined by the relative phases and amplitudes of the currents of the individual elements.” [3, p. 278]

The primary purpose or advantage of these systems is the capability to change the beam direction of the resultant wave. This change can be done physically by mechanically modifying the orientation of the antennas or electronically by using phase shifters. These last are called *electronically scanned arrays*.

The difference in the phase ϕ experienced by an electromagnetic wave is defined by (6.1), where f is the working frequency, l the length of the transmission line and v the velocity, which is, in turn, depending on the permeability and permittivity of the propagating medium.

$$\phi = 2\pi fl/v \quad (6.1)$$

Three variables can be used to develop a phase-shifting system: the frequency, the transmission line length and the velocity. The frequency was the first technique used and requires a generator per antenna. The second one, the transmission line length, became one of the most popular forms, especially when the line lengths are quantised digitally (see Fig 6.2). The last one, the velocity, can be done, for example, by changing the permeability of the medium, extensively used in ferrite phase shifters. In “Introduction to Radar Systems”, Chapter 8, from professor Skolnik [3], a complete description of all these methods can be found.

The work developed in this thesis has been centred on a digital line change with 3-bit phase shifters. The frequency must be the same to have the same electrical length; it is called a coherent system.

Previously to the phase shifters, a power division must be done. A power divider is a passive microwave device that divides an input signal into two (or more) output signals of lesser powers. It is ideally lossless, although some return and insertion losses may occur. Power dividers usually provide in-phase output signals with an equal power division ratio (3 dB), but unequal power division ratios are also possible. Given some conditions, a power divider can also be used reciprocally as a power combiner.

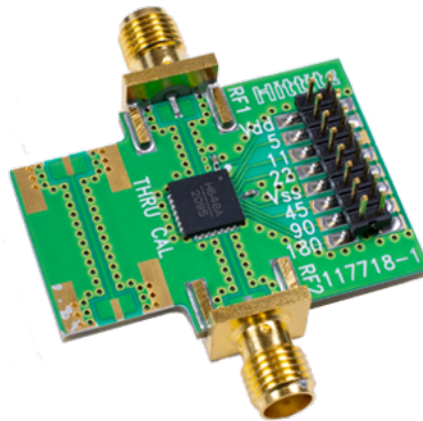


Fig 6.2. Example of a 6-bit digital phase-shifter [138].

Power dividers can be built in different technologies, mainly waveguide, stripline or microstrip, depending on the application and the power handling requirements. In waveguide technology, these can be simple, like in Fig 6.3, or complex, like Fig 6.4. Its main advantage is the high-power handling capability, while the main disadvantage is that its size becomes unpracticable for lower frequencies.

Stripline power dividers (or splitters) are very common, and their use has become extensive due to their design and manufacturing simplicity. They also allow more significant amounts of power

(around 1 kW) when using thick dielectric slabs as a substrate with dielectric constants between 2 and 10. The company Microbiotech has within their products some of these dividers (see Fig 6.5).

In the present case, power division is done with low power, so microstrip technology is also an option. Standard circuitry power dividers are going to be used for that purpose. Wilkinson divider is a well-known microstrip power divider design. These are the most common for communication purposes, and an example of it is shown in Fig 6.6.

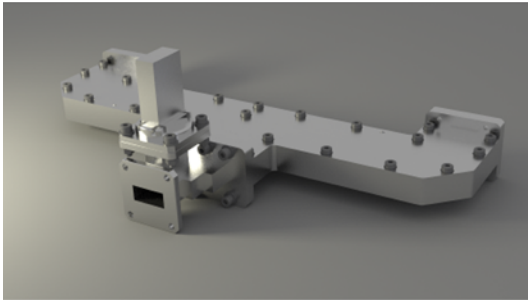


Fig 6.3. "Simple" two-way power splitter from Raditek Inc. [139]

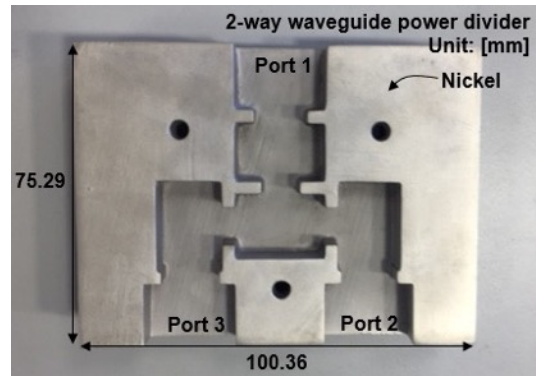


Fig 6.4. "Complex" 2-way waveguide power divider example [140]

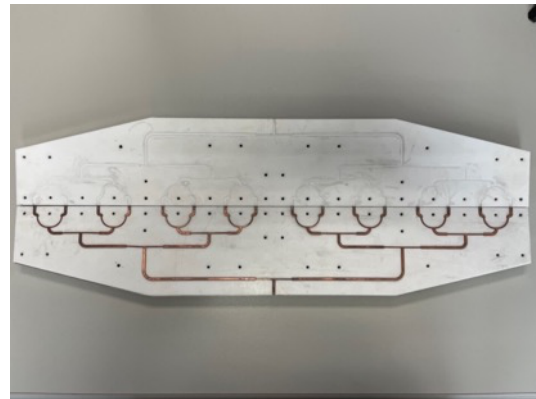
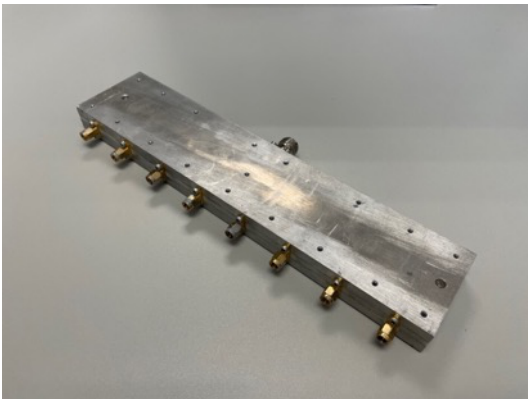


Fig 6.5. Microbiotech's stripline 1:8 (left) and 1:16 (right) power dividers.



Fig 6.6. Example of a microstrip microwave power divider [141].

6.3. Solid-state power amplifiers

After the power division, in this case, by four equal paths, each contains a solid-state power amplifier. This device is responsible for the absolute power generated by the complete system. It is responsible for controlling, gradually, the amplification over the wave. The power amplifier must contain sensing and measurement devices to manage the process, such as temperature sensors, current sensors to avoid peaks that might damage the device, directional couplers to obtain info about both transmitted and reflected power, etc.

This part of the system is critical to high temperatures produced by the working process and its higher or lower efficiency. This last parameter will determine how good a solid-state power amplifier is. Later developments give the market solid-state power amplifiers of 500 W and efficiencies around 75% from a single transistor.

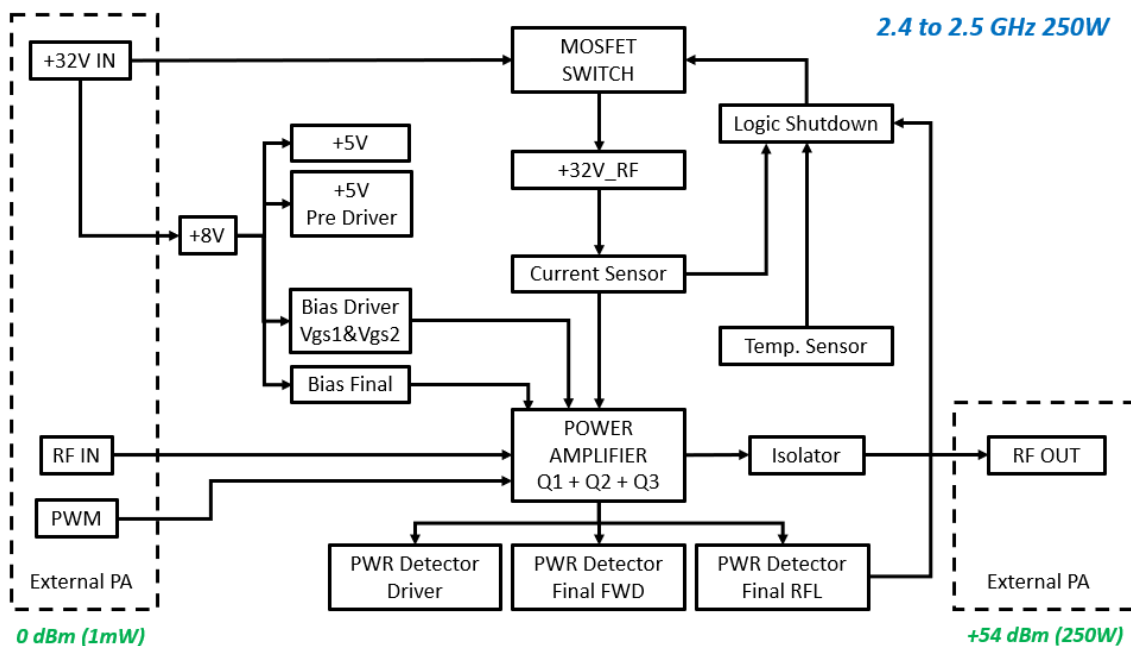


Fig 6.7. Example of the block diagram of a solid-state power amplifier at 2.45 GHz and 250 W of output power [137, Fig. 5]

This block diagram, developed by a Master's student whose work has been supervised by the author, is designed with two zones: the external, framed in Fig 6.7, and the internal. The different blocks are described below:

- a) **External.** It involves the RF IN, RF OUT, PWM and +32V IN signals. When a power amplifier is in a testbench for measure and characterisation, the user manually introduces these values. RF OUT is not defined but obtained as a result of the performance of the internal blocks; however, given that it is directly connected to the output connector, it has been defined as external.
- b) **Internal.**
 - a. DC voltage adjustment. The +32V external voltage is adjusted to a lower fixed voltage of +8V. This one, in turn, is controlled to a +5V voltage. Two

independent controllers are used to feed two circuits independently: on one hand, those related to feeding circuitry like amplifiers, logic gates or other integrated circuits; on the other hand, to feed the pre-driver transistor (Gain Block).

These +8V are also used as a voltage reference to the Driver and Final transistors' polarisation.

- b. Protection system for the amplifier. A MOSFET SWITCH, fed by the +32V, is responsible for cutting the current when one of the following three conditions happens: *Current Sensor*, *Temp. sensor*, *PWR Detector Final RFL*. The Logic Shutdown block collects these conditions, and their functions are implemented by logic gates, operational amplifiers and threshold adjustment potentiometers.
- c. Central block. The most critical nuclear block, with the POWER AMPLIFIER Q1+Q2+Q3 and its three detection subcircuits: Driver, Final FWD and Final RFL; plus the Isolator block. Here, the low power (mW) signal from the oscillator at the RF IN will be amplified and conducted to the RF OUT connector.
- d. Isolator. Finally, an isolator protects the amplifier from the possible reflected waves due to mismatching between the power transfer circuit and the antenna.

A complete design of all the elements comprising the amplifier has been made by Hernández-Bertó [142]. This master's thesis can serve as a guideline for designing and manufacturing solid-state power amplifiers.

6.4. Antennas

The Institute of Electrical and Electronical Engineers (IEEE) defines an antenna as “That part of a transmitting or receiving system which is designed to radiate or to receive electromagnetic waves” [143]. If the system is designed for other purposes than communication, an antenna can also be understood as an impedance matching device from the wires or waveguides to the free space.

Until now, industrial microwave systems, which were magnetron-driven, have had a common approach in the feeding structures for the applicators: waveguide and apertures. The idea presented in this work to operate with multiple solid-state generators allows working with TEM feeding structures. These structures can handle lower powers than the waveguide but, with a specific design, enough for the applications taken into account.

This subsection introduces the theory around the main TEM antennas used: monopole, slot, patch and PIFA. They have been designed, and the best solutions for multi-illumination real applications have been manufactured and implemented. The designs of the firsts are shown in this subsection, while the manufactured ones are introduced here and explained in detail in the following chapters.

6.4.1. Monopole antennas

One of the simplest antennas, the half-wave dipole antenna (Fig 6.8), consists of a two-wire transmission line. Each arm length of the antenna is $L \approx \lambda/4$.

A monopole antenna consists of one-half a dipole antenna mounted above the earth or a ground plane (Fig 6.9). It usually is one-quarter wavelength long. This antenna has been extensively used for commercial broadcasting in the radiofrequency AM band (500 to 1,500 kHz) and is also widely used for the land mobile-communication service [144].

These antennas have been used for frequencies in the lower RF range, so their dimensions are relatively big. However, dimensions became very feasible when using this antenna in the main ISM frequency bands. For instance, at 2,450 MHz, a monopole antenna is about 3 cm in length, which is a value that allows it to work inside microwave cavities.

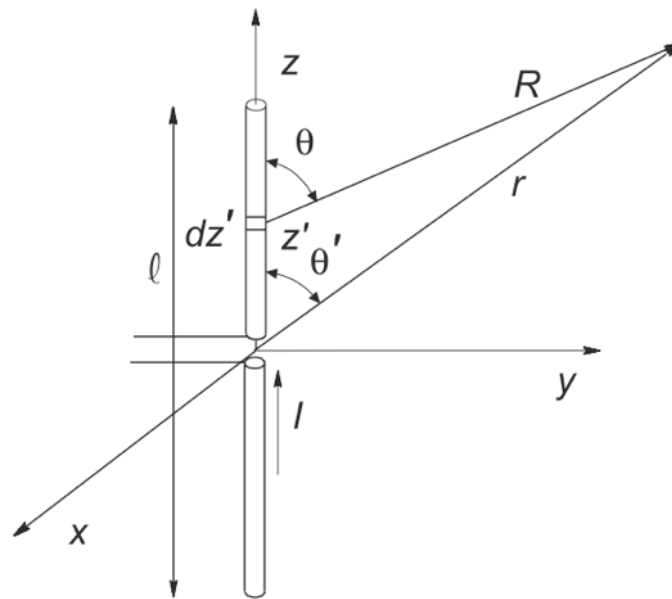


Fig 6.8. Basic dipole antenna schematic [145, Fig. 4.1]



Fig 6.9. Monopole antenna and its equivalent dipole [145, Fig. 4.16]

Two monopole antenna designs have been developed during this PhD process. 1) One economical and straightforward N-connectorized antenna at 2,450 MHz, capable of handling up to 300 W of power. 2) A novel tuneable monopole antenna, whose designs have been made for 433, 915 and 2,450 MHz with two power limits: 300 W (N-connector) and 800 W (7/16'' connector) of continuous wave (CW).

The first design is being used in an industrial application and is explained in detail in Chapter 7.

6.4.1.1 Tunable monopole antennas.

The author of this document mentored a Master's thesis called "Design and Modelling of Tunable Monopole Antennas for Power Applications in the ISM Band" [146]. The antennas designed can correct or improve the system's matching to different load sizes and properties; and cavity dimensions. This design can help create microwave systems that are more capable and versatile.

The antennas are built with a solid cylinder soldered to the coaxial connector, with its outer surface with M3 DIN metric thread. A second cylinder, wider and shorter than the first, is threaded to the main one (see Fig 6.10). The position of this element defines the antenna matching.

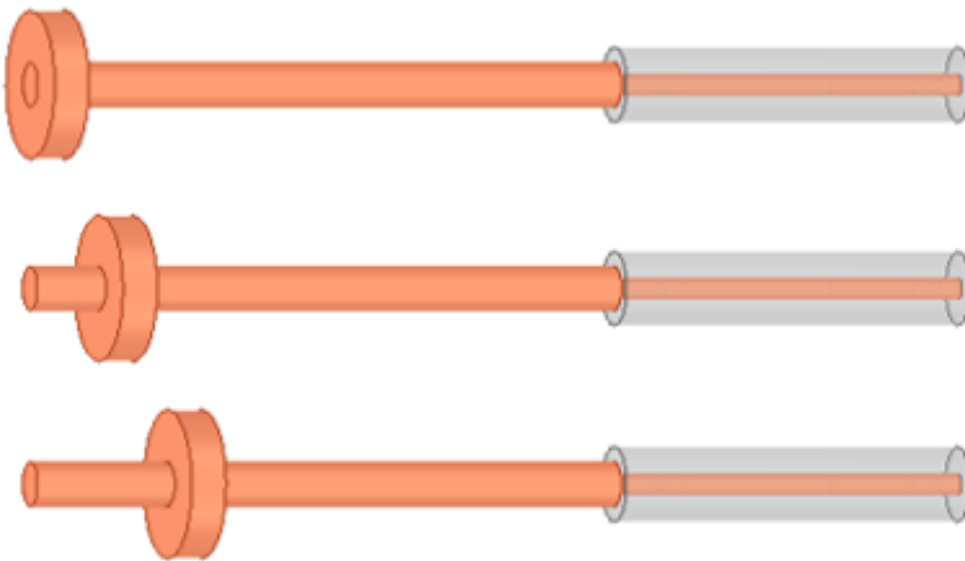


Fig 6.10. Moving cylinder example.

Six different versions of the tunable antenna have been designed: two versions for each of the three ISM frequencies discussed in this document (433, 915 and 2,450 MHz). The two versions are referred to as the maximum handling power capacity: 500 W (N-connector) and 1 kW (7/16"-connector). The design process has been carried out with the electromagnetic modelling tool HFSS.

The design antenna parameters are:

- DT, the diameter of the principal cylinder. It has to be smaller than the connector dielectric diameter: the N-connector is 4.1 mm, and the 7/16" connector is 10.2 mm. Otherwise, the antenna is in contact with the ground plane.
- AT, the principal cylinder's height or length. It is the main parameter for frequency tuning and is close to $\lambda/4$.
- DC, the diameter of the secondary cylinder or cap. It has to keep the resonance frequency obtained by DT.
- AC, the cap's height or thickness. It has been set to 5 mm for constructive reasons.

- CP, the cap position. It is responsible for achieving the best matching value depending on the load. The objective return losses are -10 dB, at least.

These variables have been used in a thorough parametric study for every one of the six designs. The cavity dimensions are 600 x 600 x 500 mm (width, length, height), and the load is defined to obtain similar responses with the three frequencies.

The final antennas have been manufactured (see Fig 6.12) and measured in a loaded cavity. Fig 6.11 shows the antenna at 433 MHz and N-connectorised as an example. The antennas dimensions are shown in Table 6.1.

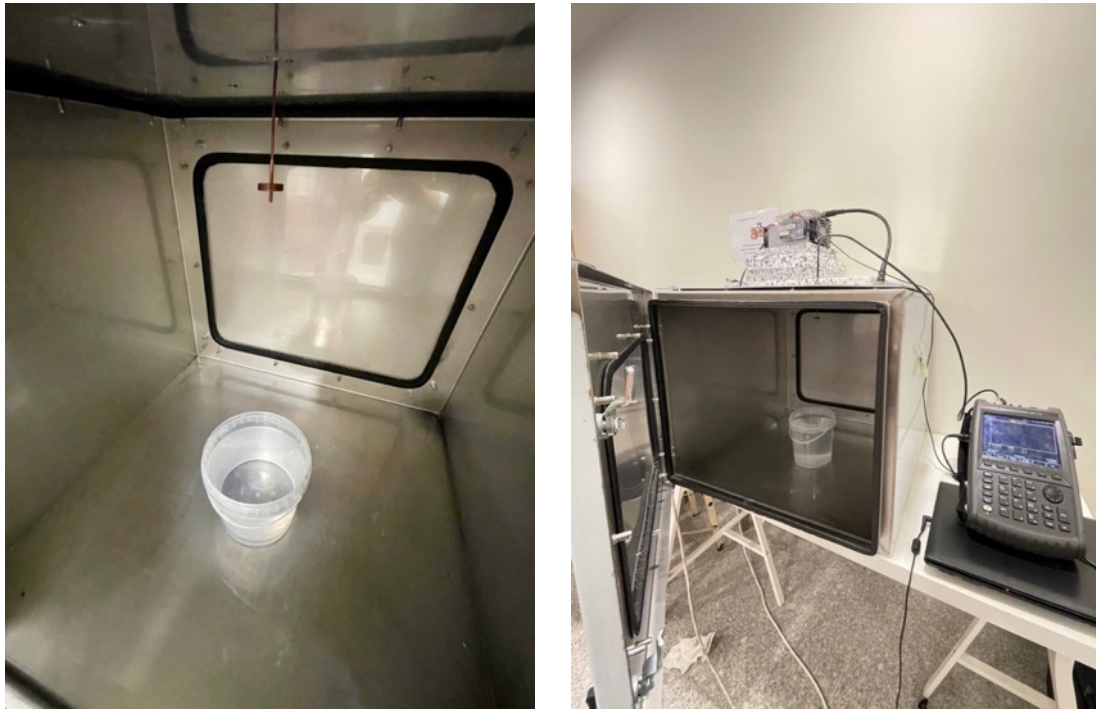


Fig 6.11. Antenna measurement. Interior view (left) and exterior view, with the VNA (right).

Table 6.1. Tunable antennas dimensions.

Parameters	Frequency					
	433 MHz		915 MHz		2,450 MHz	
	N	7/16"	N	7/16"	N	7/16"
DT	2.5 mm	8 mm	2.5 mm	8 mm	2.5 mm	8 mm
AT	80 mm	85 mm	50 mm		30 mm	
DC	20 mm		12 mm	20 mm	20 mm	
AC	5 mm					

An interesting feature of the 7/16" antennas is that the inner conductor of the connector has been prepared to replace it with the different frequency configurations. Given the price of these connectors (around 50 €), it is an interesting solution for lab equipment where tests at different frequencies are extensively used. It can be seen in Fig 6.13.

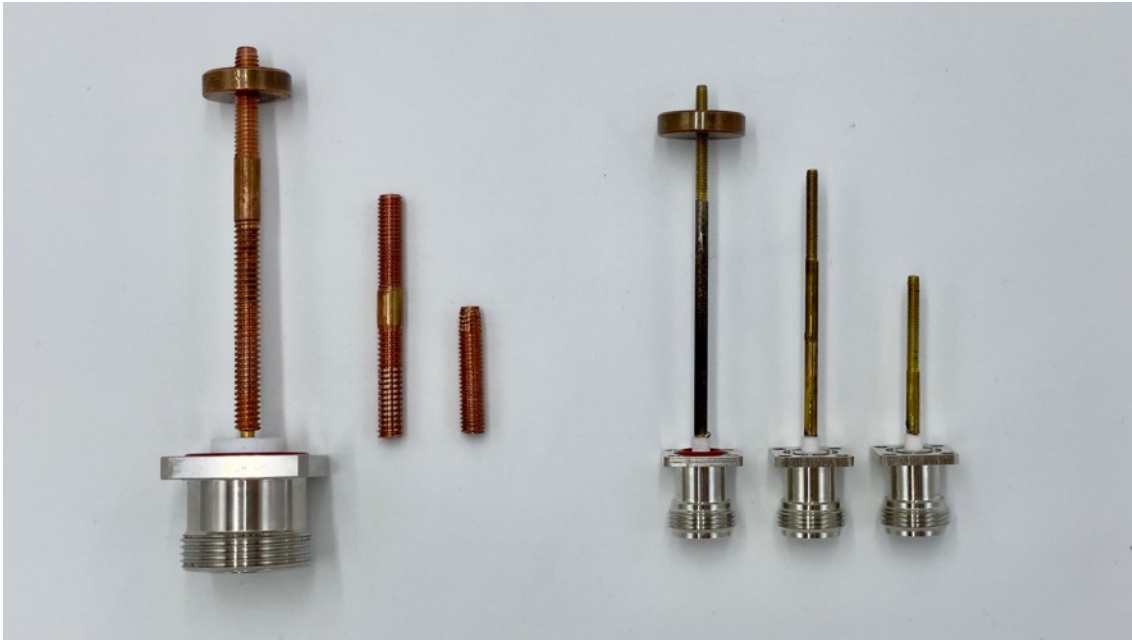


Fig 6.12. Six manufactured antennas.



Fig 6.13. Manufactured antennas with the 7/16" connector separately.

6.4.2. Slotted stripline antennas

A narrow slot, one-half wavelength long and cut in a conducting sheet of metal, is a dual half-wave dipole antenna. The slot may be excited from a coaxial line, as shown in Fig 6.14. The radiation pattern and directivity of the slot antenna are the same as those for the dipole antenna. Single-slot radiators are used as aircraft antennas where the slot is made a part of the aircraft structure itself. It is also possible to have a quarter-wave slot antenna, analogous to a monopole antenna [144]. These slot antennas have been generally integrated into resonant arrays supported by one of the faces of a waveguide.

However, for communication purposes, printed slot antennas were the most interesting ones; hence there is a lot of research effort devoted to them reported in the literature [147]–[150]. Integrated patch antennas increased their use due to the need for size and cost reduction, and integration with monolithic microwave integrated circuit (MMIC) devices [151]. At the beginning of the century, this paradigm shift was limited to low power applications. In high power heating applications, tubes and waveguides had no opponents.

The lack of suitable feeding structure designs for this kind of source hinders fully exploiting the advantages offered by this technology. To overcome it, the author worked on designing a small slot antenna with the requirements to use it as a feeding structure for a solid-state driven microwave multi-mode cavity applicator.

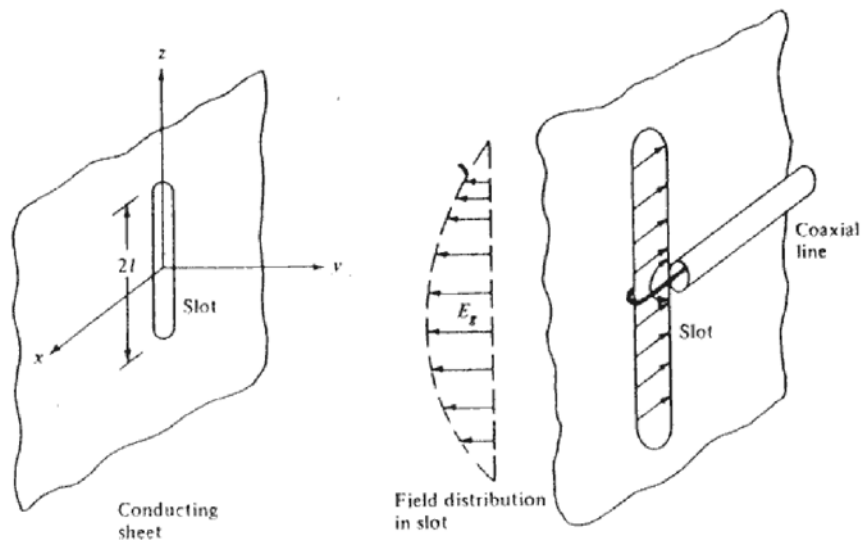


Fig 6.14. The slot antenna and its typical feeding structure [144, Fig. 4.67]

6.4.2.1 New stripline antenna design

The work devoted to this antenna design and manufacture has been published in *Electronics*, an open-access journal from MDPI, titled “Cavity-backed Slot Antenna Fed by a Stripline with SIW Structure and Vertical Coaxial Transition for Microwave Solid-State Heating Applications” [152].

The mentioned paper presents a new approach for feeding multi-mode cavities used as microwave applicators for industrial and domestic microwave ovens using solid-state sources operating in

the 2,450 MHz ISM band (commonly used for industrial microwave applications). The feeding structure consists of a slot on the top side of the applicator cavity. A shielded asymmetric stripline feeds the slot with a Substrate Integrated Waveguide structure (to preserve the stripline TEM operation within the shield) and N-connectorized.

The design of the antenna consisted of three steps. First, the slot antenna is designed on a ground plane without a cavity. This design led to the slot dimensions and the position of the feeding line. Due to the envisaged application, the stripline is shielded within a metallic box, and the slot design is modified to take into account the effect of the lateral walls. Afterwards, a SIW structure is added to suppress non-TEM modes arising in the cavity. Lastly, the vertical stripline-to-coaxial transition is designed (including a matching network) to make this antenna easy to integrate into a microwave applicator. The final model can be seen in Fig 6.15.

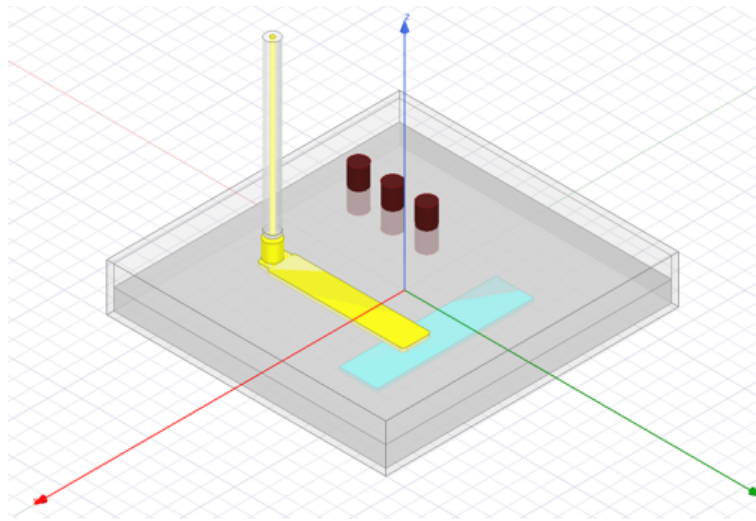


Fig 6.15. HFSS model of the slot antenna fed by the stripline.

Slot and stripline feeding line design

Following the description above and the considerations that are given by C.A. Balanis [153], a half-wave slot has been designed with a slot length $L \approx \lambda/2$ and a slot width of $W \leq 0.1\lambda$. A first approach to the slot dimensions at the working frequency is obtained from (6.2) and (6.3).

$$L = \lambda_0/2 = \frac{c_0/f_0}{2} = 61.22mm \quad (6.2)$$

$$W \leq 0.1\lambda_0 = 12.24mm \quad (6.3)$$

The slot antenna is fed using a stripline structure. The term stripline refers to a structure having a strip lying between two ground planes and parallel to them. Usually, the strip is placed at the same distance from each ground plane, but in this case, to simplify the manufacture of the antenna, the dielectric filling the space between both ground planes is split into two slabs with the same dimensions. The strip is embedded in a slot drilled on the surface of one of them, leading to a slightly off-centre stripline structure [130].

Considering the application envisaged for this antenna, the stripline used to feed it must be designed to support the propagation of high-power waves (in the order of 500 W). Therefore, a material with excellent dielectric and thermal properties (PTFE) is selected for the substrate. Once the substrate material is selected, the separation between the ground planes and the stripline width is designed keeping in mind the power requirement, leading to a set-up consisting of two sheets of 6mm height, allowing the stripline to be thick enough to support the required power. The parametric study of the strip width w has been conducted to obtain a 50Ω stripline, leading to a value of $w=8.34\text{mm}$.

After implementing the first elements in HFSS (Fig 6.18), the antenna sensitivity with L and W is studied to obtain a design baseline for the antenna that is further adjusted when the effect of the box and the feeding structure is taken into account. The analysis of Fig 6.16 and Fig 6.17 shows that the operation frequency is strongly dependent on the slot length L , whereas the slot width W mainly affects the return losses. The optimum values for L and W were 49 mm and 10.7 mm, respectively.

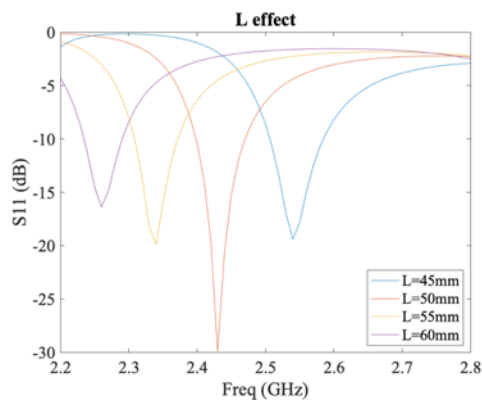


Fig 6.16. Effect on the return losses for different slot lengths (L)

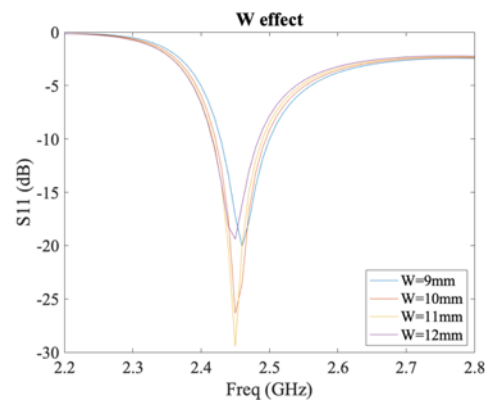


Fig 6.17. Effect on the return losses for different slot widths (W)

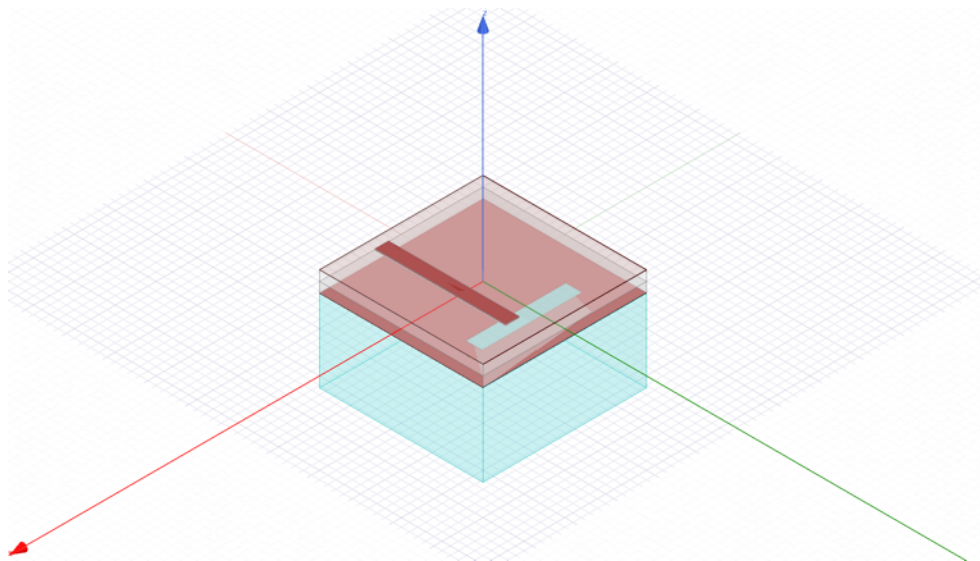


Fig 6.18. Modelling of the slot antenna fed by the stripline.

A stripline-fed slot is a well-known antenna [154]. The impedance matching of this kind of feed mainly depends on the distance between the feeding stripline and the centre of the slot. A thorough explanation of this behaviour can be found, for instance, in [155].

Once the strip and slot dimensions are defined, the position (distance to the slot centre) and the penetration over the slot width remain the two parameters governing the impedance matching (i.e., reducing the return losses). A parametric analysis using HFSS shows that the best solution is achieved when the strip is 11mm away from the slot centre and entirely covers the slot, as shown in Fig 6.18.

Shielding and SIW structures integration.

Due to the enclosed nature of the antenna (which is application-driven), it becomes a cavity, which is also known in the literature as a cavity-backed slot antenna [5]. The two main design parameters for this kind of antenna are the distance between the slot and the walls and the distance between the upper and lower ground planes (i.e., the cavity height). A thorough parametric study has been conducted to assess the design sensitivity to these variables.

As can be seen in Fig 6.19, the effect of the distance to the upper and lower walls yields a significant variation within a narrow distance sweep (from 20mm to 25mm). The figure needed to tune the antenna at 2.45 GHz is 22mm (which is close to $\lambda_{\text{eff}}/4$, a typical value for resonators design). Fig 6.20 shows the effect of the distance to the nearest parallel wall. This effect is somehow equivalent to a displacement of the slot along the transverse (Y) direction, thus is similar to that of the slot width, W (i.e., basically affects the antenna matching).

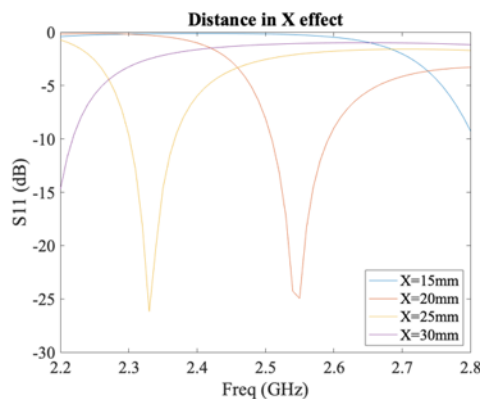


Fig 6.19. S11 parameter effect for different distances to upper and lower walls.

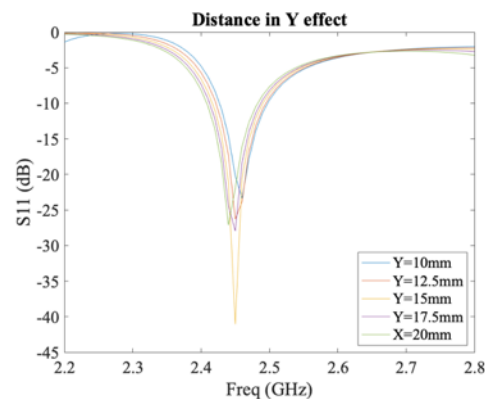


Fig 6.20. S11 parameter effect for different distances to the right wall.

A similar effect to that described above with the transverse lateral walls can also be observed on the strip. In this case, the distance of the strip to the closest wall is fixed by the slot and the position of the strip, leading to an asymmetric layout to the lateral walls parallel to the strip (see Fig 6.21). This asymmetry allows the appearance of high-order modes and is solved with the use of a new type of transmission line: Substrate Integrated Waveguides (SIW). This line consists of metallic posts with a specific diameter and separation between them. These values, the diameter of the posts, Vr (Fig 6.22), and the separation between them are obtained according to [156].

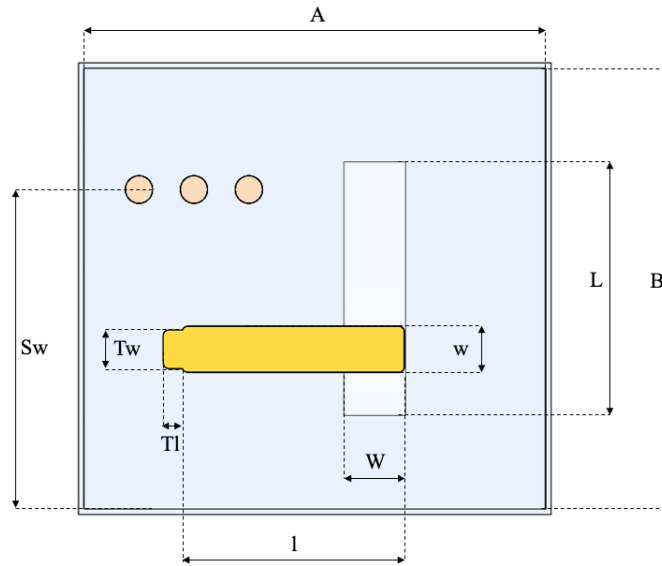


Fig 6.21. Top cut view of the antenna assembly with the widths and lengths of each component.

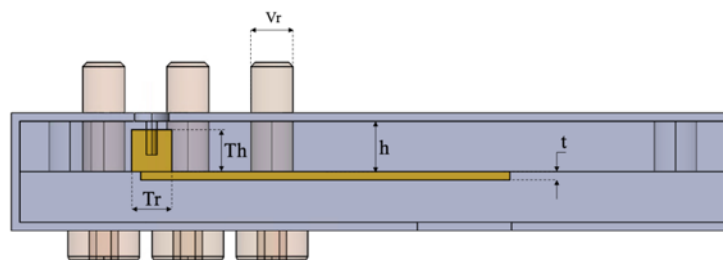


Fig 6.22. Lateral cut view of the antenna assembly with the heights and diameters of the components.

Vertical coaxial to stripline transition and final cavity matching.

This antenna has been designed to feed a cavity. Therefore, the slot and the connector must be in opposite planes, making the input microwave power easier. For that purpose, a vertical transition is needed [157].

A vertical stripline-coaxial transition usually needs two or three matching elements. In this case, a tapered strip and a cylinder reduce the return losses. The adaptation parameters for the tapered strip are the length, the width and the distance to the closest wall (i.e., that on the left in Fig 6.21). In the case of the cylinder, its radius and its height are the parameters that drive the adaptation. The final dimensions are obtained after performing several parametrical studies with the parameters above (see Fig 6.22).

When a resonant antenna such as the one discussed in the previous subsections is used to feed an empty resonant cavity, like a commercial microwave oven applicator, there are several changes in the antenna behaviour in the free space. These are: 1) the resonant frequencies of the antenna are lower than those in the free space, and 2) the resonances are also narrower. When the cavity

is loaded, the resonances are wider (leading to larger band-width), the resonant frequencies are even lower, and the resonances' level is higher due to the power absorbed by the load.

Thus, some changes to the antenna designed in the previous subsections must be made. According to the process described above in this section, an excellent approach to improving matching is modifying the slot width (W) and length (L), increasing W from 10.7 to 11.2 mm and reducing L from 49 to 46 tunes this antenna to the loaded cavity (Fig 6.23). Table 6.2 contains the final dimensions of the structure.

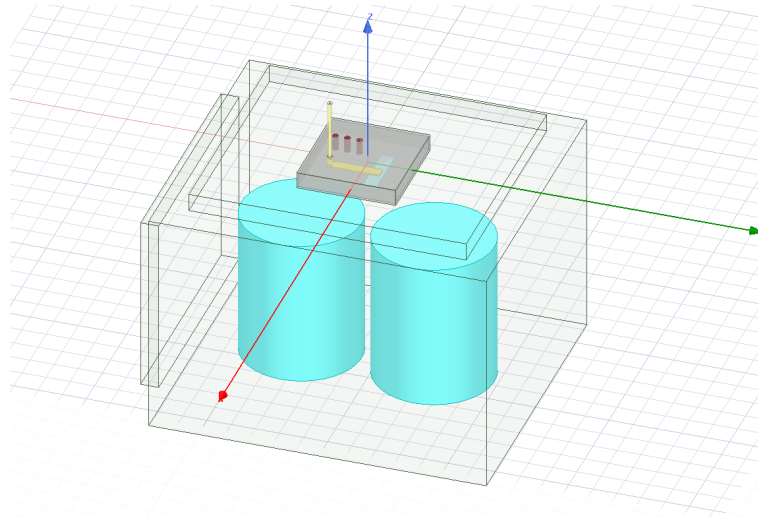


Fig 6.23. Antenna modelled feeding a box with commercial microwave oven dimensions and loaded with 2 litres of fresh water.

Table 6.2. Final antenna design parameters.

Parameter	Description	Value (mm)
w	Strip width	8.34
t	Strip thickness	1
l	Strip length	40.4
h	Dielectric thickness	6
W	Slot width	11
L	Slot length	49
A	Total length	80
B	Total width	75
V _r	Vias radius	2.5

Manufacture and validation.

The antenna has been manufactured with relatively thick components to have a simple and economical design. Two aluminium sheets are used for the shielding (with the corresponding bending); the strip is manufactured from a copper sheet (Fig 6.24); and the transition from a cylindrical copper piece. Two 6 mm Teflon sheets are used as a dielectric filling, and metric screws serve as metallic posts for the SIW. Four screws are used to secure the assembly, and, finally, an N-connector is welded into the cylindrical transition (Fig 6.25).

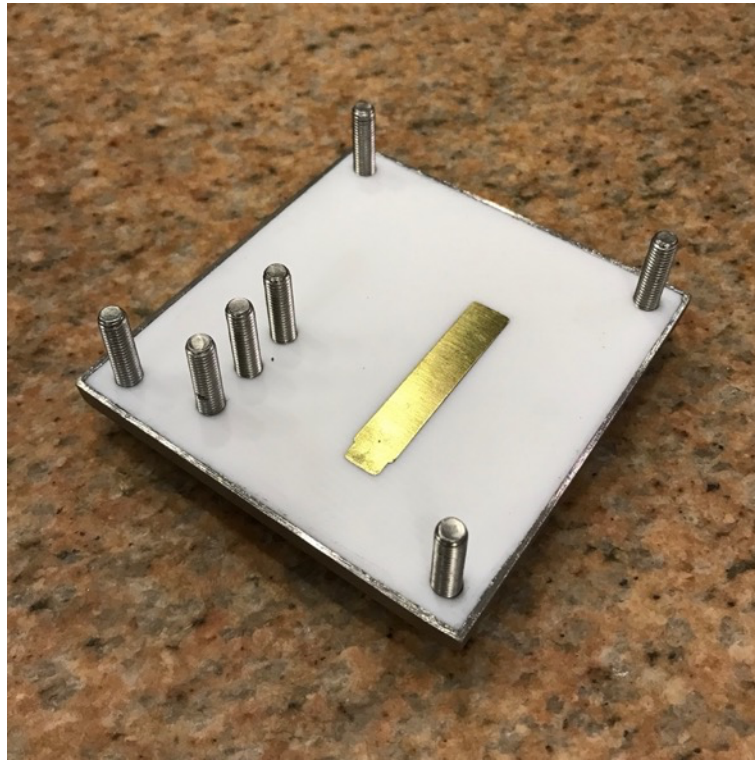


Fig 6.24. Lower part of the antenna assembly.

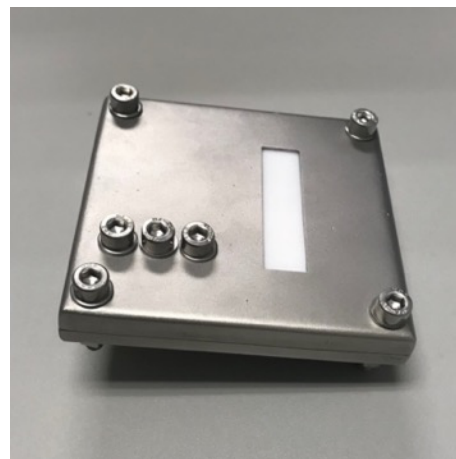
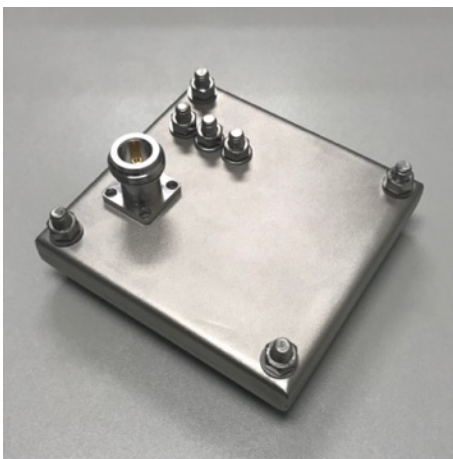


Fig 6.25. Top and bottom view of the manufactured antenna

The antenna has been measured in an anechoic chamber (Fig 6.26), leading to radiation measurements shown in Fig 6.27. These measurements also show a resonant frequency at 2.35

GHz (Fig 6.29), upholding the fact that the antenna needs to be designed with a higher resonant frequency to counter the cavity effect.

The antenna has also been installed on top of a modified commercial microwave oven (Fig 6.28), and the S_{11} parameter has been measured. Fig 6.30 shows the good agreement between the modelling and the measurement return losses values.

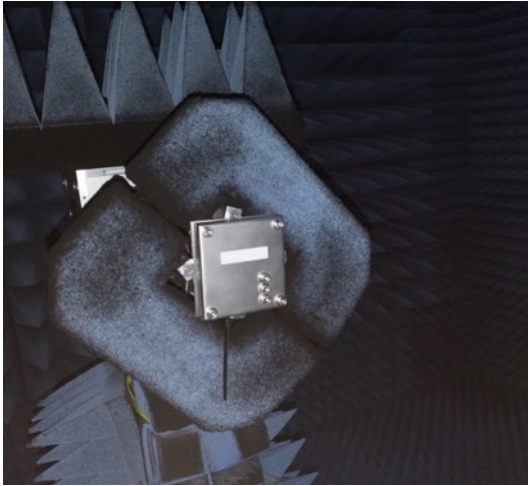


Fig 6.26. SIW antenna measured in an anechoic chamber.

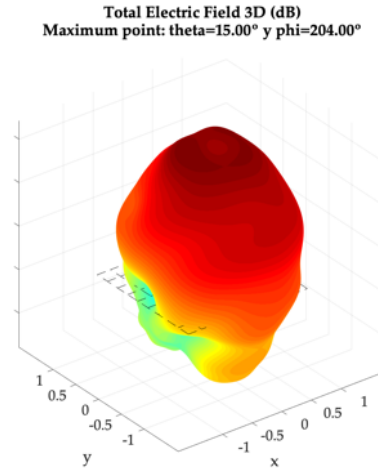


Fig 6.27. Antenna measured total electric field.



Fig 6.28. 2-litre recipients and the antenna placed in the cavity.

Finally, the IMPI 2-Liter test was performed. This test is an IMPI normalised method [158] to check the actual efficiency of a microwave oven, consisting of heating 2 litres of tempered water in two different containers for 122 seconds. The amount of transmitted power (6.6) is obtained by applying equations (6.4) and (6.5):

$$E(J) = P(W) * t(s) \quad (6.4)$$

$$E(J) = m(g) * C_e(J/gK) * \Delta T \quad (6.5)$$

$$P_{absorbed}(W) = \frac{m(g) * C_e(J/gK) * \Delta T}{t(s)} \tag{6.6}$$

The constant parameters used for this test were: 1) $m(g) = 2000g$, 2) $C_e = 4.1813J/gK$ and 3) $t = 122$ s.

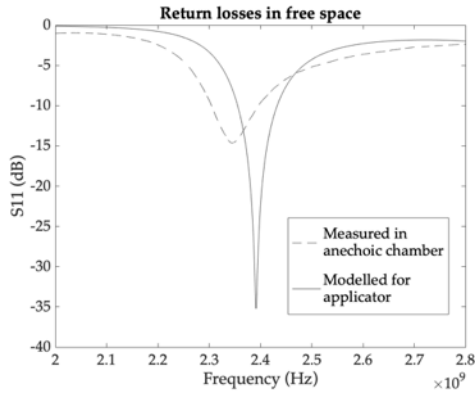


Fig 6.29. Comparison of the return losses (S11(dB)) between the model and the manufactured antenna, measured in an anechoic chamber.

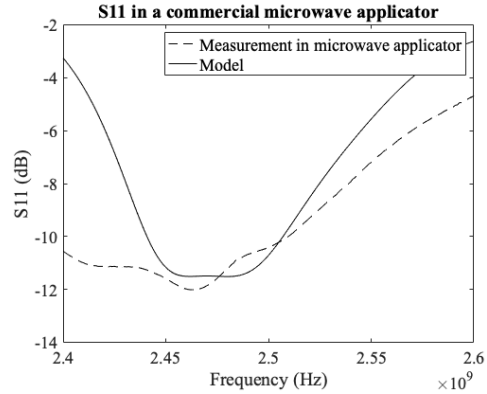


Fig 6.30. Comparison between the S11 parameters of the measurement with the antenna feeding a commercial microwave oven and the model.

The power has been generated using a solid-state power amplifier (Generator Lab Kit, Leanfa Srl, Ruvo di Puglia, Bari, IT) with an output power of 250 W and capable of measuring forward and reflected power during the test. Table 6.3 shows the average results out of ten repetitions. It can be seen that when significant power is introduced, the actual power absorption is higher than the S11 obtained in the measurements because of the effect of the load.

Table 6.3. Power and temperature measurements of the 2-litre test.

Parameter	Value
T_0 (°C)	17.5
T_F (°C)	20.5
ΔT (°C)= $T_F - T_0$	3
P_{FWD} (W)	250
$P_{absorbed}$ (W)	205.64
$P_{lost}(W)=P_{FWD} - P_{absorbed}$	44.36

This validation process showed an efficiency higher than 80%, a good value for heating processes and a standard in the current microwave oven applicators. However, considering the total electric power consumption, solid-state generators overcome the electricity to radiofrequency transformation performance, resulting in a system with greater energy efficiency.

6.4.3. Patch antennas

Planar patch antennas or microstrip antennas are the best solutions to keep a regular and clean active cavity when space reduction is needed. Patch antennas are made of a very thin metal sheet (usually copper) with $t_c \ll \lambda_0$, where t_c is the copper thickness and λ_0 is the free-space wavelength. This metallic sheet is placed at an h distance over a ground plane; being $h \ll \lambda_0$, generally $0.003\lambda_0 \leq h \leq 0.05\lambda_0$.

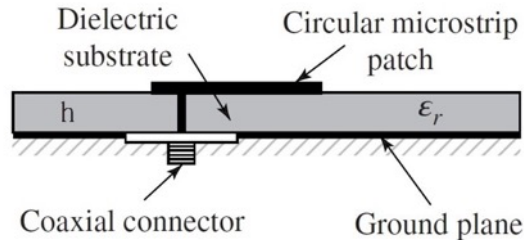


Fig 6.31. Patch antenna lateral cut [153, Fig. 14.3 (b)]

These antennas are low profile, simple and economical. They are compatible with MMIC, making them easy to be designed with a specific resonant frequency, polarisation, pattern or impedance. One of the disadvantages of these antennas is their low efficiency and low power. To overcome the first characteristic, a method used in this project is to increase the height of the substrate. The second one, the low power, has been faced using thicker patches: metallic sheets instead of printed surfaces.

6.4.3.1 Circular antennas.

The second most used patch antennas are circular. They have been used in arrays for applications like RADAR, among others. With these antennas, only one patch dimension parameter can be used to tune the antenna: the radius. The matching element is the pin (source) position, but the more centred, the better.

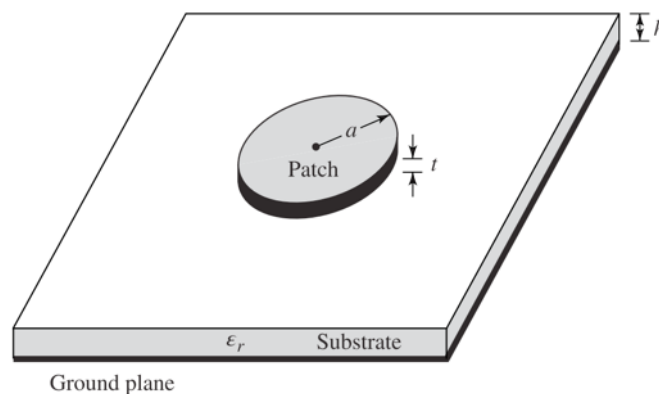


Fig 6.32. Circular patch antenna schematic [153, Fig. 1.5 (b)]

For the same substrate and ground dimensions, a larger perimeter can be obtained with squared antennas, thus, making them more interesting for the application in microwave cavities than the circular ones.

6.4.3.2 Square antennas

The square patch, or rectangular, is the most used configuration of patch antennas. The design parameters are the patch thickness, t , the substrate thickness h , and the patch dimensions L and W . The ground plane dimensions, typically some millimetres more than L and W , must be adjusted to cope with the fringing effect (see more in [153, pp. 789–790]).

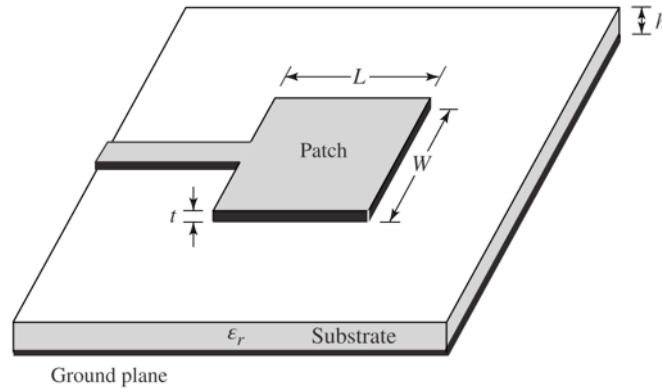


Fig 6.33. Rectangular patch antenna schematic [153, Fig. 1.5 (a)]

The patch perimeter is directly related to the tuned frequency with two freedom degrees: length and width. These antennas can be fed with a microstrip transmission line (coupled or connected) as in Fig 6.33 or with a coaxial cable and its inner conductor soldered to the patch somewhere around the middle of the patch. This position serves as the parametric value to the matching.

6.4.3.3 Antenna miniaturisation. New substrates.

Antenna miniaturisation is a process the antenna designer can exercise to reduce the dimensions of the antenna while maintaining, within reasonable limits, the original antenna radiation characteristics. It is not a simple process, and most often, some compromises have had to be accepted between reduction in dimensions and antenna performance [153, p. 619].

Since the effective wavelength is defined by (6.7), dielectric substrates with high permittivity values (ϵ_r) have been used as one of the most successful approaches to reducing antenna dimensions.

$$\lambda_{eff} = \frac{\lambda_0}{\sqrt{\epsilon_r}} \quad (6.7)$$

Two different designs have been conducted for that purpose: 1) using PEEK (Polyetheretherketone) and 2) using barium titanate as substrates.

PEEK Substrate antennas.

PEEK is a high-performance thermoplastic material that is an excellent choice for demanding applications. It withstands high temperatures and is resistant to chemicals and radiation. PEEK can be used continuously in operating temperatures up to 250° C and in hot water or steam with

no compromise to its physical properties. PEEK offers wear, moisture and chemical resistance, exceptional strength, dimensional stability and stiffness. Because of its high performance, PEEK is used in many challenging environments in the medical, nuclear, chemical processing and aerospace industries. PEEK is easily machined [159].

The author tutorised a master's thesis entitled "Patch antennas design and manufacturing for power applications in resonant cavity" [160]. It involves the complete study for the miniaturisation of patch antennas using PEEK as substrate. The results of this work are six different antennas working at the ISM frequency bands 433 MHz, 915 MHz and 2.45 GHz with two handling power capabilities: coaxial N-connectorized and coaxial 7/16'' connectorized.

The design parameters of these antennas were that they needed to have return losses lower than -10 dB in the whole frequency range and be tuned to work inside a loaded cavity. The final size dimensions (Fig 6.34) and characterisation results are shown in Table 6.4.

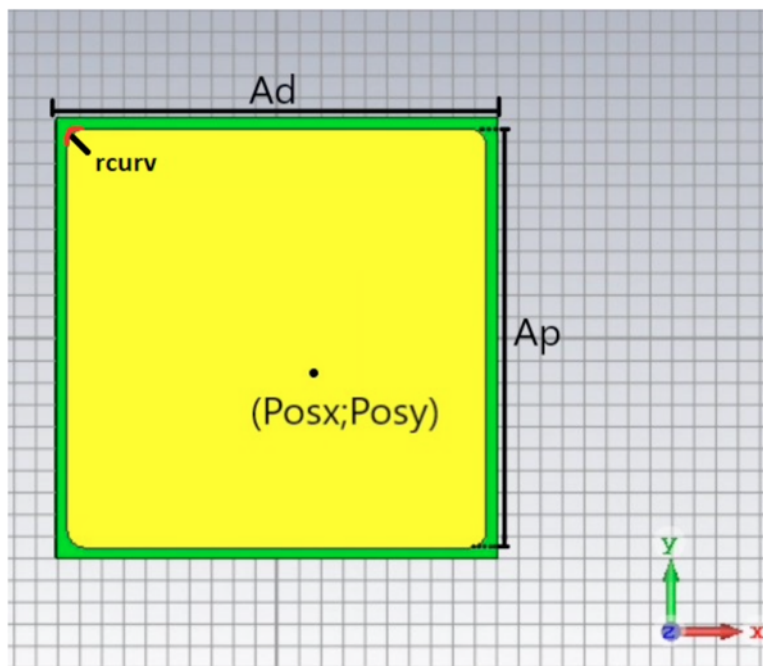


Fig 6.34. Design variables in CST for the patch antennas [160, Fig. 7]

Table 6.4. Final results of the PEEK patch antennas [160].

Frequency (MHz)	N-type connector	7/16''-type connector
433	Ad = 390 mm Ap = 380 mm Posx = 10 mm Posy = -10 mm Rcurv = 10 mm S11 = -17.3 dB BW = 14.2 MHz	Ad = 390 mm Ap = 380 mm Posx = 6 mm Posy = -6 mm Rcurv = 10 mm S11 = -14.15 dB BW = 11.93 MHz

915	Ad = 190 mm Ap = 180 mm Posx = 18 mm Posy = -18 mm Rcurv = 10 mm S11 = -21.38 dB BW = 37.89 MHz	Ad = 190 mm Ap = 180 mm Posx = 18 mm Posy = -18 mm Rcurv = 10 mm S11 = -23.35 dB BW = 42.4 MHz
2450	Ad = 76.5 mm Ap = 66.5 mm Posx = 11 mm Posy = -11 mm Rcurv = 11 mm S11 = -21.5 dB BW = 74.8 MHz	Ad = 76.5 mm Ap = 66.5 mm Posx = 11 mm Posy = -11 mm Rcurv = 11 mm S11 = -18.63 dB BW = 81.4 MHz

Barium titanate (BaTiO₃) antennas.

Numerous substrates can be used for the patch antenna design, whose dielectric constant is usually in the range of $2.1 \leq \epsilon_r \leq 12$. For good antenna performance, the most desirable ones are thick substrates whose dielectric constant is in the lower end of the range. They can provide better efficiency and larger bandwidth, but at the expense of larger element size [161]. Thin substrates with higher dielectric constants are desirable for microwave circuitry because they require tightly bound fields to minimise undesired radiation and coupling and lead to smaller element sizes. However, because of their more significant losses, they are less efficient and have relatively smaller bandwidths [161]. Since patch antennas are often integrated with other microwave circuitry, a compromise between good antenna performance and circuit design must be reached.

De Loor, in 1956, introduced in his PhD thesis the equations to obtain the dielectric properties of heterogeneous mixtures [162]. Equation (6.8) defines the dielectric constant of the mix depending on the constituents' permittivity, the inclusion percentage and a depolarisation factor.

$$\epsilon_m = \epsilon_h + \frac{v_i(\epsilon_i - \epsilon_h)}{1 + A_u \left(\frac{\epsilon_i}{\epsilon^*} - 1 \right)} \quad (6.8)$$

The parameters in this equation are:

- ϵ_m is the mixture dielectric constant.
- ϵ_h is the dielectric constant of the host material.
- ϵ_i is the dielectric constant of the inclusion.
- v_i is the inclusion rate (from 0 to 1).
- ϵ^* is the effective dielectric constant for the region immediately surrounding an included particle. For higher inclusion values, $v_i \sim 1$, $\epsilon^* = \epsilon_h$.

- A_u is the depolarisation factor, e.g., $A_u = 1$ when the inclusions are spheres.

This methodology, also developed by Tinga [163], can be devoted to reducing or incrementing the mixture's dielectric properties and creating new materials with entirely different dielectric properties.

For example, if the objective is to reduce the dielectric constant, the most efficient way is to introduce a scattered matrix of air spheres into the host material. Or, if the objective consists of having a metallic behaviour in a non-metallic material, a host like the Teflon can be modified by inserting barium titanate particles [164].

Professors Elías De los Reyes and Miguel Ferrando are currently working on designing these antennas, and the author of this thesis has been supporting this research.

6.4.3.4 Two-frequency antennas.

“Today's mobile units, such as the smartphone, provide a plethora of services, from phone calls, emails, messaging, news, sports, music, to maps, just to name a few. Also, these units have become smaller and slimmer, and less room is available to accommodate all these services efficiently. Since it is impossible to dedicate an individual antenna design for each of the services, antenna design engineers face major challenges to come up with designs whereby each antenna structure can accommodate multiple services. This requires that each physical antenna structure resonates at multiple frequencies, leading to multi-band designs. One planar antenna structure that can resonate at multiple frequencies is a rectangular microstrip with multiple slots placed on its patch in the form of a U. Each U slot is designed to resonate at a given frequency, and this is accomplished by making the overall length of each slot nearly $\lambda/2$ ” [153, p. 846].

Fig 6.35 shows an example of these antennas. The presented approach has been used to design and manufacture a two-frequency patch antenna for high-power heating microwave applications.

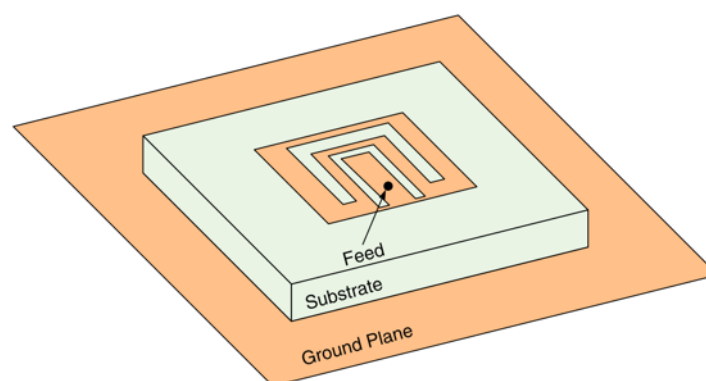


Fig 6.35. Example of a three-band U-shot microstrip/patch antenna [153, Fig. 14.55]

A common approach for microstrip antenna arrays is to have the patch backed by a rectangular or circular cavity, as shown in Fig 6.36. The first approach for this multi-frequency antenna has been made using this technique.

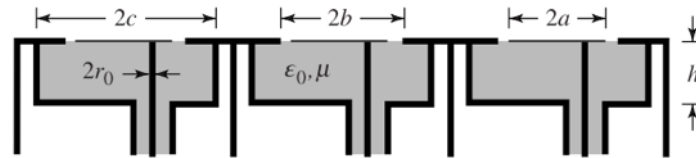


Fig 6.36. Side view of a patch array backed by circular cavities [153, Fig. 14.41 (b)]

The original design consisted of a rectangular cavity filled with Teflon[®] having a patch on top of it. A small gap was set between the cavity walls and the patch, and its feeding was modelled by a coaxial cable on the same plane as the patch (see Fig 6.37). The first variation was performed over the patch dimensions, specifically the one longitudinal to the feeding point. This parameter was defined as B and set initially to $A/2$ (see Fig 6.38); it represents the patch reduction compared to the cavity (plus the gap, g).

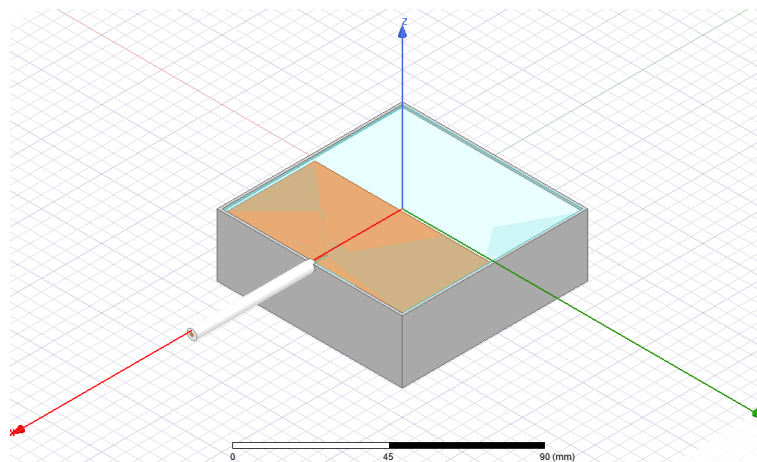


Fig 6.37. Starting point of the 2-frequencies patch antenna modelled in HFSS.

Several changes are performed, such as adding a curvature at the patch corners (r), or reducing the thickness of the dielectric and, therefore, the cavity. Another variable is the distance of the patch to the cavity ground or the top of it, and it has been defined to be over the Teflon slab rather than embedded in it.

Several parametric studies have been performed where the total perimeter, $4 \times A$, the gap, g , the cut in the patch, B , and the radius curvature of the patch corners, r , have been used to find the best matching at 915 and 2,450 MHz. The outcome of these is summarised in Table 6.5 and serves to decide the next step: to adjust these parameters for the lower frequency and use a second technique to implement the higher frequency matching.

Two symmetric slots L-shaped and cut in the patch have been designed to have the final matching of the antenna to the two frequencies. The parameters that drive the matching are the distance from the bottom of the patch to the slot, S_x , the distance from the centre to the beginning of the slot, S_y , the total length of the slot, L , and the thickness of the slot, s . All these parameters can be seen in Fig 6.38.

Table 6.5. First design parametric studies summary.

Parameter	@ 915 MHz	@ 2,450 MHz
A	Slightly over 150mm	Two solutions: 110 and 160 mm
B	58 mm for A = 160 mm	51 mm for A = 160 mm
g	Best: 6 mm, Acceptable: 1.5 mm	1.5 mm
r	Only for fine matching	Only for fine matching

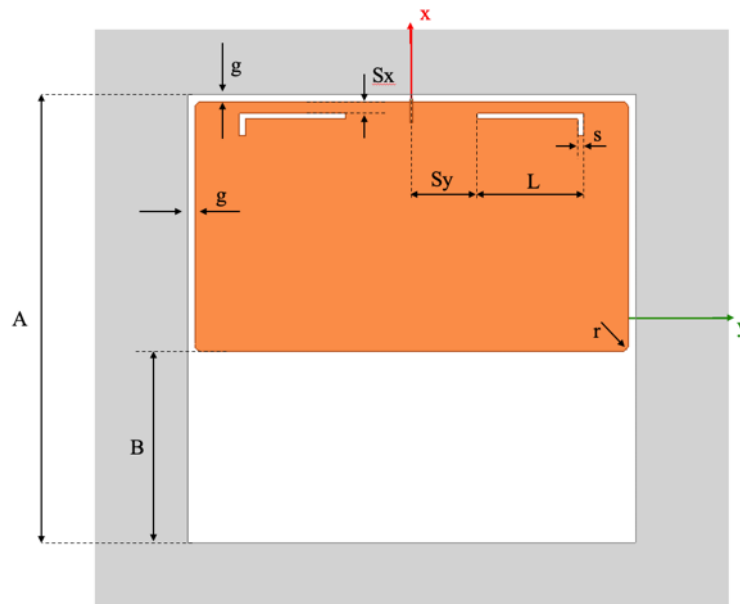


Fig 6.38. Two-frequencies antenna top view with its design parameters.

After reducing the Teflon[®] slab thickness to a commercially available standard size (8 mm), the outside length is readjusted to 190 mm. The rest of the parameters are adjusted to obtain return losses lower than -10 dB in both working frequency bands. Moreover, a vertical feeding is needed to install the antenna in a microwave cavity. Different solutions to the feeding are taken into account, including one connector divided into three feeding points, one connector per frequency with two separated feeding points, and one connector with one feeding point. This last one could be designed with the coaxial placed in the middle of the outer conductor, i.e., inside the box lateral wall or between the gap, g . This final solution can be seen implemented in Fig 6.39.

Several parametric studies have been carried out once the final thicknesses and the structure have been defined. For instance, Fig 6.40 shows how the patch dimension affects the frequency tuning. Looking at these two graphs, several values for the B parameter work fine for both frequencies (e.g., $B = 110$ mm). The symmetric L-shaped slots placed in the patch are used to match the two frequencies. 915 MHz is mainly tuned by the slot length L , as shown in Fig 6.43 (Fig 6.44 shows the minor effect of this parameter at this frequency). On the other hand, 2,450 MHz is tuned by the vertical part of the slot L_2 , as shown in Fig 6.42 (while the length nearly affects the tuned frequency, as seen in Fig 6.41).

Finally, the position of the slots is defined by the S_x and S_y parameters. The effect of these parameters has been studied, showing a strong relation between them and the matching level at 2.45 GHz (see Fig 6.45 and Fig 6.46). The effect of these parameters at 915 MHz is negligible.

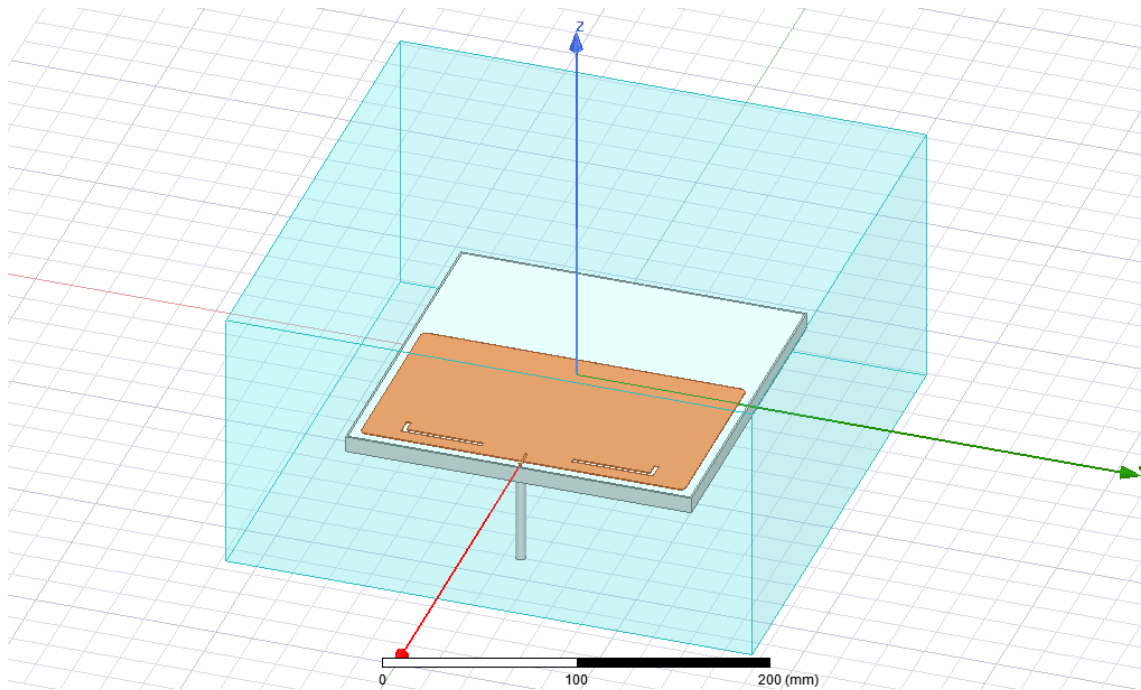


Fig 6.39. Final model of the 2-frequencies patch antenna.

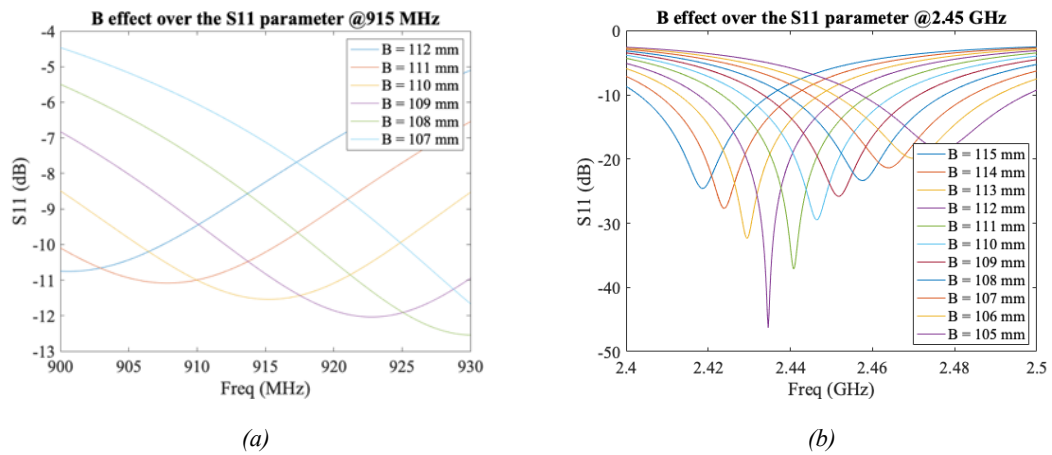


Fig 6.40. Effect of the B parameter (affecting the patch size) over the return losses at (a) 915 MHz and (b) 2,450 MHz.

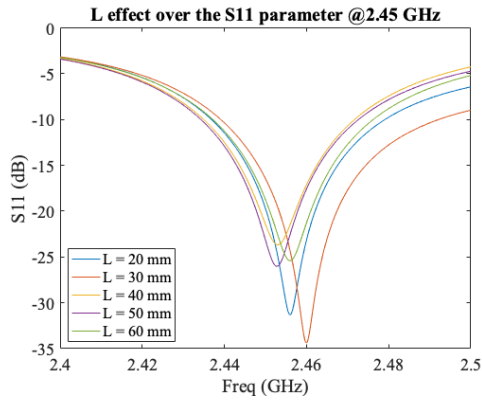


Fig 6.41. Effect of the slot length, L , over the return losses at 2.45 GHz.

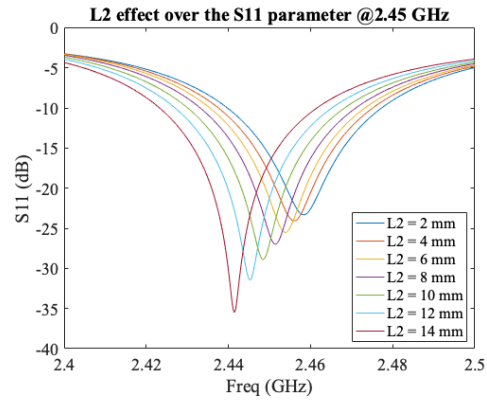


Fig 6.42. Effect of the vertical part of the slot, L_2 , over the return losses at 2.45 GHz.

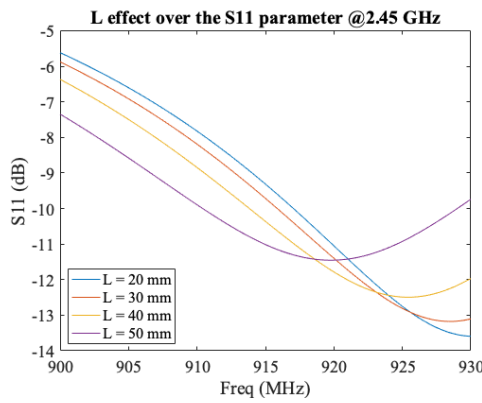


Fig 6.43. Effect of the slot length, L , over the return losses at 915 MHz.

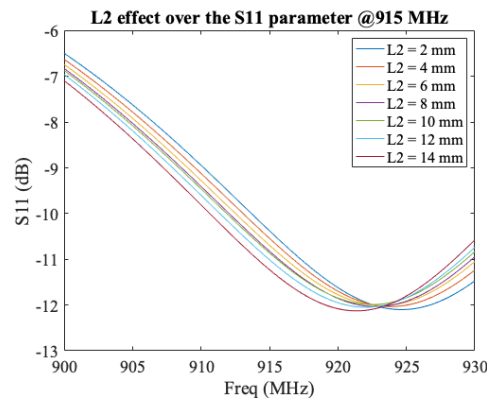


Fig 6.44. Effect of the vertical part of the slot, L_2 , over the return losses at 915 MHz.

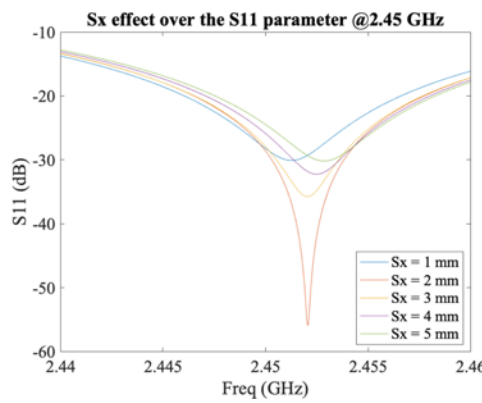


Fig 6.45. Effect of the S_x parameter over the S_{11} return losses, with $S_y = 20$ mm, at 2.45 GHz.

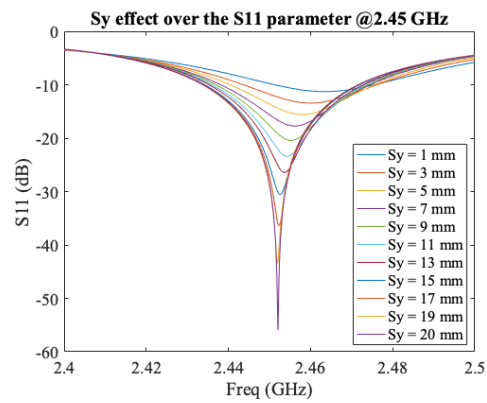


Fig 6.46. Effect of the S_y parameter over the return losses, with $S_x = 2$ mm, at 2.45 GHz.

The second part of the design of this multi-frequency antenna was adapting it to work inside a microwave cavity. To that end, several adjustments to the parameters need to be made. The final dimensions of the antenna, for both free space and cavity, are defined in Table 6.6.

Table 6.6. Final multi-frequency antenna design parameters.

Parameter	Value for free-space	Value for cavity
A	190 mm	
B	81 mm	
g	5 mm	
r	3 mm	
L	45 mm	
L2	7 mm	
Sx	8 mm	5 mm
Sy	25 mm	28 mm
s	2.5 mm	

The antenna has been manufactured (see Fig 6.47) and measured its return losses (Fig 6.48). The results pointed out in Table 6.7 show the frequency deviation introduced when the antenna design is adjusted to work inside a cavity.

Table 6.7. Marker's values from Fig 6.48 in order of appearance. Squared markers point to the objective frequencies.

Frequency (MHz)	915	943	1,746	2,274	2,450	2,560
Return Losses (dB)	-5.3382	-16.5848	-25.0681	-16.9449	-2.8614	-20.6537

Although these results are promising, the manufacture of this antenna is tricky, and the benefits of having the same antenna for different applications (i.e., frequency band) are not yet enough to take this design for the final system.

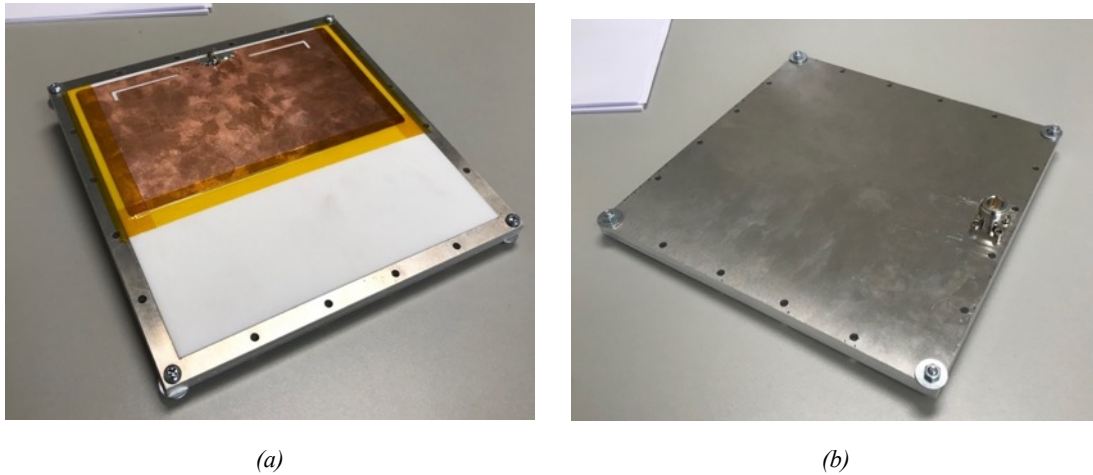


Fig 6.47. Top (a) and bottom (b) views of the multi-frequency manufactured antenna.

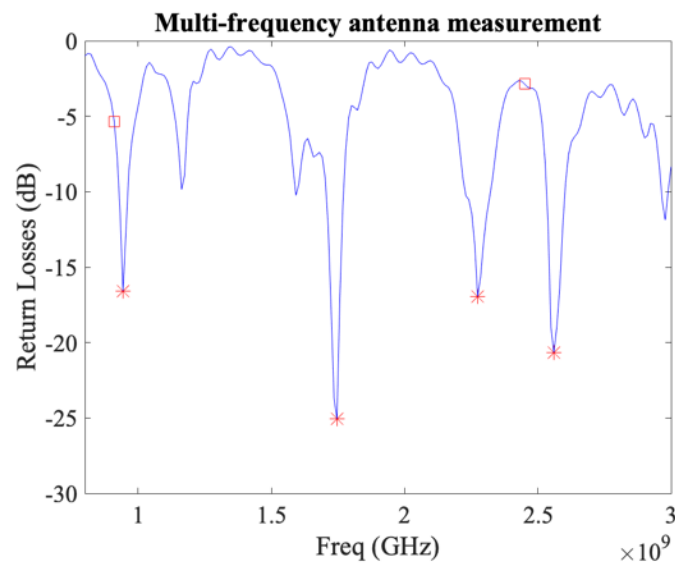


Fig 6.48. Measurement results of the multi-frequency antenna in free-space.

6.4.4. PIFA antennas

Planar Inverted-F Antenna (PIFA) is a very popular design in mobile communications. Its name is due to the resemblance of a letter F with its face down in its side view. Among its advantages are the following [153, p. 838]:

- Low backward radiation reduces the specific absorption rate (SAR) compared to other antenna types used in mobile applications.
- Both vertical and horizontal polarisations can be received.
- It can be easily integrated into mobile devices.
- It is lightweight and conformal.
- It is easy to design.
- It is low cost and reliable.

This antenna is a derivation from the rectangular patch antenna. The feeding point is located on one outer side of the antenna, and a pin, connected to the ground, is added.

The resonant frequency of the PIFA antenna is determined by the patch length (L_1) and width (L_2), the shorting sheet or pin width (W) and the substrate height (h). The relation between these parameters and the wavelength is given by (6.9) [153]:

$$L_1 + L_2 - W = \frac{\lambda}{4} + h \quad (6.9)$$

In this case, the air is used as a substrate. So, the wavelength is the free-space wavelength. For exceptional circumstances, e.g., $W = L_2$, (6.9) reduces to (6.10).

$$L_1 = \frac{\lambda}{4} + h \quad (6.10)$$

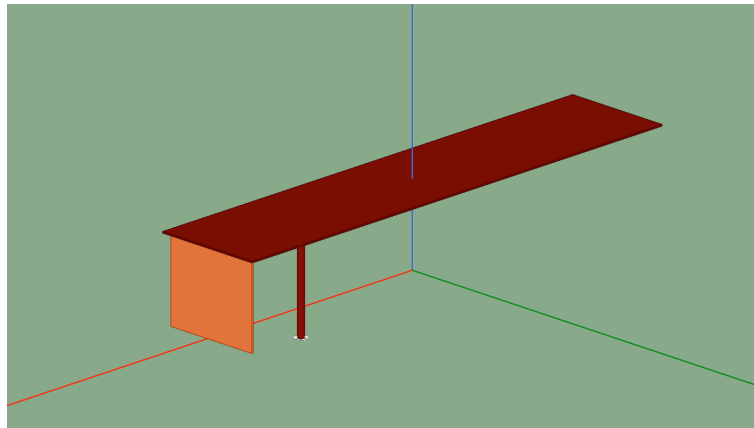


Fig 6.49. Dimetric view of the HFSS design of the PIFA antenna at 433 MHz.

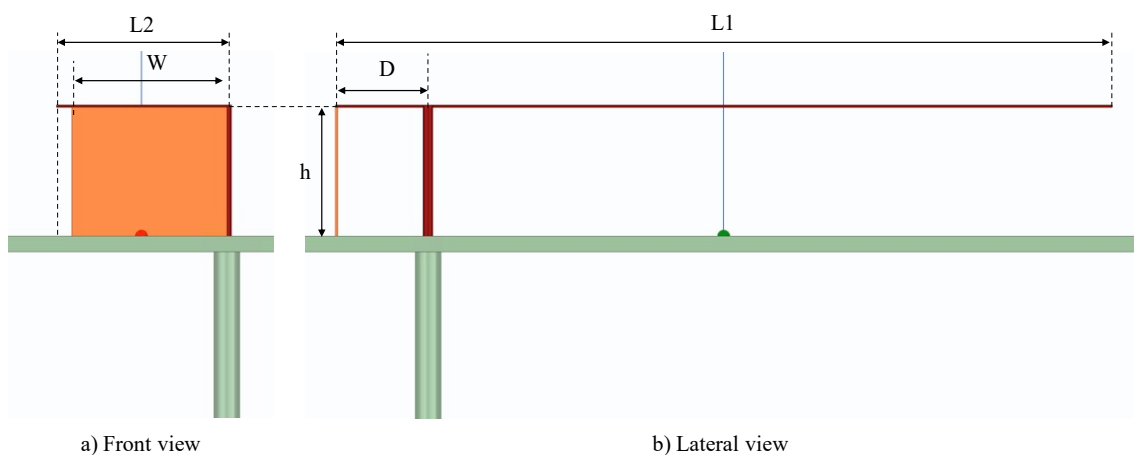


Fig 6.50. Front a) and lateral b) views of the PIFA antenna modelled in HFSS with its design parameters.

A parametric study was conducted with h , W , D , L_1 and L_2 as variables, looking for the best matching of the antenna. L_1 , L_2 and h drive the frequency tuning, while W and D match the antenna to have the lower return losses possible (see Fig 6.51).

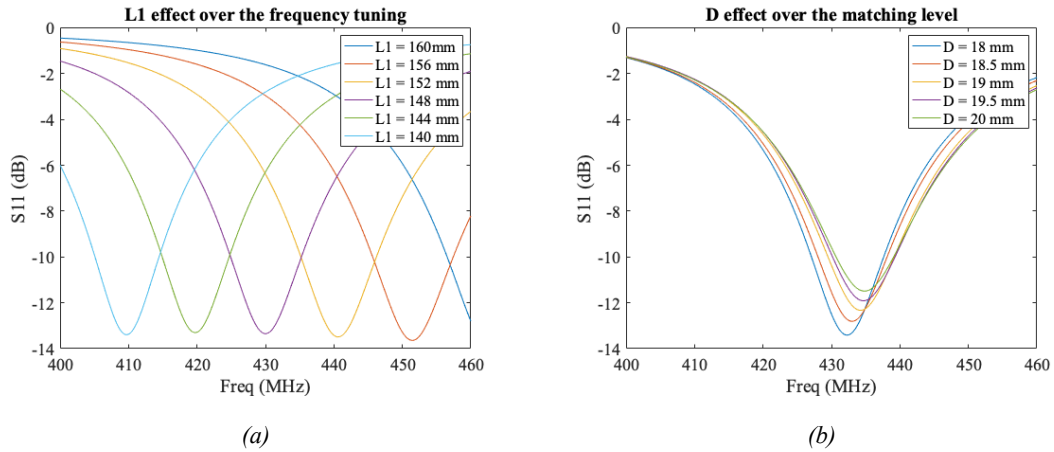


Fig 6.51. Example of the (a) L1 and (b) D parameters effect.

After the parametric study and optimisation, the final dimensions of the antenna are shown in Table 6.8. With these dimensions, the return losses obtained are shown in Fig 6.53.

Table 6.8. PIFA final dimensions

Parameter	Value (mm)
L1	151
L2	33
W	30
h	25
D	18

The antenna has also been manufactured and included in a modified commercial microwave oven (Fig 6.52) and measured. Results are shown in Fig 6.53, where the model and the measurements are compared.



Fig 6.52. Pictures of the PIFA antenna installed in a modified commercial microwave oven.

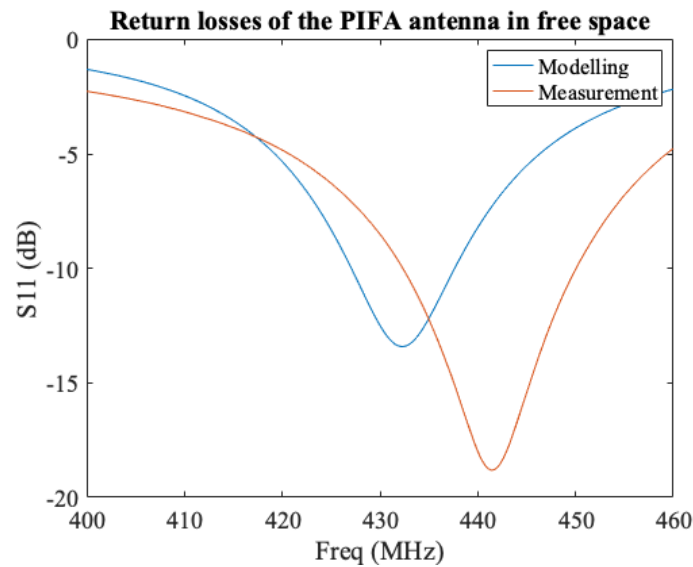


Fig 6.53. Results of the PIFA antenna at 433 MHz

6.5. Resonant cavities.

The last element of the microwave heating system is the resonant cavity, which has already been introduced in Chapter 2. The propagation modes are of great importance in the design of microwave heating systems and are highly dependent on the oven size and the working frequency.

A field propagation mode is seriously considered when the wave reflections inside the cavity define a constructive stationary wave pattern between the cavity walls in at least two out of three directions XYZ. Each propagation mode pattern is characterised by its polarisation (TE – TM) and the number of wavelengths in the three space dimensions. The number of modes, therefore, increases with the cavity size. Fig 6.54 shows the mentioned behaviour for a defined cavity to work at 2.45 GHz and is explained using a dimension factor β . The larger the mode number, the more different field patterns are found in the cavity. Fig 6.55 shows an example of this field pattern for the $\beta = 1$ dimensions.

The resonant cavity has two different behaviours considering the loading condition. When a lossy load is placed inside it, the mode resonant frequency is lower, and its bandwidth is wider (see Fig 6.56). This change implies a reduction in the quality factor Q, which is used to measure the power dissipation and to define the system efficiency. Hence, when designing applicators (antennas) for cavity integration, it is necessary to adjust the dimensions after the free-space design step.

In his Master's thesis [146], Soriano defines the Q factor in a simple, straightforward and helpful way. In summary, larger cavities offer better quality factors. This statement is considered for the application designs explained in the two following chapters.

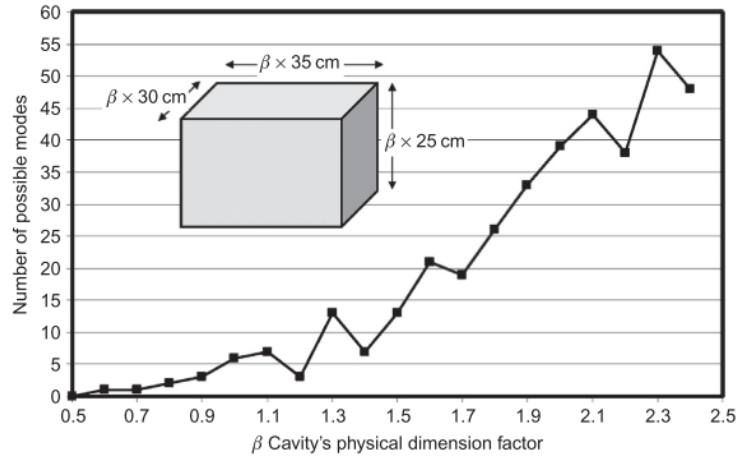


Fig 6.54. Comparison between the number of possible modes and the dimension factor [165, Fig. 5.2]

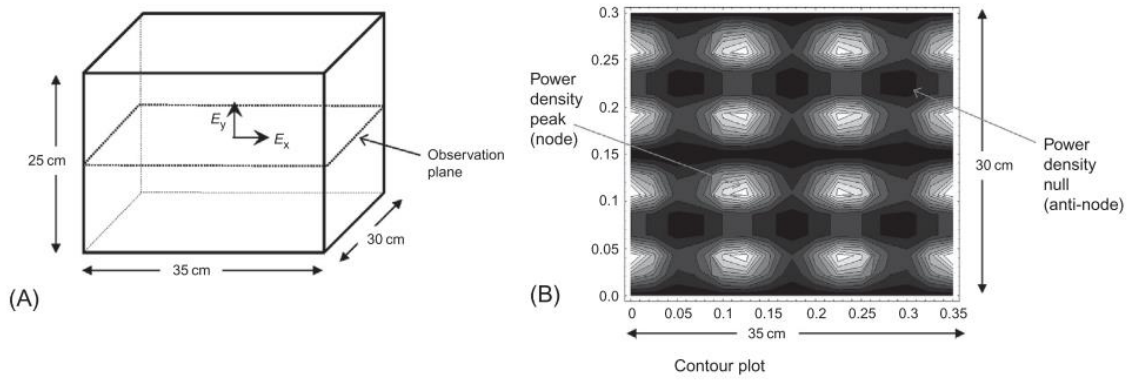


Fig 6.55. Power density distribution of the TE₃₂₄ mode in a rectangular cavity at 2452.12 MHz [165, Fig. 5.1]

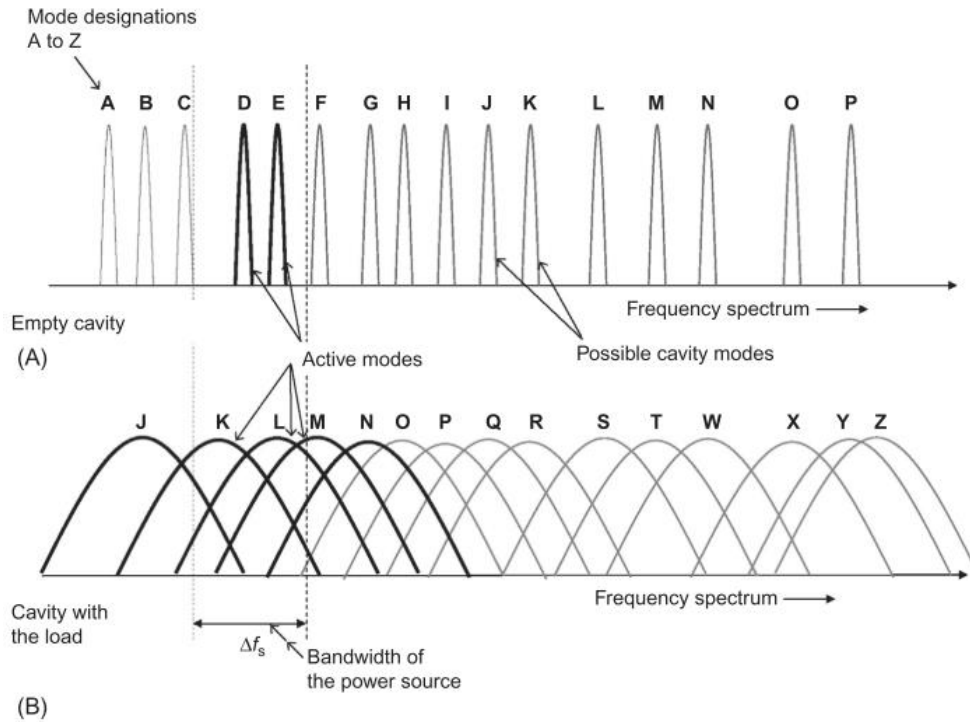


Fig 6.56. Lossy load effect over the resonant modes in a cavity [165, Fig. 5.6]

Chapter 7. Microwave assisted chemical processes – 2,450 MHz ISM band.

Microwave frequencies from 300 MHz to 300 GHz are used in many applications. However, the 2,450 MHz ISM frequency band is the most used and known. Two applications are widely known: domestic microwave ovens and Wi-Fi networks.

The main advantage of this frequency is its high interaction with the water molecules. At the frequency of domestic microwave ovens (2,450 MHz), the process of dipole rotation occurs 4.9×10^9 times per second and results in an increased rate of heat generation [1].

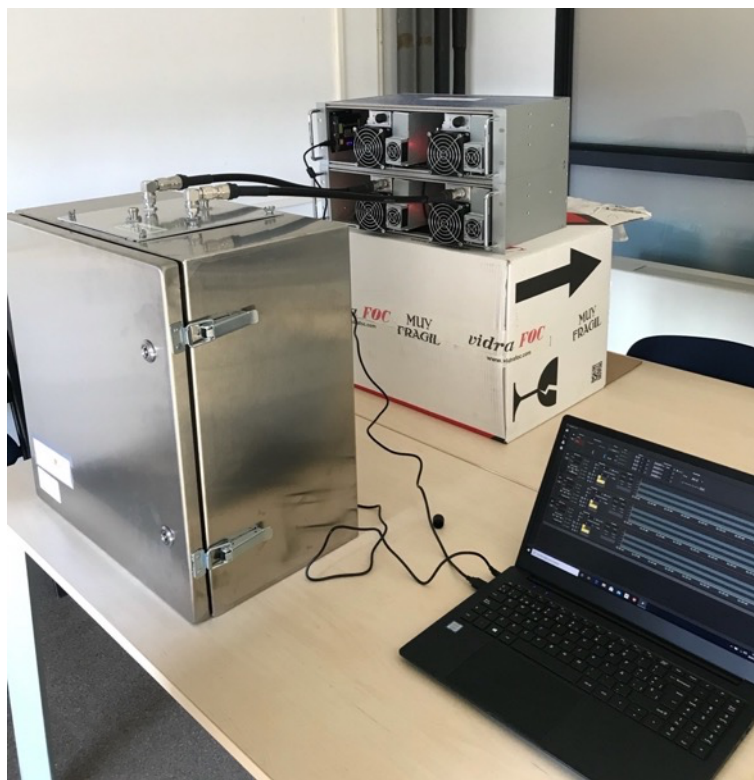


Fig 7.1. Developed SSMGS for microwave-assisted chemical processes at 2,450 MHz.

Chapter 7 comprises the work devoted to designing a microwave heating system at the 2,450 MHz frequency band with the RADAR philosophy explained in the introduction of this thesis dissertation. It includes the antenna design, applicator manufacture and results of the multi-source solid-state driven batch oven designed for chemical synthesis (see Fig 7.1).

7.1. Patch and wire antenna design.

7.1.1. Teflon-based patch antennas.

The microstrip patch of the antenna is designed so its pattern maximum is normal to the patch. For a rectangular (or square) patch, the side length, here A_p , is usually $\lambda_0/3 < A_p < \lambda_0/2$. The patch and the ground plane are separated by a dielectric sheet, referred to as the substrate. In this case, the substrate with the lower dielectric constant is Teflon[®] ($\epsilon = 2.1$). A first approach to the 2,450 MHz patch antenna size is obtained through (7.1)

$$\begin{aligned} \frac{\lambda_0}{3} = \frac{c_0/f}{3} = \frac{3e8[m/s]}{2.45e9[Hz]} = 40.82 \text{ mm} < A_p < \frac{\lambda_0}{2} = \frac{c_0/f}{2} = \\ = \frac{3e8[m/s]}{2.45e9[Hz]} = 61.12 \text{ mm} \end{aligned} \quad (7.1)$$

The antenna has been modelled with this size range and $A_d = A_p + 10 \text{ mm}$. The parametric study conducted shows a higher working frequency than the objective. So, the A_p value is incremented until the best matching values coincide with the working frequency, 2.45 GHz. This value has been encountered around $A_p = 80 \text{ mm}$.

Like the other antenna designs presented previously in the document, a coaxial connector feeds the antenna. The equivalent circuit of the so-called probe feed [153] is shown in Fig 7.2.

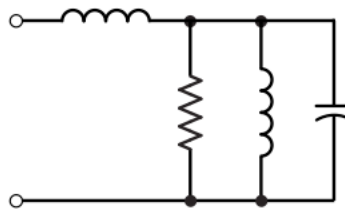


Fig 7.2. Coaxial probe feed schematic [153, Fig. 14.4 (b)]

Mathematical calculations, with the schematic elements in the figure above, can be used to obtain the perfect feeding point as described in [153]. However, parametric modelling studies are more practical in achieving the matching.

A parametric study with the feeding position (X,Y) is conducted, and the results show that the best matching is encountered across the principal axes. Fig 7.3 shows the existing symmetry (dotted against the solid line), and the best matching at 2,450 MHz is obtained when the feeding

point is in $Pos_x = 25 \text{ mm}$ and $Pos_y = 0 \text{ mm}$. The obtained matching is around -36 dB , and the bandwidth covers the whole solid-state modules' frequency range with return losses lower than -10 dB (the typical limit for antennas).

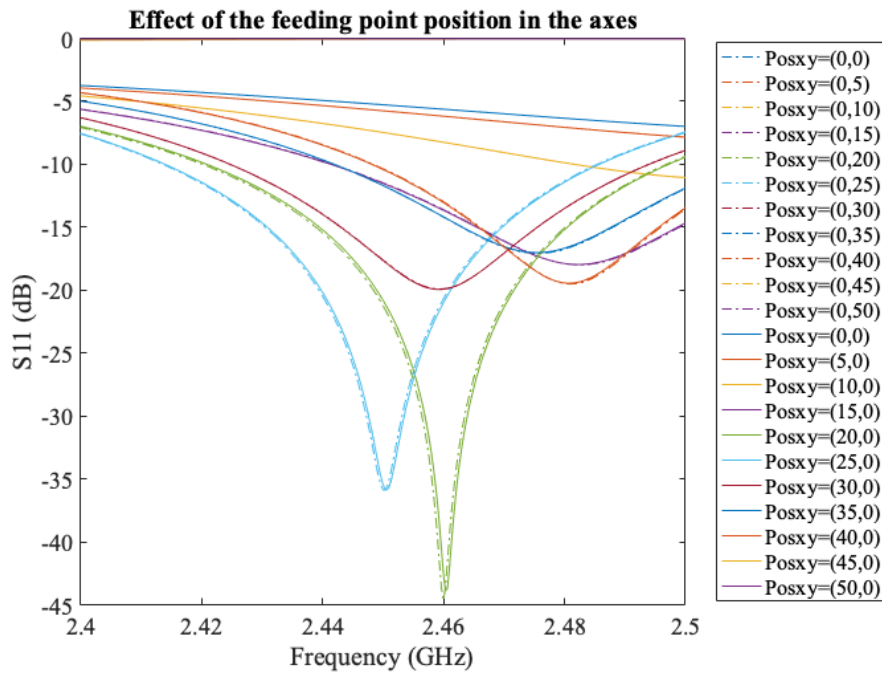


Fig 7.3. Return losses of the antenna depending on the feeding point in the axes (best option).

The other two critical parameters are $A_p = 80.5 \text{ mm}$, $A_d = 100 \text{ mm}$ and $r_{curv} = 5 \text{ mm}$.

Later, the antenna is modelled to work inside a microwave oven. Several changes have been made to maintain the matching. These have been: adjusting the patch side length, $A_p = 83.5 \text{ mm}$, increasing the curvature of the corners, $r_{curv} = 10 \text{ mm}$, and relocating the feeding point to the patch border, specifically $Pos_x = 38.74 \text{ mm}$. Fig 7.4 shows this final design, where has also been modelled a supporting nylon screw. It is centred on the patch, and its main purpose is to keep the sandwich assembly tight.

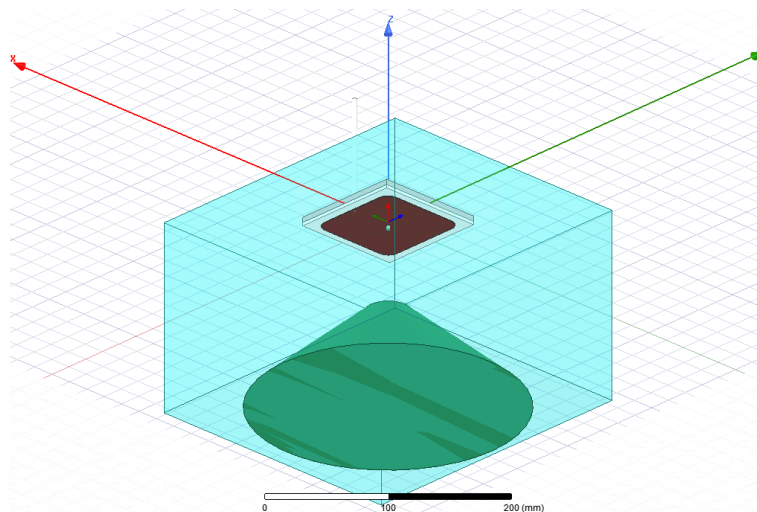


Fig 7.4. Inverted dimetric view of the antenna modelled with a loaded cavity.

The updated antenna has been manufactured and inserted in a modified commercial microwave oven (see Fig 7.5). The results in Fig 7.6 show the measurements performed and confirm the antenna's fantastic behaviour. A predominant resonance can be found at 2,460 MHz with a matching level of -29.53 dB.

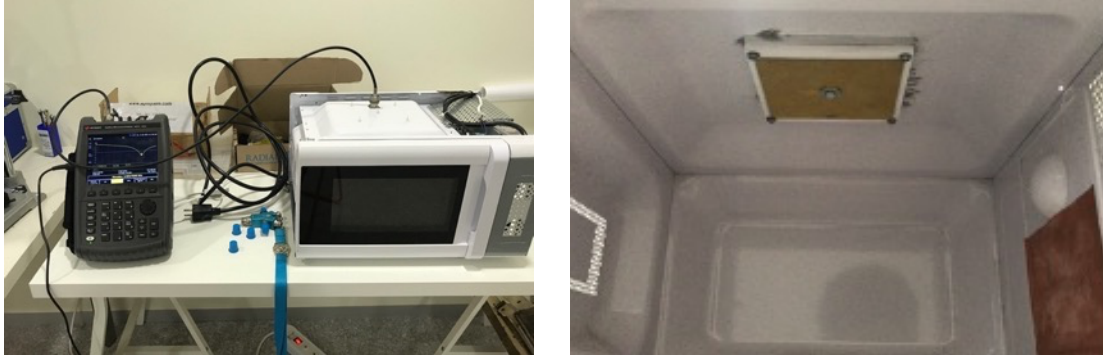


Fig 7.5. Antenna installed in a modified microwave oven (right) and measured its RL (left)



Fig 7.6. Return Losses measurement (S11) of the patch antenna. Marker M2 define the best matching frequency.

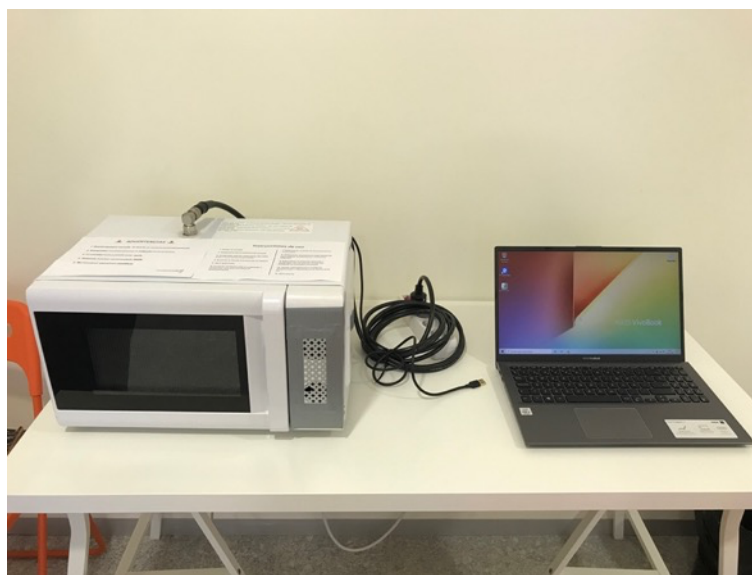


Fig 7.7. Complete system at 2,450 MHz and 250W solid-state microwave source controlled by a PC.

This antenna has been used in a solid-state-based microwave oven and sold to the labs at the University of Valencia (see Fig 7.7). The solid-state microwave generator inserted in the oven is the STARTER Evaluation Kit from Leanfa Slr. (Bari IT), that provides 250 W at 2,450 MHz. The generator is controlled by proprietary software on a computer (Windows).

7.1.2. Monopole antennas.

Sometimes simpler solutions are the better. The most straightforward way to make a monopole antenna is by soldering a copper wire to the coaxial connector inner conductor. These are the less complex TEM antennas.

Given the simplicity of the antenna, the design process is based on mathematical calculations and physical tests.

The first step is to calculate the approximate antenna size according to the wavelength:

$$l_{monopole} \approx \frac{\lambda}{4} = \frac{c/f}{4} = \frac{3e8/2.45e9}{4} = 30.61 \text{ mm} \quad (7.2)$$

A design philosophy followed is to cut slightly larger than the calculation, mount it with the connector and measure the return losses with a VNA. The initial VNA frequency range is wider than the band to detect the resonance, which will be in the lower part of the range.

Later, an iterative process is performed by cutting two mm of the wire and measuring the return losses until the perfect matching is obtained. The antenna designed at 2,450 MHz presents little deviation in the resonant frequency when it is placed feeding a resonant cavity with dimensions larger than the wavelength.

Fig 7.8 shows the antenna manufactured for the 2,450 MHz frequency band. Its power efficiency has been measured in a modified microwave oven showing very promising results: depending on the load, it is possible to reach return powers lower than 1%.

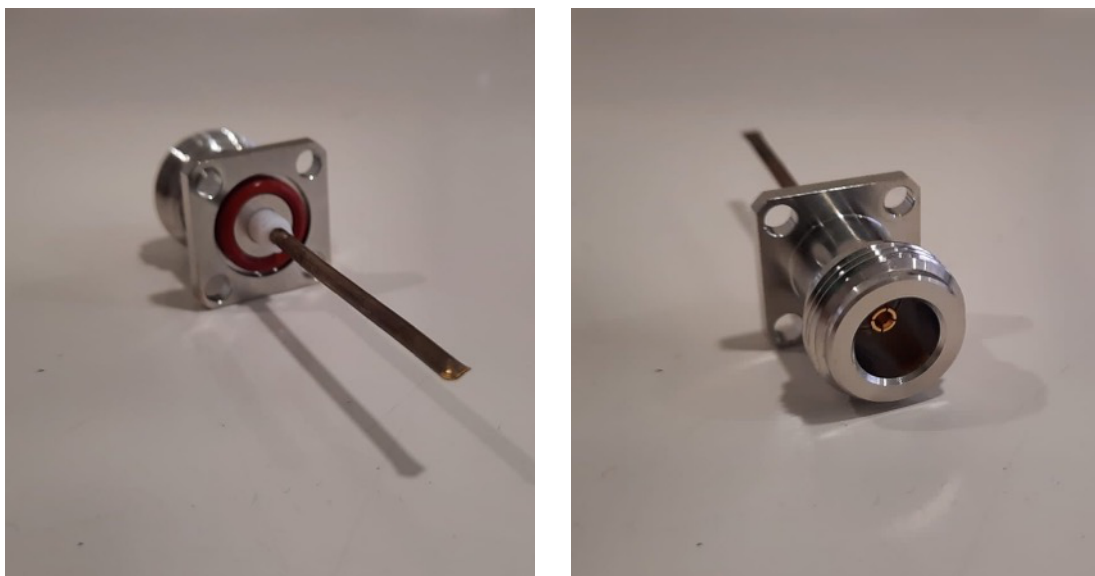


Fig 7.8. Monopole antenna with an N-connector designed at 2,450 MHz.

7.2. Application example: chemical synthesis.

This subsection describes the new microwave application on porous silica synthesis assisted by microwaves. Some of the work done is related to the research project “Valorización de un nuevo procedimiento de síntesis asistida por microondas de sílice porosa” developed conjointly with the Redolí group in the Department of Inorganic Chemistry at Valencian University (UV).

Silica is one of the most used nanomaterials because of its versatility: it forms mesoporous materials and nanoparticles, can be used as shells and integrated into composites, and can also be functionalized. As reported by Díaz de Greñu et al. in [166], where extensive research on microwave treatment of silica-based materials can be found, the development of systems and procedures for microwave-assisted silica synthesis are significantly reduced.

The work carried out and presented here is centred on the design, development and manufacture of a multi-purpose microwave heating system with complete versatility to experiment with a whole range of possibilities in microwave-assisted synthesis. The versatility is given by a multi-sources solid-state generator that can adjust the heating pattern through the power, frequency and phase control.

The load requirement defined by the research group in the chemical field is 1.5 L of liquid content. After performing initial heating tests with limited power and mass, the power rate obtained is 0.5 W/g. For 1.5 L (equivalent to 1.5 kg given the high water content), the power required would be 1,500 W. However, it has been proved that higher load volumes are related to better matching figures. Therefore, it has been decided to develop a 1kW solid-state system, which is market-ready in a combination of four 250 W modules. It is essential to state that in this system with multiple sources that operate in pairs to obtain a proper field control, the number of modules should be a two potence.

7.2.1. Applicator design and implementation.

7.2.1.1 Multi-source microwave generator.

The specific features of the SSMGS designed for the application are:

- Total power of 1 kW (4 x 250 W). The output power is controlled with watt per watt steps or sensitivity.
- A frequency sweep is available within the frequency band, 2450 MHz \pm 30 MHz, with 2 MHz steps. The frequency can be defined individually for each module or synchronised for the phase change.
- Each module's phase is controlled individually.
- The system is equipped with forced-air cooling with low-noise fans.
- It is managed with an intuitive and user-friendly control software with a computer user interface.

The SSMGS block diagram, with each needed element, is depicted in Fig 7.9.

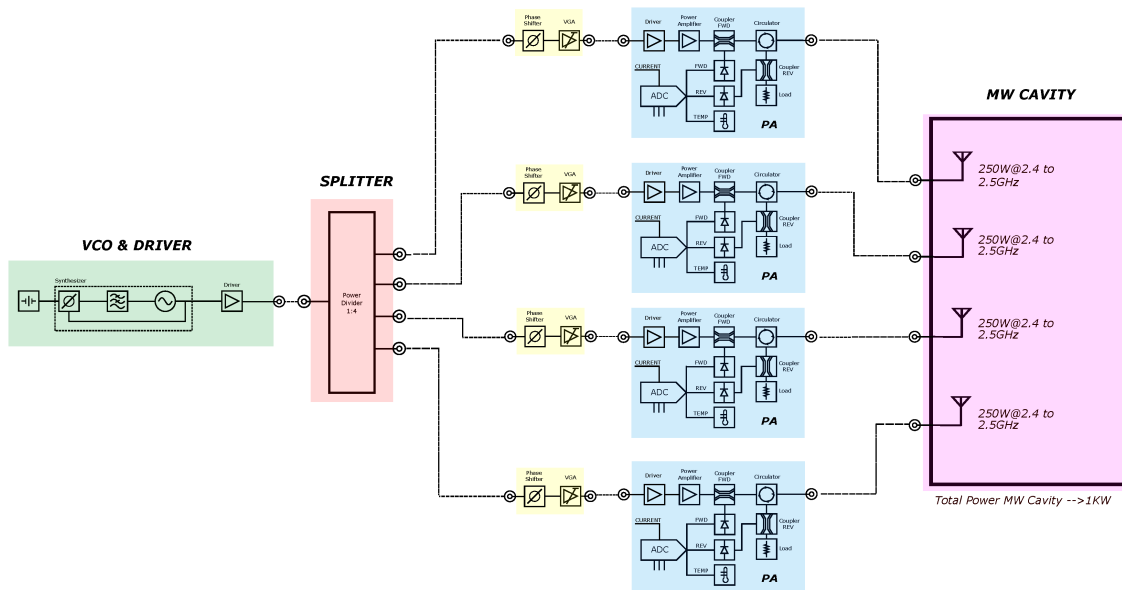


Fig 7.9. Block diagram for the 2.45GHz multi-source solid-state driven system with 1kW of total output power.

Several companies in the microwave market offer devices to form the required system, and others work with larger subsystems. After a thorough search, the selected device is the PHASESHIFTER Evaluation Kit from Leanfa Srl (Bari, IT) (see Fig 7.10). It is built around four 2450 MHz 250 W OEM (Original Equipment Manufacturer) power amplifiers. It is equipped with a forced-air cooling system and an advanced synthesizer with multiple outputs capable of accurate frequency synchronisation and 360° independent phase rotation.



Fig 7.10. PHASESHIFTER Evaluation Kit @ 2.45 GHz.

This system is very similar to the one used in the 915 MHz application. Its specific control description is explained later in 8.2.4.1.

7.2.1.2 Antennas and cavity.

The cavity in a microwave heating system is also a key feature. There are monomode and multimode cavities. The firsts are usually designed ad-hoc for a specific application, and their

main advantage is the field homogeneity in a very concrete location. These monomode cavities present limited the versatility so appreciated in lab research environments.

As explained before in Chapters 2 and 6, the number of modes in a multimode cavity depends on the frequency and size. The application this system is intended for is multipurpose and needs to work with different load volumes. A standard 500 mm x 300 mm x 500 mm (width, depth, height) cavity is proposed. These dimensions allow working with the vials' location in height, their lengths, and the different elements' location (antennas, flux air apertures, etc.)

The monopole antennas used in this prototype are made of thin hollow copper tubes soldered to the N-connectors (Fig 7.11). These, also called wire antennas, are very simple and offer good matching in cavity applications. Moreover, there is no space problem with the antennas' small size due to the operating frequency, 2,450 MHz, and the cavity dimensions. The design process has been explained previously in the text.

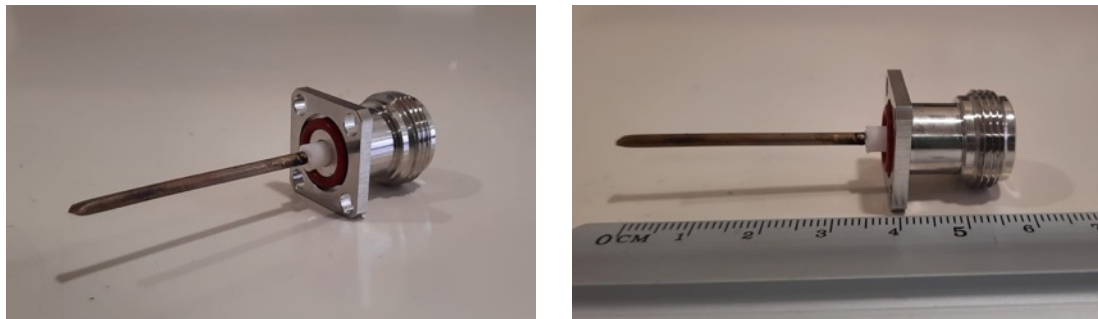


Fig 7.11. Manufactured monopole antenna and its size.

Three possible locations of these antennas have been modelled in HFSS: 1) four antennas on the top face, Fig 7.12 (a), 2) two antennas on the top and one in each lateral face, Fig 7.12 (b), and 3) two antennas in each lateral face Fig 7.12 (c). The selected option is the first.

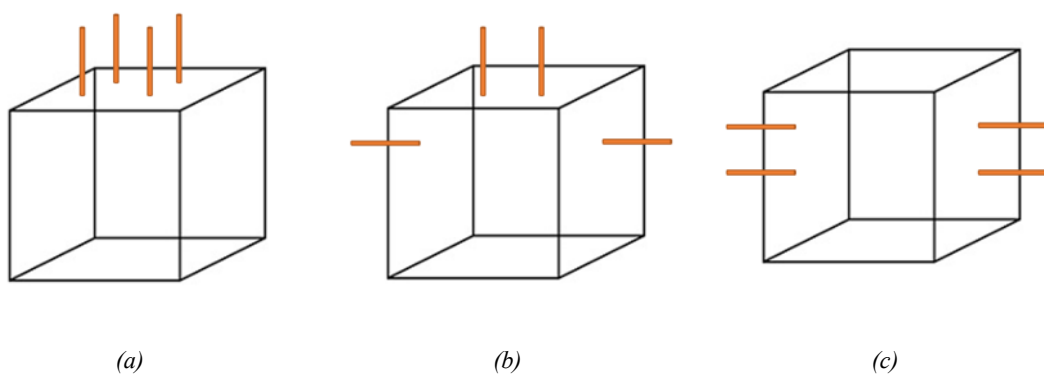


Fig 7.12. Antenna different location configuration.

Once the face is selected, the separation between the antennas is the next variable to be defined. Following the monopole theory, an approximate distance between antennas is $\lambda(@2,450 \text{ MHz}) = 122.3 \text{ mm}$, and the definitive distance is set to 120 mm. This distance presents the scattering parameters that have been measured with the VNA and are shown in Table 7.1. These values are optimised later once the load is present.

Table 7.1. Antenna array *S*-parameters.

S_{11} (dB)	S_{21} (dB)	S_{31} (dB)	S_{41} (dB)
-7.6383	-12.483	-12.485	-9.9447

The antennas have been installed in an aluminium panel, permitting a possible antenna distribution change (see Fig 7.13). EMI/EMC gaskets are used to assure the correct shielding, as shown in Fig 7.14.



Fig 7.13. Antenna array installed in metallic sheet.

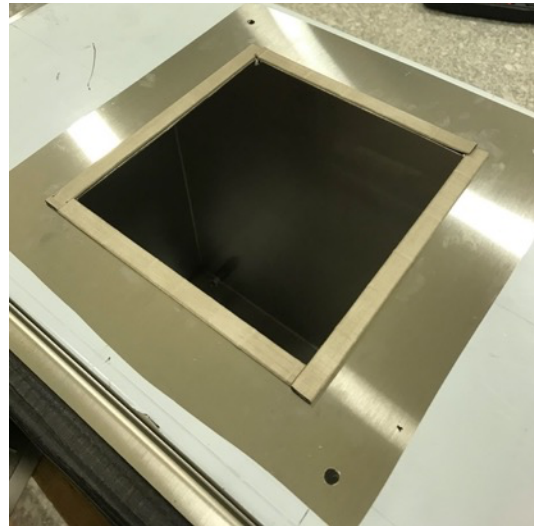


Fig 7.14. Shielding gaskets on top of the cavity.

7.2.1.3 Validation and start-up procedure.

The validation and start-up methodology consists of checking, one by one, all the elements of the system: generation and application. The generator's location and the cable connectivity are defined, the reflected power in each antenna is measured, and finally, the system efficiency is obtained. Fig 7.15 shows the system under validation.

Low-loss power cables are needed to conduct the power from the generator to the antennas. These cable's rigidity and required contained lengths are a handicap for the system integration in a lab environment. A solution has been found by using coaxial transitions with a right angle of 90°. The final assembly is shown in Fig 7.16, and the antennas' nomenclature used can be seen in Fig 7.17. The numbers refer to the SSMGS's module each antenna is connected.

The first stage consists of the antennas' individual calibration. The LeanOn software allows operating the system of each module independently. The first calibration's objective is to verify the four solid-state amplifiers' proper functioning and validate the antennas' performance and their optimum frequency. The calibration process is performed with a generic 2L water load centred in the cavity base (see Fig 7.15).



Fig 7.15. Complete system during the set-up process.

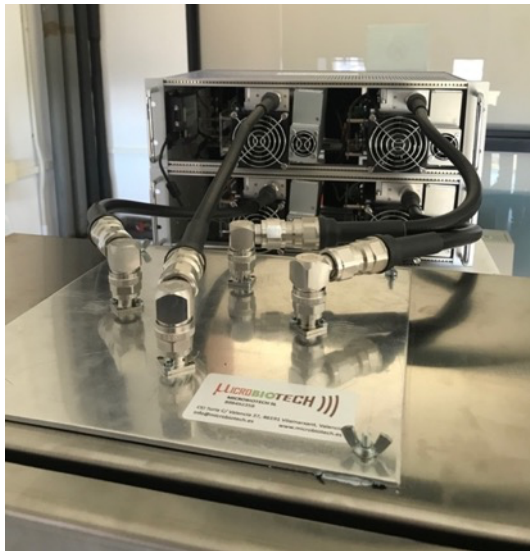


Fig 7.16. Coaxial 90° transitions and cable connections to the generator.

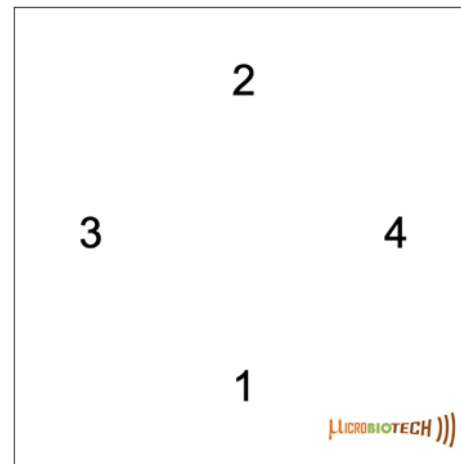


Fig 7.17. Antenna nomenclature and its position in the panel.

The three variables stored during the calibration process are:

- Forward power, P_{fwd} : the nominal power delivered to the antenna.
- Reflected power, P_{rfl} : the returning power due to the antenna's return losses (RL).
- Coupled power, P_{cp} : the power that ends in the inactive modules by the coupling between the active antenna and the other three.
- Effective power, P_{eff} : the actual power absorbed by the load. It is obtained by the following equation:

$$P_{eff} = P_{fwd} - P_{rfl} - \sum P_{cp} \quad (7.3)$$

The antenna calibration objective is to achieve the lowest reflection and coupling possible. A typical value for the antenna reflected power -10 dB (or lower than 10%).

Table 7.2-

Table 7.5 show this calibration process's measurements and the optimum frequency for each case.

Table 7.2. Antenna 1 calibration measurements.

Antenna 1	P_{fwd}	P_{rfl}	P_{cp2}	P_{cp3}	P_{cp4}	P_{eff}	Frequency
	10 W*	0 W	0 W	0 W	0 W	10 W	2420 MHz
	20 W	1 W	1 W	0 W	1 W	17 W	2425 MHz
	100 W	7 W	5 W	0 W	3 W	85 W	2425 MHz

*Given the low sensitivity, this measurement is not further performed.

Table 7.3. Antenna 2 calibration measurements.

Antenna 2	P_{fwd}	P_{rfl}	P_{cp1}	P_{cp3}	P_{cp4}	P_{eff}	Frequency
	20W	1W	1W	0W	1W	17 W	2479 MHz
	100W	6W	5W	0W	3W	86 W	2479 MHz

Table 7.4. Antenna 3 calibration measurements.

Antenna 3	P_{fwd}	P_{rfl}	P_{cp1}	P_{cp2}	P_{cp4}	P_{eff}	Frequency
	20W	0W	0W	4W	1W	15 W	2406 MHz
	100W	1W	2W	20W	3W	74 W	2406 MHz

Table 7.5. Antenna 4 calibration measurements.

Antenna 4	P_{fwd}	P_{rfl}	P_{cp1}	P_{cp2}	P_{cp4}	P_{eff}	Frequency
	20W	0W	0W	2W	1W	17 W	2462 MHz
	100W	1W	5W	11W	5W	78 W	2462 MHz

A clear conclusion is that the major coupling is encountered in the diagonals: Antenna 1 – Antenna 2 and Antenna 3 – Antenna 4. The secondary conclusion extracted is the Antenna 3 misbehaviour, solved by replacing it. Previously to the replacement, the antennas combination study was performed, and the results are shown in Table 7.6 - Table 7.8. The active antennas are labelled as reflected power though this value combines the reflected power and the coupled from the other active antenna.

Table 7.6. Antenna 1 + Antenna 2 power tests.

Antenna 1 + Antenna 2	P_{fwd} (W)	P_{rfl1}	P_{rfl2}	P_{cp3}	P_{cp4}	P_{eff}	Efficiency % (P_{eff}/P_{fwd})
	10 + 10	2 W	2 W	0 W	1 W	15 W	75 %
	20 + 20	4W	3W	1W	2W	30 W	75%
	50 + 50	8W	7W	2W	5W	78 W	78%
	100 + 100	15W	13W	4W	8W	160 W	80%
	200 + 200	29W	25W	7W	16W	323 W	80.75%

Table 7.7. Antenna 1 + Antenna 4 power tests.

Antenna 1 + Antenna 4	P_{fwd} (W)	P_{rfl1}	P_{cp2}	P_{cp3}	P_{rfl4}	P_{eff}	Efficiency % (P_{eff}/P_{fwd})
	10 + 10	1W	2W	1W	2W	14 W	70%
	20 + 20	2W	3W	2W	3W	30 W	75%
	50 + 50	4W	6W	5W	7W	78 W	78%
	100 + 100	8W	11W	9W	13W	159 W	79.5%
	200 + 200	15W	20W	17W	25W	323 W	80.75%

Table 7.8. Antenna 2 + Antenna 4 power tests.

Antenna 2 + Antenna 4	P_{fwd} (W)	P_{rfl1}	P_{cp2}	P_{cp3}	P_{rfl4}	P_{eff}	Efficiency % (P_{eff}/P_{fwd})
	10 + 10	1W	2W	1W	2W	14 W	70%
	20 + 20	2W	3W	2W	3W	30 W	75%
50 + 50	4W	6W	5W	7W	78 W	78%	

	100 + 100	8W	11W	9W	13W	159 W	79.5%
	200 + 200	15W	20W	17W	25W	323 W	80.75%

An interesting outcome of these power tests is the continuity of the optimum frequencies, independently of the powers used in the modules. Antenna 3 has been operating erratically; however, the combination of Antenna 1 + Antenna 3 has been tested at maximum power (200 W + 200 W) to check the overall efficiency. It showed an 80% efficiency.

Lastly, the power test is completed using the four sources. The overall reflected power and efficiency are shown in Table 7.9.

Table 7.9. Power test with the four modules activated.

Antenna 1 + 2 + 3 + 4	P_{fwd}	P_{rfl}	$P_{eff} = P_{fwd} - P_{rfl}$	Efficiency (P_{eff}/P_{fwd})	Comments
	4 x 50 W	50 W	150 W	75%	The reflected power in the Antenna 3 is 37% (see Fig 7.18)
	4 x 100 W	93 W	307 W	76.75%	
	4 x 200 W	175 W	625 W	78.13%	



Fig 7.18. Control software screenshot at maximum power where can be seen the Antenna 3 malfunctioning.

7.2.2. Modelling of chemical processes.

The work developed in this thesis on the manufacture of this microwave oven for chemical processes includes parametric electromagnetic and multi-physic modelling to help the lab with proper system behaviour. Both studies have been performed with Comsol Multiphysics, being the latter presented in an international conference [167]. This team will perform three operations with the oven: synthesis, calcination, and functionalisation.

7.2.2.1 Synthesis.

The original synthesis process is performed with a 4.12 mL atrane mixture with 10 mL of distilled water. After the microwave treatment, a gel white solid is obtained. The white solid is cooled in an ice bath, retrieved later by centrifugation, cleaned with water and ethanol, and dried for a whole night at 40°C. Studying the optimum recipient size for the dissolution is necessary to scale the process up to 1.5 L. Two parameters will be taken into account: the recipient diameter and height.

The microwave's penetration depth depends on the material's dielectric properties and the working frequency. Homogeneous heating strongly depends on the recipient size to have all the load equally heated. So, the electromagnetic field distribution is studied for different diameters using electromagnetic modelling tools.

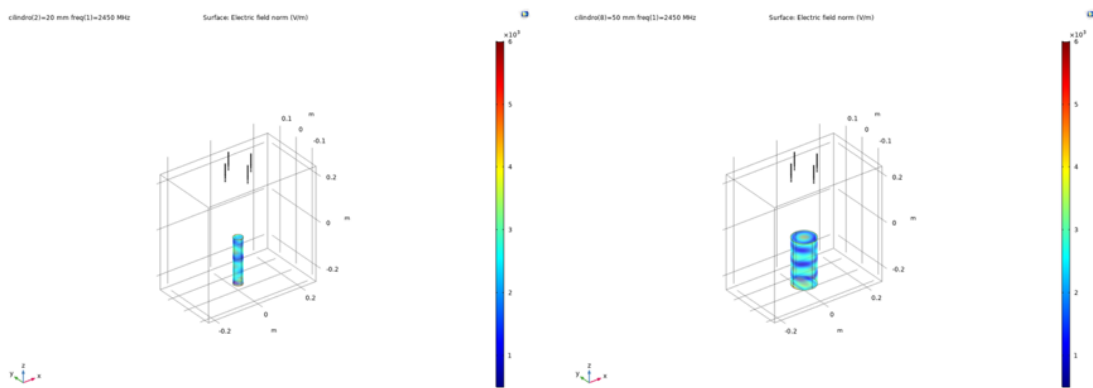


Fig 7.19. Modelling of a recipient with 40 mm (left) and 100 mm (right) diameters.

Fig 7.19(left) shows that the 40 mm diameter provides a nearly homogeneous field distribution in the recipient transversal section. Fig 7.19(right), on the other hand, shows a more intense field in the middle of the recipient, attenuated homogeneously in all radial directions.

The height needed for these two diameter options is given by:

$$V = \pi r^2 h \quad (7.4)$$

$$h_1(cm) = \frac{V}{\pi r^2} = \frac{1500mL}{\pi * (2cm)^2} = 119.37cm \quad (7.5)$$

$$h_2(cm) = \frac{V}{\pi r^2} = \frac{1500mL}{\pi * (5cm)^2} = 19.1cm \quad (7.6)$$

The cavity height needed with the first option is too large, so the selected recipient diameter is 100 mm, which forces a 191 mm height. As shown in Fig 7.19(right), there is a periodic pattern with field maximums and minimums from top to bottom. This field heterogeneity can be solved with the frequency and phase sweeps.

Moreover, a second choice: with two shorter recipients, the desired homogeneity could be obtained without needing the electronic sweeps. A two-cylinder matrix with 100 mm height separated 20 mm between centres is studied.

Fig 7.20 shows the effect of the position in height within the cavity of these two cylinders. These two locations are related to modes with high field distribution and can be equally chosen for the experiments.

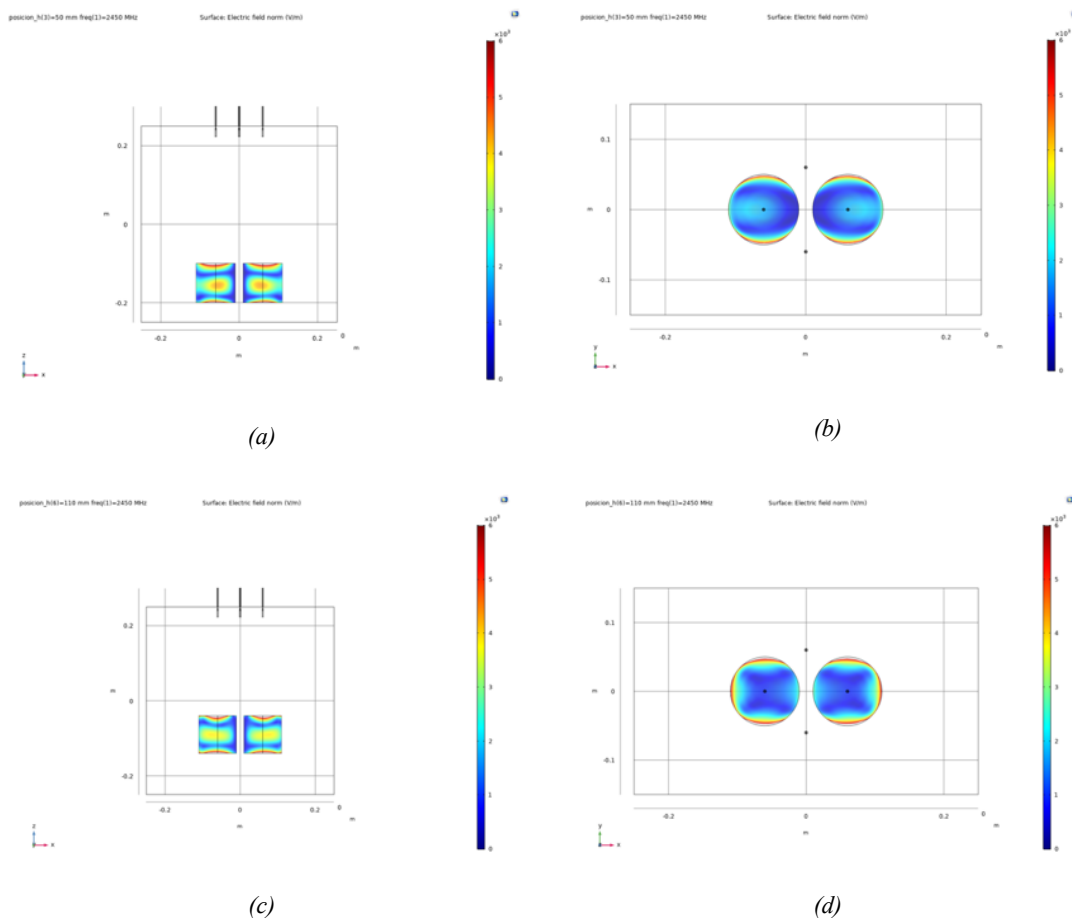


Fig 7.20. Top and front view of the modelling at 50 mm (a,b) and 110 mm (c,d) position.

7.2.2.2 Calcination.

The calcination process is performed at temperatures over 450° C. Specifically, it has been usually done inside a muffle furnace at 550° C for five hours. With this technology, the process used to be done at night to ensure smooth heating/cooling rates. Solid-state microwave ovens can be an excellent solution to speed up this process.

Replacing these devices with microwave ovens requires a microwave susceptor recipient in order to reach the mentioned temperature range. It is the main difference between the three processes; in the calcination process, the microwaves heat the recipient rather than the product itself.

The design process is centred on the recipient's structure and properties. It has to absorb the microwaves swiftly and present a high-temperature difference breaking capacity while reaching high temperatures. These are characteristic features of crucibles. Microbiotech has developed special technical ceramic crucibles that fit the application. A small quantity of dried white solid obtained from the synthesis process is calcinated inside the crucible.

Concretely, the carbon-doped ceramic crucible has to contain 20 g of dried white solid. Microbiotech's patent covers the interaction between microwaves and this material called MBT01. According to the wavelength, the recipient diameter should be 62 mm with a reduced thickness: the lesser the mass to be heated, the faster the heating. It is therefore proposed a 2 mm thickness. However, a rectangular surface is preferred by the chemical lab.

The crucible is integrated into a multi-layer set of ceramic materials with different purposes (see Fig 7.21). From the outer to the inner layer, the functions are:

- 1) A temperature-resistant isolator is responsible for keeping the temperature concealed inside the recipient, helping to the temperature increase. It must be transparent to microwaves. This layer can be built with cordierite.
- 2) The highly-susceptor recipient is responsible for the heating increase. It has been made with the MBT01 material.
- 3) The dried solid cannot be placed directly in touch with the MBT01 susceptor. A porcelain layer is used to contain the product.

The different layer dimensions are obtained from the lab requirements and the modelling results in Comsol Multiphysics (see Fig 7.22). They can be seen in Table 7.10.

Table 7.10. Multi-layer calcination recipients' dimensions.

Layer	Width (mm)	Length (mm)	Height (mm)	Thickness (mm)
Cordierite	115	230	30	15
MBT01	70	165	15	2
Porcelain	65	150	10	3



Fig 7.21. Three-layer recipient for microwave-assisted calcination.

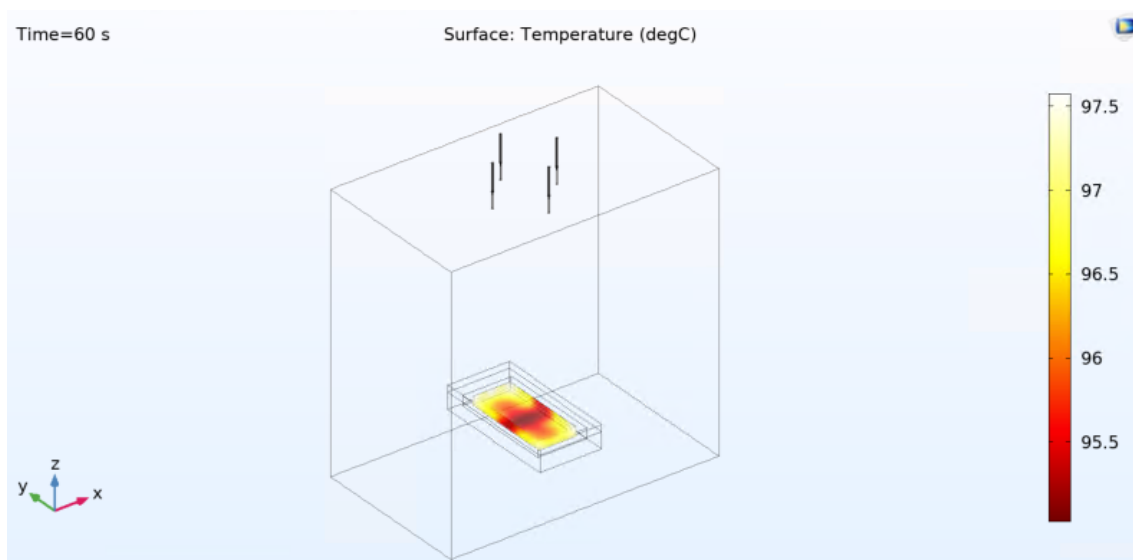


Fig 7.22. Multiphysics modelling in Comsol of the calcination structure in a multi-source solid-state driven microwave oven.

Fig 7.23 and Fig 7.24 show an example of the modelled thermal distribution compared to the actual measurement made with the final system. These results show good agreement and are used as the first step to future improvements both in the microwave system and in the calcination chemical process.

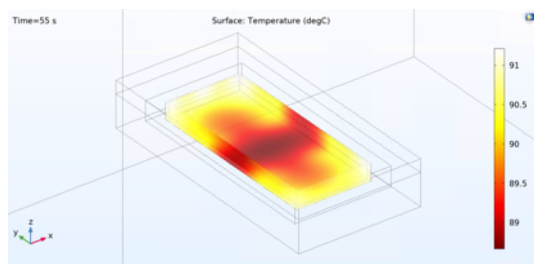


Fig 7.23. Detail of the heat pattern in the porcelain recipient after 55 seconds.

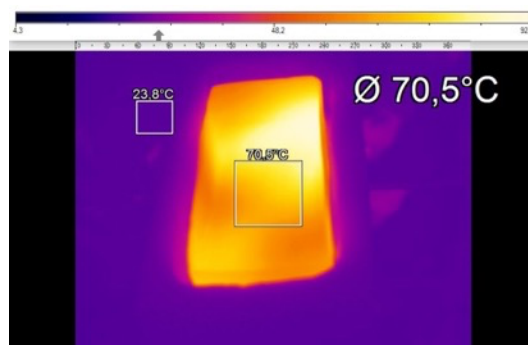


Fig 7.24. Radiation pattern captured with an infrared camera after 55 seconds.

7.2.2.3 Functionalisation.

Finally, the same microwave multi-source system can be used for the functionalisation procedure. The functionalisation process is similar to synthesis, although it is done with acetonitrile instead of distilled water. The acetonitrile dielectric constant is 37.5, which means that the penetration depth is higher than with the water volume.

The process is also made with a 1.5 L volume, and the solid used is 500 g of the calcinated material in the previous step. Fig 7.25 shows the electromagnetic field distribution for the same diameters as synthesis. It can be seen that the field patterns are very similar, showing the important effect of the cavity dimensions and the antenna configuration. The main difference is the greater electromagnetic field intensity, related to a higher penetration depth.

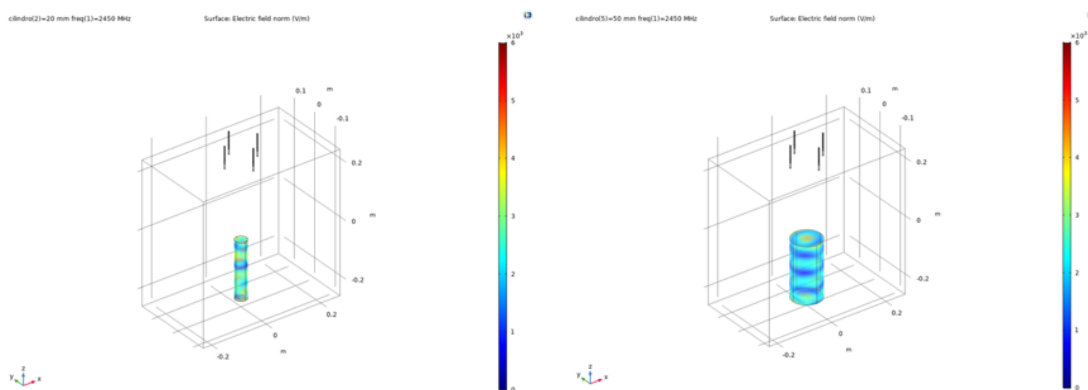


Fig 7.25. 40 mm (left) and 100 mm (right) diameters for the functionalisation.

The multi-source microwave heating system has been designed to take full advantage of the technology in multiple processes, as shown in this subsection. The later results of the processes performed with the system are being analysed for possible patentability.

7.2.3. Processes validation.

With the developed and validated system, it has been carried out the validation of the three different processes. The equipment phase, frequency and power has been configured to perform the three stages of the explained chemical process. It has been compared the results obtained with the S2MH system and the state-of-the-art oven. Table 7.11 summarises the average results out of three repetitions [168].

Table 7.11. Time improvement results on chemical processes.

Chemical process	Conventional oven		S2MH		Relative time reduction
	Quantity	Time	Quantity	Time	
Synthesis	6 g	24 h	70 g	10 min	99%
Calcination	2 g	5.5 h	1.3 g	25 min	88%
Functionalisation	3.55 mmol NH ₂ g/SiO ₂	5.5 h	0.9 mmol NH ₂ g/SiO ₂	5 min	94%

7.3. Conclusions.

This chapter has shown the different studies, electromagnetic and multiphysics modelling, designs and implementations carried out to verify the proposed thesis. Specifically, in this chapter can be seen that:

- A multi-purpose microwave equipment based on solid-state technology has been validated to work in different chemical applications.
- The monopole antennas designed and manufactured have proved to be adequate to the purpose of the system, providing high power efficiency to the oven: over 80%.
- It is possible to modify the electromagnetic field generated over the load. The different elements implemented such as phase shifters, variable power amplifiers and the frequency tuning feature allow this implementation for a wide variety of load's shape and nature (e.g., aqueous solutions, solid structures for calcination, etc.)
- The chemical processes performed with the presented equipment, have experienced an improvement in the required operation time, as can be seen in Table 7.11.

Chapter 8. Microwave assisted almond drying – 915 MHz ISM band

Among the different frequency bands available for ISM applications, two have similar wavelengths: 896 and 915 MHz. The exceptionality of this range of the radiofrequency spectre is that their use is restricted to different world regions. 915 MHz is the reserved frequency band in America, while 896 MHz is used in the UK [8]. In Europe, there is no legislation from the ITU (International Telecommunication Union) in this frequency range.

The main advantage of working with lower frequencies than the typical 2,450 MHz is the greater wavelength and its direct relation to the penetration depth. As described in Chapter 2, the American industrial sector developed microwave systems at the 915 MHz frequency band. This equipment has been used in other regions under exceptional circumstances and strict leakage prevention measures despite the regulation. The following work has been done with a Spanish company whose primary market is the United States.



Fig 8.1. Developed conveyor oven for almond drying with the SSMGS at 915 MHz.

This second chapter presenting industrial applications with the proposed system is centred on the complete description of the modular batch/continuous microwave oven operating at 915 MHz for almond drying. It has been developed to work with four patch antennas capable of handling up to 500 W each, combined with airflow management. The result of this work is a Proof of Concept (PoC) for industrial implantation development.

8.1. Patch antennas studies

Using patch antennas for this application is based on space reduction inside the cavity and the already big dimensions of the oven, which is application-driven. These antennas also offer a more directive radiation pattern, making it easier to work in an array.

The antennas have been designed and built with two different dielectric substrates: Teflon and PEEK. The first is one of the most common substrates in microwave applications, and the second is because of its rigidity and its higher temperature limit.

8.1.1. With Teflon substrate

Antennas for high power applications made with Teflon as the dielectric material are common. Following the same philosophy as in the 7.1.1 subsection, the design, manufacture, validation and integration of a patch antenna have been done, with the principal materials being a 6 mm (enough to use supporting screws) aluminium piece working as the ground plane, a 4.5 mm standard Teflon sheet and a 0.45 mm standard copper sheet.

The first approximation for the dimensions has been obtained from a simple relation between frequencies. Given the inverse relationship between the frequency and the wavelength, this factor is $2450/915 = 2.67$. The first approach for this frequency is obtained from the dimensions in 7.1.1:

$$A_{d_{915}} = 2.67 * A_{d_{2450}} = 2.67 * 100 = 267 \text{ mm} \quad (8.1)$$

$$A_{p_{915}} = 2.67 * A_{p_{2450}} = 2.67 * 80.5 = 214.94 \text{ mm} \quad (8.2)$$

where A_d is the support side's length, and A_p is the patch side's length.

The feeding element is the same as the 2.45 GHz application: a vertical wire soldered to the patch coming from the coaxial connector.

A parametric study has been conducted to analyse, in free space conditions, the effect of these two parameters on the resonance. First, the A_p parameter is studied because of its direct relation to the resonant frequency, as shown in Fig 8.2 (a). Then, the A_d parameter for the adjustment. Fig 8.2 (b) shows that the similar the patch and the ground plane are, the better.

Later, the feeding point is analysed to improve the matching of the antenna (Fig 8.3 and Fig 8.4). Finally, the effect of the corner radius is studied (Fig 8.5).

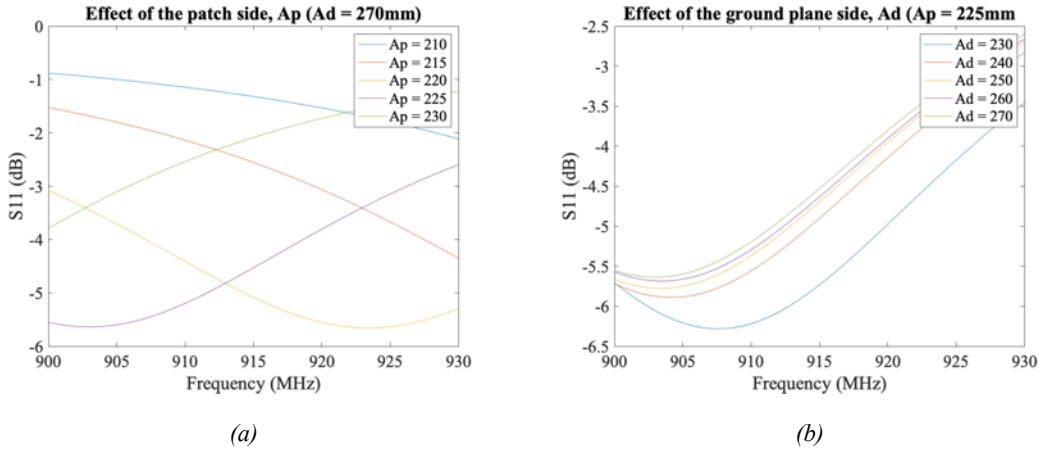


Fig 8.2. (a) A_p and (b) A_d parameters effect.

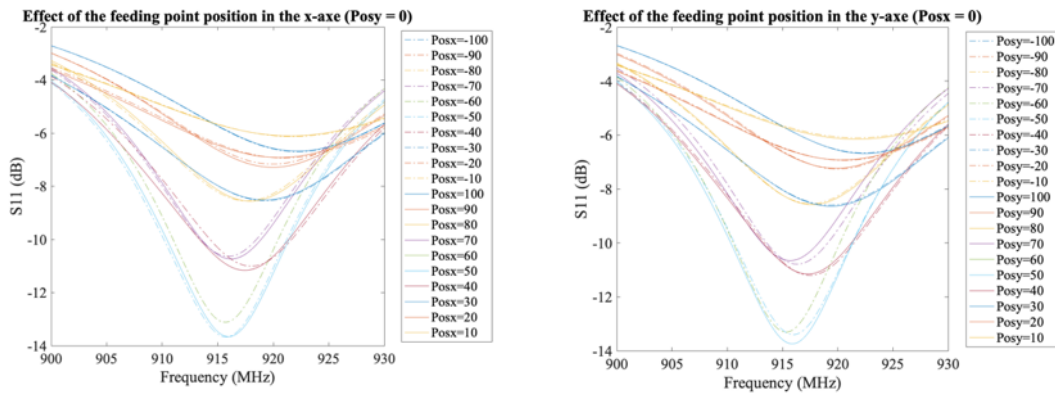


Fig 8.3. Effect of Pos_x (left) and Pos_y (right) once the patch dimensions are defined.

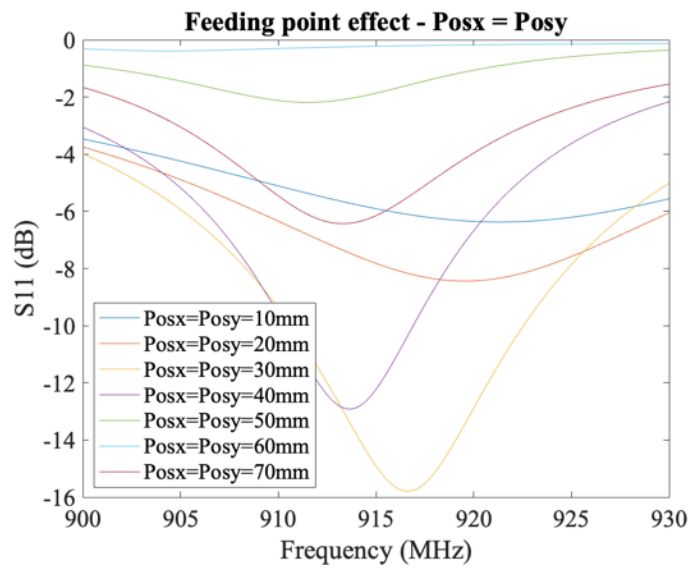


Fig 8.4. Parametric study of the feeding point: diagonal movement.

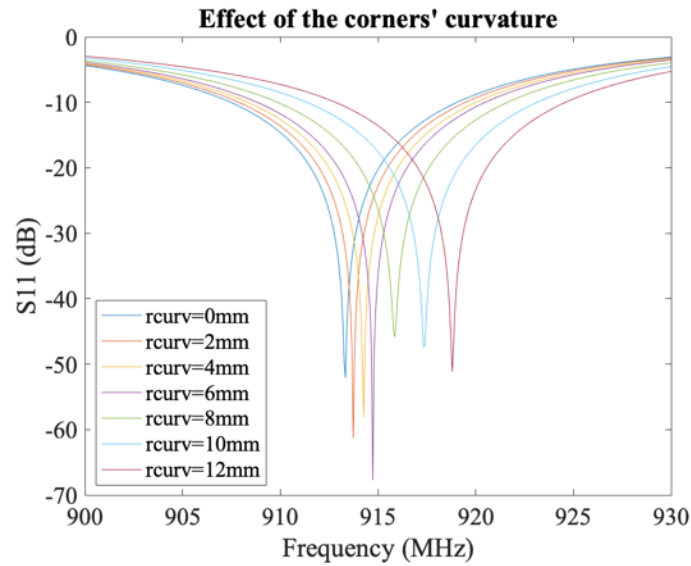


Fig 8.5. Matching adjustment with the corner's radio curvature.

Some conclusions can be extracted from these data lines:

- Exists symmetry in the feeding point.
- When the feeding point is in one of the axes ($P_{ox} = 0$ or $P_{oy} = 0$), the best solution is around 50 mm.

Finally, the optimum parameter design is obtained through a complete parametric study, and the results are shown in Fig 8.6. The design parameters for the best solution are: $A_d = 240$ mm, $A_p = 220.5$ mm, $r_{curv} = 6$ mm, $Pos_x = 30$ mm and $Pos_y = 40$ mm. The best S_{11} value is -67.5 dB @ 914.7 MHz, and the frequency range with $S_{11} < -10$ dB is [908,2 – 920,5 MHz].

Interestingly, the optimum position for the feeding point is around the medium point between the best solutions with only one axe as a variable.

Some changes can be seen in the return losses when the antenna is introduced into a loaded cavity. In the case of this antenna and the cavity used to validate it (the same as in the previous subsection), these changes are minor and depend mainly on the load (see Fig 8.6); thus, it is not necessary to make any adjustment.

The antenna has been manufactured and measured in both conditions (Fig 8.7), showing promising results. However, a problem is encountered related to the pieces assembly. A mechanism is needed to attach the patch homogeneously to the Teflon and the Teflon to the aluminium piece. At first, five screws are used, creating air gaps that make the return losses value unstable.

More screws have been set to improve it without a significant breakthrough. Since Teflon is one of the most slippery surfaces, using adhesive material is not an option. At this point, replacing the Teflon with another substrate is thought and started the materials research, with the conclusion of choosing PEEK. This material has not been used before for these purposes.

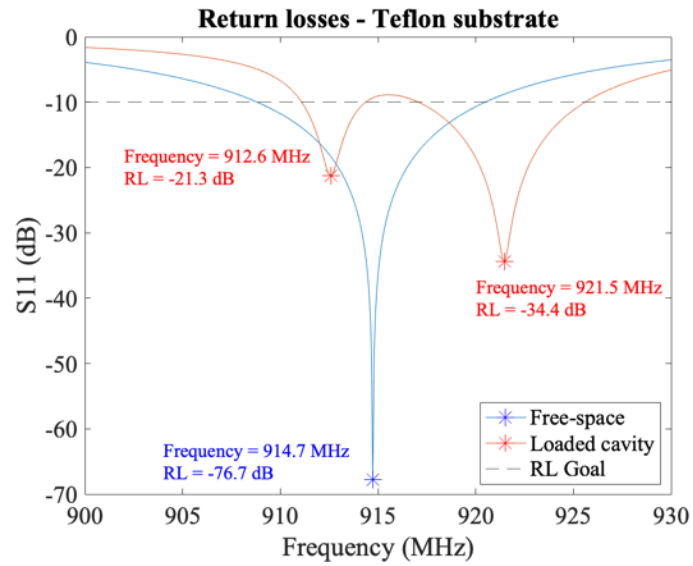


Fig 8.6. Return losses of the modelled antenna.

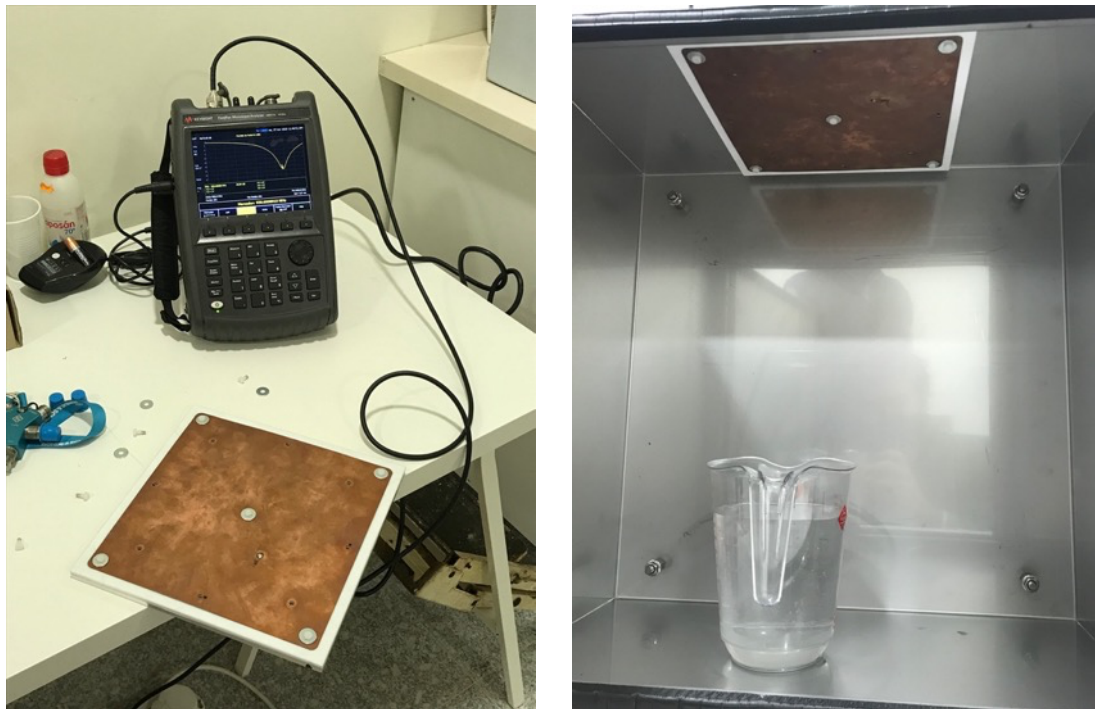


Fig 8.7. Teflon squared patch antenna at 915 MHz, measured in free space (left) and inside a cavity (right).

8.1.2. With PEEK substrate

Based on the work in 7.1.1, the patch antenna based on PEEK as a substrate is carried out. The thicknesses of the three principal elements (ground/support plane, substrate and patch) remain the same as in the Teflon study. Thus, adjusting to this new substrate is done using a simple rule of three.

Given that the wavelength in a medium, usually called λ_g , is related to the material permittivity through (8.3), an increase in the dielectric permittivity ϵ_r corresponds to size reduction.

$$\lambda_g = \frac{\lambda_0}{\sqrt{(\epsilon_r)}} \quad (8.3)$$

In this case, the permittivity of the Teflon is compared to the Peek by $2.1/3.2 = 0.656$. Introducing this factor in (8.3), i.e., applying the square root, the approximative dimensions of this new antenna are obtained:

$$A_{d_{PEEK}} = \sqrt{0.656} * A_{d_{Teflon}} = 0.81 * 240 = 194.4mm \quad (8.4)$$

$$A_{p_{PEEK}} = \sqrt{0.656} * A_{p_{Teflon}} = 0.81 * 220.5 = 178.6 mm \quad (8.5)$$

The antenna has been modelled in HFSS with these parameters for free-space. The resonance is located a bit higher than the objective central frequency. A fine adjustment in these two parameters is made to obtain the optimum resonance. Fig 8.8 shows the S_{11} for the theoretical dimensions and the behaviour after the adjustment. Concretely, the final values are $A_{p_{PEEK}} = 180 mm$ and $A_{d_{PEEK}} = 190 mm$. The feeding point has also been slightly adjusted: $Pos_x = 30 mm$ and $Pos_y = 40 mm$.

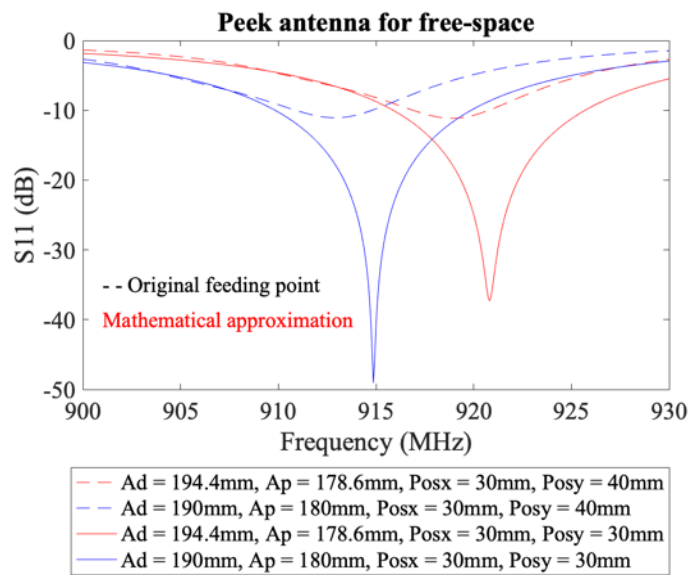


Fig 8.8. Return losses for the mathematical approximation and the later improvements.

The antenna is later modelled for the cavity mentioned before. The same situation as in the Teflon occurred: no change is needed, as shown in Fig 8.9. The corner radius is set to 12 mm instead of 6 mm to refine it.

The antenna has been manufactured with the help of the specialised company Tarí Mecanizados (Rafelbuñol, Valencia, ES). A first solution is done with Nylon screws to support the patch to the substrate (Fig 8.10). It can be seen in this picture the different possible locations for the screws. The mechanical tensions introduced by the screws produce the patch bending.

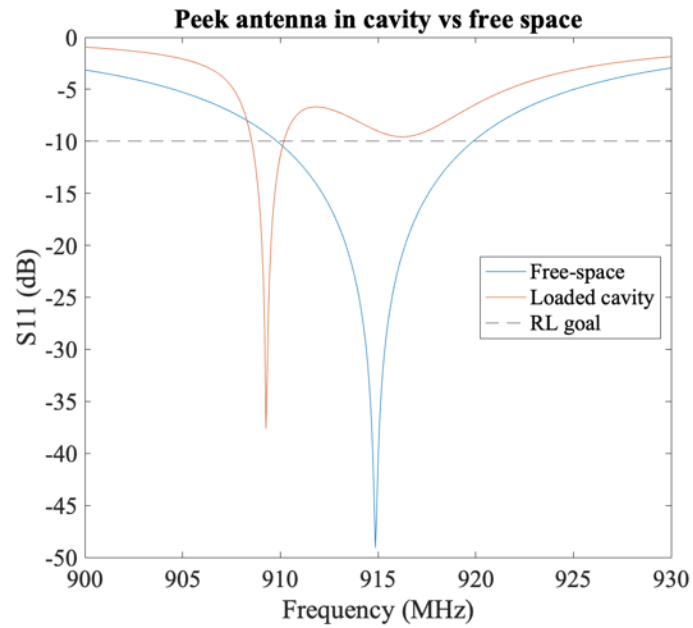


Fig 8.9. Comparison of the RL between the antenna modelled for a loaded cavity and free-space

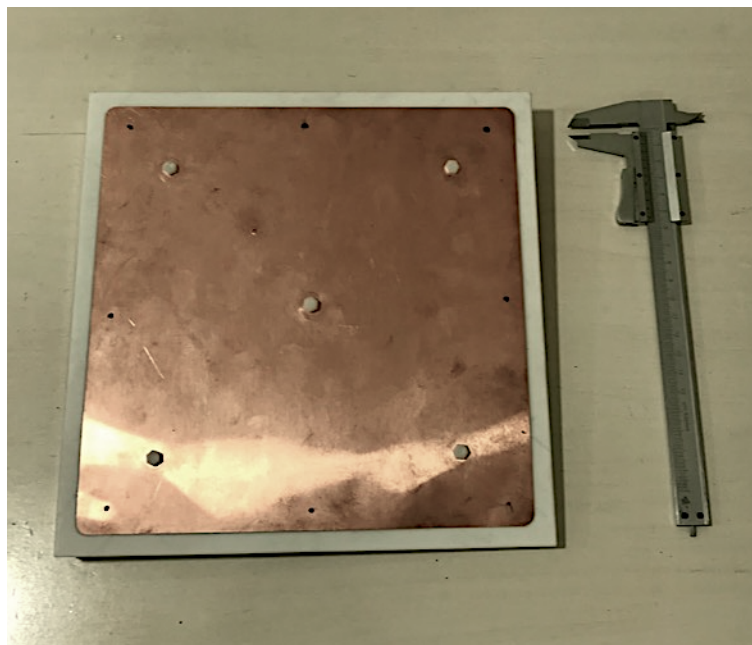


Fig 8.10. Manufactured patch antenna at 915 MHz and PEEK substrate.

An assembly improvement has been made with the introduction of a high-temperature adhesive glue and the optimisation of its applying technic, assuring the proper adhesive distribution and the, therefore, the most similar result to the modelled one. It is a complex and challenging objective. Fig 8.11 shows a plastic piece used to see how the glue is spread through the surface and the resultant pattern once cured.



Fig 8.11. Example of the actions performed to verify the proper adhesive distribution.

Once the assembling method has been verified, six antennas have been manufactured for the application presented later in this chapter (see Fig 8.12). Given the non-automatised manufacturing process, some deviations are likely to occur.



Fig 8.12. Five out of six manufactured antennas and the solid-state microwave module at 915 MHz.

The antennas are measured both in free space and inside the cavity, where power tests are performed to verify their proper response (see Fig 8.13). The results of the free-space measurement are shown in Table 8.1.

It is decided that all the antennas but the 3rd one can be used in the final system. Its resonant frequency is out of the operating frequency range of the solid-state microwave modules.



Fig 8.13. Free space measurement with VNA (left) and power tests (right).

Table 8.1. Free-space PEEK antenna measurements.

Antenna	Best matching – S11 dB	Frequency (MHz)
1	-21	916.9
2	-26	915.87
3	-22	929.54
4	-27	923.8
5	-30	918.7
6	-28	920.1

The antennas are tested, as said, to verify their behaviour when high power is applied through them to a cavity. The cavity is loaded with a centred water recipient and placed 50 mm over the cavity bottom. The power tests consist of 2 minutes on different power levels to check the stability and matching. Stability is essential because some microwave devices can change their matching with the temperature increase of their elements. Better matching values are typical when the load is water or foodstuff and its temperature increases. Table 8.2 shows, as an example, the results of the power test for the first antenna.

Table 8.2. Power tests for the antenna 1.

Transmitted Power (W)	Reflected Power (W)	Optimum working frequency
20	1	916 MHz
100	9	916.5 MHz

200	15 – 17	916.5 – 917 MHz
-----	---------	-----------------

These results confirm that the RL are lower than -10 dB, i.e., the reflected power is lower than the 10%. It was the design goal and has been achieved.

8.2. Application example: dried fruits drying process

The solid-state multi-source system using patch antennas has been applied to the industrial process of almond drying. A complete study, development and manufacture have been carried out for a research project funded by CDTI (Centro para el Desarrollo Tecnológico Industrial). This project has been developed by Microbiotech S.L., the IIAD (Instituto Universitario de Ingeniería de Alimentos para el Desarrollo) from UPV and José Borrell S.A. This last is a renowned company that manufactures all kinds of machinery for almond treatment in Denia, Valencia.

The project's objective is to develop a system capable of being integrated into the almond drying line with microwave energy generated by solid-state microwave generators. This technology will improve the heating pattern by controlling the frequency, phase, and power. It will also help improve the electric security and lifetime of the equipment.

The block diagram defined in this doctoral thesis has been updated to the specific requirements of this project and can be seen in Fig 8.14. In this schematic, the total power is 2 kW; this value is explained in detail later in the text, as well as the frequency selection and the number of antennas.

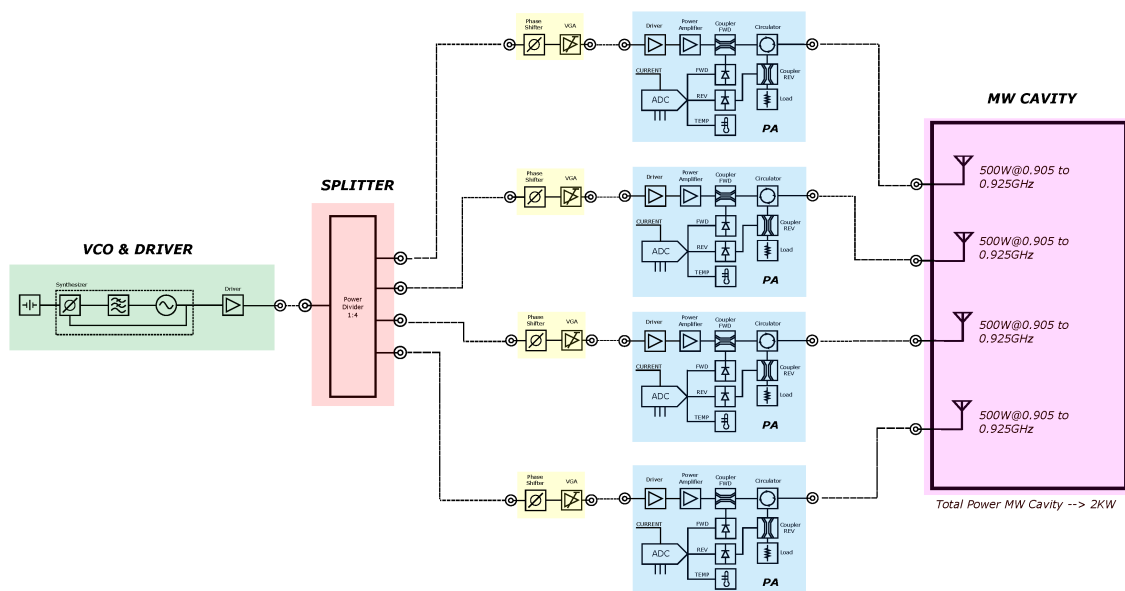


Fig 8.14. Block diagram for the 915 MHz multi-source solid-state driven system with 2kW of total output power.

The project's structure has different stages: first, the dielectric properties of the almonds have been measured to assure the microwave-almond interaction; then, the power requirements are obtained through mathematical calculations and confirmed by the first tests; after that, complete electromagnetic modelling is carried out to get the optimum oven dimensions, the number feeding structures (antennas) and their location in the cavity, the position of the load within the cavity, etc.; finally, the development and manufacture of the prototype are done. The results of this work serve as a Proof of Concept (PoC) and situate this system at a TRL 7 level.

8.2.1. Almond thermophysical and electromagnetic characterisation.

Previous to any microwave study, where electromagnetic or multiphysics modelling will take place, a proper thermophysical and electromagnetic characterisation is needed.

The raw material used for the tests has been provided by J. Borrell S.A. and consists of two kinds: whole peeled and packed almond and chopped peeled and packed almond. Previously to the measurement, the samples have been registered as shown in the example of Fig 8.15.

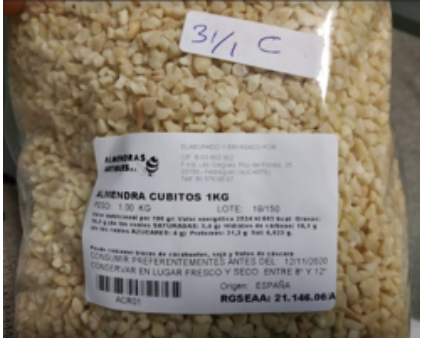
Identification 31/1 C		
	Reception date	31/01/2020
	Expiration date	12/11/2020
	Lot; origin	19/150; Spain (Alicante)
	Observations	Blanched almond in dice, 1kg
	RGSEAA	21,146,06/A
	Conservation	Cool, dry place between 8 and 12 °C
	Nutritional value (100 g)	E.V.: 603 Kcal; Fat: 5.4 g; CH: 10.1 g; Protein: 21.3 g; Salt: 0.023 g

Fig 8.15. Example of an almond sample reception register file.

8.2.1.1 Humidity characterisation

The gravimetric method [169] has been used to measure the humidity content, and the hygrometer Aqualab CX-2 (Meter Group, USA) has been used to measure the water activity. The initial humidity value, x_w , of the two samples was 4.12 ± 0.7 (% b.h), and the water activity, a_w , was 0.627 ± 0.001 .

Due to the water content dependency of the dielectric properties and its change during a drying process, it is necessary to balance the samples to different humidity values to measure the impact

on the dielectric properties. Controlled relative humidity (RH) chambers/cells were used to balance the almond samples at different humidity levels.

This method consists of the self-modification of the sample humidity once it has reached the balance with a reference material inside a closed recipient during a specified time at a constant temperature. In this case, saturated solutions of different salts have been used as reference material. The humidity content of the samples is determined after reaching the balance. Depending on the relative humidity of the cells (which is conditionate to the saturated saltwater activity, a_w , that is fixed), water absorption or desorption will happen, modulating the final balanced humidity.

The almond samples have been balanced at 20° C, up to humidity levels of 11.3, 22.5, 43.2, 57.6, 75.3, and 84.3 % on a wet basis. The cell's HR range is chosen by considering both the starting almond humidity and the usual humidity ranges available in the almond manufacturing process (15% natural almonds, 5-7% pasteurised almonds and 0.5-1% toasted almonds).

8.2.1.2 Dielectric properties measurements

As mentioned in Chapter 3, several dielectric properties measurement systems and techniques are available. This characterisation has been done using the reflection/transmission coaxial system presented by Santón et al. [70]. In these measures, the granulated material (chopped sample) was set in thin transparent plastic bags, as shown in Fig 8.16. These bags introduce a slight measurement deviation due to the transparent behaviour of the microwaves and their reduced thickness.

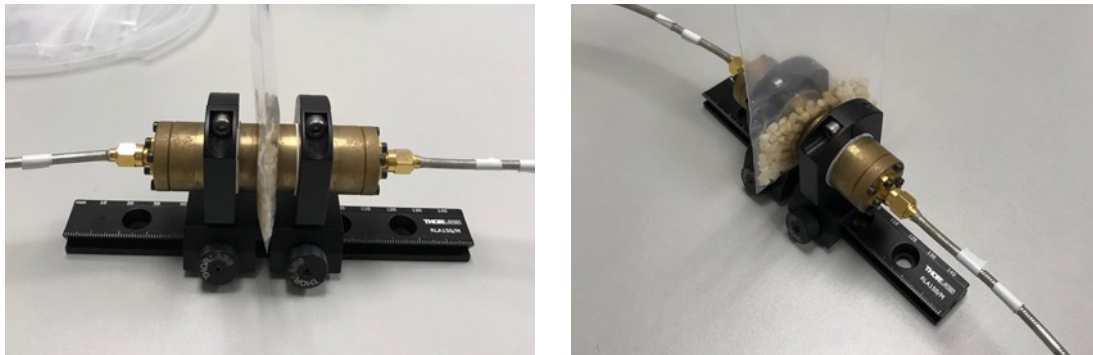


Fig 8.16. Dielectric properties measurement of an almond sample.

The samples have been balanced to different humidity contents and tempered to 20, 30, 40, 50, 60 and 70 °C, obtaining the dielectric properties in a wide range of humidity and temperature (see Table 8.3). This data is key to the microwave drying modelling in multiphysics software.

Table 8.3. Dielectric properties of chopped almonds depending on humidity and temperature.

T (°C)	x_w (%)	ϵ'	ϵ''	T (°C)	x_w (%)	ϵ'	ϵ''
20	2.1	1.83	0.21	20	11.9	4.70	1.51
30	2.1	1.72	0.22	30	11.9	4.87	1.52

40	2.1	1.76	0.24	40	11.9	5.11	1.56
50	2.1	1.92	0.25	50	11.9	5.27	1.61
60	2.1	2.14	0.26	60	11.9	5.41	1.67
70	2.1	2.39	0.31	70	11.9	5.55	1.75
20	4.2	1.82	0.31	20	15.8	7.19	2.16
30	4.2	1.72	0.32	30	15.8	7.5	2.18
40	4.2	1.74	0.34	40	15.8	7.83	2.21
50	4.2	1.82	0.35	50	15.8	8.07	2.3
60	4.2	1.94	0.36	60	15.8	8.29	2.39
70	4.2	2.06	0.41	70	15.8	8.53	2.48
20	8.0	2.55	0.55	20	19.6	7.3	3.22
30	8.0	2.6	0.58	30	19.6	7.54	3.3
40	8.0	2.66	0.62	40	19.6	7.89	3.34
50	8.0	2.74	0.71	50	19.6	8.10	3.45
60	8.0	2.81	0.79	60	19.6	8.33	3.56
70	8.0	2.87	0.82	70	19.6	8.61	3.78

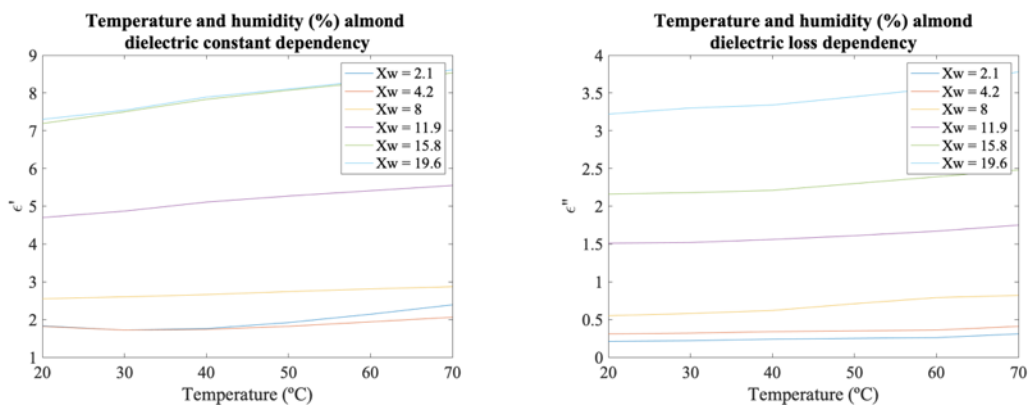


Fig 8.17. Real (left) and imaginary (right) parts of the dielectric permittivity for different humidity percentages and temperatures.

As known through the literature and shown in Fig 8.17, the lower the water content, the lower the interaction with microwaves.

8.2.2. Power requirements and first tests

Choosing 915 MHz as the frequency band for this application was first thought due to its industrial application. This industrial application requires a broad product heating surface and a relatively high thickness. The dielectric properties and the working frequency are directly related to the penetration depth by equation (8.6).

$$d_p = \frac{c_0}{2\pi f \sqrt{2\epsilon' \left[\sqrt{1 + \left(\frac{\epsilon''}{\epsilon'}\right)^2} - 1 \right]}} \quad (8.6)$$

Although the literature indicated that 915 MHz was a reasonable choice, heating tests to confirm this is needed. The objective of these tests is to ensure that the penetration depth is enough for all the product amounts, the product quality is the one required by the client (homogeneous heating without almond burnings), and the reduction in the drying time is significant. These three aspects define the feasibility of the application.

Two test benches have been set, one at 915 MHz (Fig 8.18) and the other at 2,450 MHz (Fig 8.19). The two systems have in common that they operate with a 250 W solid-state microwave generator from Leanfa Slr (Bari, IT) and a monopole antenna integrated into a metallic cavity as the applicator structure. The tests also included the study for needing a hot air stream to help the heating. The control variables are microwave power and frequency, air temperature and speed, and sample size.



Fig 8.18. Microwave heating system at 915 MHz.

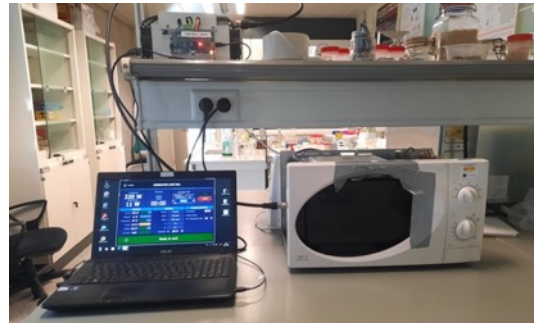


Fig 8.19. Microwave heating system at 2,450 MHz.

Frequency tuning within the frequency bands, 902.5 – 927.5 MHz and 2.42 – 2.48 GHz, respectively, is used to change the electric field distribution within the cavity. It adjusts the system reflected power, whose small load (the almond sample) could have been located low field intensity region. On the other hand, if the sample is located in a high-intensity field area, a hotspot could occur.

These parameters, along with the power, are operated via PC software. The power can be varied between 1 to 250 W, one by one. Given that the power–mass rates are between 0.5 and 2.5 W/g, the maximum sample size is 100 g with two configurations: a diameter of 40 and 80 mm (Fig 8.20). These recipients are designed to improve the airflow through the sample.

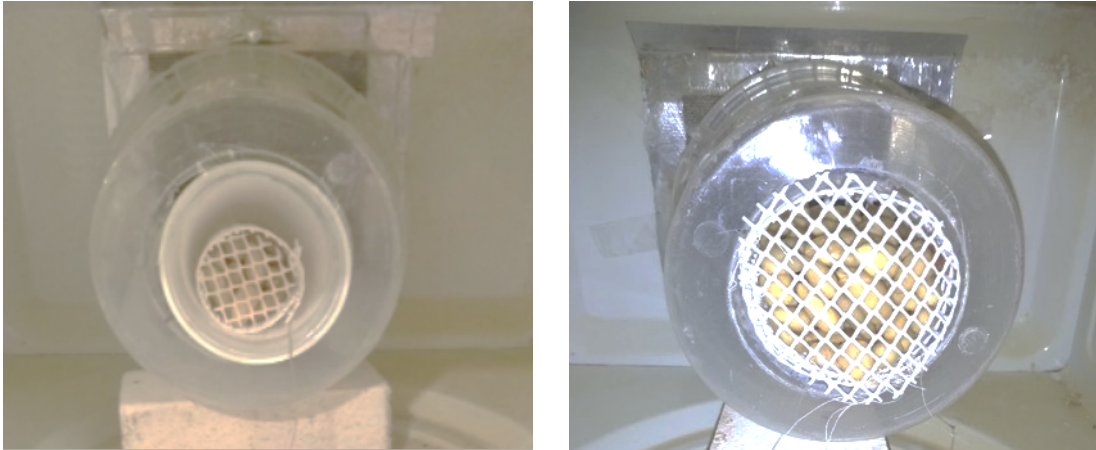


Fig 8.20. Almond sample configurations with diameters of 40 mm (left) and 80 mm (right) placed inside the multi-mode metallic cavity.

The first results showed a significant hot spot in the centre of the sample when working at 2,450 MHz, as shown in Fig 8.21. An electromagnetic model is computed to understand this behaviour. The electric field distribution in the cavity (see Fig 8.22) shows that a high-intensity spot can be found in its centre. A new configuration has been set to solve it (Fig 8.23), and 915 MHz is used as the working frequency. It has been possible to reach a homogeneous 1% humidity with these features. The drying process consisted of microwave heating of 100 g for 10 minutes with a power–mass relation of 1 W/g. At this frequency, it is possible also to reach 2.5 W/g without any overheating problem.

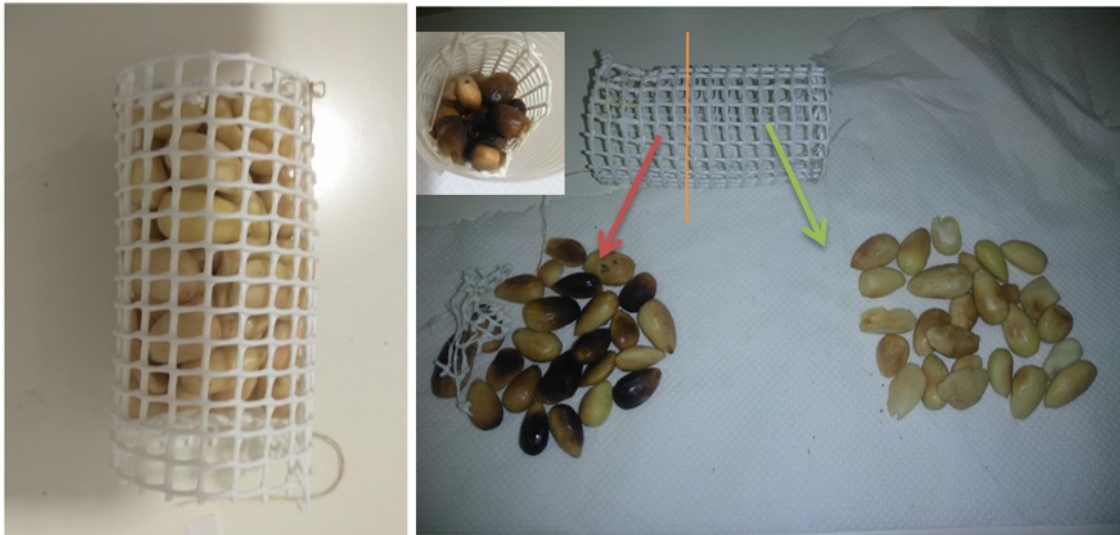


Fig 8.21. Hotspot effect on the almond sample at 2,450 MHz.

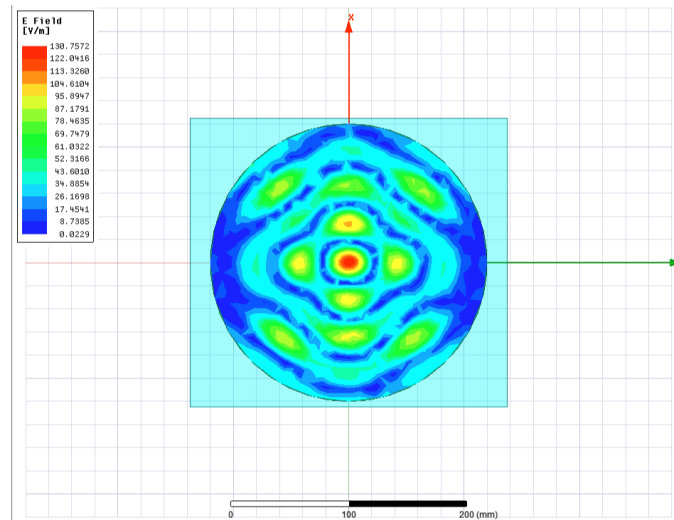


Fig 8.22. Electric field pattern modelled for the test's cavity.

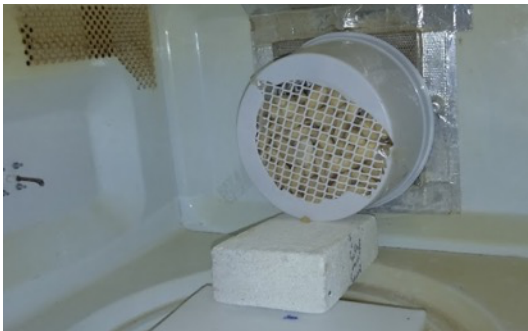


Fig 8.23. New configuration to avoid hotspots (left) and drying results at 915 MHz (right).

8.2.3. Multi-sources electromagnetic modelling

Improving heating efficiency and homogeneity is a must in industrial processes. In the almond drying sector, the product is introduced into continuous ovens on a conveyor belt, forming a rectangular nearly-homogeneous surface with a determined thickness. In the microwave terminology, it is considered the load.

Multiple and independent microwave sources are used to electronically change the electric field distribution and intensity. This change, continuous or static, allows coping with the different heating mechanisms that take place in a microwave-based heating process of a rectangular load and are described in Chapter 2.

To that end, the first studies are focused on defining the cavity dimensions and the number of sources to be used. This selection is made according to the selected frequency, 915 MHz, power requirements, industrial belt standards and product dimensions previously used by the client. A standardised system can help integrate the microwave system as a part of a multiple technologies combined system.

Different studies are performed using the antennas described in Subsection 8.1.2 to define their number and location in the cavity. These studies also include the effect of the phase-shifting to the electromagnetic pattern.

A first approach is made using two antennas located on the top face of the cavity and rotated 90° one to the other. This rotation avoids the mutual coupling effect [170]. Fig 8.24 shows an array of electric field distributions for a complete range of phases (0 to 360°) in one of the antennas while the other remains with phase 0°. It can also be seen that the electric field pattern has considerable dimensions, according to the 915 MHz frequency band.

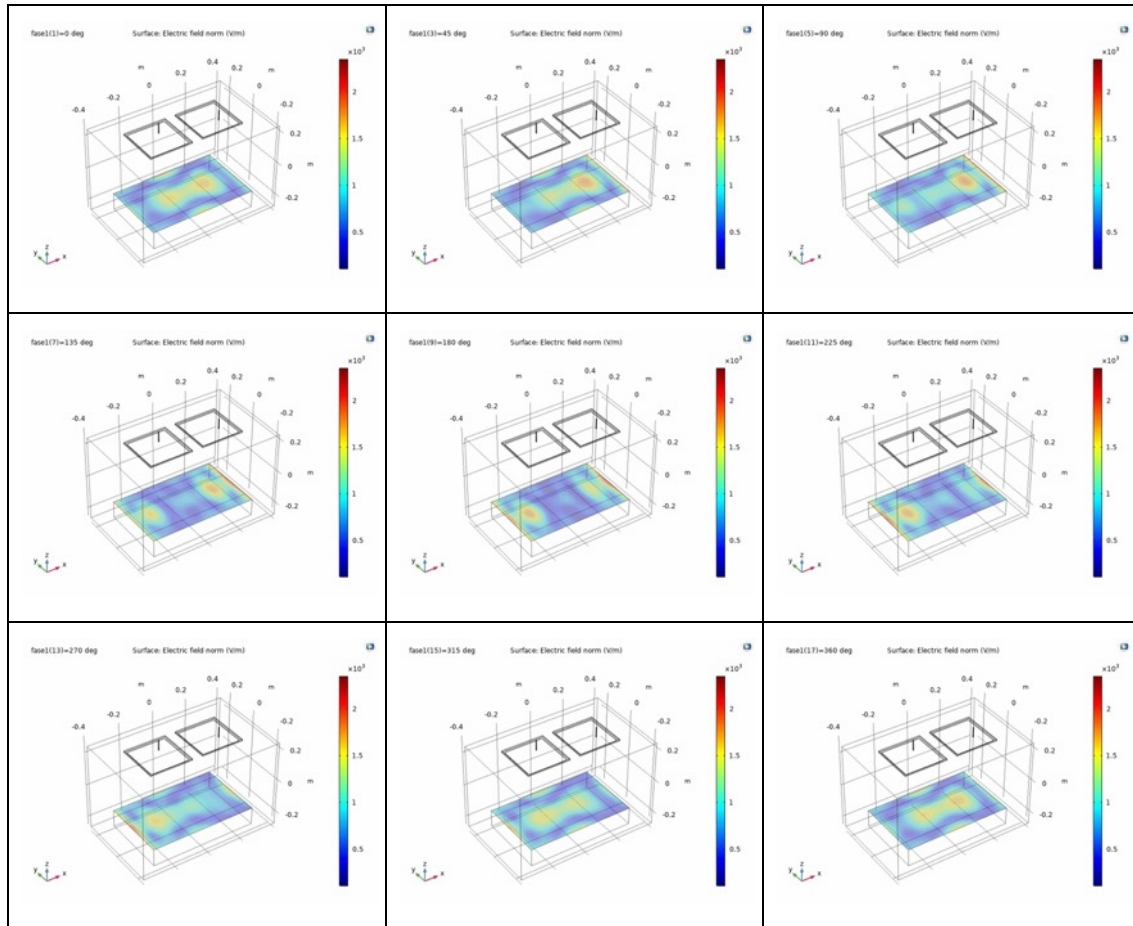


Fig 8.24. The effect over the almond surface of the phase-shifting in one of the antennas from 0 to 360 grades at 915 MHz.

Later, a study with four antennas was made. According to their position, these antennas have been treated in pairs: two share the same X position while the others share the Y position of the top surface. Fig 8.25 shows the effect when the change is made in the antenna at the right, i.e., the phase-shifting is done horizontally. This effect is not the same when the phase-shifting is vertical. Fig 8.26 shows a similar field pattern but with different behaviour with the phase.

Combining these two types of phase change gives the system great control over the electric field. The adequate velocity of this change can make these fields maximum and minimum to converge into a homogeneous average electromagnetic field pattern.

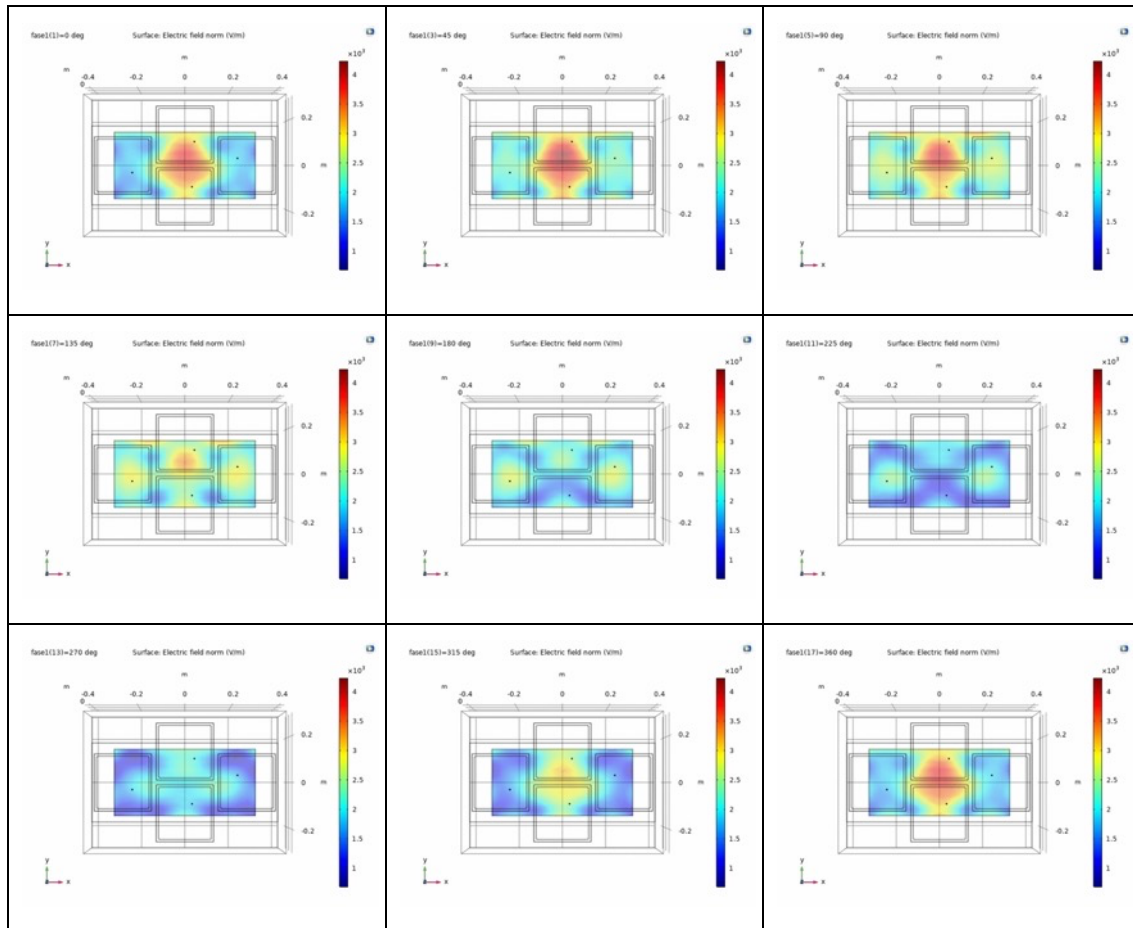
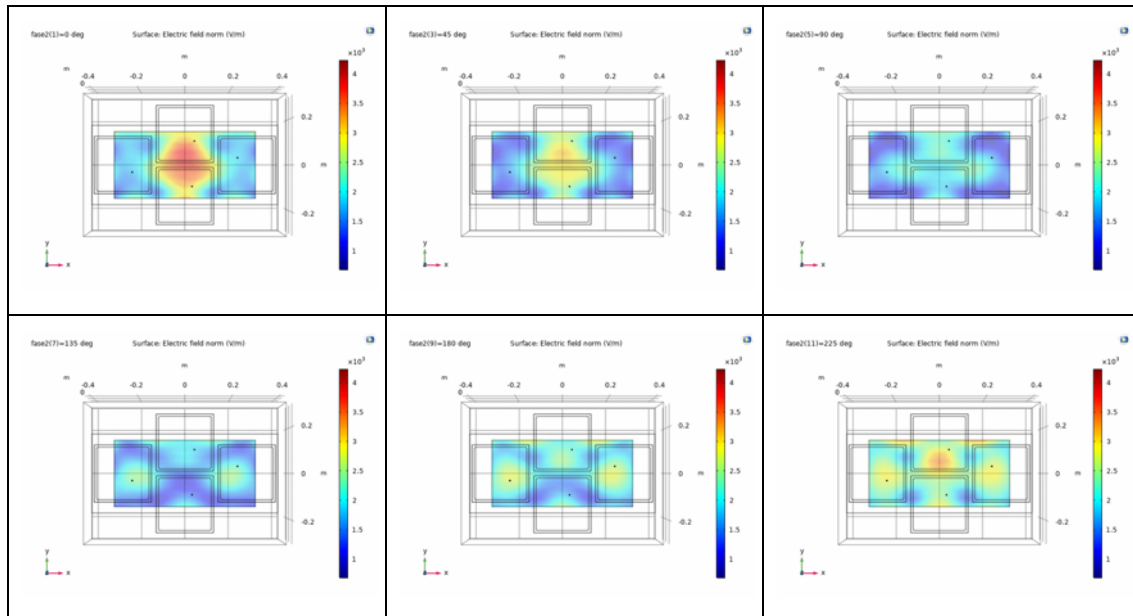


Fig 8.25. The effect over the almond surface of the phase-shifting in the right antenna from 0 to 360 grades.



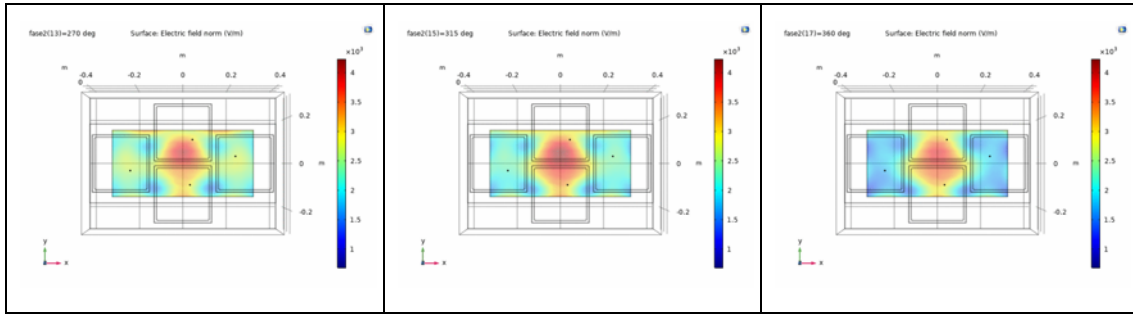


Fig 8.26. The effect over the almond surface of the phase-shifting in the bottom antenna from 0 to 360 grades.

The last study is focused on combining six antennas into the same cavity. Three columns and two rows form the array; the top row is row 1, and the left column the column 1. Among all the studies done, here are shown the results from three: phase-shifting in columns 1 and 3 (see Fig 8.27), phase-shifting in column 2 (see Fig 8.28) and phase-shifting in row 2 (Fig 8.29).

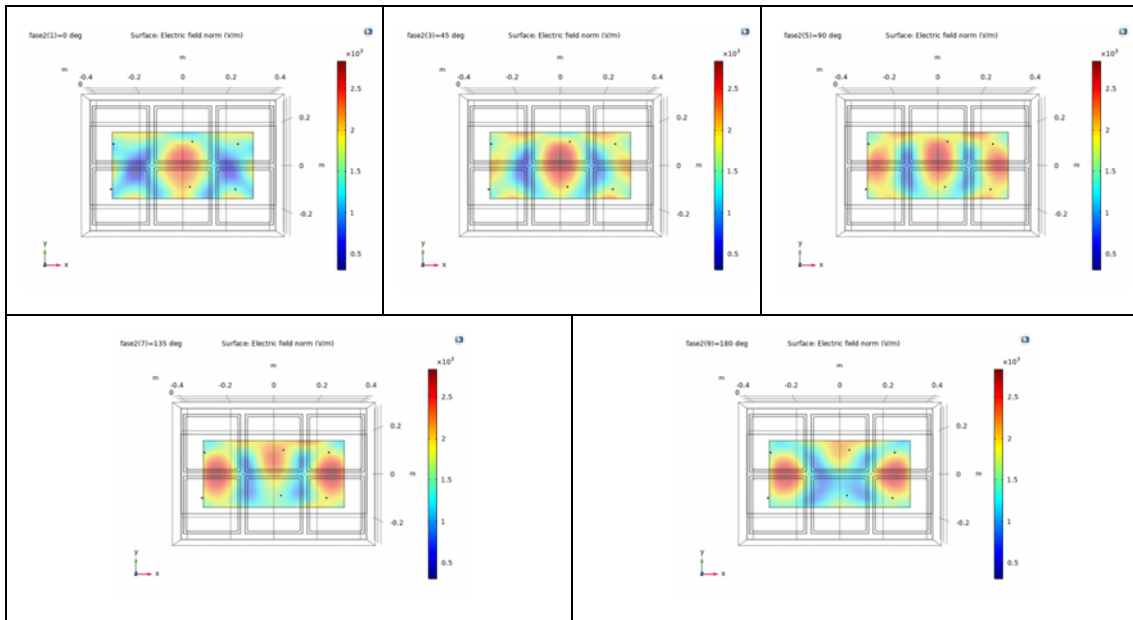
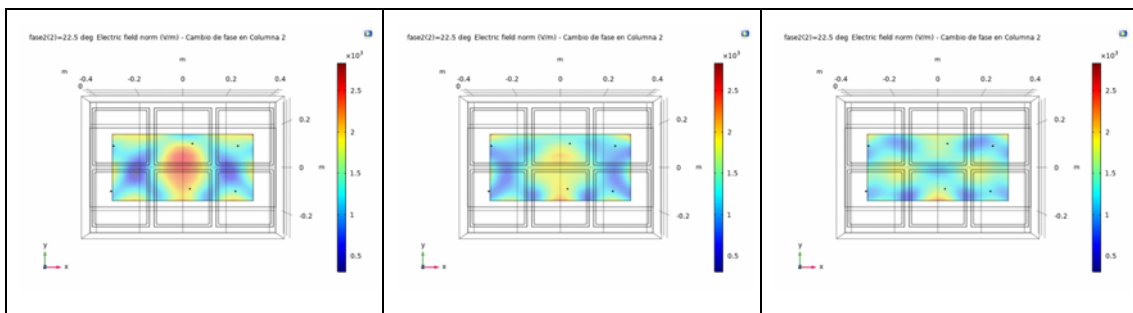


Fig 8.27. The effect over the almond surface of the phase-shifting (0-180°) in the first and third columns of antennas.



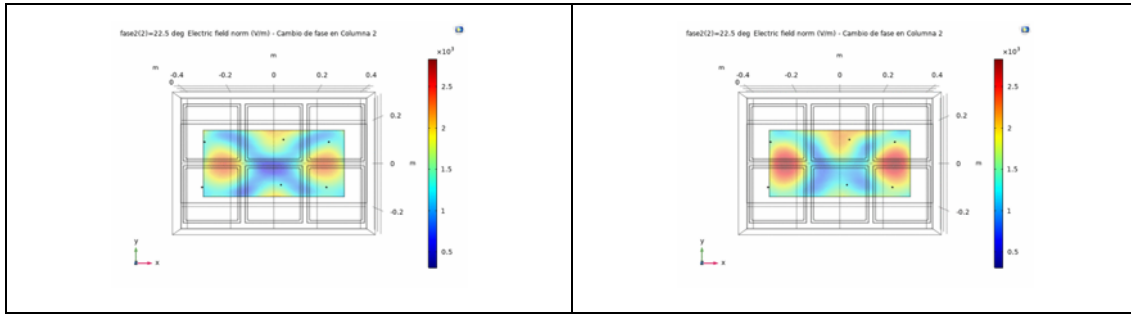


Fig 8.28. The effect over the almond surface of the phase-shifting (0-180°) in the second column of antennas.

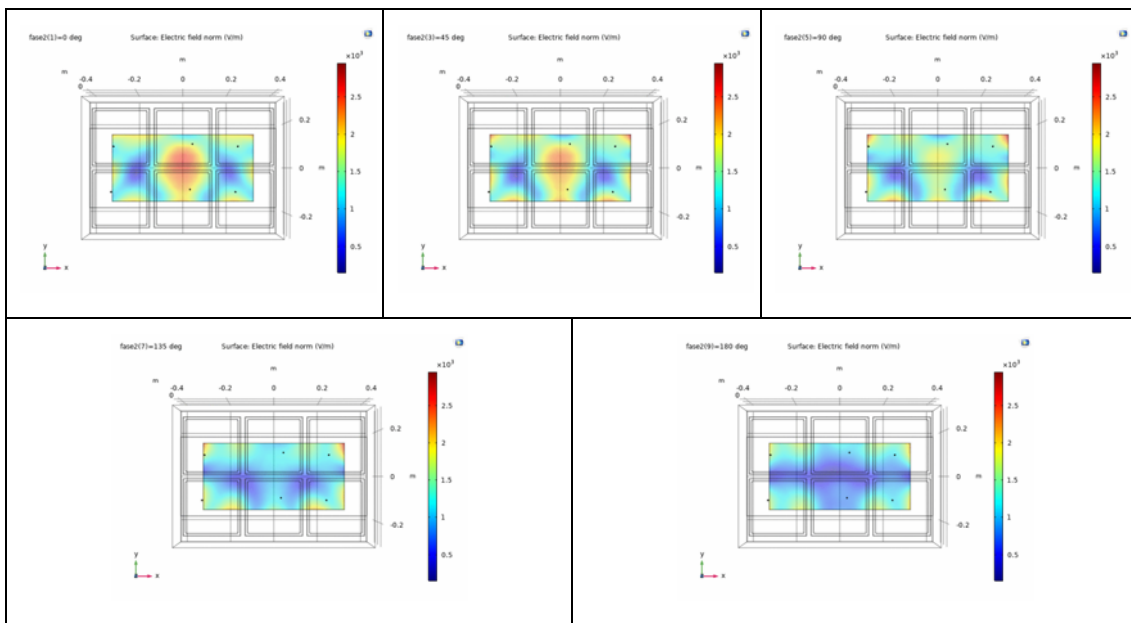


Fig 8.29. The effect over the almond surface of the phase-shifting (0-180°) in the second row of antennas.

Taking a look at the results seems reasonable to choose the second option: four antennas, making it mandatory to increase the amount of power per antenna. However, the benefits are more significant: fewer variables ease the system's control, and the observed electromagnetic field pattern is adequate to obtain homogeneous microwave heating.

As stated before, the cavity dimensions are given by three variables. First, the number of antennas, their size, and distribution on the top surface, and the necessary space between them and the cavity walls. Second, the conveyor belt and the company's different requirements, such as cleaning clearances. Third, the market available electromagnetic shielding equipment and their standard dimensions or options. With this in mind, the final dimensions chosen are 850 x 655 x 640 mm (length, width and height).

8.2.4. Development of a modular oven as a PoC (proof of concept)

8.2.4.1 Solid-state microwave generator

Following the same decision as with the 2.45 GHz chemical application (see subchapter 7.2), it has been chosen to work with already integrated solid-state microwave generators; in this case, with four coherent but independent microwave power outputs.

The microwave generation equipment acquired to build this PoC is the PHASESHIFTER Evaluation Kit from Leanfa Srl (Bari, IT). This generator (Fig 8.30) is built around four 915 MHz 750W solid-state amplifiers. With these amounts of power, these amplifiers are generally water-cooled; however, the client asked for a forced-air cooling system, so the maximum power per amplifier had to be reduced to 500W. It includes an AC/DC switching power supply system and an advanced synthesiser with four outputs capable of accurate frequency synchronisation and 360° independent phase rotation [171]. The system is controlled by a Windows software called LeanOn, and the control is based on serial communication via USB (see Fig 8.31).



Fig 8.30. Frontal isometric view of Leanfa's PhaseShifter Kit.

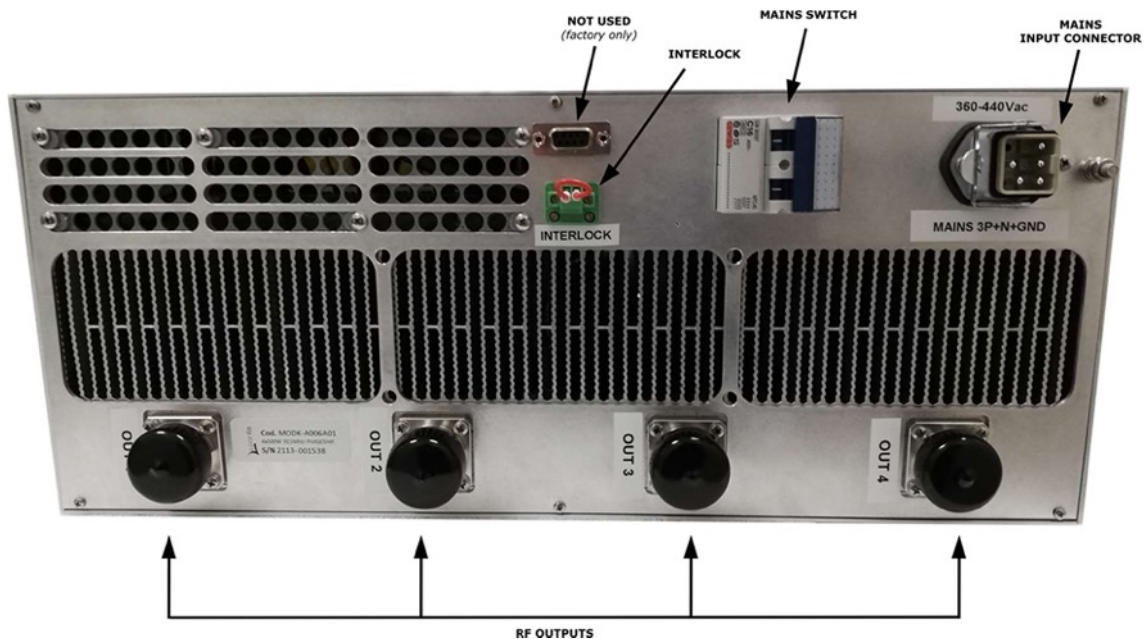


Fig 8.31. Rear panel view of the PhaseShifter Kit with the connections labelled.

Later, this system was modified (see Fig 8.32) to include a higher-level communication protocol: Modbus. This protocol allows working over Ethernet/IP making this system market-ready due to

the vast implantation of this protocol in the industrial environment. It eases the use of proprietary control software development and automation.



Fig 8.32. Modbus ethernet converter external installation.

The device has a maximum power consumption of 4kVA, and its size and weight are 620 x 490 x 180 mm and 38 kg, respectively. The microwave transmission to the oven is done by semi-rigid high-power coaxial cables connected from the 7/16” output connectors to the four patch antennas (with N connectors) located on top of the oven.

The kit can be used with the four modules operating with independent frequencies or in the so-called “sync” mode, which allows the four modules to radiate precisely synchronised at the same operating frequency. In this operating mode, each module’s relative phase can be set in the 0-360° range with a step of 1.4°.

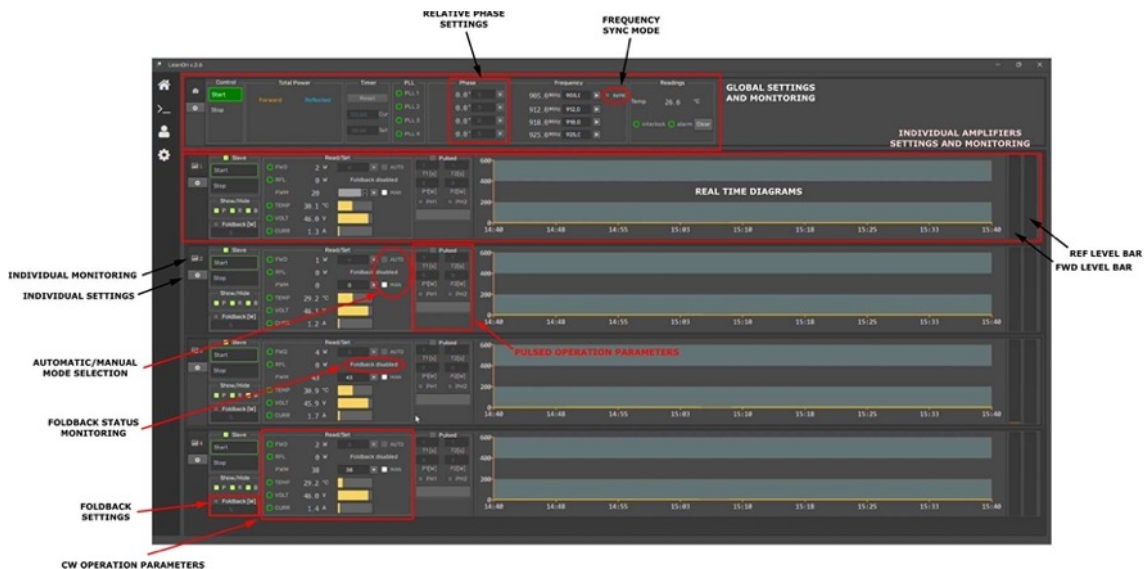


Fig 8.33. General screenshot of LeanOn control software with the different control buttons labelled.

Each power module can be operated in Continuous Wave (CW) or Pulsed Mode. The CW operation can be controlled in two different modes. The first and most recommended for regular operation is the automatic mode (AUTO) that allows selecting the desired output level in Watts thanks to a closed-loop control system that automatically implements a temperature compensated regulation of the selected output level. The second operating mode is called Manual (MAN) mode and is limited to specific testing conditions, especially during customer software development. It

is an open-loop operation driven by a PWM value, generating a constant control voltage without guaranteeing a regulated output power level, which typically decreases with the generator's temperature. The Pulsed Mode allows defining two output levels in Watts and two corresponding time durations (step of 1s), generating a periodic pulsed waveform.

The monitoring "Home page" of the LeanOn platform (see Fig 8.33) shows the global settings and monitoring in the top section, where the operating frequencies can be set. The system automatically selects the same frequency value for all four modules if the sync mode is active. Each frequency value can be set independently, within the admitted range, if sync mode is unselected. If a phase-shifting process is needed, the frequency must be in sync mode. Otherwise, the wave wouldn't be coherent.

The same area shows the status of the interlock contact, available on the rear panel of the kit, e.g., to manage safety conditions linked to doors or security contacts in microwave applicators. When the interlock is open, the outputs are automatically muted, e.g., to guarantee safe conditions in case of accidental opening of microwave applicators.

In the same top section of the home page, the user can set a Timer to select a predefined time duration of the microwave outputs generation. After choosing a defined time duration, the timer will be progressively decremented, and the system will automatically stop after reaching zero value. The Evaluation Kit can always be used with manual Start/Stop operation by leaving the timer to a zero-set value. Next to the Timer, readings of the global forward and reflected powers and the lock status of the frequency synthesisers (PLL 1-4) are available for constant monitoring.

8.2.4.2 Static or batch oven design

The PoC has been designed to be used in two modes: batch and transport oven. It was interesting to have an intermediate step between the modelling and the final design to check the possible problems. The batch oven design allows an easy transformation into a transport one. Some dimensions and features are oriented to that aspect. Moreover, it has been designed to test different antenna configurations; being these antennas, the outcome of the subsection 8.1.2.

The first design is based on tetrahedral metallic posts making a skeleton and then adding different metallic sheets to every face. However, standardised metallic enclosures for electrical purposes were found in the market for a compatible solution. Specifically, the Spanish company DelValle Global Solutions S.L. (Álava, ES) offers different products consistent with the project and the capacity to have the metallic boxes designed ad-hoc with several accessories such as windows, lock type, or preformed apertures. The Luxor model ordered, whose drawings are shown in Fig 8.34, offers certified EMI (Electromagnetic Interference) protection in the selected working frequency, 915 MHz. This metallic enclosure has been modified, for this step, with three apertures: one for the applicators (antennas) at the top, two for the forced-air flux on the lateral sides, and a last one for the viewing window in the door (front).

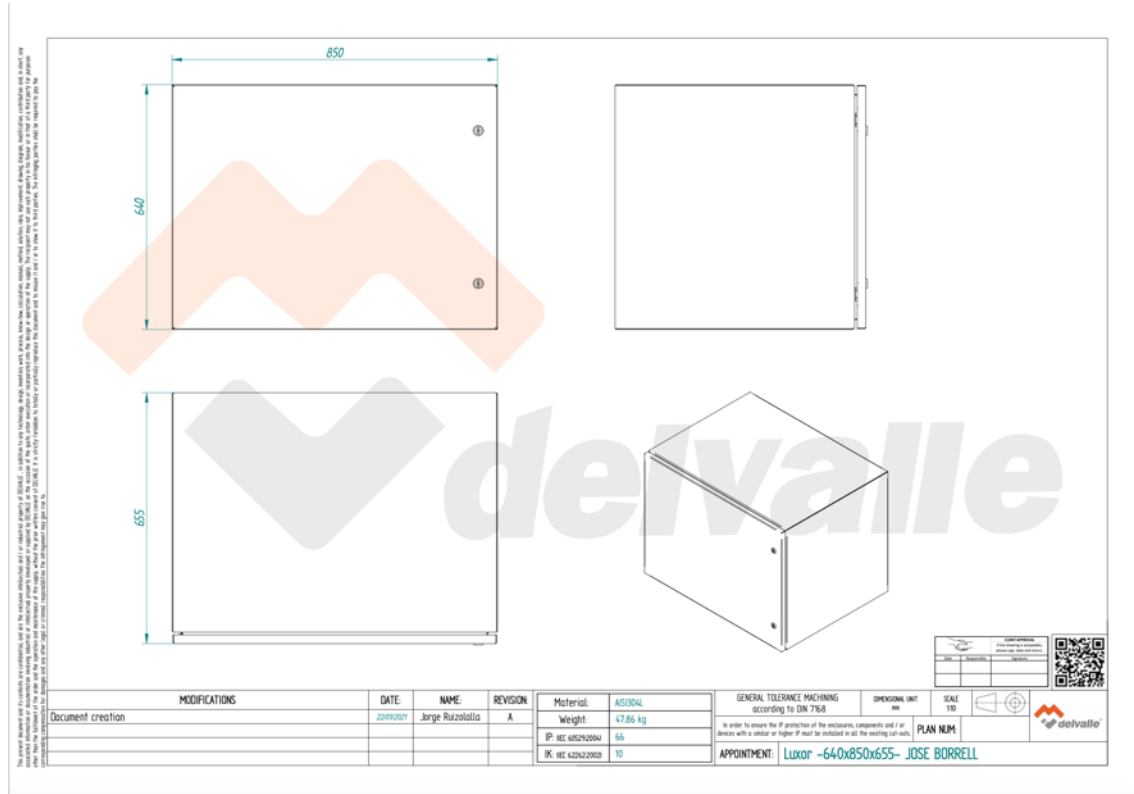


Fig 8.34. Drawings of the metallic enclosure ordered to DelValle. Luxor model.

First, a rectangular aperture covering most of the top face has been done to test different antenna configurations. Fig 8.36 shows the drawing of the metallic sheet prepared to cover the aperture with the four antennas configuration. It also shows the gasket (in blue) used to ensure good contact between both metallic surfaces and keep the proper electromagnetic shielding. The antenna configurations chosen, all of them compatible with the aperture and with an easy screws replacement method, are one antenna (centred), two antennas separated in the length direction, two antennas separated in the width direction, two antennas in diagonal and four antennas.

Second, two apertures are placed on the left and right faces. These wholes are filled with EMI compatible honeycomb shielding. These honeycomb windows need to be compatible with standard fan dimensions. The selected fan is the model HC-25-2T/H 230/400V [172] from SODECA (Gerona, ES). To protect this fan, the honeycomb shielding chosen is 9500-300-300-A-DS-A [173] with a single layer of 25,3 mm thickness from the Dutch company HOLLAND SHIELDING (Dordrecht, NL). Fig 8.35 shows that the honeycomb with the mentioned thickness offers approx. 106 dB attenuation at 916 MHz.

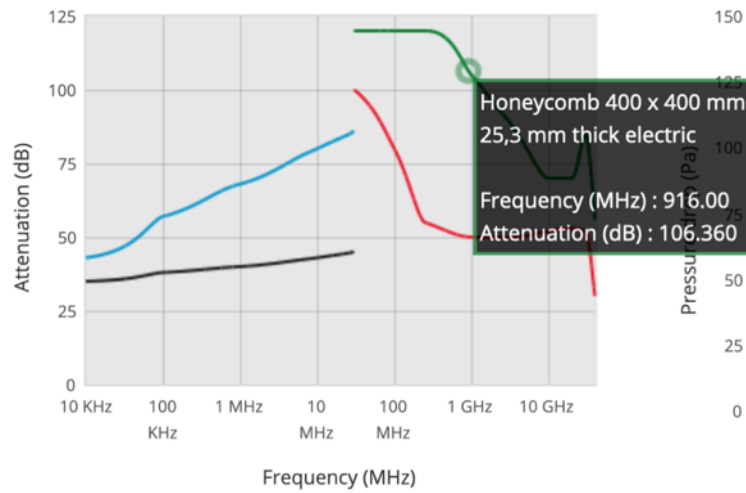


Fig 8.35. Frequency-dependent shielding behaviour of the selected honeycomb [173].

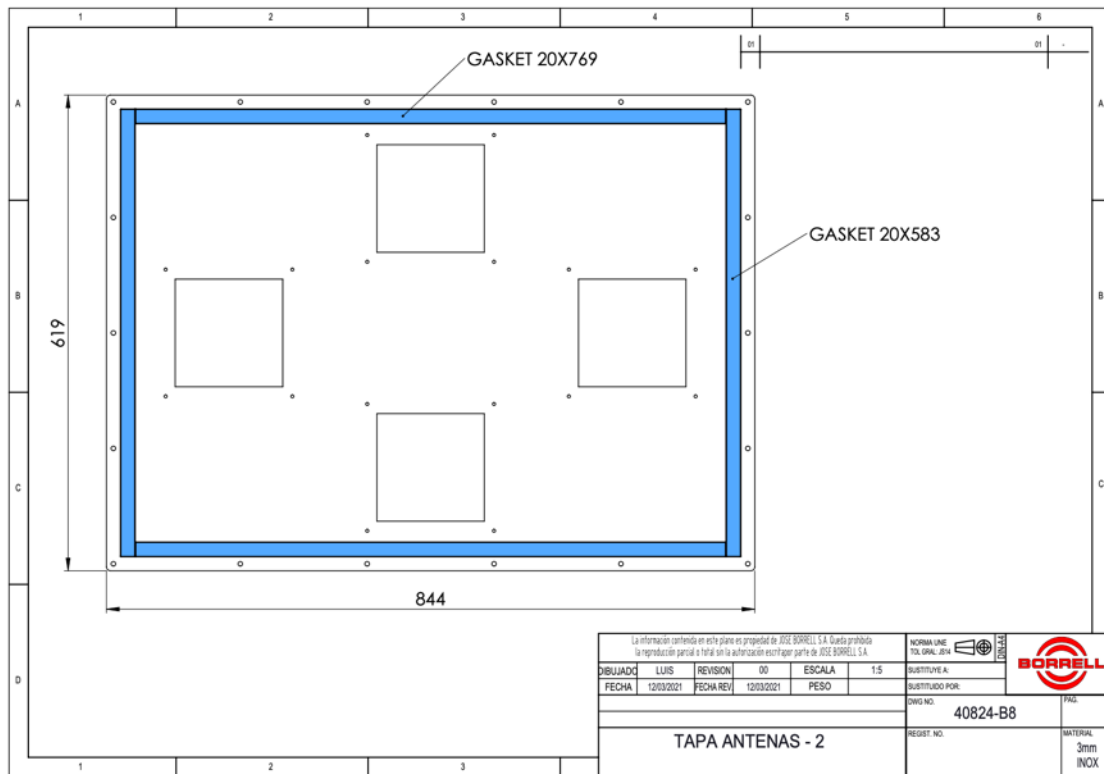


Fig 8.36. Drawing of the metallic sheet, compatible with the top oven aperture, with the four antennas configuration.

Third, a big aperture in the front face, i.e., the door, sets an EMI viewing window. The solution offered by DelValle for a viewing window is not valid because it has no microwave protection. The solution is to buy it from a specialised microwave shielding company. The model used is a *Mesh foil window* [174] with part number: 9700-300-400-G-1-3.35-SB-30 from HOLLAND SHIELDING (Dordrecht, NL). It is composed of 3 mm glass plus 0.35 mm foil.

The dimensions of the shielding window and the assembly to integrate onto the oven door are shown in Fig 8.37. The dimensions and location of every element to incorporate the window in the door are shown in Fig 8.38.

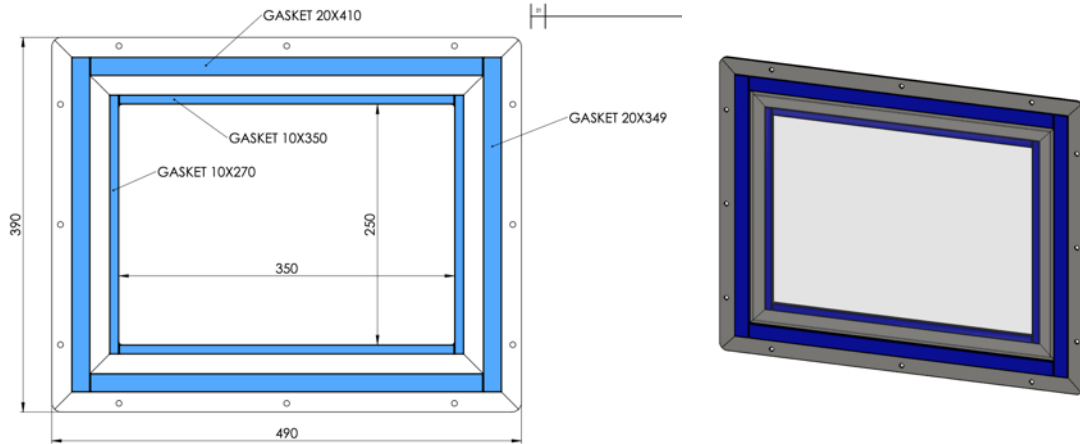


Fig 8.37. EMC viewing window and gasket dimensions drawing (left) and the 3D model (right).

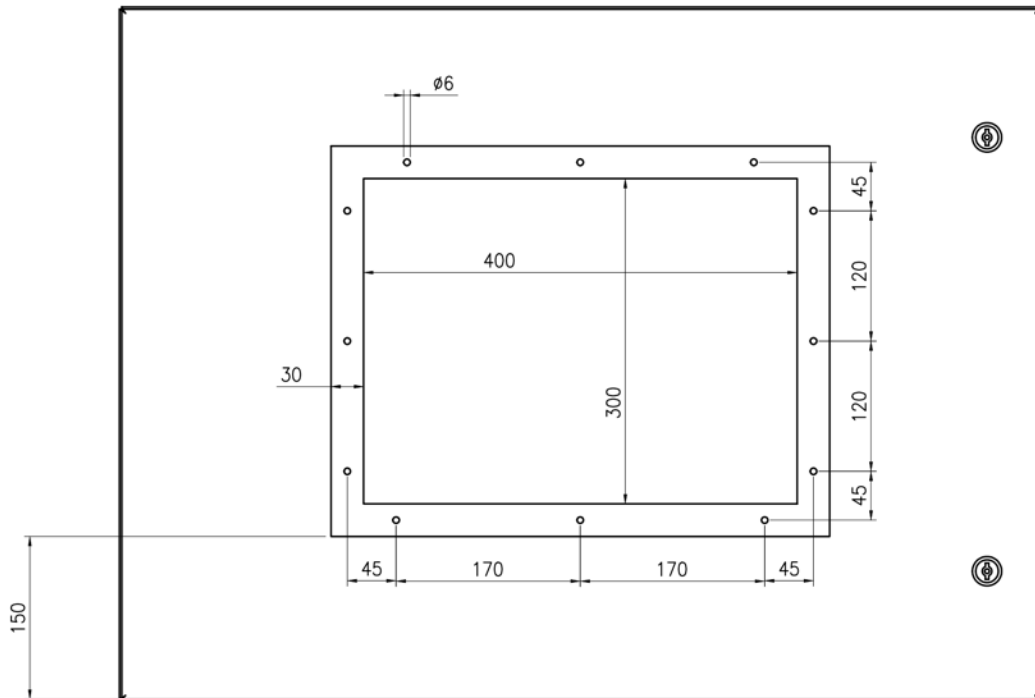


Fig 8.38. Drawing of the window location in the oven door.

Finally, the oven has been installed on a test bench with all the needed elements, as shown in Fig 8.39 and Fig 8.40.

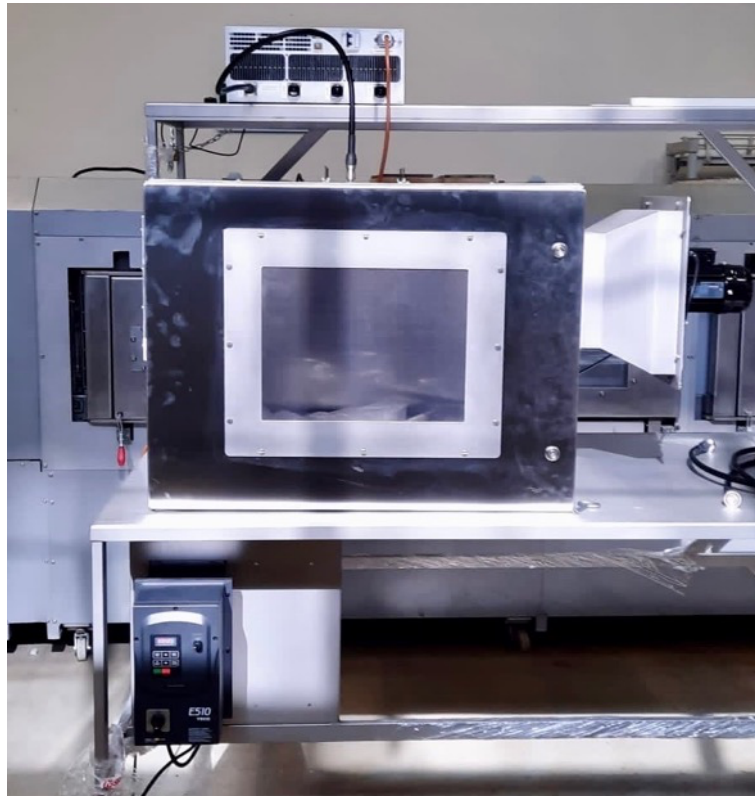


Fig 8.39. Front view of the static oven with the fan on the right and the fan controller at the bottom.

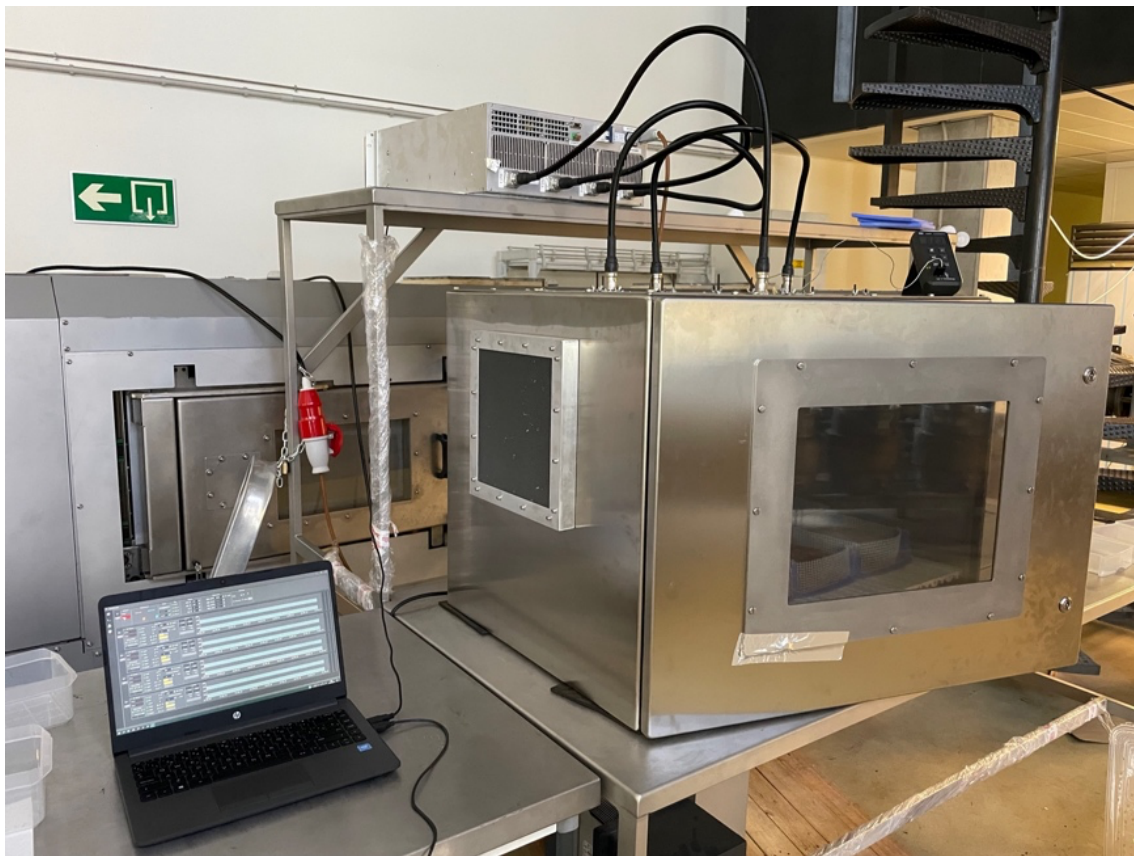


Fig 8.40. Isometric view of the static oven in the testbench with the computer for the control.

8.2.4.3 Continuous or transport oven design

Converting the static oven into a continuous one involves adding two apertures on the lateral faces below the forced-air grilles in Fig 8.40. These two apertures are the input and output accesses of the load, which is carried by a conveyor belt. While the variables in the static oven were the microwave power and phase-shifting and the air rapidity, in the continuous one, the velocity of the conveyor belt is added to them.

One of the elements to be designed is the belt supports. A solution would be using rotating bars, although the different elements that need to be used to keep microwave leakage are pretty complex, as shown in Fig 8.41. A more straightforward solution is to use Teflon sheets below the belt; given its low friction coefficient, the belt displacement is smooth and stable.

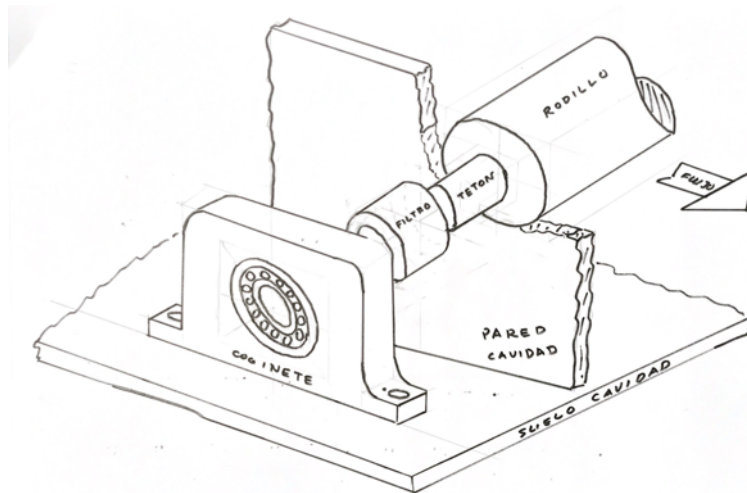


Fig 8.41. Schematic of the rolling bar with electromagnetic shielding elements.

The most challenging aspect is the microwave shielding of the accesses. Section 5.3. EMC protection elements for in-line industrial ovens., describes the complete development of the approach for keeping microwaves inside the oven based on periodic metallic structures and highly susceptor materials. The result of this study is shown in Fig 8.42.



Fig 8.42. Shielding periodic structure installed in the transport oven.

Two more elements have been used to ensure the perfect shielding of this PoC: a metallic comb-over to avoid the direct ray (Fig 8.43) and a metallic grid at the end of each access (Fig 8.44). This last impedes the expected displacement of the belt but can be solved by using feed hoppers.



Fig 8.43. Internal view of the transport oven with the almond load and the patch Peek antennas installed on top.



Fig 8.44. Rectangular grid structure that will work as a feed hopper and a shielding element.

The final view of the oven can be seen in Fig 8.45.



Fig 8.45. External view of the transport oven with the accesses.

8.2.5. Results

Different measures and heating tests have been carried out to close the design and manufacture of the solid-state microwave PoC for industrial almond drying. The almond has been prepared to be heated the most efficient way possible, different configurations have been checked, and the outcome is a system capable of improving the drying timings.

It has also defined the start-up procedure for the operation of the SSMGS.

8.2.5.1 Load location and test preparation.

The first tests carried out with the static oven have been centred on the height adjustment and thickness of the sample. A conveyor belt sample has been used as the surface to put the load on. It has been possible to check the behaviour of the load and the microwaves for different heights from the bottom using Teflon cylinders and bars like the example in Fig 8.46 (right). The range of heights has been from 15 mm to 200 mm.

For these first adjustment tests, a small load quantity has been used. The 4 kg almonds, with humidity values around 5-6%, are scattered through the surface, making it a thin layer (see Fig 8.46). This load makes it possible to study the final drying conditions and see if the first response to the microwave is adequate. After these tests, the sample's height or location (distance from the

belt's top surface to the cavity bottom) is set to 100 mm. This value is later used to design the accesses for the continuous oven.



Fig 8.46. Initial load distribution (left) and detail of the elements used to adjust the height of the belt (right).

For the heating tests, where higher power values than in the preliminary are used, the load used is set into regular plastic trays (see Fig 8.47). This method allows measuring each fragment of the total load in temperature and weight loss. The total sum of trays used is 16, making it possible to have two load thicknesses: 40 mm and 80 mm. Each tray can fit from 700 to 800 g (see Fig 8.48), making the total load (when every tray is used) between 12.5 and 14.5 kg.



Fig 8.47. Almond distribution with regular compartments for 40 mm (left) and 80 mm (right) thickness.



Fig 8.48. Sample weight measurement.

These trays are changed by hand-made HDPE (high-density polyethylene) mesh baskets to improve the results of the heating tests. The mesh permits a more active airflow, and the heat transfer is not constrained by the plastic walls (see Fig 8.49).

The temperature measurement procedure consisted of thermographic recording, with an Optris IR camera, of the maximum and minimum temperature areas. Another method used to measure the heating speed and homogeneity is weighting the baskets. That way, it is possible to see the mass loss difference between the different parts of the load.



Fig 8.49. Meshed baskets distribution of the load.

8.2.5.2 Microwave generation system adjustments.

Microwave systems like microwave heating ovens present the so-called characteristic impedance. This impedance is mainly given by the oven dimensions, the different materials used, and the shapes of every element inside it. As mentioned earlier in the document, the main of an antenna is to match the generation system impedance to the applicator and its load.

The impedance that “see” the antennas is different each time that the load is changed, e.g., variation in the amount of load (weight) or relocation in the oven or even if the thermophysical properties are different (mainly temperature and water content).

The starting up procedure each time the load changes comprises the following steps:

- 1) The frequency synchronisation must be enabled, i.e., the four sources operate coherently with the same frequency.
- 2) After checking that every door or protective element is closed and the oven loaded, a low power matching procedure is conducted by changing the frequency between the frequency band, in this case, 902.5 and 927.5 MHz. This procedure is done with only one source at a time. The nominal power has to be between 10 and 20 W, depending on the system's sensitivity to detect the changes in the frequency. The objective of this step is to find a frequency with:
 - a) Return losses lower than 5%.
 - b) Overall coupling with the other sources is lower than 5%.

- 3) Once the best frequency (or frequency range) is defined, another source-by-source tuning must be made with low powers. In this case, the phase of each source is set to reduce both the return losses and the coupling. This step can be used to improve step 2) or fulfil it if the frequency as a tuning parameter has not been enough.
- 4) For each source, the range of the phase producing the best matching is stored to be used in phase-shifting mode.
- 5) The last step is to verify with high power (over 100 W per source) the outcome of the previous actions.

8.2.5.3 Almond heating results with the static oven.

Heating tests in the static oven have been performed once the load has been defined and prepared. These tests include different antenna configurations, the position (height from the bottom) set to the optimum, and the configuration system protocol to work with that load defined.

These tests include different antenna configurations: a single antenna (Fig 8.50), two antennas with different alignments (Fig 8.51 and Fig 8.52) and the final four antennas configuration (Fig 8.54).

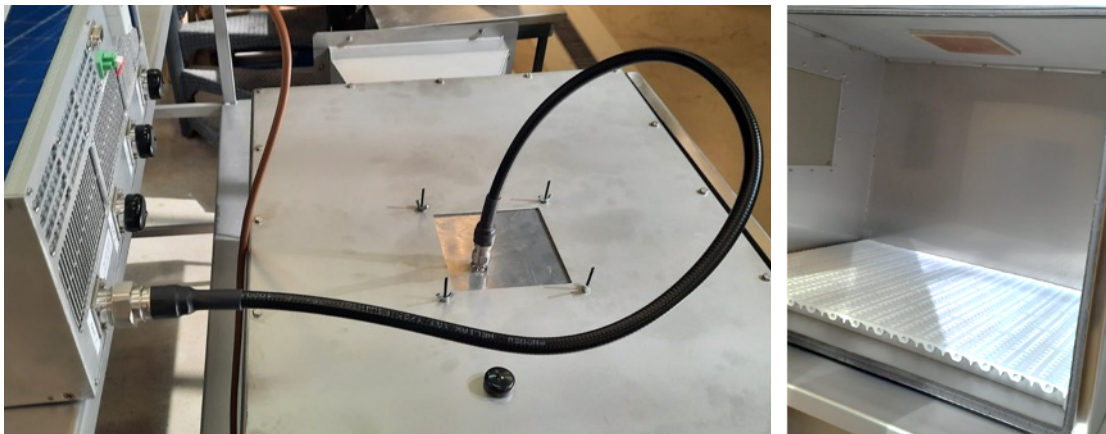


Fig 8.50. Single antenna configuration. Top view (left) and inside view (right).

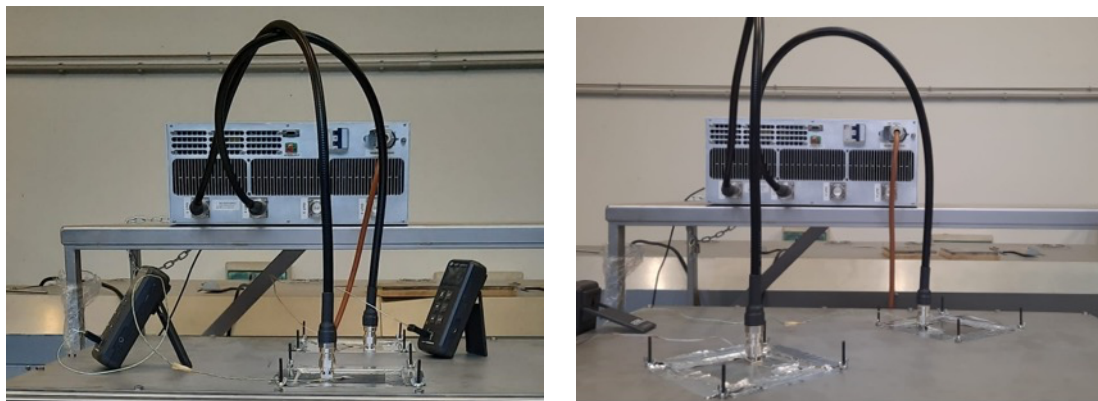


Fig 8.51. Two antennas configuration: vertical alignment (left) and diagonal alignment (right)

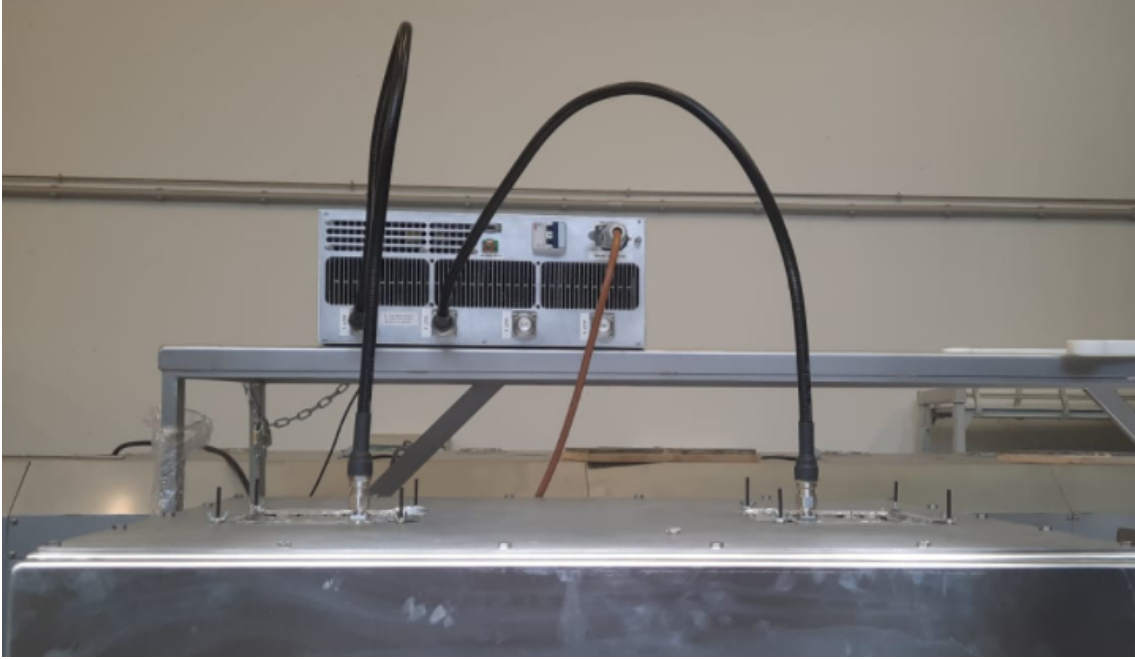


Fig 8.52. Two antennas configuration: horizontal alignment.

The first experiments, centred on the two antennas configuration, showed promising results. Fig 8.53 shows the effect of the phase change of one of the antennas (the right one in Fig 8.52) over the heating pattern. It can be seen differences of 2° C on average between cold and hot spots. These tests also showed (given the temperature differences) that the amount of load compared to the power available is limited. Thus, the most devoted work has been centred on the four antennas configuration.

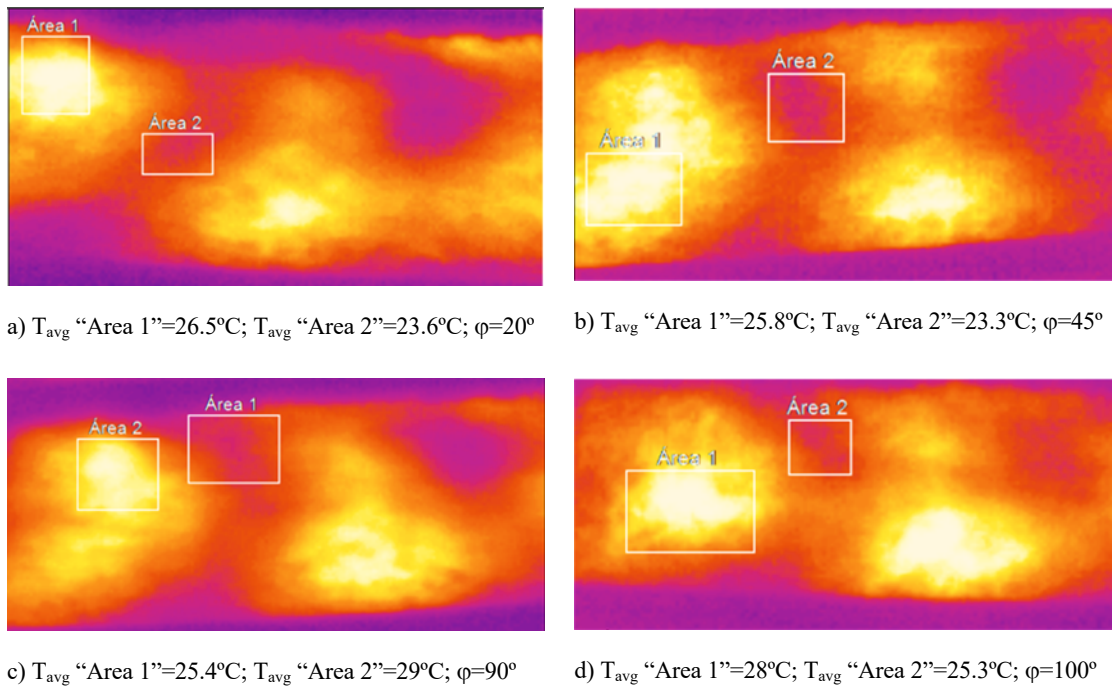


Fig 8.53. Example of the maximum and minimum temperature spots after the phase-shifting (φ) with two antennas separated horizontally.



Fig 8.54. Four antennas configuration.

First, the scattering matrix has been measured with the FoxField N9917A vector network analyser (VNA) from Keysight Technologies with the load inside the cavity. Given the system's symmetry, the scattering parameters can be simplified as (8.7). The principal diagonal contains each antenna/source's return losses, and the other parameters indicate the coupling between the antennas. This action is not necessary to be repeated each time but is done to confirm the antenna's good design and location inside the cavity.

$$S = \begin{bmatrix} S_{11} & S_{21} & S_{31} & S_{41} \\ & S_{22} & S_{32} & S_{42} \\ & & S_{33} & S_{43} \\ & & & S_{44} \end{bmatrix} \quad (8.7)$$

After performing the calibration procedure explained above, the measurement of the scattering parameters is done with the following results (8.8). The values show the excellent antennas' matching to the load and cavity (all < -10 dB), and their low coupling.

$$S(dB) = \begin{bmatrix} -11.8 & -19.4 & -20.6 & -14 \\ & -17.1 & -11.3 & -27.4 \\ & & -11.7 & -25 \\ & & & -14 \end{bmatrix} \quad (8.8)$$

Fig 8.55 shows heating with four sources with 200 W each for 10 min. The phase change has been done between the phase range defined according to step 4) of the starting up procedure. The heating pattern observed is very homogeneous (especially on the upper layer), with only 2° C of difference between the maximum (30° C) and minimum (28° C) values. The lower layer presents a more significant difference, 32° C against 27° C. These results indicate the overall load thickness adequacy for the industrial process, despite the differences in some bottom parts of the load.

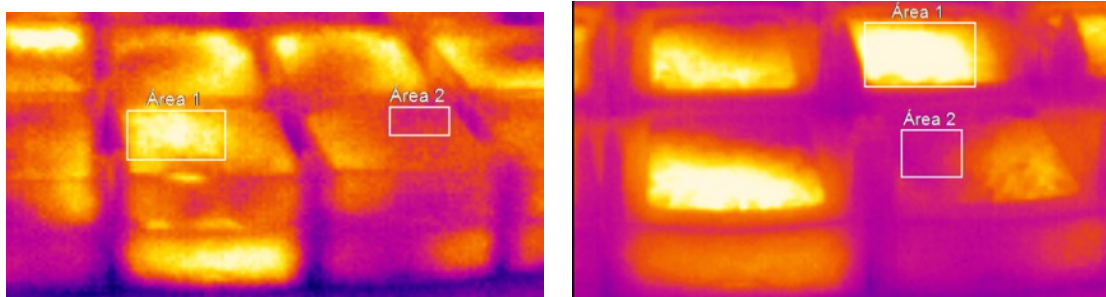


Fig 8.55. Thermal images of different parts of the load show homogeneity with four sources and 80 mm of thickness.

In the end, a single load layer (40 mm) is used for the drying tests. It permits a clearer view of the microwave capacity to improve the industrial drying process.

8.2.5.4 Drying tests.

The drying tests have been carried out with cycles of 200 W and 300 W per module. The cycles are 20 and 30 minutes with the first power, while the cycles used are 10 minutes for the second power. At the end of each cycle, the different trays are weighed to note the water loss, being the direct way to measure the drying of the almond.

The sample used for these tests is around 8000 g with 10% humidity, implying a 0.1 W/g power mass ratio, which is lower than the ideal. However, the results are satisfactory: the mass loss obtained is approximately three times that of forced hot air drying.

8.2.5.5 Results of the continuous oven.

The continuous oven manufacture has been finalised with the inclusion of the conveyor belt and its electromechanical system (see Fig 8.56 and more details in Fig 8.57 Fig 8.59). The oven has been tested with manual control of the electromagnetic system. However, the company José Borrell S.A. pointed out the need for automatism, even in the first stage. This improvement is commented on in detail in Chapter 9.



Fig 8.56. Frontal view of the definitive continuous oven with the four sources SSMGS.

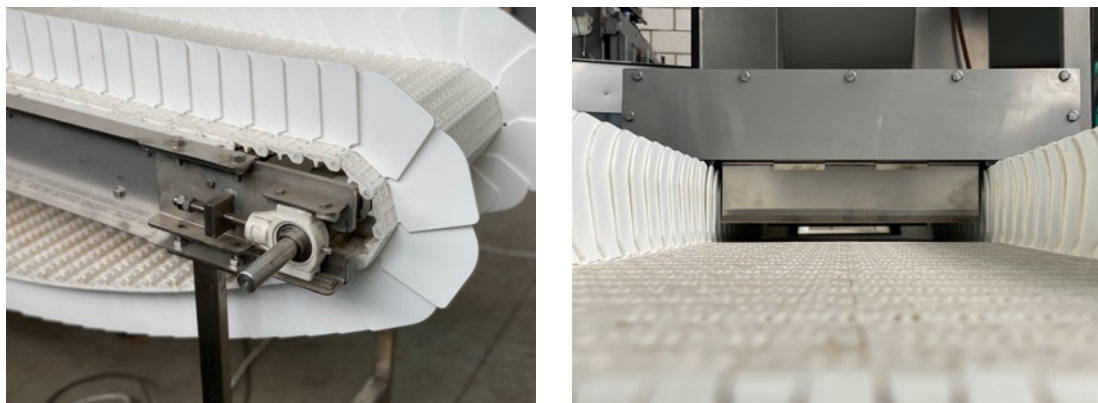


Fig 8.57. Detail of the extensor for the conveyor belt (left) and of the reduced free aperture (right).



Fig 8.58. Conveyor belt with modular lateral supports to confine the load.

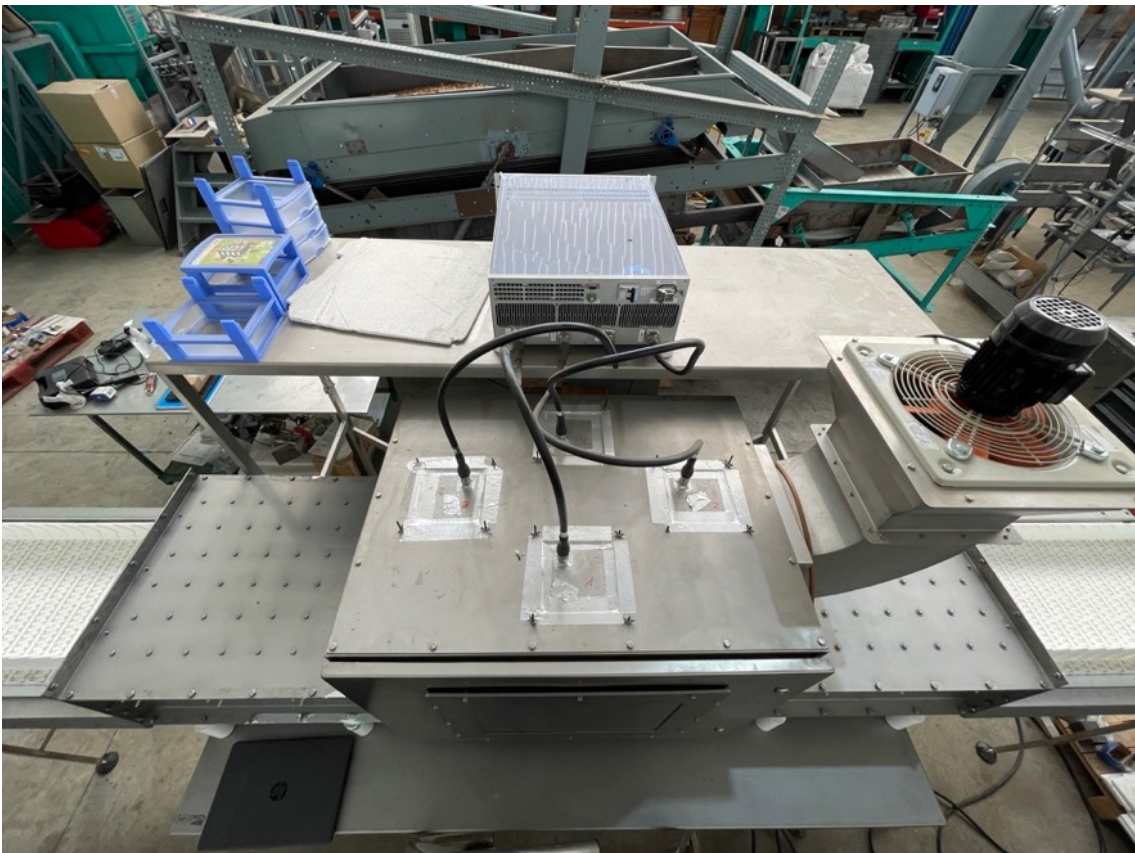


Fig 8.59. Top view of the definitive transport oven.

8.3. Conclusions.

This chapter has shown all the extensive work devoted to designing, manufacturing and validating a conveyorised microwave oven based on S2MH. It has been built around a 2 kW SSMGS at 915 MHz.

The feeding structures used in this multi-illumination system are patch antennas with PEEK as the dielectric. It presents a novelty due to the lack of use of this material in previous designs. The antennas' return losses values show adequate levels (lower than 10%) in the operating frequency band, and the coupling between them has been minimised.

It has been proved that the antennas' phase change can modify the heating pattern. Specifically, it has been seen that pairing the antennas two by two produces the same effect and reduces the number of variables to work with. To improve final heating results, e.g., borders, first and last product in the oven, more experimental tests will be necessary.

The carried out experiments have shown that the frequency used and the cavity design are optimum to heat an 8 cm thick load. Future experiments might focus on including structures that foster the heating of the product immediately above the conveyor belt.

Finally, the different shielding elements, either purchased or designed and manufactured, have proved effective for the power levels used in the oven.

Part IV

Conclusions

Chapter 9. Results discussions and future work

The last part of the PhD thesis aims to give a general summary of the work's results with the relevant discussion. The multi-frequency systems are explained, with the main challenges that it represents. It also includes the aspects pointed out as the next steps needed for the complete development of the proposed technology, with particular attention to the management of these systems related to artificial intelligence (AI), such as machine learning.

9.1. Summary and comments

The results obtained during these four years as an Industrial PhD candidate can be easily divided into microwave generation systems based on solid-state technology, antennas and industrial applications. These three aspects have been explained in detail in the third part of the document.

The so-called Solid-State Microwave Generator System (SSMGS) has been thoroughly designed to match all the applications the system is capable of working on. It has been described in detail from general subsystems to specific components providing enough freedom to decide whether to build it from scratch or integrate the different subsystems. That decision should be made considering the company selling volume and the electronic integration capability.

The result of this PhD thesis has also been the research and discovery of an affordable market-ready microwave generator solid-state-based with compatible properties for the SSMGS. It is the StarterKit from Leanfa Srl. (Bari, IT), and can be ordered ad-hoc.

A high work volume has been devoted to the applicators' design. Different antennas have been studied, designed and manufactured for the three main ISM frequencies (433, 915 and 2,450 MHz). All these antennas have in common their TEM structure, their high-power coaxial connectors feeding systems and their integration-oriented design for microwave heating cavities.

The summary of the antennas designed, their main features and the attainments achieved can be seen in Table 9.1. It is important to point out that monopole antennas provide better return losses (RL) figures than patch antennas. However, the directivity of these two antennas is different. This

property is directly related to the coupling effect of the antennas when installed in a multi-source system. A master's thesis mentored by the author studies this effect thoroughly [175].

The applicator designs also include optimising the cavity dimensions for each application and the correct location of the antennas to improve the power delivery and reduce the antenna coupling.

Table 9.1. Designed antennas summary.

Name	Frequency	Type	Features	Application
Simple wire antennas	2450 MHz	Monopole	RL < 1% N connector	Multi-purpose multi-source oven for chemical synthesis (UV)
Tunable antennas	2450 MHz	Monopole	RL < 1% N and 7/16" connector	Not used yet
	915 MHz			Multi-source almond drying system (J. Borrell S.A.)
	433 MHz			Future research and publications work (Microbiotech and ITACA)
Slotted SIW antenna	2450 MHz	Slotted stripline	RL < 10% N connector Complex design and assembly	Paper on a Q2 scientific journal (Electronics, MDPI)
Peek antenna	915 MHz	Patch	RL < 10% N connector Space reduction and increased temperature resistance PEEK substrate	Multi-source almond drying system (J. Borrell S.A.)
Teflon patch antenna	2450 MHz	Patch	RL < 10% N connector Teflon substrate	Single-source chemical lab oven (UV)

	915 MHz	Patch	RL < 10% N connector Teflon substrate	Discarded (Peek antenna used)
Two-freq. patch antenna	2450 or 915 MHz	Patch	RL \approx 10% Single N connector Teflon substrate	Discarded for its size and the challenges with multi-frequency system development
PIFA antenna	433 MHz	PIFA	RL \approx 1% N connector	Future research and publications work (Microbiotech and ITACA)

Two final applications have been boosted with the implementation of the technology proposed in this PhD dissertation.

From the lab environment, the University of Valencia has validated the research application oven developed and designed for multi-purpose chemical processes. It has been designed and manufactured using a 1 kW, four output, solid-state microwave generation system. The monopole antennas provide a final efficiency bigger than 80%, and the frequency, phase and power control permit the improvement required and sought while designing the system.

They use this system with improved control and heating precision to obtain new materials, speeding up the current synthesis, calcination and functionalisation processes. This new material is called UVM7 and is under patent consideration.

On the other hand, José Borrell S.A. is considering fully exploiting the industrial conveyor oven based on S2MH. The prototype is under further and more specific validation. Specifically, the Modbus control is being updated and adapted to the company protocols and security aspects. Once it is completed, drying tests under different air-flow conditions and heating patterns will be carried out. This process also includes the creation of control algorithms and the development of an intelligent managing system. These aspects are further explained in the next section.

9.2. Multi-frequency and AI.

Hybrid devices are very extended in the food treatment sector: resistors combined with forced-air furnaces, microwave ovens with grill functions based on resistors, resistor heaters with steam generation cooking industrial ovens, etc. The work devoted to improving heating processes with the aid of multi-source solid-state-based microwave systems includes the possibility of combining two or more frequencies at the same time.

Materials susceptible to being heated by microwaves have different dielectric properties, which define that relation. For a given size and shape, the dielectric properties of a material change with the frequency and the temperature. Moreover, this change can be similar, i.e., the increasing and decreasing rates of the dielectric constant with the temperature are identical at 915 MHz and 2.45 GHz; or completely different.

Frequency mixing in a microwave oven is an interesting solution to select intelligently, for instance, which frequency needs to be used to defrost a meat sample; to cope with the abrupt dielectric constant behaviour around the change in state from frozen to liquid water in a soup; or to achieve specific food surface finishing, among other applications.

The first idea of this thesis project was to work with a multi-frequency single system. However, the thesis development led to not implementing it. The three principal challenges encountered are the mechanical complexity, the lack of multi-frequency modelling capability with the commercial software, and the exponential growth of control variables.

9.2.1. Mechanical implications

The most used microwave device's shielding mechanism is the wave trap, also called choke. Chokes are very useful in applications like the domestic microwave oven that requires constant mechanical movement. This kind of shielding has a better lifespan, assuring the proper security normative.

When combining two or more frequencies, these shielding mechanisms need to be replicated, one per frequency. It introduces another complexity level in the design of the oven, not only with the door but also with the different apertures needed.

Enclosures with mechanical contact are used as a solution and must be designed for all the critical elements: doors, fan shieldings, conveyor belt apertures, etc. It is, therefore, clear that batch or static ovens present fewer problems than continuous ovens when various frequencies are used simultaneously (or at least in the same oven).

Fig 9.1 shows a multi-view drawing of a high-quality door for electromagnetic compatibility (EMC) from the microwave specialised Microwave Vision Group (MVG, IT). It can be seen the highly technical features that the door includes ensuring the perfect contact on all the surfaces.

Regarding the continuous ovens, periodic structures like the described and designed for the drying almond system are designed for a single frequency. The 2,450 MHz frequency won't be attenuated, and the dimensions required for this frequency will oblige to drastically reduce the amount of almonds (thickness) to have a continuous process.

A solution for this issue can be found by working with a metallic sluice system. Despite its refusal from some industrial manufacturers, the product has to be loaded in independent trays to allow a correct slice closing. This system forces to have several resonant cavities inside the oven.

Finally, given the separation between the ISM bands, there aren't antennas capable of performing adequately in such a wideband range. Integration of different antennas is needed in the same oven. A solution was proposed by designing a multi-frequency antenna (see subsection 6.4.3.4) to

connect the microwave generator needed each time (different frequency) without replacing the antenna.

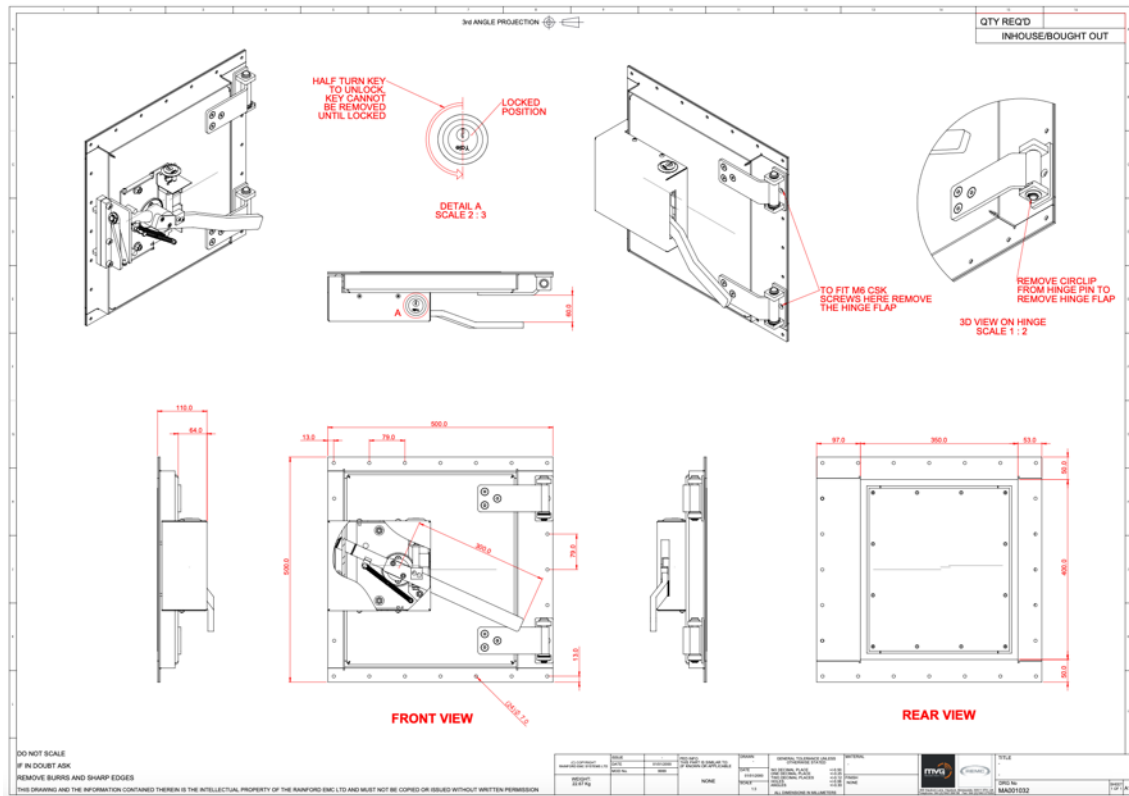


Fig 9.1. High-quality EMC shielding door from MVG.

9.2.2. Modelling implications

Among the first actions carried out during the design of microwave devices, one of the most important is proper electromagnetic modelling. Then, multiphysics modelling helps to understand the interaction between the designed electromagnetic equipment and the heated material with time.

The two main FEM electromagnetic modelling tools are HFSS and CST. Neither of these allows assigning a different frequency in the wave ports. Comsol Multiphysics has been used for the multiphysics modelling and presents the same problem: multi-frequency is not an integrated feature.

Matlab can be used to cope with this issue. It is necessary to collect the electromagnetic fields created by each frequency, combine them outside the modelling tool, apply the electromagnetic equations inside the load, and obtain the generated energy. This process has to be done for both frequency ranges with enough resolution to control the changes with the frequency. Moreover, all the equations need to be recalculated for each phase change. It is possible to understand the extraordinary complexity this involves when multiphysics studies are carried out.

9.2.3. Managing implications

Last but not least, multi-frequency systems mean an escalation in the managing variables. For instance, with the two SSMGS used in the previous applications, the possible controlling combinations (without considering the sensing variables) can add up to two hundred thousand billion (200.000×10^9). Table 9.2 shows the different parameters involved in understanding the mentioned figure.

Therefore, it is mandatory to use algorithms, databases, and machine learning technology to take the entire profit of a system like it.

Table 9.2. Example of the possible input combinations of a 2-frequencies microwave system.

Leanfa STARTERKIT configuration		
Frequency band	915 MHz	2450 MHz
Available frequency range	902.5 MHz – 927.5 MHz	2420 MHz – 2480 MHz
Frequency step	0.5 MHz	2 MHz
Max. power / module	500 W	250 W
Power step	1 W	1 W
Phase step	1.4°	1.4°
Number of possible combinations		
Frequency	50	30
Modules	4	4
Power	500	250
Phase	257	257
Total	25.7e6	7.71e6
Aggregate	198.147e12	

9.2.3.1 Artificial Intelligence (AI) techniques

“Artificial Intelligence (AI) is that activity devoted to making machines intelligent, and intelligence is that quality that enables an entity to function appropriately and with foresight in its environment” [176]. Intelligence often follows a process that a computer system can mimic as part of a simulation:

- a) Set a goal.
- b) Assess the currently known parameters information.
- c) Gather additional information.
- d) Manipulate the data to achieve consistent form with the current information.
- e) Define relationships and truth values between existing and new information.
- f) Determine whether the goal is achieved.
- g) Update the goal in light of the new data and its effect on the success probability.
- h) Repeat steps b) to g).

Even though algorithms can be created and access to data is provided in support of this process within a computer, a computer’s capability to achieve intelligence is severely limited [177]. There are two types of AI: strong and weak. The first is considered a generalized intelligence that can adapt to various situations, and the second is a specific intelligence designed to perform a particular task well. Moreover, a second classification can be made:

- Reactive machines: A reactive machine has no memory or experience upon which to base a decision. Instead, it relies on pure computational power and smart algorithms to recreate every decision every time. This is an example of a weak AI used for a specific purpose, e.g., a chess computer game.
- Limited memory: These machines rely on a small amount of memory to provide experiential knowledge of various situations. When the machine sees the same situation, it can rely on experience to reduce reaction time and provide more resources for making new decisions that haven’t yet been made. This is an example of the current level of strong AI, e.g., a self-driving car or autonomous robots.
- Theory of mind: A machine that can assess both its required goals and the potential goals of other entities in the same environment has a kind of understanding that is feasible to some extent today but not in any commercial form. It is the technology needed in the future truly autonomous cars.
- Self-awareness: The AI of the movies require technologies that aren’t even remotely possible now because such a machine would have a sense of both self and consciousness. In addition, instead of merely intuiting the goals of others based on environment and other entity reactions, this type of machine would be able to infer the intent of others based on experiential knowledge.

The proposed SSMGS are currently ready to be controlled with a weak AI like the defined as reactive machines. This technology is based on algorithms and data, which is very extensive in the system (see Fig 9.2) but need to be appropriately collected, prepared and organised.

However, the ideal heating machine based on the SSMGS needs to be developed with a superior AI with limited memory. The correct decision at the precise moment is the key to the microwave heating improvement the proposed system can provide.

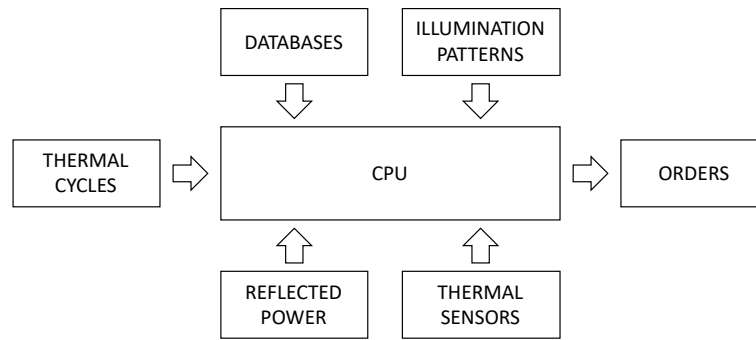


Fig 9.2. Input and outputs of the control system.

9.3. Future work

Microbiotech S.L. and the Institute of Information and Communication Technologies (ITACA) of the Polytechnic University of Valencia have been the principal support for this PhD thesis. The results obtained from it, have opened the possibility to achieve the development of a more definitive smart microwave heating system.

To cope with the challenges presented early in the chapter, it is necessary to add an important processing part to the system. Being able to manage the information provided by the transmitted and reflected power, the thermal images and temperature sensors arrays data; is the first step of a smart control of the microwave heating patterns.

These two groups have created a consortium with a third partner, SWAT ID, to deepen in the data managing for an improved SSMGS. The work proposed is to relate the available data, provided from the systems developed and presented in this PhD dissertation, with changes in the food dielectric properties, change of state, humidity reduction, structural changes like meat protein's coagulation, butter or chocolate fusion, etc.

The outcome of this future research would be an improved version of the SSMGS, with better control, reliable communication protocols and integration of automatised protocols (see Fig 9.3).

The S2MH systems will be benefited from this improvement, but also further work in the applicator design can help it. Among the possible updates, the tunable monopole antennas have relevant implication.

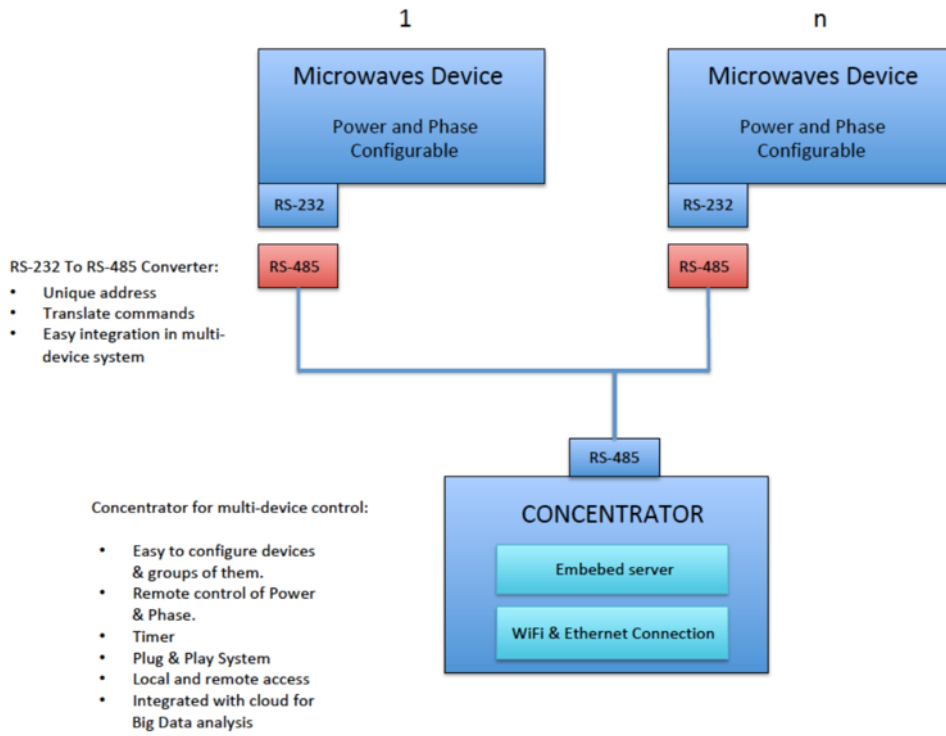


Fig 9.3. Diagram block of the improved SSMGS.

Chapter 10. Final conclusions

This last chapter summarises this PhD dissertation with some final and general conclusions. The devices and subsystems identified in the market and those specifically designed and manufactured to foster the advantages of S2MH have proven successful in improving heating applications, making them more versatile. The main conclusions drawn by this PhD thesis are:

1. A multi-source coherent microwave generator system has been designed based on solid-state technology, the SSMGS. Working side by side with a solid-state power amplifier company, we have guided the manufacture of a device, the StarterKit, and used it in two completely different applications. The main feature of this SSMGS is the capability to digitally control the frequency, power and phase of the four amplifying modules.
2. The use of specific TEM feeding structures, like monopole and patch antennas, allows space reduction and multi-illumination. With this feature, electronic control over the heating pattern is feasible. Challenges with the patch's dielectric have been found, leaving the door open to further research on new substrates for this purpose.
3. It has also been proved that an intelligent selection of the frequency for each application is necessary, considering different requirements such as the load volume, thickness, and dielectric properties.
4. The original idea of introducing multiple frequencies in a single applicator seems interesting for subtle effects over the load, such as defrosting control or food browning. Nonetheless, the shielding mechanical implications and the reduced modelling possibilities led us to postpone its implementation. We have applied for funding for a new research project on this aspect.
5. Implementing RADAR techniques for heating purposes is a good approach. However, it is not a direct application due to the effect of the cavity. Plane-wave and wavefront concepts cannot be used in heating applications, first for the relatively small size of the applicator cavity (related to the wavelength) and second for the multiple reflections on the metallic walls. Therefore, it is essential to work carefully on the cavity design too.

6. Including AI techniques would extend the process design's improvement, managing materials properties databases and controlling a system with many variables. It is necessary specific knowledge in this field to afford its application.

Bibliography

- [1] R. F. Schiffmann, "Microwave Processes for the Food Industry," in *Handbook of Microwave Technology for Food Applications*, A. K. Datta and R. C. Anantheswaran, Eds. Marcel Dekker, Inc., 2001, pp. 299–338.
- [2] G. W. Stimson, *Introduction to Airborne Radar*, Third. SciTech Publishing, 2014. doi: 10.1049/sbra101e.
- [3] M. I. Skolnik, *Introduction to Radar Systems*, Second Edi. McGraw-Hill, Inc, 1988. doi: 10.1017/CBO9780511608117.001.
- [4] J. C. Maxwell, *A Dynamical Theory of the Electromagnetic Field*. Eugene, Oregon: Wipf and Stock Publishers, 1996.
- [5] C. A. Balanis, *Advanced Engineering Electromagnetics*. J. Wiley & Sons, 2012.
- [6] S. O. Nelson, *Dielectric Properties of Agricultural Materials and Their Applications*. 2015. doi: 10.1016/C2014-0-02694-9.
- [7] A. R. Von Hippel, *Dielectrics and Waves*. Artech House Inc., 1995.
- [8] A. C. Metaxas and R. J. Meredith, *Industrial microwave heating*. London: Institution of Electrical Engineers, 1983. [Online]. Available: <https://trove.nla.gov.au/work/13331450?q&versionId=25335578>
- [9] S. Ryyänen, "The electromagnetic properties of food materials: A review of the basic principles," *J. Food Eng.*, vol. 26, no. 4, pp. 409–429, 1995, doi: 10.1016/0260-8774(94)00063-F.
- [10] P. H. Fang, "Cole—Cole Diagram and the Distribution of Relaxation Times," *J. Chem. Phys.*, vol. 42, no. 10, pp. 3411–3413, May 1965, doi: 10.1063/1.1695743.
- [11] L. F. Chen, C.K.Ong, C.P.Neo, V. V Varadan, and V. K. Varadan, *Microwave Electronics Measurement and Materials Characterisation*. John Wiley & Sons, 2004. doi: 10.1002/0470020466.
- [12] "Silver," *Wikipedia.org*. <https://en.wikipedia.org/wiki/Silver> (accessed Feb. 03, 2022).
- [13] "Aluminium," *Wikipedia.org*. <https://en.wikipedia.org/wiki/Aluminium#/media/File:Aluminium-4.jpg> (accessed Feb. 03, 2022).
- [14] Vazbros, "Teflón PTFE Blanco Natural Redondo y Placa," www.vazbros.com. <https://www.vazbros.com/materiales/teflon-ptfe/> (accessed May 06, 2022).
- [15] Rogers Corporation, "RT/duroid® 6202 Laminates ," www.rogerscorp.com. <https://rogerscorp.com/advanced-electronics-solutions/rt-duroid-laminates/rt-duroid-6202-laminates> (accessed May 06, 2022).

- [16] Wikipedia, "Silicon," *www.wikipedia.org*. <https://en.wikipedia.org/wiki/Silicon> (accessed May 06, 2022).
- [17] Wikipedia, "Gallium." <https://en.wikipedia.org/wiki/Gallium> (accessed May 06, 2022).
- [18] T. Seymour and A. Shaheen, "History of Wireless Communication," *Rev. Bus. Inf. Syst.*, vol. 15, no. 2, pp. 37–42, 2011, doi: 10.19030/rbis.v15i2.4202.
- [19] P. Spencer, "Method of treating foodstuffs," US Patent 2495429 A, 1950
- [20] D. M. Pozar, *Microwave Engineering*, 4th Ed. J. Wiley & Sons, 2005. doi: TK7876.P69 2011.
- [21] R. H. Edgar and J. M. Osepchuk, "Consumer, Commercial and Industrial Microwave Ovens and Heating Systems," in *Handbook of Microwave Technology for Food Applications*, A. K. Datta and R. C. Anantheswaran, Eds. Marcel Dekker, Inc., 2001, pp. 215–278.
- [22] W. Hammack, "The greatest discovery since fire [microwave oven]," *IEEE Microw. Mag.*, vol. 6, no. 4, pp. 62–70, 2005, doi: 10.1109/MMW.2005.247999.
- [23] N. S. Cooper, "Microwave ovens," in *Development of Packaging and Products for Use in Microwave Ovens*, 2nd ed., U. Erle, P. Pesheck, and M. Lorence, Eds. Woodhead Publishing, 2020, pp. 177–199.
- [24] Sutori.com, "Percy Spencer." <https://www.sutori.com/es/elemento/spencer-began-conducting-further-experiments-to-gain-a-greater-understanding-of> (accessed Feb. 10, 2022).
- [25] P. O. Risman, "METHOD AND DEVICE FOR PRODUCING HEATING OF MOISTURE-CONTAINING OBJECTS," US3839616A, 1974
- [26] H. S. Hauck, "Design Considerations for Microwave Oven Cavities," *IEEE Trans. Ind. Gen. Appl.*, vol. 6, no. 1, pp. 74–80, 1970.
- [27] U. Erle, P. Pesheck, and M. Lorence, *Development of Packaging and Products for Use in Microwave Ovens*, 2nd ed. Woodhead Publishing, 2020.
- [28] M. Vollmer, "Physics of the microwave oven," *Phys. Educ.*, vol. 39, no. 1, pp. 74–81, 2004, doi: 10.1088/0031-9120/39/1/006.
- [29] ApplianceCare, "How to Replace a Microwave Diode," *www.appliancecareusa.com*. <https://appliancecareusa.com/microwave-repair/how-to-replace-a-microwave-diode/> (accessed Mar. 02, 2022).
- [30] Authorized Service, "Microwave Not Heating? How to Safely Discharge the Microwave High-Voltage Capacitor," *www.authorizedco.com*. <https://authorizedco.com/microwave-repair/microwave-not-heating-how-to-safely-discharge-the-microwave-high-voltage-capacitor/> (accessed Mar. 02, 2022).
- [31] A. K. Datta and R. C. Anantheswaran, *Handbook of Microwave Technology for Food Applications*, vol. 1. Marcel Dekker, Inc., 2001.
- [32] J. M. Catalá, D. S. Hernández, and E. De los Reyes, "Rubber vulcanisation for the footwear industry using microwave energy in a pressure-aided cavity," 1998.
- [33] B. Velázquez Martí, "Estudio de la aplicación de microondas en la desinfección de suelos," PhD Thesis, Universidad Politécnica de Valencia, Valencia, 2003.
- [34] R. Wesson, "Solid-State Microwave Cooking," *AMPERE Newsletter. Special Issue on Solid-State Microwave Heating*, no. 89, pp. 27–32, 2016.
- [35] E. Schwartz, "Historical Notes on Solid-State Microwave Heating," *AMPERE Newsletter. Special Issue on Solid-State Microwave Heating*, no. 89, pp. 4–7, 2016.

- [36] M. Golio, *RF and Microwave Semiconductor Device Handbook*, 1st ed. CRC Press LLC, 2003.
- [37] S. M. Sze and M. K. Lee, *Semiconductor Devices. Physics and Technology*, 3rd ed. John Wiley & Sons, Inc., 2012. doi: 10.1002/9780470068328.
- [38] P. Colantonio, F. Giannini, and E. Limiti, *High Efficiency RF and Microwave Solid State Power Amplifiers*. Roma: John Wiley & Sons Ltd, 2009.
- [39] F. H. Raab *et al.*, “RF and microwave power amplifier and transmitter technologies,” *High Freq. Electron.*, vol. 2, no. 5, pp. 22–36, 2003, [Online]. Available: <http://www.feng.pucrs.br/~decastro/pdf/RF&MicrowavePowerAmp&XMTRs.pdf>
- [40] Leanfa Slr, “EVALUATION KITS. Laboratory Kits for Microwave Generators.” Accessed: Feb. 08, 2022. [Online]. Available: <https://www.leanfa.com/public/download/brochure-evaluation-kits-english.pdf>
- [41] Leanfa Slr, “Generator Lab Kit. Kit for Scientific Experimentation.” Accessed: Feb. 08, 2022. [Online]. Available: <https://www.leanfa.com/public/download/generator-lab-kit-ver1-en.pdf>
- [42] PinkRF B.V., “About us – PinkRF.” <https://www.pinkrf.com/about-us/> (accessed Feb. 08, 2022).
- [43] PinkRF B.V., “RF Energy Toolkits – PinkRF.” <https://www.pinkrf.com/products/rf-tool-kits/> (accessed Feb. 08, 2022).
- [44] Muegge GmbH, “Solid-State-Microwave-Generator - MR1000D-200ML - Muegge.” <https://muegge.de/en/product/solid-state-microwave-generator-mr1000d-200ml/> (accessed Feb. 08, 2022).
- [45] Sairem S.A., “Industrial solid-state microwave generators.” <https://www.sairem.com/industrial-solid-state-microwave-generators/> (accessed Feb. 09, 2022).
- [46] A. Grandemenge, J.-M. Jacomino, M. Radoiu, and L. Latrasse, “FACILITY FOR MICROWAVE TREATMENT OF A LOAD,” WO2012146870, Apr. 25, 2012 Accessed: Feb. 09, 2022. [Online]. Available: <https://patentscope.wipo.int/search/en/detail.jsf?docId=WO2012146870>
- [47] Sairem S.A., “GMS 1000 solid state microwave generator.” Accessed: Feb. 09, 2022. [Online]. Available: <https://www.sairem.com/wp-content/uploads/2020/04/SAIREM-GMS1000-MK106-EN.pdf>
- [48] Sairem S.A., “GMS 450 solid state microwave generator.” Accessed: Feb. 09, 2022. [Online]. Available: <https://www.sairem.com/wp-content/uploads/2020/04/SAIREM-GMS450-MK079-EN.pdf>
- [49] WATTSINE ELECTRONIC, “915MH-25kW solid state microwave generator .” <https://www.wattsine.com/productview-13-31.html> (accessed Feb. 09, 2022).
- [50] WATTSINE ELECTRONIC, “433MHz-200W Solid State Microwave Power Generator.” <https://www.wattsine.com/productview-11-1.html> (accessed Feb. 09, 2022).
- [51] WATTSINE ELECTRONIC, “433MHz-200W-CMFA Solid State Microwave Power Generator.” <https://www.wattsine.com/productview-11-24.html> (accessed Feb. 09, 2022).
- [52] Ampleon, “Ampleon and Midea collaboration results in world’s first solid state oven,” 2016. <https://www.ampleon.com/news/press-releases/ampleon-and-midea-collaboration-results-in-world-s-first-solid-state-oven.html> (accessed Feb. 01, 2022).
- [53] NXP Semiconductors, “NXP Smart Cooking Appliance Concept.” <https://www.nxp.com/products/radio-frequency/rf-cooking/smart-cooking-concept:RF-SMART-COOKING-PG> (accessed Feb. 01, 2022).

- [54] Miele, “The Miele Dialog oven - Be part of the revolution.” <https://www.miele.com/brand/en/revolutionary-excellence-38683.htm> (accessed Feb. 01, 2022).
- [55] M. Wolf, “Miele Shipping the Dialog, their Oven With Solid State Cooking Tech, to 20 Countries,” *TheSpoon.tech*. <https://thespoon.tech/miele-shipping-the-dialog-their-oven-with-solid-state-cooking-tech-to-20-countries/> (accessed Feb. 01, 2022).
- [56] Goji Food Solutions, “RF cooking with Goji.” <http://www.gojifoodsolutions.com/> (accessed Feb. 01, 2022).
- [57] B. Manz, “RF Energy Is Finally Cooking ,” *Microwaves & RF*, 2017. <https://www.mwrf.com/community/article/21848854/microwaves-rf-rf-energy-is-finally-cooking> (accessed Feb. 02, 2022).
- [58] IBEX, “IBEX - Digital Cooking | Homepage.” <https://www.ibexoven.com/> (accessed Feb. 02, 2022).
- [59] K. Achkasov, L. Latrasse, and J. Jacomino, “Plasma Generation Using Solid-State Microwave Technology,” *AMPERE Newsletter. Special Issue on Solid-State Microwave Heating*, no. 89, pp. 22–26, 2016.
- [60] Ansys, “Ansys HFSS | 3D High-Frequency Simulation Software,” www.ansys.com. <https://www.ansys.com/en-GB/products/electronics/ansys-hfss> (accessed Jun. 05, 2022).
- [61] COMSOL Inc., “The COMSOL® Software Product Suite,” www.comsol.com. <https://www.comsol.com/products> (accessed Jun. 05, 2022).
- [62] The MathWorks Inc., “What Is MATLAB?,” www.es.mathworks.com. <https://es.mathworks.com/discovery/what-is-matlab.html> (accessed Jun. 06, 2022).
- [63] Keysight Technologies, “N9917A FieldFox Handheld Microwave Analyzer, 18 GHz,” www.keysight.com. <https://www.keysight.com/es/en/product/N9917A/fieldfox-a-handheld-microwave-analyzer-18-ghz.html> (accessed Jun. 06, 2022).
- [64] Testo SE & Co. KGaA, “testo 890 – Thermal imager,” www.testo.com. <https://www.testo.com/en-UK/testo-890/p/0563-0890-X1> (accessed Jun. 06, 2022).
- [65] P. Santón, B. Wäppling Raaholt, R. De los Reyes, E. De los Reyes, and J. V. Balbastre, “Multiphysics Modeling of the Thawing and Tempering Process of Beef Meat in a Solid-State Based Microwave Cavity,” in *18th International Conference on Microwave and High Frequency Applications*, 2021, no. September, pp. 236–243. doi: 10.5281/zenodo.5644776.
- [66] N. E. Bengtsson and T. Ohlsson, “Microwave Heating in the Food Industry,” *Proc. IEEE*, vol. 62, no. 1, pp. 44–55, 1974, doi: 10.1109/PROC.1974.9384.
- [67] R. De los Reyes, “Medida de propiedades dieléctricas en alimentos y su aplicación en el control de calidad de productos y procesos,” Universidad Politécnica de Valencia, 2007.
- [68] J. M. Catalá, “Conceptos básicos del Procesado de Materiales con Microondas.”
- [69] D. Misra, M. Chhabra, B. R. Epstein, M. Mirotznik, and K. R. Foster, “Noninvasive Electrical Characterization of Materials at Microwave Frequencies Using an Open-Ended Coaxial Line: Test of an Improved Calibration Technique,” *IEEE Trans. Microw. Theory Tech.*, vol. 38, no. 1, pp. 8–14, 1990, doi: 10.1109/22.44150.
- [70] P. Santón, J. V. Balbastre, E. De los Reyes, R. De los Reyes, and M. Baquero-Escudero, “Transmission/reflection system for dielectric characterization using coaxial probes,” in *Proceedings of the 2019 21st International Conference on Electromagnetics in Advanced Applications, ICEAA 2019*, 2019, pp. 378–381. doi: 10.1109/ICEAA.2019.8878983.
- [71] S. Roberts and A. Von Hippel, “A New Method for Measuring Dielectric Constant and Loss in the Range of Centimeter Waves,” *J. Appl. Phys.*, vol. 17, no. 7, pp. 610–616, Jul.

- 1946, doi: 10.1063/1.1707760.
- [72] S. O. Nelson, C. W. Schlaphoff, and L. E. Stetson, "A Computer Program for Short-Circuited Waveguide Dielectric-Properties Measurements on High-or Low-Loss Materials," *J. Microw. Power*, vol. 8, no. 1, pp. 13–22, Jan. 1973, doi: 10.1080/00222739.1973.11689016.
- [73] S.-H. Chao, "An uncertainty analysis for the measurement of microwave conductivity and dielectric constant by the short-circuited line method," *IEEE Trans. Instrum. Meas.*, vol. IM-35, no. 1, pp. 36–41, Mar. 1986, doi: 10.1109/TIM.1986.6499053.
- [74] J. Bhattacharyya, S. Bakhtiari, N. Qaddoumi, D. Brandenburg, and R. Zoughi, "Microwave Diagnosis of Rubber Compounds," *IEEE Trans. Microw. Theory Tech.*, vol. 42, no. 1, pp. 18–24, 1994, doi: 10.1109/22.265523.
- [75] H. B. Sequeira, "Extracting mu and epsilon of solids from one-port phasor network analyzer measurements," *IEEE Trans. Instrum. Meas.*, vol. 39, no. 4, pp. 621–627, 1990, doi: 10.1109/19.57244.
- [76] A. M. Nicolson and G. F. Ross, "Measurement of the Intrinsic Properties Of Materials by Time-Domain Techniques," *IEEE Trans. Instrum. Meas.*, vol. 19, no. 4, pp. 377–382, 1970, doi: 10.1109/TIM.1970.4313932.
- [77] T. L. Blakney and W. B. Weir, "Comments on 'Automatic Measurement of Complex Dielectric Constant and Permeability at Microwave Frequencies,'" *Proc. IEEE*, vol. 63, no. 1, pp. 203–205, 1975, doi: 10.1109/PROC.1975.9725.
- [78] J. Baker-Jarvis, E. J. Vanzura, and W. A. Kissick, "Improved technique for determining complex permittivity with the transmission/reflection method," *IEEE Trans. Microw. Theory Tech.*, vol. 38, no. 8, pp. 1096–1103, 1990, doi: 10.1109/22.57336.
- [79] A. H. Boughriet, C. Legrand, and A. Chapoton, "Noniterative stable transmission/reflection method for low-loss material complex permittivity determination," *IEEE Trans. Microw. Theory Tech.*, vol. 45, no. 1, pp. 52–57, 1997, doi: 10.1109/22.552032.
- [80] S. Lefrançois, D. Pasquet, and G. Mazé-Merceur, "A new model for microwave characterization of composite materials in guided-wave medium," *IEEE Trans. Microw. Theory Tech.*, vol. 44, no. 9, pp. 1557–1562, 1996, doi: 10.1109/22.536604.
- [81] J. J. Laurin, G. Tanneau, and C. Akyel, "Waveguide permittivity measurement using variable-length samples and an uncalibrated reflectometer," *IEEE Trans. Instrum. Meas.*, vol. 45, no. 1, pp. 298–301, 1996, doi: 10.1109/19.481351.
- [82] R. Thomas and D. C. Dube, "Extended technique for complex permittivity measurement of dielectric films in the microwave region," *Electron. Lett.*, vol. 33, no. 3, pp. 218–220, 1997, doi: 10.1049/el:19970137.
- [83] S. S. Kim, S. B. Jo, K. I. Gueon, K. K. Choi, J. M. Kim, and K. S. Churn, "Complex Permeability and Permittivity and Microwave Absorption of Ferrite-Rubber Composite in X-band Frequencies," *IEEE Trans. Magn.*, vol. 27, no. 6, pp. 5462–5464, 1991, doi: 10.1109/20.278872.
- [84] Hewlett Packard, "Basics of Measuring the Dielectric Properties of Materials. Application Note 1217-1." 1993. [Online]. Available: <http://scholar.google.com/scholar?hl=en&btnG=Search&q=intitle:Basics+of+Measuring+the+Dielectric+Properties+of+Materials#2>
- [85] S. Soriano, E. De los Reyes, and P. Santón, "Sistema Multifrecuencia de Medida de Propiedades Dieléctricas Mediante Líneas Coplanares," Polytechnic University of Valencia, 2020.
- [86] P. Santón, J. V. Balbastre, M. Baquero, R. D. los Reyes, and E. De Los Reyes,

- “Multifrequency Dielectric Properties Measurement Method Based on Coplanar Waveguide,” in *IMPI's 56th Annual Microwave Power Symposium*, 2022, pp. 133–135.
- [87] N. E. Bengtsson and P. O. Risman, “Dielectric Properties of Foods at 3 GHz as Determined by a Cavity Perturbation Technique,” *J. Microw. Power*, vol. 6, no. 2, pp. 107–123, 1971, doi: 10.1080/00222739.1971.11688789.
- [88] A. Mansingh, “Measurement of Dielectric Parameters at Microwave Frequencies by Cavity-Perturbation Technique,” *IEEE Trans. Microw. Theory Tech.*, vol. 27, no. 9, pp. 791–795, 1979, doi: 10.1109/TMTT.1979.1129731.
- [89] A. W. Kraszewski and S. O. Nelson, “Observations on resonant cavity perturbation by dielectric objects,” *IEEE Trans. Microw. Theory Tech.*, vol. 40, no. 1, pp. 151–155, 1992, doi: 10.1109/22.108334.
- [90] M. A. Rzepecka and M. A. K. Hamid, “Modified Perturbation Method for Permittivity Measurements at Microwave Frequencies,” *J. Microw. Power*, vol. 9, no. 4, pp. 317–328, Jan. 1974, doi: 10.1080/00222739.1974.11688929.
- [91] Shihe Li, C. Akyel, and R. G. Bosisio, “Precise Calculations and Measurements on the Complex Dielectric Constant of Lossy Materials Using TM/sub 010/ Cavity Perturbation Techniques,” *IEEE Trans. Microw. Theory Tech.*, vol. 29, no. 10, pp. 1041–1048, Oct. 1981, doi: 10.1109/TMTT.1981.1130496.
- [92] V. Pohl, D. Fricke, and A. Mühlbauer, “Correction Procedures for The measurement of Permittivities with the Cavity Perturbation Method,” *J. Microw. Power Electromagn. Energy*, vol. 30, no. 1, pp. 10–26, Jan. 1995, doi: 10.1080/08327823.1995.11688253.
- [93] J. M. Rius Casals *et al.*, “Tomografía de microondas: algoritmos en coordenadas cilíndricas,” in *RSI'86: III Symposium Nacional del Comité Español de la Unión Científica Internacional de Radio*, 1986, pp. 227–229. [Online]. Available: hdl.handle.net/2117/85219
- [94] L. Jofre *et al.*, “A cylindrical system for quasi-real time microwave tomography,” *1986 16th Eur. Microw. Conf. EUMA 1986*, no. 1, pp. 599–604, 1986, doi: 10.1109/EUMA.1986.334258.
- [95] P. O. Risman, “Advanced topics in heating uniformity - theory and experimental methods,” in *Development of Packaging and Products for Use in Microwave Ovens*, 2nd ed., U. Erle, P. Pesheck, and M. Lorence, Eds. Woodhead Publishing, 2020, pp. 95–176.
- [96] B. W. Raaholt, “Influence of food geometry and dielectric properties on heating performance,” in *Development of Packaging and Products for Use in Microwave Ovens*, 2nd ed., U. Erle, P. Pesheck, and M. Lorence, Eds. Woodhead Publishing, 2020, pp. 73–93.
- [97] Y. Choi and M. R. Okos, “Effects of temperature and composition on the thermal properties of foods,” *Food Eng. Process Appl.*, vol. 1, pp. 93–101, 1986.
- [98] American Society of Heating Refrigerating and Air-Conditioning Engineers, “Thermal properties of food,” in *ASHRAE Handbook Refrigeration (SI)*, American Society of Heating Refrigerating and Air-Conditioning Engineers, Ed. 2006.
- [99] M. A. Rao, S. S. H. Rizvi, A. K. Datta, and J. Ahmed, *Engineering properties of foods*, 4th ed. 2014. doi: 10.1201/b16897.
- [100] D. Samuel and S. Trabelsi, “Measurement of Dielectric Properties of Intact and Ground Broiler Breast Meat over the Frequency Range from 500 MHz to 50 GHz,” *Int. J. Poult. Sci.*, vol. 11, no. 3, pp. 172–176, 2012.
- [101] J. G. Lyng, L. Zhang, and N. P. Brunton, “A survey of the dielectric properties of meats and ingredients used in meat product manufacture,” *Meat Sci.*, vol. 69, no. 4, pp. 589–602, 2005, doi: 10.1016/j.meatsci.2004.09.011.

- [102] D. M. Phinney, J. C. Frelka, and D. R. Heldman, "Composition-Based Prediction of Temperature-Dependent Thermophysical Food Properties: Reevaluating Component Groups and Prediction Models," *J. Food Sci.*, vol. 82, no. 1, pp. 6–15, 2017, doi: 10.1111/1750-3841.13564.
- [103] T. Ohlsson, M. Henriques, and N. E. Bengtsson, "Dielectric Properties of Model Meat Emulsions at 900 and 2800 MHz in Relation to their Composition," *J. Food Sci.*, vol. 39, no. 6, pp. 1153–1156, 1974, doi: 10.1111/j.1365-2621.1974.tb07341.x.
- [104] O. Sipahioğlu, S. A. Barringer, and C. Bircan, "The dielectric properties of meats as a function of temperature and composition," *J. Microw. Power Electromagn. Energy*, vol. 38, no. 3, pp. 161–169, 2003, doi: 10.1080/08327823.2003.11688496.
- [105] J. A. Gómez-salazar *et al.*, "Dielectric properties of fresh rabbit meat in the microwave range," *J. Food Sci.*, vol. 0, no. 0, 2021, doi: 10.1111/1750-3841.15631.
- [106] L. Malafrente, G. Lamberti, A. A. Barba, B. Raaholt, E. Holtz, and L. Ahrné, "Combined convective and microwave assisted drying: Experiments and modeling," *J. Food Eng.*, 2012, doi: 10.1016/j.jfoodeng.2012.05.005.
- [107] P. O. Risman and B. Wäppling-Raaholt, "Retro-modelling of a dual resonant applicator and accurate dielectric properties of liquid water from -20 °c to +100 °c," 2007. doi: 10.1088/0957-0233/18/4/001.
- [108] B. W. Raaholt, E. Holtz, S. Isaksson, and L. Ahrné, "Application of Microwave Technology in Food Preservation and Processing," in *Conventional and Advanced Food Processing Technologies*, 2014. doi: 10.1002/9781118406281.ch18.
- [109] B. Wäppling-Raaholt, H. Janestad, and T. Ohlsson, "Modelling of microwave tempering, defrosting and heating of frozen foods using a coupled finite difference approach," 2005.
- [110] B. W. Raaholt and S. Isaksson, "Combined microwave infrared/convective baking of bread," 2013.
- [111] B. W. Raaholt and B. Waldén, "Modelling of a combined microwave-infrared baking process of bread," 2011.
- [112] B. Wäppling Raaholt, "Microwave modelling and applications in the food industry," 2015.
- [113] B. W. Raaholt, L. Hamberg, and S. Isaksson, "Continuous tubular microwave heating of particulate foods at high temperatures," *J. Microw. Power Electromagn. Energy*, 2017, doi: 10.1080/08327823.2017.1388942.
- [114] B. W. Raaholt, S. Isaksson, L. Hamberg, A. Fhager, and Y. Hamnerius, "Continuous tubular microwave heating of homogeneous foods: evaluation of heating uniformity," *J. Microw. Power Electromagn. Energy*, 2016, doi: 10.1080/08327823.2016.1157318.
- [115] B. Bodakian, "The Dielectric Properties," *IEEE Trans. Dielectr. Electr. Insul.*, vol. 1, no. 2, pp. 181–187, 1994.
- [116] L. Zhang, J. G. Lyng, N. Brunton, D. Morgan, and B. McKenna, "Dielectric and thermophysical properties of meat batters over a temperature range of 5-85 °C," *Meat Sci.*, vol. 68, no. 2, pp. 173–184, 2004, doi: 10.1016/j.meatsci.2004.02.009.
- [117] L. Zhang, J. G. Lyng, and N. P. Brunton, "The effect of fat, water and salt on the thermal and dielectric properties of meat batter and its temperature following microwave or radio frequency heating," *J. Food Eng.*, vol. 80, no. 1, pp. 142–151, 2007, doi: 10.1016/j.jfoodeng.2006.05.016.
- [118] K. W. Farag, J. G. Lyng, D. J. Morgan, and D. A. Cronin, "Dielectric and thermophysical properties of different beef meat blends over a temperature range of -18 to +10 °C," *Meat Sci.*, vol. 79, no. 4, pp. 740–747, 2008, doi: 10.1016/j.meatsci.2007.11.005.
- [119] S. Trabelsi, "Variation of the dielectric properties of chicken meat with frequency and

- temperature,” *J. Food Meas. Charact.*, vol. 9, no. 3, pp. 299–304, 2015, doi: 10.1007/s11694-015-9235-6.
- [120] P. O. Risman, “Measurements of dielectric properties of foods and associated materials,” in *Development of Packaging and Products for Use in Microwave Ovens*, 2nd ed., U. Erle, P. Pesheck, and M. Lorence, Eds. Woodhead Publishing, 2020, pp. 200–223.
- [121] T. Ohlsson and N. E. Bengtsson, “Dielectric Food Data for Microwave Sterilization Processing,” *J. Microw. Power*, vol. 10, no. 1, pp. 93–108, 1975, doi: 10.1080/00222739.1975.11688945.
- [122] N. P. Brunton, J. G. Lyng, L. Zhang, and J. C. Jacquier, “The use of dielectric properties and other physical analyses for assessing protein denaturation in beef biceps femoris muscle during cooking from 5 to 85 °c,” *Meat Sci.*, vol. 72, no. 2, pp. 236–244, 2006, doi: 10.1016/j.meatsci.2005.07.007.
- [123] S. Trabelsi, “Frequency and temperature dependence of dielectric properties of chicken meat,” *2012 IEEE I2MTC - Int. Instrum. Meas. Technol. Conf. Proc.*, pp. 1515–1518, 2012, doi: 10.1109/I2MTC.2012.6229560.
- [124] COMSOL Inc., “Use Functions to Define a Material Property,” www.comsol.com. <https://www.comsol.com/video/use-functions-define-material-property> (accessed Jun. 04, 2022).
- [125] COMSOL Inc., *Microwave Oven*. 2018.
- [126] COMSOL Inc., “Frequency-Transient,” www.comsol.com. https://doc.comsol.com/5.5/doc/com.comsol.help.comsol/comsol_ref_solver.27.052.html (accessed Jun. 04, 2022).
- [127] J. F. Fernandez, E. De los Reyes, R. De los Reyes, J. García, E. Vela, and A. Jara, “Célula calefactora,” 2014 [Online]. Available: <http://invenes.oepm.es/InvenesWeb/detalle?referencia=P201431449>
- [128] N. Ida, *Engineering Electromagnetics*, 3rd Ed. Springer, 2015. doi: 10.1007/978-3-319-07806-9.
- [129] E. De los Reyes and A. Elias, “Adaptación de impedancias mediante doble ‘slug’ con elementos concentrados, semiconcentrados y distribuidos,” *Simp. Nac. la Unión Científica Int. Radio*, pp. 73–77, 1980, [Online]. Available: <http://hdl.handle.net/2117/85999>
- [130] B. C. Wadell, *Transmission Line Design Handbook*. Norwood: Artech House Inc., 1991.
- [131] E. De los Reyes, A. Jara, R. De los Reyes, and J. García, “Microwave energy transduction using planar technology,” *Electron. Lett.*, vol. 51, no. 6, pp. 499–501, 2015, doi: 10.1049/el.2014.3816.
- [132] P. Santón, J. V. Balbastre, E. De los Reyes, and R. De los Reyes, “Fully Asymmetric Stripline Structure for Fast Heating,” in *International Conference on Heating by Electromagnetic Sources*, 2019, no. Induction, Dielectric and Microwaves, Conduction & Electromagnetic Processing, pp. 359–362.
- [133] P. Santón, J. V. Balbastre, E. De Los Reyes, and R. De los Reyes, “Spiral Asymmetric Stripline Structure for Fast Microwave Heating,” in *International Conference on Electromagnetics in Advanced Applications (ICEAA 2019)*, 2019, pp. 690–692. doi: 10.1109/ICEAA.2019.8878948.
- [134] W. H. Bailey *et al.*, “IEEE Standard for Safety Levels with Respect to Human Exposure to Electric, Magnetic, and Electromagnetic Fields, 0 Hz to 300 GHz,” 2019. doi: 10.1109/ACCESS.2019.2954823.
- [135] International Commission on Non-Ionizing Radiation Protection (ICNIRP), “ICNIRP GUIDELINES. For limiting exposure to electromagnetic fields (100 kHz to 300 GHz),”

2020. doi: 10.1097/HP.0000000000001210.
- [136] B. W. Salski and M. Olszewska-Placha, “FDTD Modeling of Industrial Microwave Power Applicators,” in *IMPI’s 56th Annual Microwave Power Symposium*, 2022, pp. 81–83.
- [137] A. P. S. Khanna, “State of the Art in Microwave VCOs,” *www.microwavejournal.com*, May 14, 2015. <https://www.microwavejournal.com/articles/24333-state-of-the-art-in-microwave-vcos> (accessed Mar. 03, 2022).
- [138] Mouser, “HMC648ALP6E 6-bit Digital Phase Shifters,” *www.mouser.es*, Jul. 28, 2016. <https://www.mouser.es/new/analog-devices/adi-hmc648alp6e-phase-shifter/> (accessed Mar. 28, 2022).
- [139] Raditek Inc., “Waveguide Power Splitters | Raditek,” *www.raditek.com*. <https://raditek.com/waveguide-power-splitter.html> (accessed Mar. 28, 2022).
- [140] Y. Lee *et al.*, “Two-way Waveguide Power Divider using 3D Printing and Electroless Plating,” *2018 48th Eur. Microw. Conf. EuMC 2018*, pp. 219–222, 2018, doi: 10.23919/EuMC.2018.8541546.
- [141] Kimitosfu, “500-2500MHz Wilkinson Power Splitter Power Combiner Board 1Way Entrada 2Way Salida : Electrónica,” *www.amazon.com*. <https://www.amazon.com/500-2500MHz-Wilkinson-Divider-Combiner-Output/dp/B08J2VHT8N> (accessed Mar. 28, 2022).
- [142] M. Hernández-Bertó, E. De los Reyes, and P. Santón, “Amplificador de potencia en 2.45 GHz para aplicaciones ISM,” Polytechnic University of Valencia, 2021.
- [143] Institute of Electrical and Electronic Engineers, “IEEE Std 145-1983 IEEE Standard Definitions of Terms for Antennas,” 1983.
- [144] R. E. Collin, *Antennas and Radiowave Propagation*. McGraw-Hill, Inc, 1988.
- [145] Á. Cardama *et al.*, *Antenas*. Edicions UPC, 2002.
- [146] S. Soriano, E. De Los Reyes, and P. Santón, “Design and Modelling of Tunable Monopole Antennas for Power Applications in the ISM Band,” Polytechnic University of Valencia, 2022.
- [147] D. M. Pozar, “A Reciprocity Method of Analysis for Printed Slot and Slot-Coupled Microstrip Antennas,” *IEEE Trans. Antennas Propag.*, no. 12, 1986.
- [148] J. Sze and K. Wong, “Bandwidth Enhancement of a Microstrip-Line-Fed Printed Wide-Slot Antenna,” *IEEE Trans. Antennas Propag.*, vol. 49, no. 7, pp. 1020–1024, 2001.
- [149] H. Iwasaki, “A Circularly Polarized Small-Size,” *IEEE Trans. Antennas Propag.*, vol. 44, no. 10, pp. 1399–1401, 1996.
- [150] D. Peroulis, K. Sarabandi, and L. P. B. Katehi, “Design of reconfigurable slot antennas,” *IEEE Trans. Antennas Propag.*, vol. 53, no. 2, pp. 645–654, 2005, doi: 10.1109/TAP.2004.841339.
- [151] A. Bhattacharyya, O. Fordham, and Y. Liu, “Analysis of stripline-fed slot-coupled patch antennas with vias for parallel-plate mode suppression,” *IEEE Trans. Antennas Propag.*, vol. 46, no. 4, pp. 538–545, 1998, doi: 10.1109/8.664118.
- [152] P. Santón, R. De los Reyes, and J. V. Balbastre, “Cavity Backed Slot Antenna Fed by a Stripline with SIW Structure and Vertical Coaxial Transition for Microwave Solid-State Heating Applications,” *Electronics*, vol. 11, no. 3, p. 327, Jan. 2022, doi: 10.3390/electronics11030327.
- [153] C. A. Balanis, *Antenna Theory, Analysis and Design*, Forth. J. Wiley & Sons, 2016. doi: 10.1016/S1574-0099(05)02014-0.
- [154] P. K. Park and A. Science, “Design of Transverse Slot Arrays Fed by Boxed Stripline,”

- pp. 428–431, 1981.
- [155] A. Hernandez-Escobar, E. Abdo-Sanchez, and C. Camacho-Petnalosa, “On the Matching of Stripline-Fed Cavity-Backed Slots as a Series-Fed Array Element,” *Proc. 2019 9th IEEE-APS Top. Conf. Antennas Propag. Wirel. Commun. APWC 2019*, pp. 247–249, 2019, doi: 10.1109/APWC.2019.8870464.
- [156] P. Debnath and S. Chatterjee, “Substrate Integrated Antennas and Arrays,” 2017. doi: 10.1201/b18685.
- [157] R. Shen, D. Kong, and D. Sun, “A design of stripline-coaxial vertical transition with ultra-broadband,” *2010 Int. Conf. Microw. Millim. Wave Technol. ICMMT 2010*, pp. 1514–1517, 2010, doi: 10.1109/ICMMT.2010.5524919.
- [158] C. R. Buffler, *Microwave Cooking and Processing*. 1993. doi: 10.1007/978-1-4757-5833-7.
- [159] Dielectric Manufacturing, “Material Properties of Thermoplastic PEEK - Polyetheretherketone,” *www.dielectricmfg.com*, Feb. 27, 2019. <https://dielectricmfg.com/knowledge-base/peek/> (accessed Feb. 23, 2022).
- [160] N. Paz García, E. De los Reyes, and P. Santón, “Diseño y fabricación de antenas de parche para aplicaciones de potencia en cavidad resonante.,” Polytechnic University of Valencia, 2021.
- [161] D. M. Pozar, “Microstrip antennas,” in *Proceedings of the IEEE*, 1992, vol. 80, no. 1, pp. 79–91. doi: 10.1109/5.119568.
- [162] G. P. De Loor, “Dielectric properties of heterogeneous mixtures,” University of Leiden, 1956.
- [163] W. R. Tinga, W. A. G. Voss, and D. F. Blossey, “Generalized approach to multiphase dielectric mixture theory,” *J. Appl. Phys.*, vol. 44, no. 9, pp. 3897–3902, Sep. 1973, doi: 10.1063/1.1662868.
- [164] F. De Paulis, M. H. Nisanci, M. Y. Koledintseva, J. L. Drewniak, and A. Orlandi, “HOMOGENIZED PERMITTIVITY OF COMPOSITES WITH ALIGNED CYLINDRICAL INCLUSIONS FOR CAUSAL ELECTROMAGNETIC SIMULATIONS,” *Prog. Electromagn. Res. B*, vol. 37, pp. 205–235, 2012, doi: 10.2528/PIERB11072805.
- [165] M. Mehdizadeh, *Microwave/RF Applicators and Probes for Material Heating, Sensing and Plasma Generation*, 2nd ed. Elsevier, 2015. doi: 10.1016/C2014-0-00010-X.
- [166] B. Díaz de Greñu, R. de los Reyes, A. M. Costero, P. Amorós, and J. V. Ros-Lis, “Recent progress of microwave-assisted synthesis of silica materials,” *Nanomaterials*, vol. 10, no. 6, pp. 1–21, 2020, doi: 10.3390/nano10061092.
- [167] P. Santón, E. D. L. Reyes, R. D. L. Reyes, J. V. Balbastre, and J. V. Ros-Lis, “On the Multiphysics Modelling of Chemical Processes with Solid-State Driven Microwave Systems,” in *IMPI's 56th Annual Microwave Power Symposium*, 2022, no. June, pp. 90–92.
- [168] M. Benitez and J. V. Ros-Lis, “Valorización de un nuevo procedimiento de síntesis asistida por microondas de sílice porosa. ValoraSiO,” Burjassot, 2020.
- [169] S. L. Galas and J. B. Enns, “Humidity-Conditioned Gravimetric Method to Measure the Water Content of Hydrogel Contact Lens Materials,” *Optom. Vis. Sci.*, vol. 70, no. 7, pp. 577–586, 1993, doi: 10.1097/00006324-199307000-00009.
- [170] H. T. Hui, M. E. Bialkowski, and H. S. Lui, “Mutual coupling in antenna arrays,” *Int. J. Antennas Propag.*, vol. 2010, 2010, doi: 10.1155/2010/736701.
- [171] Leanfa Srl., “PHASESHIFTER Evaluation Kit 4x500W 915MHz. Reference Manual.”

- [172] Sodeca, “Ventiladores Helicoidales,” www.sodeca.es. <https://www.sodeca.es/productos/hc-p82?cs=s12&fil=50#prod> (accessed May 11, 2022).
- [173] Holland Shielding Systems BV, “Paneles de ventilación Honeycomb | Filtro de aire blindado EMI y parrillas EMC,” www.hollandshielding.es. <https://hollandshielding.es/Paneles-de-ventilación-Honeycomb> (accessed May 11, 2022).
- [174] Holland Shielding Systems BV, “EMI / RFI Pantallas blindadas de revestimiento y malla conductora eléctrica y Windows,” www.hollandshielding.es. <https://hollandshielding.es/serie-Ventanas-de-lámina-de-malla-blindada-EMI-RFI> (accessed May 11, 2022).
- [175] Á. Miró, E. De Los Reyes, and P. Santón, “Modelado Multifísico de un Sistema de Calentamiento por Microondas con Estado Sólido y Antenas con Estructura TEM,” Polytechnic University of Valencia, 2022.
- [176] IEEE, “Artificial Intelligence. IEEE Position Statement.,” no. June. IEEE, 2019.
- [177] J. P. Mueller and L. Massaron, *Artificial Intelligence for Dummies*. Hoboken: John Wiley & Sons, Inc., 2018.

Annex A

Foodstuff dielectric properties

The dielectric properties of meats as a function of temperature and composition (Sipahioglu, 2003)

Beef comparison with previous works											
Measured by Sipahioglu: Mc(%) 70.6 Ash(%) 1.02				Measured by Sun et al				Measured by Calay et al			
e'		e''		e'		e''		e'		e''	
T (°C)	Value	T (°C)	Value	T (°C)	Value	T (°C)	Value	T (°C)	Value	T (°C)	Value
20,29	52,02	20,23	17,57	20,31	81,62	20,3	160	20,27	44,05	20,23	17,57
25,35	51,7	25,18	17,15	25,36	81,16	25,18	155,78	25,4	43,32	25,18	17,9
30,41	51,52	30,29	16,34	30,34	80,3	30,36	150,43	30,38	42,33	30,29	18,99
35,47	51,06	35,39	16,29	35,48	79,98	35,39	145,46	35,59	41,73	35,31	18,57
40,44	50,6	40,27	16,63	40,46	79,25	40,27	140,49	40,42	41,28	40,27	19,66
45,34	50,28	45,3	16,96	45,36	78,8	45,22	136,28	45,31	40,42	45,3	19,23
50,4	49,83	50,48	16,53	50,33	78,21	50,4	131,68	50,29	39,83	50,4	19,94
55,46	49,51	55,43	17,62	55,39	77,34	55,35	126,71	55,43	39,37	55,35	19,89

Chicken breast comparison with previous works											
Measured by Sipahioglu: Mc(%) 74.8 Ash(%) 1.02				Measured by Sun et al				Measured by Calay et al			
e'		e''		e'		e''		e'		e''	
T (°C)	Value	T (°C)	Value	T (°C)	Value	T (°C)	Value	T (°C)	Value	T (°C)	Value
15,42	57,17	15,1	18,14	15,54	91,18	15,28	178,34	15,42	57,29	15,28	191,94
20,42	56,56	20,26	18,14	20,54	90,68	20,33	172,29	20,33	57,02	20,43	191,44
25,23	56,06	25,41	19,14	25,35	90,07	25,48	166,75	25,23	56,99	25,4	191,44
30,32	55,91	30,47	18,64	30,44	89,34	30,44	162,22	30,42	56,83	30,45	190,93
35,32	55,53	35,43	18,64	35,34	88,61	35,59	156,68	35,32	56,68	35,51	192,95
40,22	55,03	40,39	18,14	40,33	87,88	40,45	151,13	40,23	56,3	40,47	192,95
45,41	54,53	45,35	18,64	45,42	87,15	45,41	146,6	45,42	56,15	45,34	191,44
50,31	54,38	50,51	19,65	50,42	86,43	50,37	141,56	50,32	56,12	50,59	191,94
55,21	54	55,37	19,14	55,22	85,7	55,52	136,52	55,23	55,97	55,45	191,94
60,4	53,5	60,33	20,65	60,41	84,97	60,39	131,99	60,41	55,7	60,42	192,44

Beef			
Measured by Sipahioglu			
e'		e''	
T (°C)	Value	T (°C)	Value
15,28	54,69	15,23	17,01
20,41	54,7	20,29	16,68
25,34	54,5	25,34	16,43
30,37	54,25	30,27	16,39
35,4	53,86	35,44	16,43
40,33	53,44	40,36	16,55
45,36	52,83	45,41	16,7
50,29	52,1	50,33	16,94
55,32	51,28	55,37	17,17
60,35	51,11	60,41	17,72

Chicken breast				Chicken thigh			
Measured by Sipahioglu				Measured by Sipahioglu			
e'		e''		e'		e''	
T (°C)	Value	T (°C)	Value	T (°C)	Value	T (°C)	Value
15,19	55,97	15,2	18,47	15,28	55,83	15,26	16,09
20,41	55,98	20,25	18,21	20,41	55,76	20,33	15,79
25,34	55,9	25,42	18,12	25,34	55,55	25,41	15,71
30,27	55,74	30,23	18,12	30,27	55,17	30,34	15,7
35,4	55,45	35,51	18,2	35,4	54,79	35,41	15,72
40,43	55,06	40,44	18,41	40,33	54,45	40,33	15,9
45,36	54,72	45,36	18,7	45,36	53,98	45,4	16,11
50,2	54,21	50,16	19,11	50,39	53,68	50,31	16,6
55,32	53,65	55,32	19,55	55,32	52,81	55,38	16,9
60,35	53,09	60,35	20				
65,09	52,75	65,03	20,65				

Salmon				Cod				Perch			
Measured by Sipahioglu				Measured by Sipahioglu				Measured by Sipahioglu			
e'		e''		e'		e''		e'		e''	
T (°C)	Value	T (°C)	Value	T (°C)	Value	T (°C)	Value	T (°C)	Value	T (°C)	Value
15,28	51,92	15,25	16,51	15,28	62,47	15,23	17,37	15,19	59,83	15,2	18,62
20,41	51,45	20,3	16,31	20,31	62,13	20,4	16,86	20,31	58,88	20,25	18,33
25,34	51,24	25,35	16,17	25,34	61,71	25,34	16,54	25,24	58,58	25,3	18,25
30,27	51,13	30,28	16,19	30,27	61,19	30,27	16,38	30,27	58,16	30,23	18,32
35,4	50,7	35,44	16,33	35,4	60,59	35,44	16,4	35,3	57,16	35,39	18,41
40,43	50,36	40,36	16,67	40,43	60,03	40,36	16,65	40,33	56,64	40,31	18,76
45,36	49,54	45,4	16,84	45,36	59,29	45,4	16,86				
50,29	48,58	50,33	16,98	50,29	58,43	50,33	17,15				

Dielectric and thermophysical properties of meat batters over a temperature range of 5-85 °C (Zhang and Lyng, 2004)

Pork luncheon roll: Moisture (%) 60.4, Fat (%) 15.1, Protein (%) 11.3, Carbohydrate (%) 11.4, Ash (%) 1.8, Salt (%) 1.2						
Temperature (°C)	896 MHz		915 MHz		2450 MHz	
	e'	e''	e'	e''	e'	e''
5	40,13	28,48	40,03	28,01	36,08	17,14
25	39,71	32,86	39,61	32,27	35,9	18,03
45	36,49	34,49	36,39	33,85	33,01	18,32
65	39,6	41,22	39,49	40,43	35,63	21,03
85	34,93	32,45	34,82	31,85	31,16	16,24

White pudding: Moisture (%) 61.2, Fat (%) 15.8, Protein (%) 10.8, Carbohydrate (%) 9.1, Ash (%) 3.1, Salt (%) 2.3						
Temperature (°C)	896 MHz		915 MHz		2450 MHz	
	e'	e''	e'	e''	e'	e''
5	37,48	42,09	37,38	41,32	33	21,92
25	36,72	48,31	36,57	47,42	32,83	23,09
45	38,83	59,82	38,72	58,68	34,64	26,85
65	35,67	58,59	35,56	57,46	31,45	25,61
85	33,84	50,64	33,72	49,64	29,97	23,34

A survey of the dielectric properties of meats and ingredients used in meat product manufacture
(Zhang and Lyng, 2005)

Pork shoulder. Mc(%) 73.9, Protein(%) 20.1, Fat(%) 4.4, Ash(%) 1.13, Salt (%) 0.08		Pork back. Mc(%) 19, Protein(%) 3.9, Fat(%) 76.1, Ash(%) 0.2, Salt (%) 0.07	
2450 MHz		2450 MHz	
e'	e''	e'	e''
49	16,1	7,9	0,76

Turkey breast. Mc(%) 74.5, Protein(%) 24.1, Fat(%) 0.4, Ash(%) 0.98, Salt (%) 0.07	
2450 MHz	
e'	e''
56,3	18
Lamb leg. Mc(%) 73.0, Protein(%) 21.9, Fat(%) 3.6, Ash(%) 1.48, Salt (%) 0.14	
2450 MHz	
e'	e''
49,4	15
Chicken breast. Mc(%) 73.6, Protein(%) 24.3, Fat(%) 1.2, Ash(%) 0.86, Salt (%) 0.13	
2450 MHz	
e'	e''
49	16,1
Beef. Mc(%) 71.5, Protein(%) 21.3, Fat(%) 6.1, Ash(%) 0.83, Salt (%) 0.11	
2450 MHz	
e'	e''
43.7 (4°C)	13.7

Beef with additives in percentage				
2450 MHz				
Ingredient	Content (%)	e'	e''	
Pork fat		20	12,1	40,6
Potato starch		4	14,7	47,5
Gluten		0,15	15,5	49,4
No additives	NA		15,6	50,8
Nitrite		0,015	15,6	50,6
Water		25	15,8	56
Phosphate (P22)		3	22,1	48,3
Salt		1,5	24,4	47,8

Other ingredients usually added			
2450 MHz			
Ingredient	e'	e''	dp (cm)
Deionised water	6,9	76,8	5
Antioxidant BHA	7,1	68,4	4,5
Soya concentrate	7,3	43,3	3,5
Natex rusk	7,5	47,9	3,5
Potato starch	8,3	77,8	4,2
Natex grits	9	57,7	3,3
Wheat flour	9,1	74,4	3,7
Boiled potato starch	9,2	76,1	3,7
Sucrose	9,4	76,1	3,6
Caseinate	9,9	74,3	3,4
Whey protein	10,2	74,2	3,3
Soya protein isolate	10,2	75,9	3,3
Rusk	10,3	77,2	3,3
Wheat gluten	10,3	74,5	3,3
Soya protein	10,9	76,3	3,1
Gluconolactone	11,5	76,1	3
Carrageenan	11,6	76,8	2,9
Sodium alginate	13,6	76,1	2,5
Sodium ascorbate	18,7	74,1	1,8
Red 2G	21,2	72,7	1,6
MSG	23,2	74,5	1,5
Sodium benzoate	24,9	73,1	1,4
Potassium sorbate	30,1	74,1	1,1
Phosphate (P22)	34,4	73,8	1
White pudding spice	42,8	71,2	0,8
Sodium sulphite anhydrous	44,7	70,7	0,77
Nitrate	44,9	70,9	0,76
Nitrite	53,1	69,6	0,65
Salt	65,5	67,3	0,53

The effect of fat, water and salt on the thermal and dielectric properties of meat batter and its temperature following microwave or radio frequency heating (Zhang, 2007)

Beef: salt effect				
Salt added (%)	915 MHz		2450 MHz	
	e'	e''	e'	e''
0,4	54,21	34,84	48,8	20,88
1,4	51,05	52,15	45,42	26,18
2,4	45,52	62,26	41,38	29,76
Beef: fat effect				
Fat added (%)	915 MHz		2450 MHz	
	e'	e''	e'	e''
12,4	62,51	62,43	56,85	32,18
22	56,76	56,55	51,79	30,08
29,7	52,07	51,58	47,78	26,96
Beef: water effect				
Water added (%)	915 MHz		2450 MHz	
	e'	e''	e'	e''
21	54,78	61,8	50,22	31,49
25	55,83	64,83	51,31	33,44
29	59,9	68,84	55,74	35,52

Dielectric and thermophysical properties of different beef meat blends over a temperature range of -18 to +10 °C (Frag, 2008)

Lean beef: Mc(%) 67.8, Fat(%) 11.8, Protein(%) 17.9, Ash(%) 0.8							
896 MHz				2450 MHz			
e'		e''		e'		e''	
T (°C)	Value	T (°C)	Value	T (°C)	Value	T (°C)	Value
-18,07	17,97	-18,02	6,25	-18,07	15,48	-18,02	6,25
-15,08	20,04	-15,03	6,99	-15,08	18,1	-15,03	6,99
-10,06	23,2	-9,96	7,78	-10,06	20,85	-9,96	7,78
-5,09	32,44	-4,99	12,02	-5,09	28,71	-4,99	12,02
-3,06	39,63	-2,96	14,13	-3,06	34,51	-2,96	14,13
-1,08	49,86	-0,98	15,55	-1,08	44,88	-0,98	15,55
0,9	52,89	1,05	16,97	0,95	47,36	1,05	16,97
4,96	50,66	5,01	16,35	4,96	46,24	5,01	16,35
9,93	50,23	10,03	17,83	9,93	46,35	10,03	17,83

50:50. Mc(%) 48.2, Fat(%) 36.1, Protein(%) 13.7, Ash(%) 0.6							
896 MHz				2450 MHz			
e'		e''		e'		e''	
T (°C)	Value	T (°C)	Value	T (°C)	Value	T (°C)	Value
-18,03	11,22	-17,97	3,41	-18,03	9,97	-17,97	3,41
-15,04	11,22	-14,93	4,04	-15,04	10,25	-14,93	4,04
-10,03	13,16	-9,97	3,94	-10,03	11,77	-9,97	3,94
-5,07	15,37	-4,96	4,53	-5,01	13,99	-4,96	4,53
-3,09	20,22	-2,98	5,87	-3,04	17,73	-2,98	5,87
-1,02	25,07	-0,95	7,9	-1,02	22,71	-0,95	7,9
0,9	30,89	1,07	9,24	1,01	27,56	1,07	9,24
4,86	27,15	5,02	7,78	4,96	24,79	5,02	7,78
9,97	32,69	10,04	11,13	9,97	30,19	10,04	11,13

Fat. Mc(%) 26.3, Fat(%) 65.7, Protein(%) 7.8, Ash(%) 0.3							
896 MHz				2450 MHz			
e'		e''		e'		e''	
T (°C)	Value	T (°C)	Value	T (°C)	Value	T (°C)	Value
-18,03	6,09	-18,05	1,68	-18,03	5,4	-18,05	1,68
-14,99	4,58	-15,05	0,93	-14,99	4,58	-15,05	0,93
-9,97	5,98	-10,03	0,84	-9,97	5,84	-10,03	0,84
-4,96	5,59	-5,01	0,74	-4,96	5,59	-5,01	0,74
-2,99	7,11	-3,03	1,39	-2,99	6,7	-3,03	1,39
-1,01	8,5	-1	2,03	-1,01	8,23	-1	2,03
1,01	9,2	0,97	1,31	0,96	8,23	0,97	1,31
5,02	8,25	5,03	1,91	5,02	8,11	5,03	1,91
10,03	8,55	10	1,82	10,03	8,27	10	1,82

Variation of the dielectric properties of chicken meat with frequency and temperature (Trabelsi, 2015)

Chicken breast meat (pH 5.82, WHC = 5%, M = 75.5 %)												
0.5 GHz				1.55 GHz				7.96 GHz				
e'		e''		e'		e''		e'		e''		
T (°C)	Value	T (°C)	Value	T (°C)	Value	T (°C)	Value	T (°C)	Value	T (°C)	Value	
-19,59	5,49	-19,52	0,96	-19,21	4,94	-19,42	0,38	-19,55	4,66	-19,56	0,49	
-18,97	5,54	-19,06	0,89	-15,84	5,6	-15,77	0,66	-19,17	4,66	-19,19	0,49	
-15,98	5,76	-15,71	1,06	-11,04	6,34	-10,92	0,94	-15,95	4,78	-15,97	0,6	
-11,01	6,52	-11,28	1,37	-6,05	8,2	-5,88	1,79	-15,57	4,78	-15,59	0,6	
-6,03	8,63	-5,8	2,33	-4,63	9,3	-4,5	1,86	-11,04	5,13	-11,07	0,96	
-5,15	9,27	-4,9	2,59	-3,62	10,41	-3,52	2,33	-10,66	5,14	-10,69	0,96	
-4,48	10,27	-4,42	2,81	-2,79	11,69	-2,82	2,93	-6,01	6,11	-6,05	1,84	
-3,58	11,25	-3,66	3,32	-2,03	17,18	-2,07	5,03	-5,66	6,11	-5,67	1,84	
-2,96	13,15	-3,08	4,01	-1,78	16,94	-1,8	4,87	-4,63	6,74	-4,63	2,32	
-1,97	19,42	-2,27	6,32	-1,53	17,44	-1,57	5,14	-4,25	6,73	-4,27	2,32	
-1,4	42,81	-1,66	13,22	-1,44	37,83	-1,45	13,07	-3,62	7,38	-3,66	2,83	
-0,89	62,89	-0,79	23,43	-1,19	37,55	-1,22	12,91	-3,27	7,21	-3,29	2,73	
0,09	63,32	0,49	24,12	-0,94	56,31	-0,99	13,19	-3,04	8,35	-3,04	3,54	
0,8	63,26	0,94	24,29	-0,94	38,04	-0,94	18,76	-2,66	8,36	-2,68	3,55	
2	63,29	1,79	24,51	-0,69	56,04	-0,69	18,63	-2,03	11,27	-2,03	5,99	
2,98	63,28	2,9	24,91	-0,44	56,55	-0,44	18,91	-1,65	11,26	-1,68	5,99	
3,81	63,26	3,78	25,23	0,65	56,86	0,65	18,72	-1,44	21,67	-1,45	16,34	
4,34	63,38	4,24	25,41	0,9	56,57	0,9	18,57	-1,07	21,67	-1,07	16,33	
9	62,79	9,09	26,96	1,15	57,07	1,15	18,87	-0,94	31,85	-0,94	26,66	
9,47	63	9,4	27,13	1,95	57	1,94	18,6	-0,56	31,85	-0,57	26,65	
14,4	62,31	14,56	29,32	2,2	56,71	2,19	18,44	0,65	33,09	0,65	26,71	
14,88	62,49	14,87	29,56	2,72	57,26	2,71	18,65	1,03	33,09	1,02	26,71	
18,98	61,67	18,77	31,78	3,14	56,94	3,13	18,38	1,99	33,93	1,94	26,7	
19,45	61,81	19,12	31,52	3,31	56,77	3,32	18,35	2,35	33,93	2,32	26,7	
24,01	61,27	24,13	34,04	3,75	57,19	3,77	18,45	3,08	34,62	3,03	26,63	
24,48	61,43	24,43	34,2	4,15	56,83	4,13	18,25	3,48	34,71	3,41	26,63	
				4,44	57,28	4,43	18,5	4	35,2	3,95	26,5	
				8,95	56,94	8,93	18,09	4,36	35,2	4,33	26,49	
				9,2	56,63	9,2	17,94	8,95	37,99	8,93	25,54	
				9,43	57,13	9,43	18,21	9,33	37,99	9,31	25,54	
				14,36	56,52	14,33	18,01	14,36	39,99	14,33	24,12	
				14,61	56,23	14,6	17,86	14,73	40	14,7	24,12	
				14,84	56,73	14,83	18,13	18,97	40,83	18,93	22,39	
				18,97	55,87	18,93	18,13	19,34	40,82	19,31	22,39	
				19,2	55,57	19,18	17,96	23,95	41,96	23,95	21,29	
				19,45	56,1	19,43	18,25	24,33	41,96	24,33	21,29	
				23,95	55,47	23,95	18,36					
				24,2	55,17	24,18	18,21					
				24,44	55,68	24,43	18,5					

Chicken breast meat (pH 5.82, WHC = 5%, M = 75.5 %)							
T = 25°C							
e'		e''		e'		e''	
Freq (GHz)	Value	Freq (GHz)	Value	Freq (GHz)	Value	Freq (GHz)	Value
0,2	67,14	0,2	72,84	2,31	52,96	2,04	17,45
0,21	67,15	0,21	72,83	2,43	52,75	2,15	17,37
0,22	66,6	0,22	66,08	2,54	52,83	2,22	16,91
0,23	66,59	0,23	66,08	2,67	52,15	2,31	16,98
0,24	66,03	0,24	61,03	2,77	52,41	2,44	16,36
0,26	66,02	0,25	61,03	2,89	51,35	2,56	16,52
0,27	65,16	0,27	56,27	3,04	51,52	2,7	16,94
0,28	65,33	0,28	56,27	3,13	50,72	2,89	16,96
0,29	64,56	0,29	52,49	3,26	50,82	3,05	17,06
0,3	64,88	0,3	52,49	3,47	50,63	3,14	16,67
0,31	63,8	0,31	49,53	3,64	50,61	3,26	16,79
0,33	63,81	0,33	49,53	3,85	49,95	3,5	17,1
0,35	63,47	0,35	45,35	4,04	49,96	3,67	17,2
0,36	63,47	0,36	45,35	4,21	49,2	3,89	17,5
0,39	62,61	0,39	41,87	4,38	49,43	4,11	17,75
0,41	62,64	0,4	41,87	4,56	48,39	4,18	17,3
0,42	61,95	0,42	39,16	4,76	48,56	4,32	17,97
0,44	62,12	0,44	39,16	4,93	47,36	4,54	17,95
0,46	61,46	0,46	36,8	5,16	47,36	4,61	18,59
0,48	61,77	0,48	36,8	5,51	45,74	4,86	19,06
0,5	60,99	0,5	34,79	5,75	45,74	5,1	19,12
0,52	61,15	0,52	34,79	6,1	44,56	5,52	18,65
0,55	60,45	0,55	32,24	6,37	44,61	5,76	18,73
0,58	60,44	0,58	32,24	6,66	43,36	6,11	19,78
0,61	59,92	0,61	30,05	6,95	43,42	6,44	20,09
0,64	60,02	0,64	30,05	7,22	41,66	6,79	20,49
0,67	59,42	0,67	28,36	7,23	42,41	7,27	20,39
0,7	59,62	0,7	28,4	7,54	42,09	7,64	20,54
0,73	58,9	0,73	27,25	7,79	40,27	7,86	19,88
0,76	59,21	0,73	26,55	7,81	41,09	8,17	20,01
0,79	58,46	0,76	27,03	8,16	40,63	8,74	19,93
0,82	58,62	0,79	25,72	8,74	38,71	9,17	19,99
0,87	58,03	0,82	25,72	9,13	38,71	9,73	20,41
0,92	58,03	0,88	24,11	9,63	37,77	10,21	20,46
0,97	57,54	0,92	24,13	10,1	37,75	10,61	19,81
1,02	57,61	0,97	22,88	10,59	36,92	11,16	19,92
1,11	57,23	1,01	22,95	11,02	37,03	11,72	19,88
1,15	56,67	1,06	21,78	11,45	35,27	12,13	19,9
1,21	56,91	1,11	21,78	11,47	36,02	12,42	20,75
1,24	56,14	1,15	20,87	12,06	35,66	12,95	20,72
1,3	56,3	1,21	21,07	12,42	34,72	13,86	20,72
1,39	55,66	1,25	20,19	12,95	34,82	14,56	20,86
1,45	55,64	1,3	20,31	13,79	33,67	15,15	20,82
1,54	55,01	1,39	19,43	14,41	33,68	15,49	21,41
1,61	55,06	1,46	19,42	15,28	31,94	16,29	21,54
1,68	54,3	1,54	18,69	15,96	31,96	16,55	21,11
1,76	54,51	1,61	18,74	16,67	30,5	17,12	21,77
1,83	53,97	1,69	18	17,46	30,5	17,92	21,6
1,93	54,11	1,75	18,22	18,11	28,82	18,26	22,3
2,03	54,12	1,83	17,02	19,49	27,14	19,25	22,03
2,09	54,12	1,93	17,31	19,57	27,96	20,23	22
2,2	52,95	1,94	16,61	20,49	27,47	20,83	21,94

Development of Packaging and Products for Use in Microwave Ovens (Erle, 2020)

Distilled water				Raw beef			
2800 MHz				2800 MHz			
e'		e''		e'		e''	
T (°C)	Value	T (°C)	Value	T (°C)	Value	T (°C)	Value
-15,58	4,21	-20	0,85	-15,41	3,83	-21,35	0,43
-6,23	6,16	-9,34	2,33	-6,4	5,78	-11,21	1,49
5,78	83,55	2,33	22,33	3,31	49,06	-0,21	16,82
21,68	78,48	19,24	11,56	6,14	50,03	2,49	18,17
26,8	77,18	39,2	7,39	21,85	49,34	19,41	16,23
40,4	72,1	59,66	5,95	40,22	47,14	39,7	14,44
59,12	67,23			59,47	41,14	59,66	14,19
Cooked carrots				Cooked beef			
2800 MHz				2800 MHz			
e'		e''		e'		e''	
T (°C)	Value	T (°C)	Value	T (°C)	Value	T (°C)	Value
-15,41	4,59	-20	0,59	-15,23	5,36	-19,32	0,85
-6,58	5,21	-10,36	0,55	-6,58	6,54	-10,02	1,32
6,49	76,13	2,66	25,3	6,14	36,51	2,49	13,92
21,85	72,2	19,24	18,18	21,85	36,58	19,41	12,32
40,75	67,91	39,53	15,55	40,57	35,15	39,53	10,96
59,47	62,09	59,66	15,12	59,29	32,95	59,32	10,79
Mashed potatoes				Cooked ham			
2800 MHz				2800 MHz			
e'		e''		e'		e''	
T (°C)	Value	T (°C)	Value	T (°C)	Value	T (°C)	Value
-16,29	4,4	-20,51	0,68	-15,41	6,69	-20	1,78
-6,4	5,97	-10,7	1,23	-6,23	9,97	-10,36	4,04
5,96	67,17	2,66	25,81	6,14	44,7	3,34	22,24
22,03	65,34	19,07	21,67	21,85	43,82	19,07	23,2
40,75	61,05	39,7	20,13	40,75	49,24	39,53	29,14
59,47	56,57	59,66	19,54	59,12	50,66	59,83	32,62
Corn oil							
2800 MHz							
e'		e''					
T (°C)	Value	T (°C)	Value				
-6,58	2,35						
21,5	2,86						
40,57	3,15						
59,82	3,62						

Dielectric properties of fresh rabbit meat in the microwave range (Gómez-Salazar, 2021)

Rabbit											
Muscle type	Temp (°C)	Parameter	Frequency			Muscle type	Temp (°C)	Parameter	Frequency		
			915 MHz	2450 MHz	5800 MHz				915 MHz	2450 MHz	5800 MHz
Biceps femoris 100 days old male	20	e'	65,06	60,55	53,51	Tensor fasciae latae 100 days old female	20	e'	62,01	57,2	29,64
		e''	23,52	16,94	20,89			e''	19,62	15,84	20,32
		dp (cm)	1,81	0,9	0,29			dp (cm)	2,12	0,93	0,29
	40	e'	65,25	60,98	56,58		40	e'	55,21	50,99	47,17
		e''	32,87	18,67	18,49			e''	24,54	14,25	14,33
		dp (cm)	1,31	0,82	0,33			dp (cm)	1,61	0,98	0,39
	60	e'	44,25	38,74	34,74		60	e'	53,18	48,87	44,56
		e''	23,91	13,9	12,2			e''	23,4	13,96	14,12
		dp (cm)	1,5	0,88	0,4			dp (cm)	1,66	0,98	0,39
Longissimus thoracis 100 days old male	20	e'	66,74	62,67	56,68	Biceps femoris 180 days old female	20	e'	60,97	56,11	49,2
		e''	21,12	15,45	19,75			e''	21,43	15,96	19,64
		dp (cm)	2,04	1	0,31			dp (cm)	1,92	0,92	0,29
	40	e'	53,53	49,71	44,77		40	e'	57,92	54,31	50,38
		e''	19,48	13,14	14,44			e''	25,19	14,66	16,03
		dp (cm)	1,99	1,05	0,38			dp (cm)	1,61	0,98	0,36
	60	e'	49,92	44,56	39,44		60	e'	40,92	40,92	36,84
		e''	27,23	15,93	13,99			e''	20,01	12,29	12,12
		dp (cm)	1,4	0,82	0,37			dp (cm)	1,79	1,02	0,41
Tensor fasciae latae 100 days old male	20	e'	64,35	59,82	52,29	Longissimus thoracis 180 days old female	20	e'	52,67	48,41	42,33
		e''	21,35	16,28	20,49			e''	18,19	13,34	15,78
		dp (cm)	1,98	0,93	0,29			dp (cm)	2,11	1,02	0,34
	40	e'	58,74	54,47	49,77		40	e'	49,66	45,91	41,32
		e''	24,21	15,09	16,74			e''	17,6	11,94	13,6
		dp (cm)	1,68	0,96	0,35			dp (cm)	2,1	1,11	0,39
	60	e'	60,95	56,03	51,29		60	e'	54,36	50,08	45,63
		e''	34,58	19,17	17,4			e''	28,72	16,14	14,93
		dp (cm)	1,22	0,77	0,34			dp (cm)	1,38	0,86	0,37
Biceps femoris 100 days old female	20	e'	62,39	57,72	50,27	Tensor fasciae latae 100 days old female	20	e'	62,44	58,31	51,38
		e''	20,24	15,62	20,22			e''	18,05	14,74	19,72
		dp (cm)	2,06	0,95	0,29			dp (cm)	2,3	1,01	0,3
	40	e'	64,32	60,63	55,66		40	e'	57,76	53,76	49,01
		e''	23,66	15,84	18,31			e''	21,48	13,94	15,52
		dp (cm)	1,79	0,96	0,33			dp (cm)	1,87	1,03	0,37
	60	e'	57,68	53,97	50,33		60	e'	54,55	50,19	45,81
		e''	23,64	15,2	15,04			e''	22,64	13,98	14,84
		dp (cm)	1,7	0,95	0,39			dp (cm)	1,73	0,99	0,38
Longissimus thoracis 100 days old female	20	e'	50,72	45,95	39,62						
		e''	18,6	13,72	16,02						
		dp (cm)	2,03	0,97	0,32						
	40	e'	34,95	32,53	29,64						
		e''	13,05	8,23	8,81						
		dp (cm)	2,4	1,36	0,51						
	60	e'	41,86	38,04	34,56						
		e''	16,37	19,34	10,61						
		dp (cm)	2,1	1,17	0,46						